MECHANISTIC STUDIES ON QUINOLINATE PHOSPHORIBOSYLTRANSFERASE

Gemma R. Catton

A Thesis Submitted for the Degree of PhD
at the
University of St. Andrews

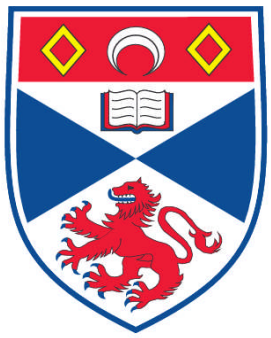

2007

Mechanistic Studies on Quinolinate Phosphoribosyltransferase

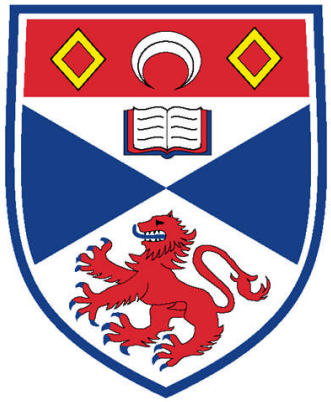

University
of
St Andrews

A thesis presented for the degree of

Doctor of Philosophy

to the

University of St. Andrews

Submitted September 2007

By

Gemma R. Catton

I, Gemma R. Catton, hereby certify that this thesis, which is approximately 55,000 words in length, has been written by me, that it is a record of work carried out by me and that it has not been submitted in any previous application for a higher degree.

Date…… Signature of candidate…….....

I was admitted as a research student in October 2003 and as a candidate for the degree of PhD in September 2004; the higher study for which this is a record was carried out in the University of St Andrews between 2003 and 2007.

Date…… Signature of candidate…….....

I hereby certify that the candidate has fulfilled the conditions of the Resolution and Regulations appropriate for the degree of PhD in the University of St Andrews and that the candidate is qualified to submit this thesis in application for that degree.

Date…… Signature of supervisor…….....

In submitting this thesis to the University of St Andrews I wish access to it to be subject to the following conditions: for a period of 1 year from the date of submission, the thesis shall be withheld from use. I understand, however, that the title and abstract of the thesis will be published during this period of restricted access; and that after the expiry of this period the thesis will be made available for use in accordance with the regulations of the University Library for the time being in force, subject to any copyright vested in the work not being affected thereby, and a copy of the work may be made and supplied to any bona fide library or research worker, that my thesis will be electronically accessible for personal or research use, and that the library has the right to migrate my thesis into new electronic forms as required to ensure continued access to the thesis. I have obtained any third-party copyright permissions that may be required in order to allow such access and migration.

Date…… Signature of candidate…….....

Acknowledgements

Firstly, I would like to thank my supervisor, Dr Nigel Botting, for all his help, advice and enthusiasm throughout this project.

I would like to thank Dr Huanting Liu for his help with all aspects of molecular biology. Thanks also to Dr Huanting Liu and Prof. Jim Naismith for all their hard work on the crystal structure.

I am grateful for all the assistance from the analytical and technical staff of the School of Chemistry at the University of St Andrews. Thanks to Catherine Botting (MS), Caroline Horsborough (MS), Melanja Smith (NMR), Sylvia Williamson (Microanalysis), Marjory Parker (stores), Colin Millar (stores), Colin Smith (glass blowing) and Bobby Cathcart (workshop).

I would like to thank all the members of the Botting research group I have had the pleasure of working alongside, many of whom became good friends; Aga, Anna, Dave, Gareth, Graham, John, Kate, Kati, Kerry, Laura, Mike, Nawaf and Qing. In particular, I would like to thank Kerry for her help at the beginning and her continued support and friendship throughout.

Thanks to Calum for keeping me entertained – lunchtimes will never be the same again!

A big thank you to Stewart for his friendship and support over the past 8 years. My time in St Andrews would not have been the same without him.

Most importantly, I would like to thank my family who have helped me so much in many different ways. A very special thank you to my Mum, my Dad and my sister and best friend, Emily for their love, support and encouragement in everything I do.

Abbreviations

AIDS	Acquired immune deficiency syndrome
Ala	Alanine
AMP	Adenosine 5'-monophosphate
Arg	Arginine
ATP	Adenosine triphosphate
AZT	Azidothymine
BH_4	Tetrahydrobiopterin
BMP	1-(Phosphoribosyl)barbituric acid
bp	Base pairs
BSA	Bovine serum albumin
Caspase	Cysteine aspartate specific protease
CD	Circular dichroism
CMP	Cytidine 5'-monophosphate
CNS	Central nervous system
CSF	Cerebrospinal fluid
DNA	Deoxyribonucleic acid
DTT	Dithiothreitol
Gln	Glutamine
GMP	Guanosine 5'-monophosphate
3-HAO	3-Hydroxyanthranilic acid oxidase
HIV	Human immunodeficiency virus
5-HT	5-Hydroxytryptamine
IDO	Indoleamine-2,3-dioxygenase
IPTG	Isopropyl-β,D-thiogalactoside
K_i	Enzyme inhibition constant
K_m	Michaelis-Menten constant
KAT	Kynurenine aminotransferase
KIE	Kinetic isotope effect
LDA	Lithium diisopropylamide
Lys	Lysine
mp	Melting point

NAD	Nicotinamide adenine dinucleotide
NAMN	Nicotinic acid mononucleotide
NMDA	*N*-Methyl-D-aspartic acid
NMR	Nuclear magnetic resonance
NOS	Nitric oxide synthase
OD	Optical density
OMP	Orotidine 5'-monophosphate
OPi	Phosphate
OPPi	Pyrophosphate
PARP-1	Poly [ADP-ribose] polymerase-1
PBS	Phosphate buffered saline
PCR	Polymerase chain reaction
PDB	Protein data bank
PLP	Pyridoxal-5'-phosphate
PMSF	Phenylmethylsulfonyl fluoride
ppm	Parts per million
PRPCP	5-Phosphoribosyl-1-(β-methylene)pyrophosphate
PRPP	5-Phosphoribosyl-1-pyrophosphate
PRTase	Phosphoribosyltransferase
QA	Quinolinic acid
QPRTase	Quinolinate phosphoribosyltransferase
Rib-Pi	Phosphoribosyl
rpm	Revolutions per minute
SDS-PAGE	Sodium dodecyl sulfate – polyacrylamide gel electrophoresis
Ser	Serine
SOD	Superoxide dismutase
TDO	Tryptophan-2,3-dioxygenase
TEV	Tobacco etch virus
TLC	Thin layer chromatography
TMP	Thymidine 5'-monophosphate
V_{max}	Maximum rate of substrate turnover at saturation

Contents

Abstract

Quinolinate phosphoribosyltransferase (QPRTase, EC 2.4.2.19) is an intriguing enzyme which appears to catalyse two distinct chemical reactions; transfer of a phosphoribosyl moiety from 5-phosphoribosyl-1-pyrophosphate to the nitrogen of quinolinic acid and decarboxylation at the 2-position to give nicotinic acid mononucleotide. The chemical mechanism of QPRTase is not fully understood. In particular, enzymatic involvement in the decarboxylation step is yet to be conclusively proven. QPRTase is neurologically important as it degrades the potent neurotoxin, quinolinic acid, implicated in diseases such as Huntington's disease and AIDS related dementia. Due to its neurological importance and unusual chemistry the mechanism of QPRTase is important. Described here is a mechanistic study on human brain QPRTase.

Human brain QPRTase was successfully expressed in *E. coli* BL21 (DE3) from the pEHISTEV-QPRTase construct and the protein was efficiently purified by nickel affinity chromatography. The crystal structure was solved using multiwavelength methods to a resolution of 1.9 Å. Human brain QPRTase was found to adopt an energetically stable hexameric arrangement. The enzyme was also found to exist as a hexamer during gel filtration under physiological conditions.

Kinetic studies allowed the measurement of the kinetic parameters for quinolinic acid. The data gave a K_m of 13.4 ± 1.0 μM and a V_{max} of 0.92 ± 0.01 μM min^{-1}. There was no evidence for cooperative binding of quinolinic acid to the six subunits of the QPRTase hexamer. The enzyme showed maximum activity at approximately pH 6.

The active site of human brain QPRTase is a deep pocket with a highly positive electrostatic surface composed of three arginine residues, two lysine residues and one histidine residue. Mutation of these residues resulted in either complete loss or significant reduction in enzymatic activity showing they are important for binding and/or catalysis. A possible mechanism involving QPRTase in the decarboxylation of quinolinic acid mononucleotide was proposed.

A series of quinolinic acid analogues were synthesised and tested as inhibitors of QPRTase. The inhibition studies highlighted some key interactions in the active site.

Chapter One

Introduction

1.1 Tryptophan metabolism

In mammals, tryptophan cannot be generated biosynthetically and is therefore essential in mammalian nutrition. For humans, the average daily requirement for tryptophan is low; 250 mg and 160 mg per day for men and women, respectively, and as such is met entirely by dietary intake.[1] In lower organisms, however, tryptophan is generated biosynthetically via a multi-step pathway.

Tryptophan **1** can be metabolised by several pathways to produce a number of biologically active molecules. Tryptophan metabolites with an intact indole nucleus arise by way of four possible routes.[2] The first route is the serotonin pathway, an important pathway in mammalian tryptophan metabolism.[1] This is a short metabolic pathway consisting of two enzyme catalysed steps, tetrahydrobiopterin (BH_4) mediated hydroxylation followed by decarboxylation, and leads to the formation of 5-hydroxytryptamine **3** (5-HT or serotonin) (Scheme 1.1).

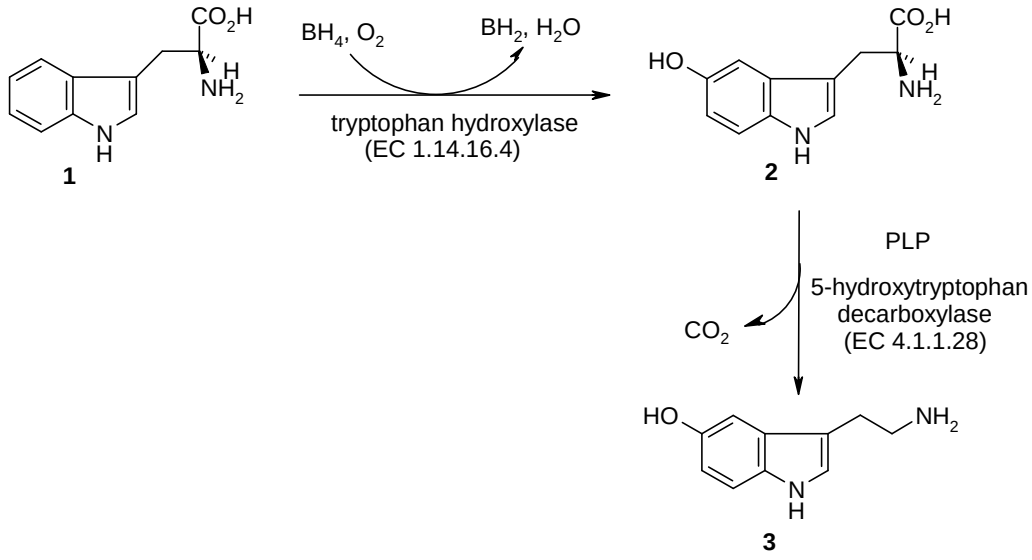

Scheme 1.1: *The serotonin pathway of tryptophan metabolism.*

The second possible pathway involves decarboxylation of tryptophan to form tryptamine, which in turn acts as a precursor for other compounds including indole, *β*-carboline and ergoline alkaloids and auxins. This is therefore an important pathway for tryptophan metabolism in plants and some bacteria but is not important in mammalian metabolism.

The third route involves cleavage of the tryptophan side chain to release indole, a reaction catalysed by tryptophanase (EC 4.1.99.1). This is essentially the reverse of the final stage of tryptophan biosynthesis in bacteria and plants. Again, this reaction is not important in mammalian tryptophan metabolism.

The fourth route to indolic tryptophan metabolites involves transamination of tryptophan to produce indole-3-pyruvate, although this is also a minor pathway in mammalian tryptophan metabolism.

Tryptophan metabolites that do not contain an intact indole nucleus arise via the kynurenine pathway, which was first described as a major route for the metabolism of tryptophan in 1947.[3] The kynurenine pathway (Scheme 1.2) begins with the oxidative cleavage of the heterocyclic ring of tryptophan **1** to give *N*-formylkynurenine **4**. This reaction is catalysed by one of two different haem-dependent oxygenase enzymes, tryptophan 2,3-dioxygenase (TDO, EC 1.13.11.11), which in mammals is confined almost exclusively to the liver,[4] or indoleamine 2,3-dioxygenase (IDO, EC 1.13.11.17), which is found in most other tissues.[5] *N*-Formylkynurine is then hydrolysed by a formamidase enzyme (EC 3.5.1.9) to give kynurenine **5**, with release of formate. Kynurenine is at a branch point in the pathway and can be metabolised by three different routes. Firstly, kynurenine can undergo hydrolysis catalysed by kynureninase (EC 3.7.1.3), a pyridoxal-5'-phosphate (PLP) dependent enzyme, resulting in the removal of the aliphatic side chain as L-alanine. This yields anthranilic acid **6** which, in lower organisms, may then be utilised in the biosynthesis of aromatic amino acids. Alternatively, kynurenine may undergo a transamination reaction catalysed by another PLP dependent enzyme, kynurenine aminotransferase (KAT, EC 2.6.1.7), to give kynurenic acid **7**, a stable aromatic metabolite sometimes employed in the biosynthesis of quinolines in lower organisms. The third possibility involves oxidation of the benzene ring catalysed by kynurenine 3-hydroxylase (EC 1.14.13.9) to produce 3-hydroxykynurenine **8**, which can then be converted to 3-hydroxyanthranilic acid **9** also by reaction with kynureninase. 3-Hydroxyanthranilic acid then undergoes a rearrangement catalysed by 3-hydroxyanthranilic acid oxidase (3-HAO, EC 1.13.11.6) to form quinolinic acid **10**. Quinolinic acid is then converted to nicotinic acid mononucleotide **11** by the

action of quinolinate phosphoribosyltransferase (QPRTase, EC 2.4.2.19). Further transformations may then follow, leading to the nicotinamide coenzymes.

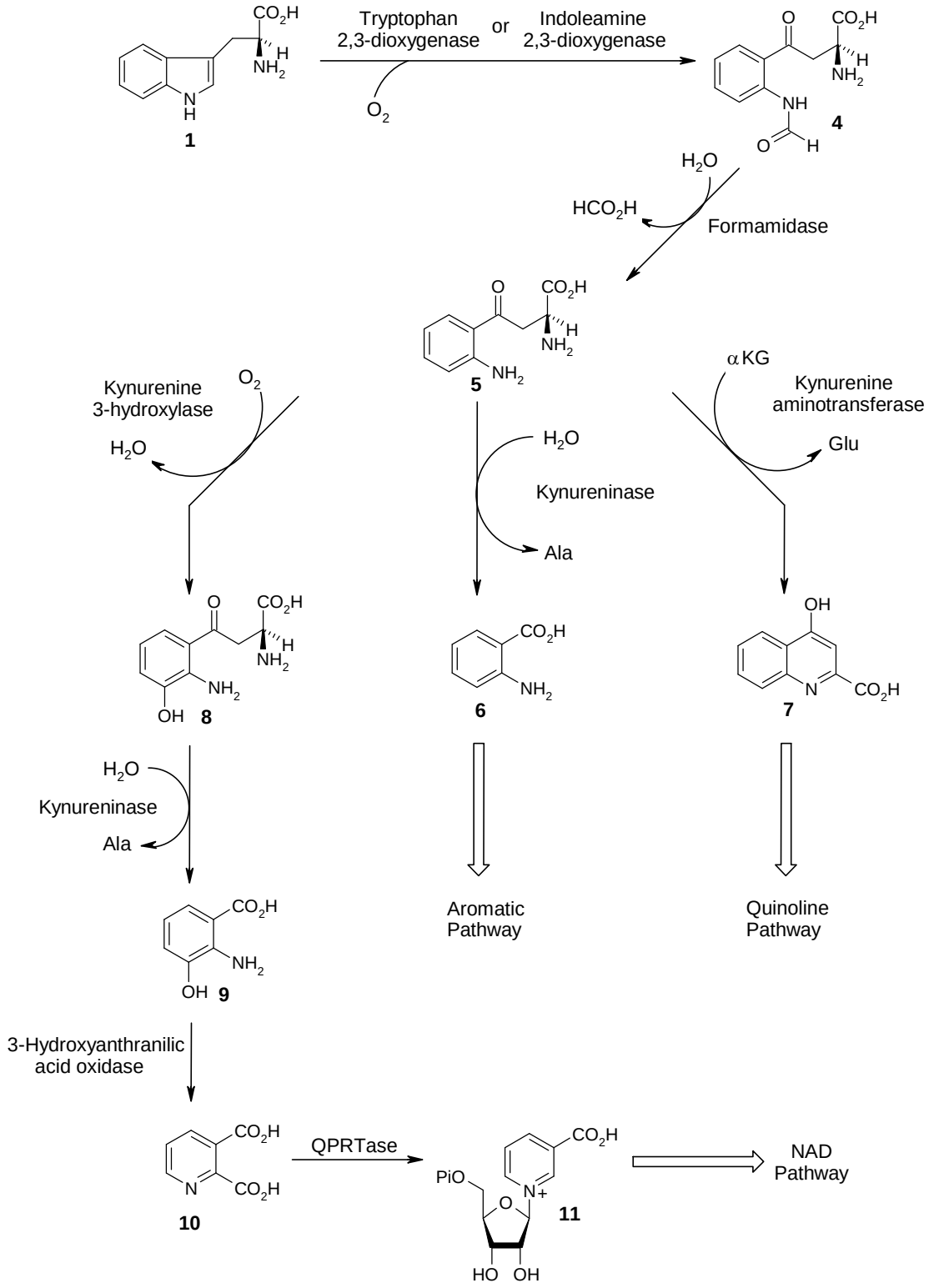

Scheme 1.2: *The kynurenine pathway of tryptophan metabolism.*

Scientific interest in the kynurenine pathway was primarily centred around both its importance as a source of nicotinamide, an important intermediate in the synthesis of the essential co-factor nicotinamide adenine dinucleotide (NAD) and also as the first metabolic pathway to be affected by vitamin B-6 deficiency.[6] Vitamin B-6 **12** is oxidised and phosphorylated in the body to pyridoxal-5'-phosphate (PLP) **13**, which is an essential cofactor for a number of enzymes involved in the kynurenine pathway i.e. kynureninase and kynurenine aminotransferase.

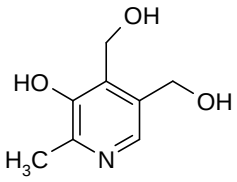

12

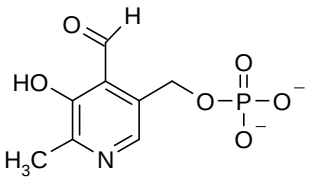

13

With the discovery that neurons and other cells release 5-hydroxytryptamine (5-HT) as a neurotransmitter or local hormone respectively, the major focus of tryptophan research shifted to the investigation of its role as a precursor of 5-HT via the serotonin pathway. 5-HT is involved in controlling sleep, appetite, mood and behaviour.[7] Dysfunction of the serotonin pathway can lead to reduced levels of cerebral 5-HT, which can result in disorders such as insomnia and depression. It was initially thought that such illnesses could be treated simply by the administration of high doses of tryptophan. However, due to the complex metabolism of tryptophan this would not only augment levels of 5-HT, but also the biosynthesis of various kynurenines via the kynurenine pathway, which are thought to be implicated in a number of neurological disorders (section 1.3). Consequently, tryptophan is no longer used to treat 5-HT deficient disorders.[8]

The discovery that some kynurenine metabolites possess interesting biological properties triggered a resurgence of interest in the kynurenine pathway. The most important work concerns the neurological activity of quinolinic acid (section 1.2). The kynurenine pathway, once perceived to be less important than the serotonin pathway, is in fact the quantitatively dominant pathway for mammalian tryptophan metabolism. In peripheral tissue, only 1% of dietary tryptophan is actually converted to 5-HT, while greater than 95% is metabolised to kynurenines.[9]

1.2 Neurological activity of quinolinic acid

The *N*-methyl-D-aspartic acid (NMDA) receptor is abundant and ubiquitously distributed throughout the brain. Activation of the receptor mediates neurotransmission across most excitatory synapses in the mammalian central nervous system (CNS). In 1981, it was discovered that one member of the kynurenine pathway, quinolinic acid, could excite neurons in the CNS by acting as an agonist at the NMDA receptor.[10] This first report of the excitatory activity of quinolinic acid resulted from experiments in the cerebral cortex of anaesthetised rats, in which it was demonstrated that quinolinic acid could excite all 54 neurons tested with an apparently similar potency to NMDA itself. By comparing the structures of quinolinic acid **10** and NMDA **14** it can be seen that they share a similar backbone, shown in red, hence quinolinic acid is able to interact with the NMDA receptor.

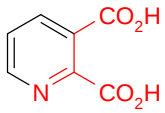

10

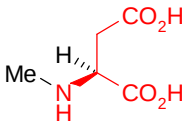

14

The NMDA receptor is important because it is implicated in key aspects of brain function such as development, learning and memory. These functions are mediated by calcium entry through the NMDA receptor-associated calcium channel upon activation of the receptor by NMDA. However, over-activation of NMDA receptors by agonists such as quinolinic acid triggers an excessive entry of Ca^{2+} ions into the cell.[11] Uncontrolled calcium influx overloads the transport systems and buffers which normally act to reduce the concentration of free Ca^{2+} in the cell. The excess Ca^{2+} triggers a series of processes that promote neuronal cell death[12,13] and hence quinolinic acid possesses neurotoxic activity.[10] The ways in which quinolinic acid-induced Ca^{2+} influx through NMDA-coupled ion channels leads to neuronal cell death are outlined in Figure 1.1.

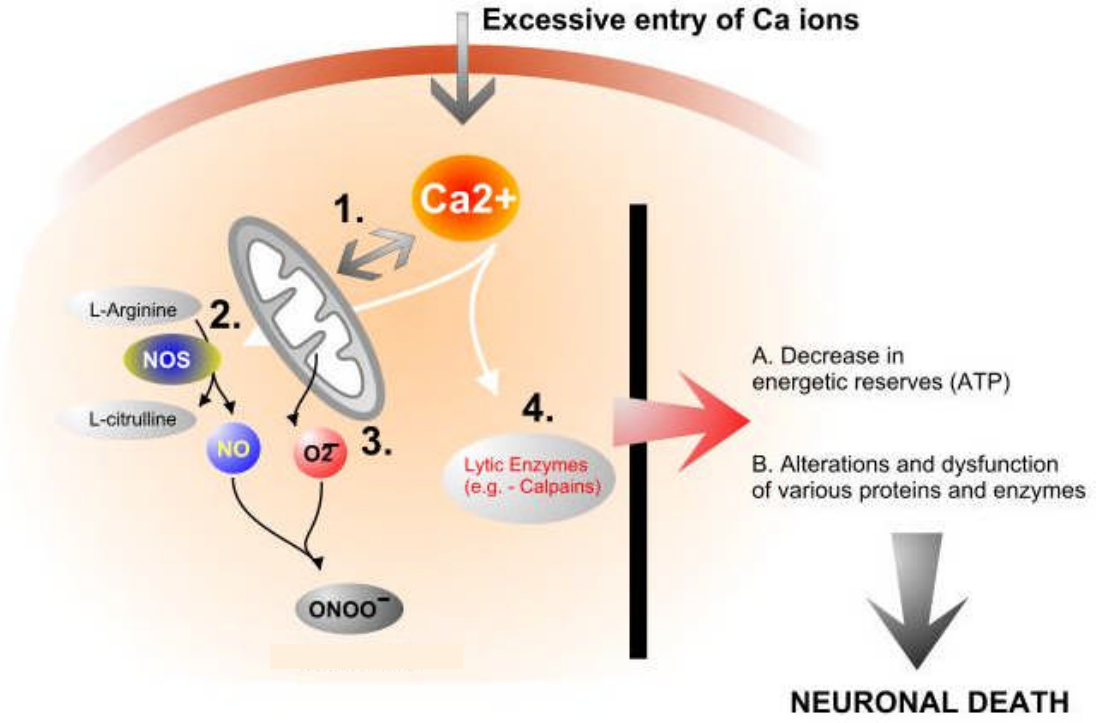

Figure 1.1: *Quinolinic acid induced neurotoxicity – the intracellular cascade of biochemical events leading to excitotoxic cell death.*[14]

Firstly, excessive Ca^{2+} influx leads to an elevation of the intracellular free Ca^{2+} concentration to a point that results in Ca^{2+} overload of mitochondria (Figure 1.1, **1**). The excess Ca^{2+} causes depolarization of the mitochondrial membrane potential, malfunction of the mitochondrial electron transport chain and a decrease in ATP synthesis.[15] The resulting dramatic decrease in cellular ATP concentrations means that energy requiring processes are severely compromised, leading to cell dysfunction and ultimately neuronal cell death (Figure 1.1, **A**).

Secondly, studies have shown that oxidative/nitrosative stress is involved in NMDA receptor-mediated excitotoxic neuronal cell damage by quinolinic acid. Quinolinic acid-induced Ca^{2+} influx into cells triggers a series of processes that lead to increased production of the highly toxic compound peroxynitrite ($ONOO^-$) (Figure 1.1). Peroxynitrite is formed in biological systems by the reaction of nitric oxide (NO) with superoxide (O_2^-). It has been shown that stimulation of NMDA receptors leads to the Ca^{2+}-dependent activation of nitric oxide synthase (NOS, EC 1.14.13.39), resulting in the increased production of nitric oxide in neurons (Figure 1.1, **2**).[16,17] Also the increased entry of Ca^{2+} into the mitochondria, and subsequent malfunctioning of the

mitochondrial electron transport chain, leads to increased production of reactive oxygen species such as superoxide (O_2^-) (Figure 1.1, **3**).[18] The most powerful cellular antioxidant system protecting against superoxide is the enzyme superoxide dismutase (SOD, EC 1.15.1.1). However, it has been shown that the activity of superoxide dismutase is significantly reduced in the presence of quinolinic acid and this further contributes to the build up of superoxide.[19] This simultaneously enhanced production of nitric oxide and superoxide leads to the rapid formation of the highly toxic compound peroxynitrite (Figure 1.1).

Peroxynitrite is a powerful oxidant and reacts with a variety of biomolecules to produce a wide array of tissue damaging effects.[20,21] Peroxynitrite is a particularly effective oxidant of aromatic molecules and organosulfur compounds including free amino acids and peptide residues. Peroxynitrite oxidises cysteine to the disulfide and methionine to the sulfoxide. Tyrosine and tryptophan undergo single-electron oxidations to radical cations, which are competitively hydroxylated, nitrated and dimerised.[22,23] These changes may lead to the dysfunction of essential proteins, for instance tyrosine nitration has been suggested as a key factor in the case of reduced superoxide dismutase activity.[24]

The reaction of peroxynitrite with lipids leads to lipid peroxidation (malondialdehyde and 4-hydroxynonenal formation)[25] and formation of nitrito-, nitro-, nitrosoperoxo- and/or nitrated lipid oxidation adducts,[26] all of which cause damage to cellular membranes. Quinolinic acid (100 μM) has been shown to produce an 80% increase in lipid peroxidation, evidence that quinolinic acid-induced toxicity involves the early formation of peroxynitrite.[27]

In addition, peroxynitrite causes damage to DNA since purine nucleotides are vulnerable to oxidation and adduct formation, resulting in the production of 8-hydroxydeoxyguanosine or 8-nitroguanine. Peroxynitrite is also a potent trigger of DNA strand breakage.[28]

Peroxynitrite therefore causes extensive cellular damage leading to cellular dysfunction. When peroxynitrite-induced cellular damage reaches a level where it cannot be handled by the repair mechanisms, cells undergo one of the basic cell death pathways i.e. apoptosis or necrosis (Figure 1.1, **B**).

Furthermore, quinolinic acid-induced Ca^{2+} overload of cells can result in sustained activation of a number of Ca^{2+}-dependent degradative enzymes, the uncontrolled action of which terminally disrupts cell function (Figure 1.1, **4, B**). Calpains are Ca^{2+}-dependent proteolytic enzymes. The cellular targets for these enzymes are a number of structural components of the neuronal cytoskeleton, including spectrin, microtubule-associated proteins, tubulin and neurofilaments.[29] The proteolytic activity of the calpain enzymes disrupts the links that anchor the cytoskeleton to integral proteins of the plasma membrane, and this may lead to membrane blebbing and ultimately to the loss of plasma membrane integrity.[30] Similarly, phospholipase activation by sustained increase in intracellular Ca^{2+} can result in enhanced breakdown of membrane phospholipids and loss of plasma membrane integrity.[31]

Ca^{2+} overload of cells can also trigger endonuclease activation which results in fragmentation of DNA.[32] In addition, Ca^{2+} overload may stimulate other enzymatic processes that result in DNA damage. For example, elevated Ca^{2+} levels can lock the enzyme topoisomerase II (EC 5.99.1.2) in a form that cleaves but does not re-ligate DNA, leading to DNA fragmentation.[33]

Further damage to DNA results from the Ca^{2+}-dependent activation of the *c*ysteine *asp*artate specific prote*ase* (caspase) cascade, which results ultimately in the activation of caspase-3 (EC 3.4.22.B9).[34] Studies have shown that the caspase enzymes are important in excitotoxin-induced neuronal apoptosis of cerebrocortical neurons,[35] in particular caspase-3.[36] The caspase enzymes have a significant proteolytic activity and induce the degradation of a series of cytosolic and nuclear targets. In particular, caspase-3 cleaves poly [ADP-ribose] polymerase-1 (PARP-1, EC 2.4.2.30), a key DNA repair enzyme that is activated by DNA strand breakage. The cleavage of PARP-1 by caspase-3 results in the separation of the two zinc-finger DNA-binding motifs from the automodification and catalytic domains, thus preventing the recruitment of the enzyme to sites of DNA damage.[37] Caspase-3

protease activity leads to chromatin condensation and DNA fragmentation in the neuronal nucleus, suggesting these proteases play a central role in NMDA-mediated neuronal apoptosis.

In summary, quinolinic acid exerts its neurotoxic activity by overstimulating NMDA receptors; the target neurons are overexcited, the result being energy disturbance and a series of pathobiochemical changes that culminate in nerve cell death. Studies have shown that micromolar concentrations of quinolinic acid are toxic when cells are exposed to those concentrations for several hours,[38-40] and sub-micromolar concentrations can produce neurotoxicity in culture if maintained for several weeks, with some neurons being killed on exposure to only 100 nM quinolinic acid.[41]

1.3 Quinolinic acid and neurological diseases

Excitotoxicity due to excessive NMDA receptor activation is a final common path for cell death in a number of neurodegenerative conditions. The observation that quinolinic acid is an excitotoxic NMDA receptor agonist raises the potential involvement of this metabolite in many neurodegenerative and convulsant disorders. Elevation of quinolinic acid to neurotoxic levels has now been observed in a number of neurological disorders, suggesting quinolinic acid may play an important pathological role in these conditions.[5]

1.3.1 Non-inflammatory neurological diseases

1.3.1.1 Huntington's disease

Huntington's disease is a progressive neurodegenerative disorder characterised by specific and regional neuronal cell loss in the striatum and neocortex of the brain. Its clinical phenotype includes motor and psychiatric manifestations with a decline in cognitive function, resulting in the progressive development of involuntary movements and, in its later stages, dementia.

Quinolinic acid was first proposed to be an important factor in Huntington's disease because it produced nerve cell damage very similar to that caused by the disease.[42] Animal studies by Schwarcz found that intrastriatal injection of quinolinic acid resulted in the formation of lesions which closely resemble those observed in the post-mortem brains of Huntington's disease victims, suggesting quinolinic acid may be causally involved in the disease.[43]

Studies involving the quantification of various kynurenine pathway metabolites have revealed some interesting pathway alterations in Huntington's disease. Firstly, a recent study involving a mouse model of Huntington's disease has shown that quinolinic acid levels are elevated in the cortex and striatum, the two brain areas that suffer the most pronounced neuron loss in Huntington's disease, further supporting the idea that quinolinic acid might be involved in the progression of the disease.[44] Quinolinic acid is formed from a precursor, 3-hydroxyanthranilic acid, by the enzyme 3-hydroxyanthranilic acid oxidase (3-HAO). Quinolinate phosphoribosyltransferase (QPRTase) is the only enzyme responsible for the catabolism of quinolinic acid. Kinetic studies have shown that the maximum enzymatic rate for 3-HAO is approximately 80-fold higher than that for QPRTase, although the Michaelis-Menten constant (K_m) for both enzymes is about the same.[45] QPRTase is therefore the rate-limiting enzyme in quinolinic acid metabolism. A study of post-mortem brains of Huntington's disease victims revealed a 3- to 4-fold increase in the activity of 3-HAO in the corpus striatum, the area of the brain most affected by the disease.[46] In contrast, the activity of QPRTase is relatively unchanged in Huntington's disease.[47] Therefore, if QPRTase was unable to metabolise the excess quinolinic acid, this would account for the observed increased levels of the neurotoxin.

In addition, reduced levels of kynurenic acid have been observed in both the post-mortem brain[48,49] and cerebrospinal fluid (CSF)[50] of Huntington's disease victims. Kynurenic acid is an NMDA receptor antagonist and is therefore able to block neuronal damage induced by neurotoxins.[51] It has been proposed that kynurenic acid and quinolinic acid concentrations must be finely balanced in order to maintain the NMDA receptor activity at its optimum level. A drop in the level of the neuroprotectant, kynurenic acid, as observed in the post-mortem brains and CSF of

Huntington's disease victims, shifts the balance in favour of the neurotoxin, quinolinic acid.

A crucial role for quinolinic acid and NMDA receptors in the neuronal dysfunction and loss which occurs in Huntington's disease has thus been postulated. In a study of post-mortem brains of Huntington's disease victims, Young *et al.* detected a loss of NMDA receptors, which is consistent with an increased loss of cells bearing these receptors in response to an excitotoxic process mediated by quinolinic acid.[52]

In addition, there is growing evidence for a degree of oxidative stress in Huntington's disease which could result from the over-activation of NMDA receptors by quinolinic acid. In an animal model for Huntington's disease, a significant increase in lipid peroxidation has been reported which parallels the neurological phenotype.[53] Also, results from a recent study of Huntington's disease patients were consistent with elevated oxidative stress as reflected in the significantly raised (almost eight-fold higher) plasma levels of lipid peroxidation products compared to control subjects.[54]

While there is growing evidence for a role for quinolinic acid in Huntington's disease, there is also strong evidence that overexpression of the abnormal huntingtin gene contributes to the induction of Huntington's disease symptoms in humans and to the striatal characteristics of Huntington's disease in mouse models.[55] However, the two situations may be closely linked since it has been shown that administration of quinolinic acid into the striatum can induce increased expression of huntingtin[56] and as such it has been proposed that perhaps a primary toxicity caused by quinolinic acid could induce huntingtin expression as a cytoprotective response.[57,58]

1.3.1.2 Temporal lobe epilepsy

Studies have shown that injection of quinolinic acid into the hippocampus of rats causes convulsions reminiscent of human temporal lobe epilepsy.[59] Examination of the activity of QPRTase in post-mortem brain tissue from epilepsy victims revealed reduced activity of the enzyme relative to controls.[60] It was inferred that the decreased QPRTase activity may lead to a build up of quinolinic acid which may be involved in epileptogenesis.

1.3.2 Inflammatory neurological diseases

A study by Heyes *et al.* showed that inflammatory diseases (bacterial, viral, fungal and parasitic infections, meningitis, autoimmune diseases and septicaemia) are associated with accumulation of quinolinic acid.[50] In this study, the CSF and post-mortem brain tissue quinolinic acid levels of inflammatory disease patients who had demonstrable clinical neurological deficits were increased between ten-fold to one thousand-fold compared to control groups and exceeded the 100 nM concentrations that are toxic to certain types of neurons *in vitro*.[41]

It has been demonstrated that macrophages, cells which are activated and can infiltrate the brain following an immune response to neutralise the effects of foreign substances, have a particularly high capacity for synthesising quinolinic acid.[61] Similarly microglial cells, the resident immune cells within the brain, are capable of biosynthesising quinolinic acid.[62] Activated microglia and macrophage infiltrates into the brain might therefore be an important source of quinolinic acid within the CNS in inflammatory diseases. This is discussed further using specific examples of inflammatory diseases as case studies.

1.3.2.1 Alzheimer's disease

Alzheimer's disease is a progressive neurological disorder which causes defects in memory, cognition, attention and motivation. It is the most common cause of dementia in the elderly. Two significant abnormalities occur in the brains of people affected by Alzheimer's disease, particularly in the neocortex, hippocampus and amygdale regions. These are the formation of extracellular plaques, which consist largely of an insoluble sticky protein called β-amyloid, and the formation of intracellular neurofibrillary tangles, which are made from an abnormal, hyperphosphorylated state of tau, a protein normally associated with microtubule formation. Dementia is significantly correlated with the density of β-amyloid deposits and the number of neurofibrillary tangles. However, studies have shown that isolated plaques do not have direct cytotoxic effects upon neuronal tissues.[63]

Microglial clusters around the plaques are a distinctive feature of Alzheimer's disease pathology. Studies have shown that microglia and β-amyloid deposits appear almost simultaneously at an early stage in Alzheimer's disease and the density of plaques and microglia are strongly correlated.[64] Recently, it has been shown that, in culture, the microglia in contact with the plaques typically have a "reactive" morphology similar to those found in Alzheimer's disease tissue.[63] It would appear, therefore, that β-amyloid plaques are able to activate microglia, although the way in which this occurs is unknown. Plaque-stimulated microglia are capable of a range of secretory functions, and studies suggest that it is these reactive microglia that are the source of brain neurotoxins in Alzheimer's disease.[63] Activated microglia are capable of synthesising quinolinic acid in neurotoxic concentrations, raising the possibility that quinolinic acid could play an important role in the neurodegeneration associated with Alzheimer's disease.[62] In support of this hypothesis, Guillemin *et al.* have demonstrated that β-amyloid plaques can induce quinolinic acid production by human microglia.[65] Furthermore, up-regulation of the kynurenine pathway and accumulation of quinolinic acid have been detected in the cortical microglia and neurons in the hippocampus of the Alzheimer's disease brain.[66]

1.3.2.2 HIV and AIDS

It has been reported that almost 20% of patients with acquired immune deficiency syndrome (AIDS) develop marked CNS symptoms, with cognitive decline, motor dysfunction and behavioural abnormalities.[67] There is growing evidence, gathered from both human studies and animal model studies, for a role for quinolinic acid in this AIDS-dementia complex.

In patients who are affected by AIDS-related dementia, the levels of quinolinic acid in the CSF are increased up to 20-fold.[68] The levels of quinolinic acid observed correlate with the degree of cognitive and motor dysfunction in the affected patients. The amount of quinolinic acid in the brain of patients infected with human immunodeficiency virus (HIV) can increase up to levels 300 times of those measured in the CSF.[69] The quinolinic acid found in the AIDS brain is likely to originate from cells activated by the immune system as part of the generalised inflammatory reaction

to the viral invasion. Studies have shown that immune stimulation of macrophages can activate components of the kynurenine pathway including indoleamine-2,3-dioxygenase (IDO), kynurenine-3-hydroxylase, kynureninase and 3-hydroxyanthranilic acid oxidase (3-HAO).[70] In AIDS-related dementia, there is evidence for increased activity of IDO.[71] Such IDO induction will result in enhanced tryptophan degradation along the kynurenine pathway, leading to increased generation of quinolinic acid. It has been demonstrated that the activated macrophages present in AIDS patients are capable of generating enough quinolinic acid to cause neuronal damage.[72]

Studies have shown that the concentration of quinolinic acid declines in parallel with neurological improvement when AIDS patients are treated with the drug azidothymine (AZT).[73] This drug inhibits the replication of the HIV virus. As a result the immune response is suppressed, presumably resulting in a decrease in quinolinic acid biosynthesis by immune stimulated cells and leading to improvement of motor and cognitive processes.

1.3.2.3 Cerebral malaria

Malaria, caused by *Plasmodium falciparum* infection, is one of the most important global health problems, potentially affecting more than one third of the world's population. A major, life-threatening complication of malaria infection is cerebral malaria. Cerebral malaria is characterised by neurological manifestations, such as convulsions and coma. This condition chiefly afflicts children aged 2-6 years in sub-Saharan Africa and adults in South East Asia.[74]

The contribution of excitatory mediators to the initiation and maintenance of seizures and neurodegeneration during cerebral malaria has been studied in both human populations[75,76] and mouse models.[77] The studies showed that quinolinic acid levels are elevated in the CSF of children suffering from cerebral malaria. For example, Kenyan children suffering from cerebral malaria exhibit a fourteen-fold increase in CSF quinolinic acid levels.[76] Similarly, elevated levels of quinolinic acid have been observed in the mouse model of cerebral malaria.[77] These studies suggest that

quinolinic acid may contribute to some of the neurological symptoms of cerebral malaria.

The increased level of quinolinic acid is thought to arise from activation of the kynurenine pathway as a result of immune stimulation. Studies on the mouse model of cerebral malaria have shown that the activity of IDO, the first enzyme of the kynurenine pathway, is dramatically increased in the brain.[77] One of the earliest events in cerebral malaria pathogenesis appears to be a mild increase in the permeability of the blood-brain barrier.[78] The significance of changes in the blood-brain barrier in cerebral malaria is that they would allow cytokines and malaria antigens to enter the brain compartment from which they are normally excluded. Interferon-γ, a cytokine known to be produced in malaria infection,[79] is a powerful inducer of IDO expression.[80]

Currently there is no specific treatment for cerebral malaria. Recently, however, studies have shown that inhibition of the kynurenine pathway results in prolonged survival using a murine model of cerebral malaria.[81] The enzyme targeted in this inhibition study was kynurenine-3-hydroxylase. Inhibiting the kynurenine pathway at this stage prevents synthesis of quinolinic acid and therefore prevents over-activation of NMDA receptors and subsequent neuronal damage and neurological symptoms associated with the disease. Therefore, compounds which inhibit the kynurenine pathway may potentially be effective in the treatment and prevention of human cerebral malaria.

1.3.2.4 Poliomyelitis

The importance of quinolinic acid in poliomyelitis has been investigated using model animal studies involving infection of the lumbar spinal cord of macaques with poliovirus.[82] Such an infection causes neurodegeneration and produces inflammatory lesions within the target areas of the central nervous system. The study found that the concentration of quinolinic acid in poliovirus-infected spinal cord and CSF was substantially increased and exceeded levels reported to kill spinal cord neurons *in vitro*. As with other inflammatory neurological disorders, the production of quinolinic acid is believed to reflect local induction of IDO by cytokines in reactive

cells and inflammatory cell infiltrates within the CNS. All the poliovirus-infected macaques showed motor impairments, which were classified as either weakness of leg muscles, partial paralysis or complete paralysis. The magnitude of the increase in quinolinic acid concentration in the spinal cord was proportional to both the degree of motor impairment and the severity of lesions. This suggests that quinolinic acid may contribute to nerve cell death in the spinal cord and other poliovirus target areas.

1.3.2.5 Lyme disease

Neurological dysfunction frequently occurs in patients with Lyme disease, which is caused by infection with the bacterium *Borrelia burgdorferi*. The levels of quinolinic acid are raised significantly in the CSF of Lyme disease patients with CNS involvement, and those levels correlate strongly with the invasion of the CNS by leukocytes, cells involved in inflammatory and immune responses.[83] The presence of quinolinic acid may contribute to the neurological and cognitive deficits seen in many Lyme disease patients.

1.3.2.6 Traumatic CNS damage

It has been demonstrated that quinolinic acid levels are significantly elevated in the CSF following traumatic brain injury in humans.[84] Similarly, in animal studies, Blight *et al*. have demonstrated a contributory role for quinolinic acid in secondary neurological deficits following a compression injury of the spinal cord of guinea pigs.[85] It has been clearly established that an inflammatory reaction occurs in response to brain injury. A recent study by Mackay *et al*. showed that increases in inflammatory indicators were linked to increases in kynurenine pathway metabolites for patients with chronic brain injury and those patients with more inflammation showed greater activation of the pathway.[86] This is consistent with the view that activation of the kynurenine pathway is a consequence of inflammation. The results of this study showed that for brain-damaged patients the raised levels of inflammation, increased activation of the kynurenine pathway and oxidative stress continue many years after the original insult, possibly contributing to the continuing cerebral dysfunction in these patients.

1.4 Quinolinate phosphoribosyltransferase (QPRTase)

The enzyme quinolinate phosphoribosyltransferase (QPRTase) provides the only route for the metabolism of the neurotoxin quinolinic acid. QPRTase belongs to a family of ten phosphoribosyltransferase (PRTase) enzymes, an important group of enzymes which utilise 5-phosphoribosyl-1-pyrophosphate (PRPP) in substitution reactions. Each PRTase enzyme is highly specific for a nitrogenous, generally aromatic, base (Table 1.1). The PRTase enzymes are involved in *de novo* and salvage reactions of purine, pyridine and pyrimidine nucleotide biosynthesis,[87] as well as in histidine[88] and tryptophan[89] biosynthesis.

Enzyme	**Substrate**	**Enzyme**	**Substrate**
Adenine PRTase (EC 2.4.2.7)	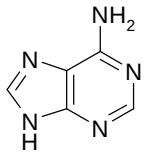	Nicotinamide PRTase (EC 2.4.2.12)	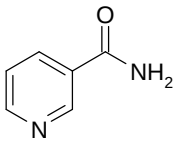
Anthranilate PRTase (EC 2.4.2.18)	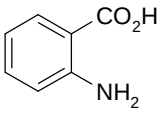	Nicotinate PRTase (EC 2.4.2.11)	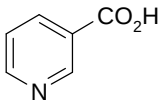
ATP PRTase (EC 2.4.2.17)	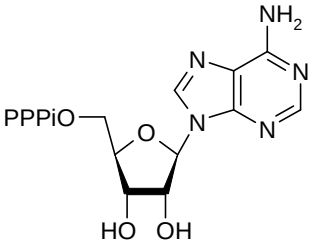	Orotate PRTase (EC 2.4.2.10)	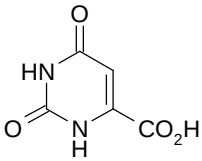
Glutamine-amido PRTase (EC 2.4.2.14)	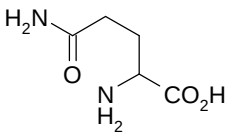	Quinolinate PRTase (EC 2.4.2.19)	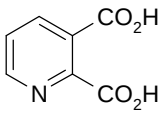
Hypoxanthine-guanine PRTase (EC 2.4.2.8)	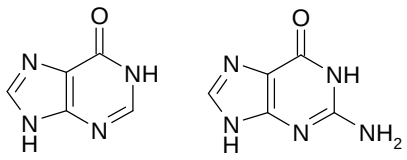	Uracil PRTase (EC 2.4.2.9)	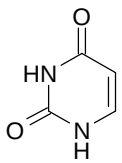

Table 1.1: *Phosphoribosyltransferase enzymes and their substrates.*

However, QPRTase is an unusual phosphoribosyltransferase enzyme in that it appears to catalyse a second reaction. QPRTase was first isolated and purified from rat liver acetone powder by Nakamura *et al.* in 1963.[90] The stoichiometry of the reaction was determined and found to involve the reaction of one molecule of quinolinic acid **10** with one molecule of PRPP **15** in the presence of Mg^{2+} to generate one molecule of nicotinic acid mononucleotide **11**, carbon dioxide and pyrophosphate. The reaction presumably involves the initial formation of quinolinic acid mononucleotide **16** which is subsequently decarboxylated to form the nicotinic acid mononucleotide product **11** (Scheme 1.3). No quinolinic acid mononucleotide **16** was detected. Thus a single enzyme, QPRTase, appeared to be responsible for two consecutive chemical reactions, phosphoribosyl transfer and decarboxylation.

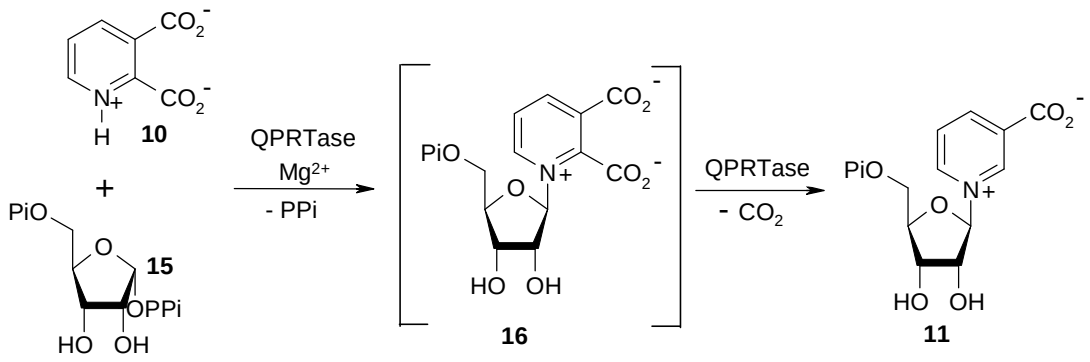

Scheme 1.3: *Metabolism of quinolinic acid.*

Since its initial discovery, QPRTase has been isolated and purified from many sources. QPRTase is widely distributed in micro-organisms, fungi and plants including *Pseudomonas fluorescens*, *E. coli*, *Neurospora crassa*, yeast, persimmon leaf, shiitake mushroom, *Pseudomonas riboflavin*,[91] castor bean endosperm,[92] *Mycobacterium tuberculosis*, *Salmonella typhimurium*[93] and the root and leaves of the tobacco plant *Nicotiniana tobaccum*.[94] In addition, hog liver[95,96] and kidney,[97,98] rat brain, liver and kidney[99] and human brain and liver[100] have all been identified as sources of QPRTase. In all systems investigated to date, both the phosphoribosyltransferase activity and the decarboxylation are catalysed by a single protein.

1.5 Mechanism of QPRTase

QPRTase is an intriguing enzyme which appears to catalyse two distinct chemical reactions; the Mg^{2+}-dependent transfer of a phosphoribosyl moiety from PRPP to the nitrogen of quinolinic acid and decarboxylation at the 2-position to give nicotinic acid mononucleotide. The mechanism of the QPRTase catalysed reaction is not well understood. The elucidation of the mechanism is important because of the unusual chemistry and neurological significance of the QPRTase reaction.

1.5.1 Kinetic mechanism of QPRTase

Essentially, there are two main possibilities for the kinetic mechanism of QPRTase. The first possibility is the ping-pong mechanism which is a two-step process whereby PRPP binds first and reaction takes place to eliminate pyrophosphate and leave a reactive phosphoribosyl intermediate at the active site. The quinolinic acid then binds and reacts with this intermediate to form the mononucleotide (Scheme 1.4).

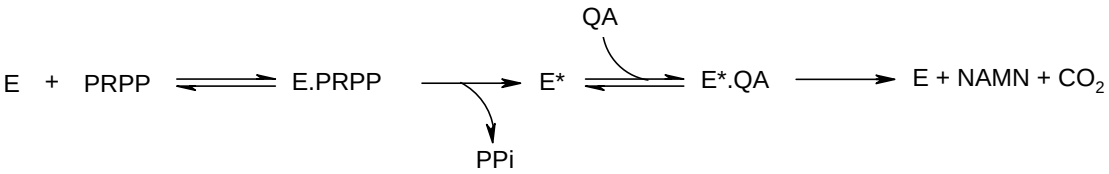

Scheme 1.4: *Two-step kinetic mechanism for QPRTase.*

Such a kinetic mechanism has been observed for three members of the PRTase family; adenine PRTase,[101] orotate PRTase[102,103] and uracil PRTase.[104] However, kinetic studies on QPRTase from *E. coli* by Calvo *et al.* have ruled out a ping-pong mechanism for QPRTase.[105] They reported that the true enzyme substrate was the magnesium complex of PRPP and showed that a double reciprocal plot of initial rate as a function of the concentration of quinolinic acid at various fixed concentration levels of $MgPRPP^{3-}$ resulted in an intersecting pattern. These results indicate a sequential mechanism in which both PRPP and quinolinic acid bind before pyrophosphate, carbon dioxide or nicotinic acid mononucleotide is released.

A sequential kinetic mechanism involves simultaneous binding of PRPP and quinolinic acid at the enzyme active site, giving a ternary complex, and the transfer reaction then takes place in one step. Three possible orders of substrate binding to form the ternary complex may be proposed (Scheme 1.5).

A. Ordered sequential mechanism with PRPP leading.

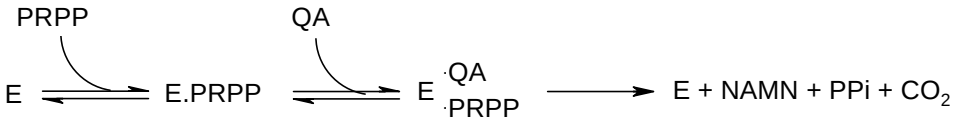

B. Ordered sequential mechanism with QA leading.

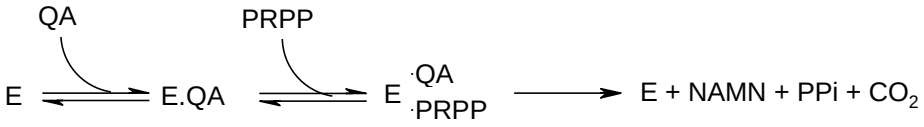

C. Random sequential mechanism.

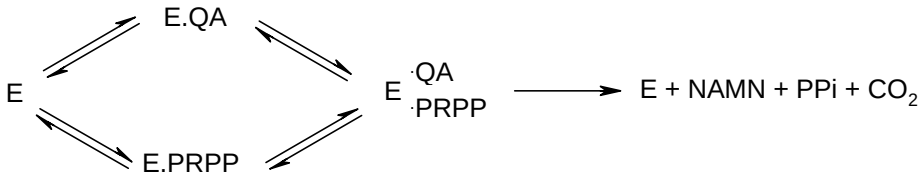

Scheme 1.5: *Sequential kinetic mechanism for QPRTase.*

Having deduced a sequential kinetic mechanism for QPRTase, Calvo *et al*. then carried out inhibition studies on QPRTase from *E. coli* to establish the order of substrate binding.[106] Inhibition by phthalic acid was found to be competitive with respect to quinolinic acid and uncompetitive with respect to PRPP. The uncompetitive pattern was explained by the formation of a dead-end complex between QPRTase·PRPP and phthalic acid. This requires that PRPP binds to QPRTase first followed by quinolinic acid to form a ternary complex (Scheme 1.5, A). Fructose-1,6-bisphosphate was found to be a competitive inhibitor with respect to PRPP and noncompetitive with respect to quinolinic acid. These inhibition patterns were interpreted in terms of the formation of a dead-end binary complex of QPRTase·fructose-1,6-bisphosphate, again supporting the ordered addition of PRPP followed by quinolinic acid (Scheme 1.5, A).

Recently, Grubmeyer *et al.* carried out a more detailed study on the kinetic mechanism of *Salmonella typhimurium* QPRTase.[107] Firstly, equilibrium gel filtration experiments were employed to assess substrate binding to the enzyme. The results showed that both quinolinic acid and PRPP can bind to free QPRTase, but did not indicate whether the resultant binary complexes are catalytically competent. This was determined by performing isotope trapping experiments, which measured the partitioning of binary and ternary enzyme-substrate complexes in the reaction pathway. Complexes of QPRTase with radiolabeled substrate were formed and then injected into a chase solution containing the second substrate, together with a large concentration of the non-radioactive form of the substrate whose behaviour was to be analysed. When QPRTase·[β-^{32}P]-PRPP complexes were injected into chase mixtures containing quinolinic acid and non-radioactive PRPP, no [β-^{32}P]-PRPP was trapped as pyrophosphate. However, [^{3}H]-quinolinic acid was trapped as [^{3}H]-nicotinic acid mononucleotide when the QPRTase·[^{3}H]-quinolinic acid complexes were injected into buffer containing PRPP and non-radioactive quinolinic acid. These results are inconsistent with an ordered sequential mechanism with PRPP as the leading substrate (Scheme 1.5, A) in which the QPRTase·[β-^{32}P]-PRPP complex should be trapped. They are consistent with an ordered sequential mechanism with quinolinic acid as the leading substrate (Scheme 1.5, B) or the random sequential mechanism (Scheme 1.5, C) if PRPP is able to dissociate rapidly from the QPRTase·PRPP·QA ternary complex. To differentiate between random and ordered sequential mechanisms, the partitioning of the QPRTase·PRPP·QA ternary complex was examined by steady-state isotope trapping experiments with [^{3}H]-quinolinic acid and [5-^{32}P]-PRPP. In these experiments, mixtures of QPRTase and radioactive substrates allowed to reach the steady state were injected into a quench solution or a trap solution containing a vast excess of the non-radioactive substrates. Trap samples were then allowed to react for ~10 additional turnover times, and then the reactions were quenched. The amount of radioactive substrate bound in the steady state and committed to catalysis was indicated by the difference between the trap and quench samples. The results clearly indicated that nearly all the [^{3}H]-quinolinic acid and about one-third of the [5-^{32}P]-PRPP in QPRTase·PRPP·QA ternary complexes partition forward to product formation. Therefore, in contrast to the kinetic mechanism previously determined by Calvo *et al.*, the conclusion from this study was that *Salmonella typhimurium*

QPRTase follows an ordered substrate binding mechanism in which binding of quinolinic acid precedes that of PRPP (Scheme 1.5, B).

To resolve some of the differences between their conclusions and those previously reported Grubmeyer *et al.* carried out selected steady-state kinetic measurements. It was found that PRPP behaves as an inhibitor at high concentrations. This is consistent with the observation that the QPRTase·PRPP complex is catalytically non-productive since QPRTase·PRPP complexes deplete the concentration of free QPRTase. Substrate inhibition was not observed by Calvo as the range of concentrations examined was too low to cause inhibition. Thus the major discrepancies result from the existence of a non-productive side branch on the reaction pathway, leading to the formation of a dead-end QPRTase·PRPP complex (Scheme 1.6).

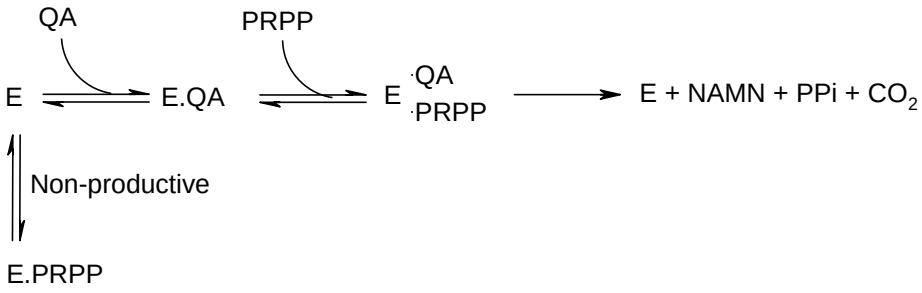

Scheme 1.6: *Kinetic mechanism for QPRTase proposed by Grubmeyer et al.*

This mechanism is consistent with the structural data for this enzyme, which show quinolinic acid is buried much deeper in the active site than PRPP, which is closer to the surface.[108] In addition, the binding of PRPP in the active site appears to block access for quinolinic acid.

1.5.2 Chemical mechanism of QPRTase – Phosphoribosyl transfer

Phosphoribosyltransferase enzymes catalyse the transfer of a phosphoribosyl moiety from PRPP to the nucleophilic nitrogen of purines, pyridines and pyrimidines. The coupling reaction requires a divalent metal ion, usually Mg^{2+}. In all cases the reaction proceeds with inversion of stereochemistry at the anomeric C-1 of PRPP,[109] although the chemical mechanism for this reaction has been disputed for many years. A direct S_N2-type displacement, shown in Scheme 1.7 for the QPRTase catalysed reaction, is possible given the inversion of the configuration at the anomeric carbon position of PRPP. This is compatible with the ternary complex kinetic mechanism where both reactants bind to the active site simultaneously.

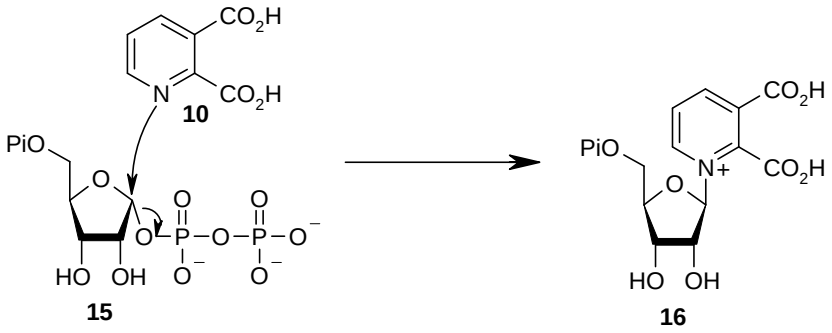

Scheme 1.7: *S_N2 mechanism.*

However, the pyrophosphate leaving group is among the most acidic found in biological glycosides and the furanose ring oxygen can readily stabilise positive charge.[110] Both of these factors will favour carbocation S_N1-type mechanisms over S_N2-type mechanisms. If it is the case that QPRTase catalysed phosphoribosyl transfer proceeds via a two step S_N1-type mechanism (Scheme 1.8), then the active site must shield the oxocarbonium ion **17** such that nucleophilic attack by quinolinic acid **10** can only occur from one face to give the observed stereochemistry.

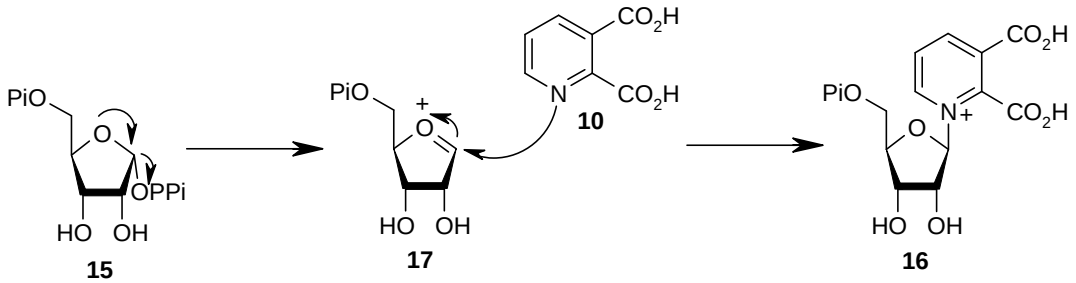

Scheme 1.8: *S_N1 mechanism.*

Determination of the kinetic isotope effects (KIE) for an enzyme catalysed reaction provides a powerful tool for the elucidation of the chemical mechanism for the reaction. Isotope effects are caused by the substitution of a lighter atom for a heavier one, for example replacing hydrogen with deuterium or tritium, or replacing ^{12}C with ^{13}C or ^{14}C. A KIE is the ratio of reaction rates for molecules containing the lighter and heavier atoms. A primary isotope effect is observed when the bond to the heavy atom is being cleaved or formed during the rate-determining step of the reaction. An α-secondary isotope effect occurs when the heavy atom is directly attached to the atom undergoing bond cleavage or formation, while a β-secondary isotope effect occurs when there is a further bond between the heavy atom and the site of reaction.

Secondary hydrogen isotope effects can often be used to obtain an insight into the changes in hybridisation at the site of substitution as a reaction proceeds from the ground state to the rate limiting transition state. One situation in which they have been frequently employed is in attempts to distinguish between S_N1 and S_N2 mechanisms. α-Secondary hydrogen isotope effects arise from changes in the zero-point energy of normal vibrations. The changes in zero-point energy are a result of changes in hybridisation of the carbon atom in going from the ground state to the transition state. Primarily, changes in C-H bending vibration are involved. In going from an sp^3 to an sp^2 hybridised carbon, the out-of-plane bending frequency decreases from 1350 cm^{-1} to 800 cm^{-1}. Therefore, if the transition state arising from an sp^3 ground state closely resembles the sp^2 structure, it will generally have less total zero-point vibrational energy compared to the ground state. Consequently, the activation energy for reaction of a molecule containing a heavier hydrogen isotope bonded to the reaction centre is larger, resulting in slower reaction for the substituted molecule. In contrast, S_N2 reactions generally exhibit much smaller α-secondary KIEs. This is because the S_N2 transition state has more nearly equal total zero-point vibrational energy compared to the sp^3 ground state, resulting in more nearly equal reaction rates for substituted and unsubstituted molecules. Thus determination of α-secondary hydrogen isotope effects is useful in differentiating between S_N1 and S_N2 mechanisms.

However, a problem may arise in enzyme catalysed reactions if the α-secondary hydrogen KIE is suppressed by steady state features of the enzymatic reaction, so that an S_N1 reaction could be mistaken for S_N2. This ambiguity often can be resolved by determination of the primary ^{14}C KIE for the same enzymatic reaction. For an S_N1 reaction, a small primary ^{14}C isotope effect would be expected because of the asymmetric transition state. However, the S_N2 transition state is more symmetrical and a larger primary ^{14}C isotope effect should be observed. Thus the primary and α-secondary kinetic isotope effects tend to be complementary. Carbocation-like transition states exhibit large α-secondary isotope effects and small primary effects, whereas S_N2-like transition states exhibit smaller α-secondary isotope effects and larger primary effects (Table 1.2).[111] Thus, in a reaction that demonstrates an α-secondary deuterium or tritium isotope effect near 1.00, observation of a significant primary ^{14}C isotope effect eliminates the possibility that a significant α-secondary effect was suppressed by steady state factors. This would unambiguously identify the catalytic mechanism as being S_N2-like. Thus a combination of primary and secondary isotope effects is required to fully elucidate a reaction mechanism.

Reaction type	**^{2}H α - Secondary KIE**	**^{14}C Primary KIE**
S_N1	1.15 – 1.25	1.00 – 1.08
S_N2	1.00 – 1.06	1.09 – 1.15

Table 1.2: *Comparison of kinetic isotope effects for S_N1 and S_N2 reactions.*

Such an approach has been used in studies on the chemical mechanism of the PRTase family.[112] In a study by Goitein *et. al*, PRPP was synthesised with ^{14}C at C-1 or with ^3H bonded to the C-1 or C-5 carbon atoms. Appropriate pairs of these compounds were then used to determine the primary ^{14}C and α-secondary ^3H kinetic isotope effects on three PRTase reactions (Table 1.3).

PRTase	^{3}H Secondary KIE	^{14}C Primary KIE
Hypoxanthine-guanine PRTase	1.30	1.05
Orotate PRTase	1.17	1.03
ATP PRTase	1.11	1.01

Table 1.3: *Comparison of the primary and secondary KIEs for three PRTase enzymes.*

By itself, the observation of a moderate α-secondary tritium KIE of 1.11, which corresponds to an α-secondary deuterium effect of 1.08, for the ATP PRTase reaction makes it probable that this enzyme utilises a carbocation mechanism. However, this KIE is near the upper limit of that expected for S_N2-like reactions (Table 1.2) and some uncertainty might exist as to the real mechanism were it not for the additional information available from the primary ^{14}C KIE. A primary ^{14}C KIE of 1.01 suggests that the ATP PRTase reaction utilises a carbocation intermediate. The hypoxanthine-guanine PRTase and orotate PRTase catalysed reactions exhibited large α-secondary tritium kinetic isotope effects, which clearly indicate that these enzymes also utilise carbocation S_N1-type mechanisms.

Furthermore, computational studies have been used to model the transition state structure for which the calculated KIE values match the measured KIE values for the orotate PRTase reaction.[113] The results strongly suggest that the reaction undergoes an S_N1-like mechanism, with a substantially developed oxocarbonium ion in the transition state.

Since all three of the PRTases examined utilised carbocation S_N1-type catalytic mechanisms, it seems likely on chemical grounds that this is the case for all PRTase reactions, including QPRTase, although this is as yet unconfirmed.

1.5.3 Chemical mechanism of QPRTase – Decarboxylation

QPRTase is an unusual PRTase enzyme in that it appears to catalyse a second reaction, decarboxylation of the quinolinic acid mononucleotide **16** to form the corresponding nicotinic acid mononucleotide **11**. This decarboxylation reaction is considered to have an analogous mechanism to that observed for the decarboxylation of pyridine carboxylic acids in chemical studies. The mechanism proposed by Hammick *et al.* involves loss of carbon dioxide to form a nitrogen ylide, which is then protonated to give the product (Scheme 1.9).[114] In the model studies, the intermediate ylide was trapped with a suitable electrophile, such as acetone or benzaldehyde (Scheme 1.9).

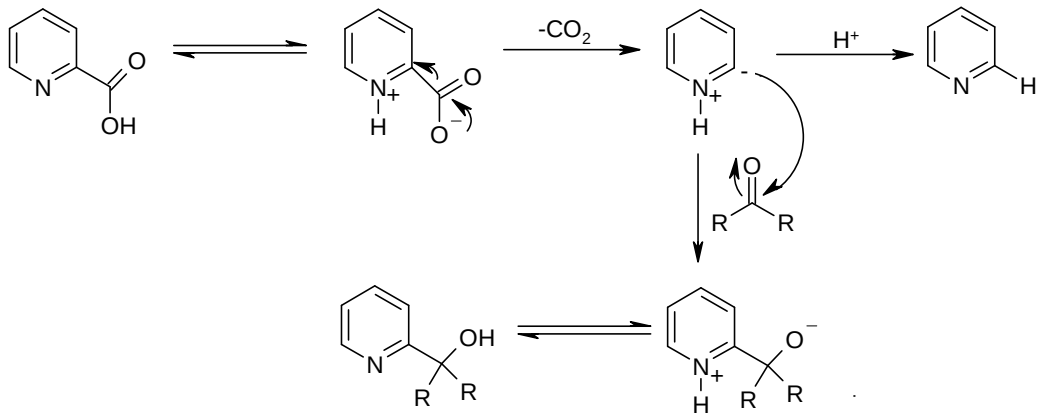

Scheme 1.9: *Mechanism for the decarboxylation of pyridine carboxylic acids.*

An analogous mechanism can be envisaged for the decarboxylation of quinolinic acid mononucleotide **16**, proceeding via the nitrogen ylide **18** (Scheme 1.10).

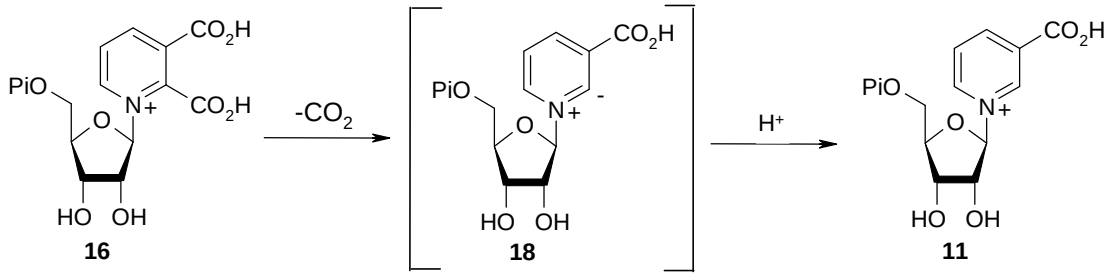

Scheme 1.10: *Decarboxylation of quinolinic acid mononucleotide.*

However, enzymatic involvement in the decarboxylation step is yet to be conclusively proven. As similar reactions were observed to occur spontaneously, it was suggested that QPRTase played no part in the decarboxylation step and it occurred after the mononucleotide had been released from the active site. In order to test this theory, experiments were conducted involving the non-enzymatic decarboxylation of pyridine carboxylic acids.[115] Quinolinic acid was the most rapidly decarboxylated of all the pyridine carboxylic acids studied, but the reaction was still very slow and required harsh conditions. Quinolinic acid was shown to decarboxylate in aqueous hydrochloric acid (pH 1) at 95 °C, with a half life of *ca.* 3 days. Clearly the harsh conditions whereby decarboxylation was observed are quite remote from the physiological conditions (pH 7 and 37 °C) under which the QPRTase catalysed reaction takes place. Some enzymatic involvement would therefore seem to be necessary. Ideally, examination of the non-enzymatic decarboxylation of quinolinic acid mononucleotide would solve this problem. However, to date this has not been possible since quinolinic acid mononucleotide has proved to be a very difficult compound to synthesise.

Orotidine 5'-monophosphate decarboxylase (OMP decarboxylase, EC 4.1.1.23) carries out a very similar decarboxylation reaction to QPRTase and thus information on the mechanism of this enzyme can be used as a guide in evaluating the mechanism of QPRTase. OMP decarboxylase catalyses the decarboxylation of orotidine 5'-monophosphate (OMP) **19** to form uridine 5'-monophosphate **20** in the final step of *de novo* pyrimidine nucleotide biosynthesis. The previous step in the biosynthesis involves the transfer of a phosphoribosyl group to orotate **21** to form orotidine 5'-monophosphate **19**. This reaction is catalysed by orotate phosphoribosyltransferase (OPRTase, EC 2.4.2.10). Therefore the two enzymes (OPRTase and OMP decarboxylase) catalyse the transfer of a phosphoribosyl group to the nitrogen of a heterocycle followed by decarboxylation (Scheme 1.11), the same two reactions catalysed by the single QPRTase protein.

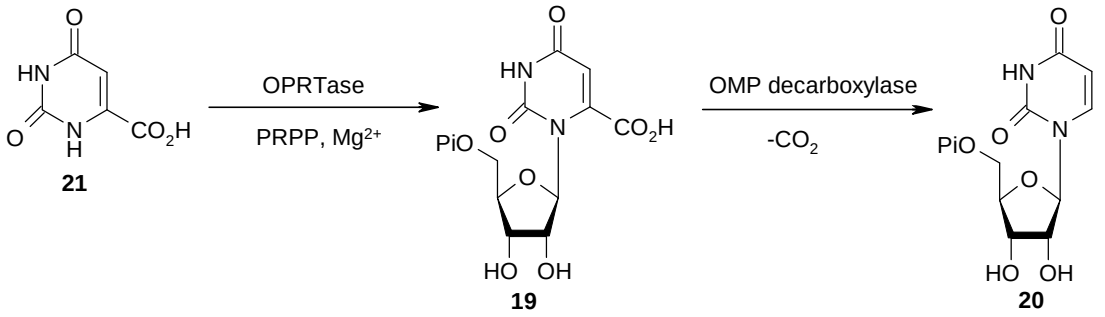

Scheme 1.11: *Conversion of orotate to uridine 5'-monophosphate.*

A mechanism involving a nitrogen ylide intermediate has been proposed for OMP decarboxylase.[116] On the basis of the observation of rates of non-enzymatic decarboxylation of various OMP analogues and other heterocyclic acids resembling OMP, Beak and Siegel suggested that the active site of OMP decarboxylase might function to catalyse the formation of a zwitterionic intermediate **22**, followed by decarboxylation to a stabilised nitrogen ylide **23** (Scheme 1.12). Protonation of the ylide would then give the product **20**.

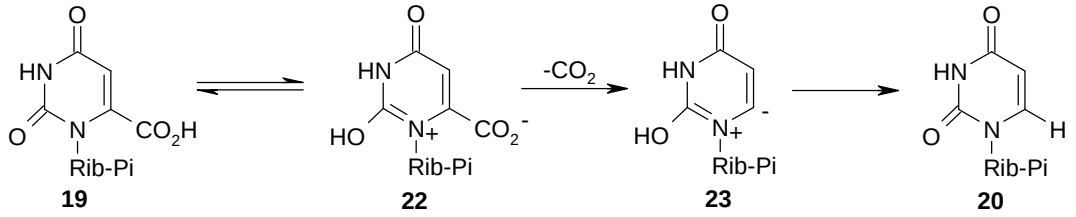

Scheme 1.12: *Ylide mechanism for OMP decarboxylase.*

This ylide mechanism is supported by results from inhibition studies.[117] Levine *et al.* observed that 1-(phosphoribosyl)barbituric acid (BMP) **24** was a very strong inhibitor of OMP decarboxylase and suggested that this compound might act as a transition state analogue because of its resemblance to the nitrogen ylide intermediate that Beak and Siegel had proposed.

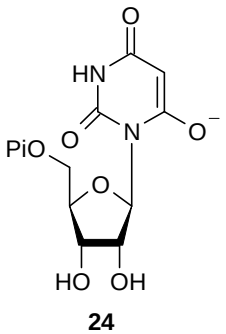

However, on the basis of model studies, Silverman and Groziak proposed an alternative mechanism for OMP decarboxylase.[118] They proposed a covalent catalytic mechanism involving addition of an enzymic nucleophile across the C5-C6 double bond of the pyrimidine ring system (Scheme 1.13, A) followed by the concerted elimination of CO_2 and the enzymic nucleophile to give the product (Scheme 1.13, C).

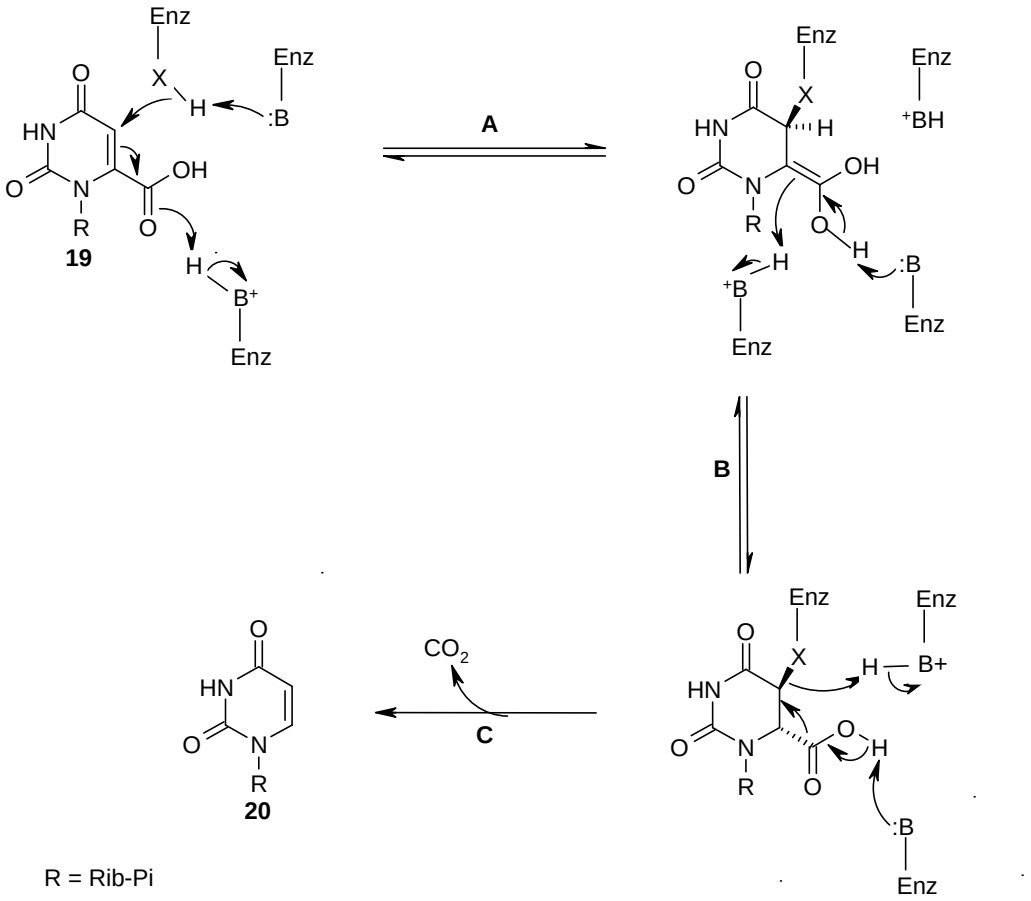

Scheme 1.13: *Covalent catalytic mechanism for OMP decarboxylase.*

In an effort to distinguish between these two possible mechanisms, Acheson *et al.* synthesised the inhibitor BMP **24** enriched in ^{13}C at C-5 of the pyrimidine ring and examined its interaction with OMP decarboxylase by NMR.[119] Formation of a covalently bound adduct with either substrate or inhibitor would result in a change in geometry at C-5 from trigonal (sp^2) to tetrahedral (sp^3), and a significant upfield shift of the ^{13}C NMR C-5 resonance would be expected. In the nitrogen ylide mechanism, however, C-5 remains trigonal throughout the catalytic sequence. When OMP decarboxylase was titrated with the ^{13}C enriched BMP, a new resonance at 78.5 ppm was observed. The signal was situated only 0.6 ppm downfield from the resonance of

the free inhibitor and so it seems unlikely that covalent attack by an enzymic nucleophile occurs at C-5 of the inhibitor. Consistent with this conclusion, the UV difference spectrum of the enzyme-inhibitor complex was virtually identical with the spectrum of the inhibitor-free solution.

As an additional test for a change in geometry at C-5, Acheson *et al.* synthesised the substrate OMP with deuterium substituted for hydrogen at C-5 and determined the effect of this substitution on the rate constants for enzymatic decarboxylation. No significant secondary hydrogen isotope effect was observed. Similarly, Smiley *et al.* measured ^{13}C kinetic isotope effects for the enzymatic reaction.[120] The observation of large ^{13}C isotope effects for OMP decarboxylase suggests that no covalent chemical step is occurring prior to decarboxylation. Only an unusually fast covalent step could allow the decarboxylation step to be fully rate-limiting. Therefore, these experiments do not support the existence of covalently bound intermediates on the reaction pathway catalysed by OMP decarboxylase. The results appear, instead, to be consistent with a mechanism involving a nitrogen ylide intermediate.

More recently, Harris *et al.* determined the structure of OMP decarboxylase from *E. coli* co-crystallised with the inhibitor BMP and used their structural results to evaluate the different catalytic mechanisms.[121] The structural studies strongly supported the ylide-type mechanism and identification of the active site enabled the elucidation of the residues involved in the mechanism (Scheme 1.14). Site-directed mutagenesis studies on yeast OMP decarboxylase have confirmed Lys73 is an essential catalytic residue.[122]

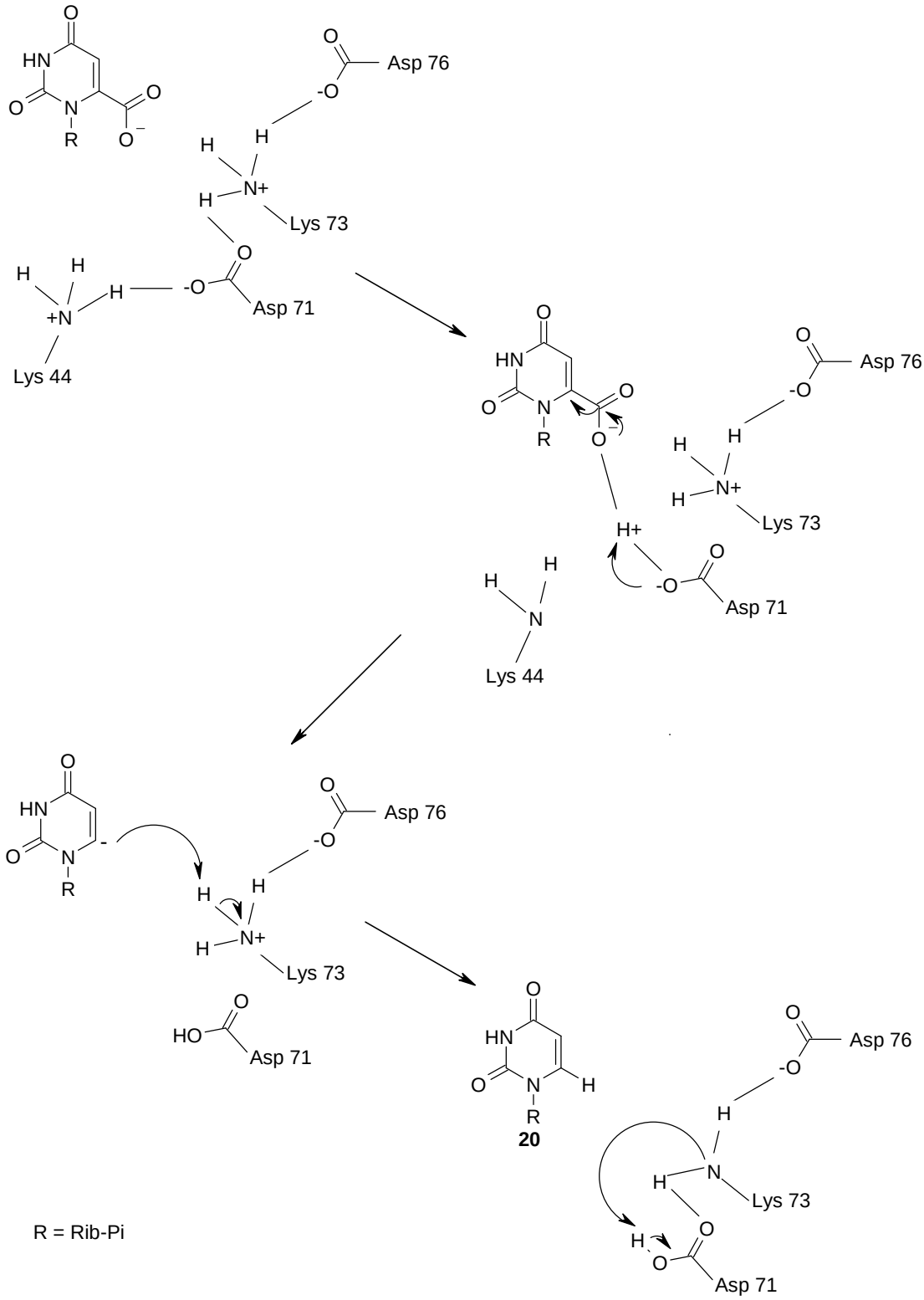

Scheme 1.14: *Ylide mechanism for OMP decarboxylase.*

The decarboxylative step catalysed by QPRTase is similar in many respects to that catalysed by OMP decarboxylase and therefore it is possible that QPRTase catalyses the decarboxylation of quinolinic acid mononucleotide in an analogous manner.

1.6 Inhibition of QPRTase

Investigation into the inhibition of an enzyme system is an extremely important part of understanding the enzyme. The use of inhibitors is vital, not just to prevent the enzyme from functioning, but also to examine possible mechanisms for the catalysed reaction. Several inhibition studies have been reported for QPRTase.

1.6.1 Quinolinic acid analogues

Studies involving the inhibition of QPRTase by quinolinic acid analogues may provide useful mechanistic information. Phthalic acid **25** is a potent competitive inhibitor of QPRTase, which suggests that the ring nitrogen is not essential for binding at the active site.[99,106,107,123] Picolinic acid **26** is also a good competitive inhibitor. In contrast, nicotinic acid **27** is not an inhibitor, which implies that the carboxylic acid function at the 2-position is absolutely necessary for binding. The methyl esters of phthalic acid and picolinic acid also do not inhibit, implying that the free acid is required at the 2-position for binding at the active site.[92]

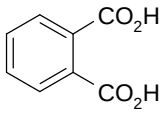

25

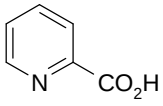

26

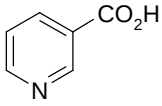

27

In order to gain more information on the mechanism, a series of 2-substituted nicotinic acids and 2-substituted 3-nitropyridines were investigated as inhibitors of QPRTase from ATCC strain 23269 by Calvo *et al.*.[105] The 2-hydroxy and 2-thiopyridines used in the study were all shown to inhibit QPRTase, with the 2-thio-3-nitropyridine derivative **31** showing the greatest inhibitory effect (Table 1.4). The type of inhibition was determined for this compound and was found to be competitive with respect to quinolinic acid.

The 2-hydroxypyridines exist mostly in a tautomeric form where the oxygen is present as a carbonyl and the ring is really an unsaturated lactam (Scheme 1.15). The same is true for the 2-thiol derivatives. It was estimated based on NMR studies that only about 4% of compound **28** is present as the hydroxypyridine. The corresponding 2-thiopyridine **29** was found to have slightly larger amounts of the thiol tautomer, 8% based on NMR studies. It was shown that the general effect of the nitro substituent at the 3-position of the pyridine ring was to increase the amount of the hydroxyl or thiol form relative to the lactam or thiolactam (Table 1.4).

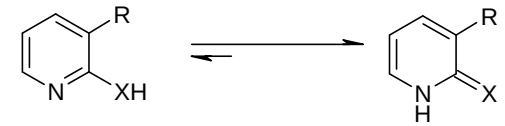

R = CO_2H, NO_2
X = O, S

Scheme 1.15: *Tautomerisation of 2-hydroxy and 2-thiopyridines.*

Compound	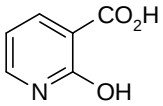 **28**	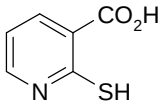 **29**	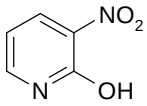 **30**	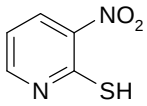 **31**
% Inhibition	0 (pH 7) 6.3 (pH 9)	8.3 (pH 7) 20 (pH 9)	16 (pH 7) 23 (pH 9)	95 (pH 7)
pKa	Not determined	Not determined	10.3	6.9
Summary	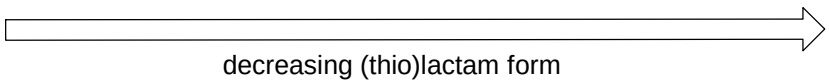 decreasing (thio)lactam form decreasing pKa increasing inhibitory effect			

Table 1.4: *Inhibitors of QPRTase.*

Due to the strong electron withdrawing ability of the nitro group, the pK_a of a hydroxyl or thiol at the 2-position would be expected to be lower than in the case of the pyridine with a carboxylate at the 3-position (Table 1.4). Based upon this argument, it can be concluded that the pyridines with a 3-nitro substituent will exist to a greater extent in the hydroxyl or thiol form relative to the lactam or thiolactam, and the hydroxyls and thiols at the 2-position will be more acidic. The fact that the compound with the lowest pK_a, **31**, was also the best inhibitor implies that negative charge on the 2-substituent is an important contributor to tight binding to the enzyme. Furthermore, the percentage inhibition was found to be pH dependent, a result consistent with a requirement for a negative charge at C-2 of the pyridine ring (Table 1.4).

This evidence supports the postulated decarboxylation mechanism. It is envisaged that these inhibitors mimic the intermediate ylide **18** that is formed immediately following decarboxylation.

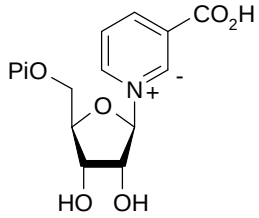

18

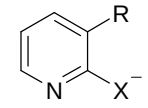

R = CO_2H, NO_2
X = O, S

1.6.2 PRPP analogues

1-Phosphorothioate analogues of PRPP, in which a non-bridging oxygen atom is replaced with sulfur, have been prepared.[124] Such analogues of PRPP have direct application as mechanistic probes, and in particular probes of the structure of the Mg^{2+}-PRPP complex at the active site of QPRTase. The analogues prepared were 5-phosphoribosyl 1-*O*-(2-thiodiphosphate) (PRPPβS) and the Sp and Rp diastereomers of 5-phosphoribosyl 1-*O*-(1-thiodiphosphate) (PRPPαS). In a study by Kunjara *et al.*, these compounds were tested as substrates for QPRTase from hog kidney.[125] The study showed that with Mg^{2+} as the divalent cation, the order of effectiveness as substrates was PRPP > PRPPβS > PRPPαS. The Sp diastereomer of

PRPPαS was a better substrate than the Rp diastereomer with Mg^{2+}, whereas with Cd^{2+} as the activating metal ion the Rp diastereomer was better. The apparent reversal of enzyme stereospecificity with the change of the divalent cation suggests that the metal ion remains ligated to the 1-phosphate moiety in the rate determining step. This rationale is based on the preferential ligation of hard metal ions (Mg^{2+}) to oxygen, and of soft metal ions (Cd^{2+}) to sulfur (Figure 1.2).

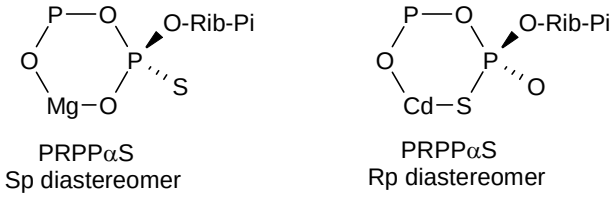

Figure 1.2: *Simplified structures of the metal ion – PRPP analogue complexes.*

Although these compounds were tested as substrates for QPRTase, the fact they bound to the enzyme implies they could also be inhibitors of the reaction.

Fructose-1,6-bisphosphate **32** is one of the few analogues of PRPP **15** to be examined as an inhibitor of QPRTase. Kinetic studies by Calvo *et al.* showed that this compound was a competitive inhibitor with respect to PRPP and a noncompetitive inhibitor with respect to quinolinic acid.[106]

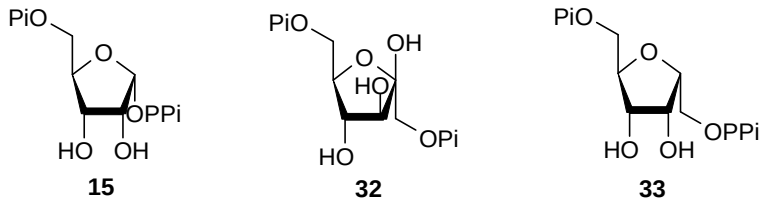

5-Phosphoribosyl-1-(β-methylene)pyrophosphate (PRPCP) **33** is a stable analogue of PRPP **15**. PRPCP has been employed in crystallisation studies and has proved useful in probing binding interactions at the active site of QPRTase (section 1.7).[108] However, this compound has not yet been examined as an inhibitor in kinetic studies.

1.6.3 Other applications of QPRTase inhibitors

As discussed in sections 1.6.1 and 1.6.2, inhibitors of QPRTase are useful mechanistic tools for the elucidation of the chemical mechanism of QPRTase. Inhibitors of QPRTase may also allow the neurological effects of quinolinic acid to be investigated by blocking the active site of the enzyme, inhibiting its action and therefore artificially raising quinolinic acid levels. The biological effect of this increase could be investigated and compared with neurological disorders. Thus inhibitors of QPRTase may also be important as biological tools.

In addition to their use as tools for mechanistic and biological studies, inhibitors of QPRTase may also possess antimycobacterial properties.[108] *Mycobacterium tuberculosis* is the single most deadly human pathogen and is responsible for nearly three million deaths every year. Recent elucidation of the mode of action of isoniazid, a frontline antimycobacterial drug, suggests that nicotinamide adenine dinucleotide (NAD) metabolism is extremely critical for this microorganism. QPRTase is a key enzyme in the *de novo* biosynthesis of NAD, which is an essential coenzyme that functions as a hydrogen transfer agent. In addition to the *de novo* synthesis of NAD, salvage pathways (pyridine nucleotide cycles) exist that allow recycling of NAD, usually via degradation of NAD **34** in several steps to nicotinic acid **27**, followed by conversion of nicotinic acid to nicotinic acid mononucleotide **11** by nicotinate phosphoribosyltransferase (NPRTase) (Scheme 1.16).

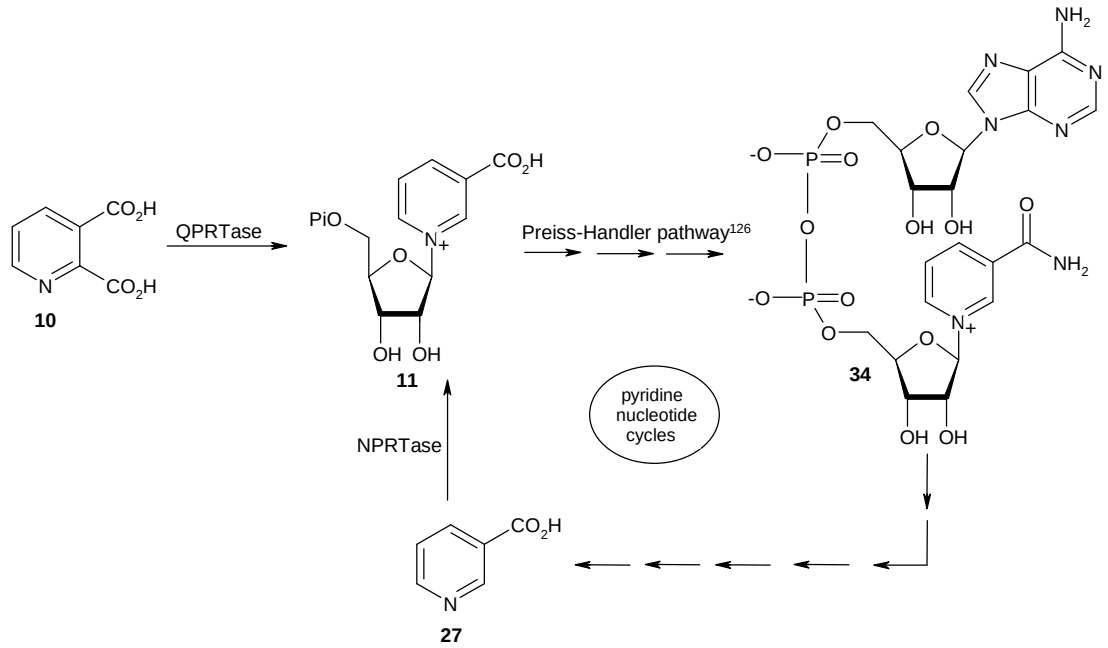

Scheme 1.16: *NAD metabolism.*

Despite the similarity between their enzymatic reactions, QPRTase and NPRTase exhibit exclusive specificity for their respective substrates.[109] In *Mycobacterium tuberculosis*, unlike most organisms, the salvage pathway appears to be disrupted. This is proposed to be a consequence of the lack of detectable NPRTase activity and results in secretion of nicotinic acid **27**, as NAD **34** cannot be recycled, although the NAD degradation enzymes remain very active.[127] Thus *Mycobacterium tuberculosis* depends solely on the *de novo* pathway to meet its NAD demand, making this organism extremely vulnerable to drugs targeted against QPRTase. Subtle differences between the active sites of the mycobacterial and human enzymes – in the quinolinic acid binding site (Leu170 → Met) or PRPP binding site (Arg48 → Lys, Ala268 → Ser, Ala271 → Met and His274 → Gln) - could be exploited in the design of drugs specific for mycobacterium QPRTase.[108]

Similarly, fungi rely entirely on the *de novo* pathway for their NAD requirements. Therefore, compounds which block this biosynthetic pathway, including analogues of quinolinic acid as inhibitors of QPRTase, could act as anti-fungal agents.[128]

1.7 Crystal structure of QPRTase

The availability of the crystal structures of QPRTase with and without its substrates and products would provide a detailed perspective for the active site interactions in pre-catalytic, catalytic and post-catalytic stages of the enzyme. Hence useful information could be obtained concerning the mechanism of the QPRTase reaction. In addition, knowledge of the design of the QPRTase active site and of any substrate induced conformational changes could be exploited in designing novel inhibitors for the enzyme.

1.7.1 QPRTase apoenzyme structure

Structural studies have been carried out on bacterial QPRTase from both *Mycobacterium tuberculosis*[108] and *Salmonella typhimurium*.[129] The structure of the apoenzyme from *Mycobacterium tuberculosis* has been solved at high-resolution (2.4 Å). *Mycobacterium tuberculosis* QPRTase is a homodimer with each 29 kDa subunit consisting of 285 amino acids. Each subunit was found to be comprised of eleven β-strands and ten α-helices arranged into two structural domains. The N-terminal open-face β-sandwich domain is composed of a four stranded anti-parallel β-sheet stacked against three α-helices and the C-terminal α/β-barrel domain is composed of seven β-strands and six α-helices. The connection between the two domains is through the longest α-helix.

Similarly, QPRTase from *Salmonella typhimurium* is a dimer of identical 32 kDa subunits. The X-ray crystal structure of this enzyme has also been solved at high resolution and revealed an analogous two-domain structure for each subunit.[129]

The QPRTase α/β-barrel is unlike any other α/β-barrel structure reported to date. A conventional α/β-barrel involves eight β-strands and eight α-helices arranged in a regular $(\beta\alpha)_8$ topology. The seven stranded α/β-barrel observed in QPRTase differs significantly, following an $\alpha\beta\alpha\beta(\beta\alpha)_4\beta$ topology.

Furthermore, QPRTase shows a completely novel fold for a PRTase enzyme. QPRTase belongs to a family of ten enzymes that catalyse phosphoribosyltransfer reactions. The crystal structures of several PRTase enzymes are known and include the structures of orotate PRTase,[130] hypoxanthine-guanine PRTase,[131] glutamine-amido PRTase[132] and uracil PRTase.[133] All these enzymes possess a common fold composed of a central parallel five-stranded β-sheet surrounded by four α-helices. These PRTase enzymes contain a conserved motif of thirteen residues that serves to bind the ribose-phosphate moiety of the substrate PRPP and is found at the centre of the PRTase fold. The phosphoribosyltransferase enzymes can therefore be divided into two structurally distinct groups, type I, the most commonly observed PRTase fold, and type II, of which QPRTase is the only known example. This observation shows that members of the PRTase group of enzymes have evolved convergently to perform similar enzymatic functions utilising different protein architectures.

The QPRTase dimer is formed by a twofold symmetry that places the N-terminal domain of one subunit next to the C-terminal domain of the other (Figure 1.3). The two active sites are located at the interfaces between the α/β-barrel of one subunit and the β-sandwich of the second subunit and are composed of residues from both subunits. A dimeric structure is therefore essential for activity of the enzyme.

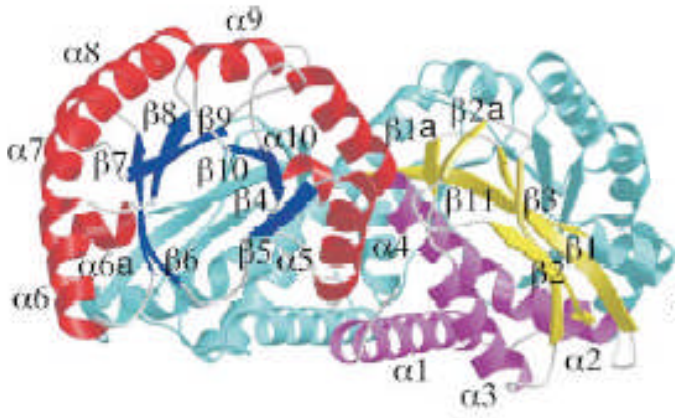

Figure 1.3: *Mycobacterium tuberculosis QPRTase dimer. For one of the monomers the α/β-barrel is shown with helices in red and strands in blue, and the open face of the β-sandwich is shown with purple helices and yellow strands; the second monomer is shown in cyan.*[108]

The asymmetric unit of the crystal of *Mycobacterium tuberculosis* QPRTase was found to contain three dimers, which are related by a threefold noncrystallographic symmetry (Figure 1.4). The interface between dimers is largely solvent accessible and hydrated in character. Stacking interactions between the side chains of Arg48 and Trp227 were identified as the major protein – protein contact at this interface.

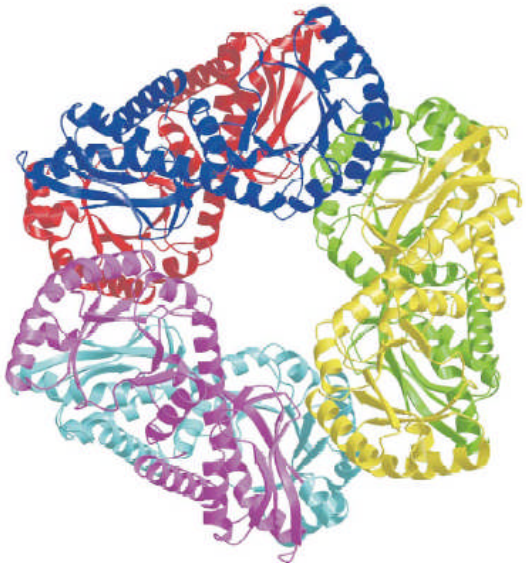

Figure 1.4: *Mycobacterium tuberculosis QPRTase hexamer. Each subunit is shown in a different colour.*[108]

1.7.2 QPRTase complex structures

In addition to the *Mycobacterium tuberculosis* QPRTase apoenzyme structure, the structures of three binary complexes (with substrate quinolinic acid **10**, product nicotinic acid mononucleotide **11** and inhibitor phthalic acid **25**) and a ternary complex (with bound phthalic acid **25** and 5-phosphoribosyl-1-(β-methylene)pyrophosphate (PRPCP) **33**) have been determined.[108]

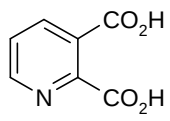

10

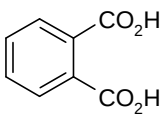

25

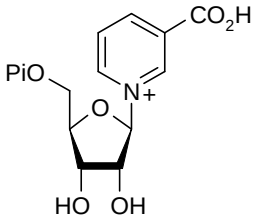

11

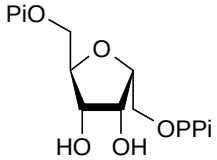

33

The quinolinic acid binding site of *Mycobacterium tuberculosis* QPRTase is a deep pocket located at the centre of the α/β-barrel with a highly positive electrostatic surface. This surface is composed of three arginine residues (Arg139, Arg162 and Arg105'), two lysine residues (Lys140 and Lys172) and one histidine residue (His161). These residues are highly conserved among QPRTase enzymes and adopt similar conformations in the structures of *Mycobacterium tuberculosis* QPRTase and *Salmonella typhimurium* QPRTase.

The orientations of quinolinic acid and phthalic acid are essentially identical in their respective complexes with QPRTase. Both of the carboxylate groups are involved in hydrogen bonding interactions with the active site residues (Figure 1.5). The C-3 carboxylate group forms hydrogen bonds with the sidechain atoms Nε and Nη of Arg162 and Nε of Arg139, whereas the C-2 carboxylate group is within hydrogen bonding distance of the mainchain NH of Arg139, the sidechain of Arg105' and the sidechain Nηof Lys172. In addition, the sidechains of the residues Thr138, His161, Leu170 and Leu220 are within van der Waals distance of the substrate.

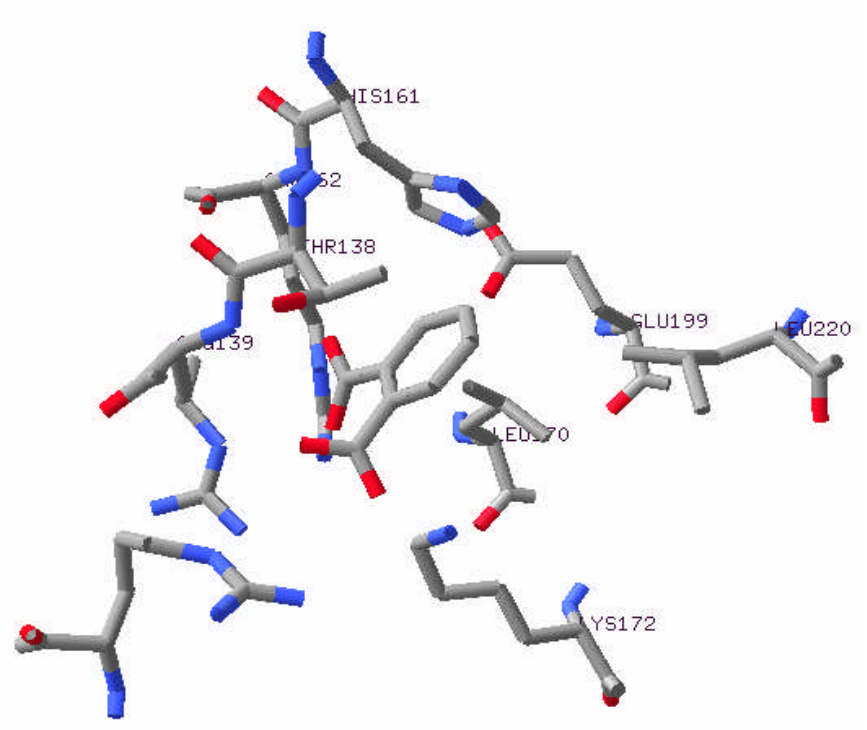

Figure 1.5: *Active site of Mycobacterium tuberculosis QPRTase with phthalic acid bound.*

By comparing the structures of the QPRTase apoenzyme and the QPRTase-quinolinic acid complex, it was noticed that the binding of quinolinic acid is accompanied by substantial structural changes in the active site of *Mycobacterium tuberculosis* QPRTase. These include reorientation of the sidechains of a number of binding site residues such as His161, Leu170, Lys172 and Leu220. In particular, the conformational flexibility in the sidechain of residue Lys172, which orients in an altogether different fashion in the two structures, results in significant structural changes. In the structure of the apoenzyme, the sidechain of Lys172 hydrogen bonds with the sidechains of residues Asn174 and Glu104', whereas in the structure with quinolinic acid bound it orients towards the C-2 carboxylate. This results in a 5 Å movement of the Lys172 sidechain Nε atom and a 2 Å displacement of its Cα atom.

The enzyme conformational changes are retained in the ternary QPRTase-phthalic acid-PRPCP complex. Use of phthalic acid and PRPCP, stable analogues of quinolinic acid and PRPP, respectively, enables examination of the binding of the ternary complex in the active site without turnover. Phthalic acid binds in a conformation identical to that seen in its binary complex with QPRTase. A divalent cation is required for PRPP binding as well as catalysis, and the structural studies showed that one divalent metal ion is coordinated by two ribose hydroxyl groups, two pyrophosphate oxygen atoms and two water molecules, while another divalent metal ion is coordinated by two PRPCP oxygen atoms and four water molecules. The 5-phosphate interacts with the backbone amide of Gly270, the backbone carbonyl of Gly249 and the sidechains of residues Lys140 and His274. The hydroxyl groups of the ribose ring form hydrogen bonds with the sidechains of Glu201, Asp222 and Lys172. The pyrophosphate group of PRPCP is within hydrogen bonding distance of Arg105', Arg173, Lys140, Asp222 and Asp173.

The alteration in the conformation of Lys172 on quinolinic acid binding has several implications for the specificity and mechanism of the QPRTase reaction. The interaction of Lys172 with the negatively charged C-2 substituent appears to determine the specificity of QPRTase for quinolinic acid. In terms of mechanism, kinetic data[107] for *Salmonella typhimurium* QPRTase implied an ordered sequential mechanism with quinolinic acid binding prior to PRPP and this is consistent with the

structural data, which show the quinolinic acid bound more deeply in the active site.[129] Moreover, comparison of the various complex structures suggests that the conformational changes in the active site brought about by the binding of quinolinic acid appear to facilitate PRPP binding and the subsequent reaction.[108]

The structure of *Mycobacterium tuberculosis* QPRTase with the product nicotinic acid mononucleotide (NAMN) bound in the active site has also been determined. In this binary complex, NAMN was found to adopt a conformation such that the nicotinate ring occupies a very similar position to quinolinic acid in the QPRTase-quinolinic acid complex (Figure 1.6). The C-3 carboxylate provides the only hydrogen bonding interactions for the nicotinate ring with the protein (to the side chains of residues His161 and Arg162). The lack of a C-2 carboxylate and a planar geometry at the positively charged nitrogen atom results in the movement of the pyridine ring by 1 Å relative to the QPRTase-quinolinic acid complex. The ribose hydroxyl group oxygen atoms of NAMN are within hydrogen bonding distance of Asp222, Glu201, Gly249, Ser248 and Gly270. Similarly, the oxygen atoms of the phosphate group hydrogen bond with residues Gly270, Ala271, His274 and Lys140.

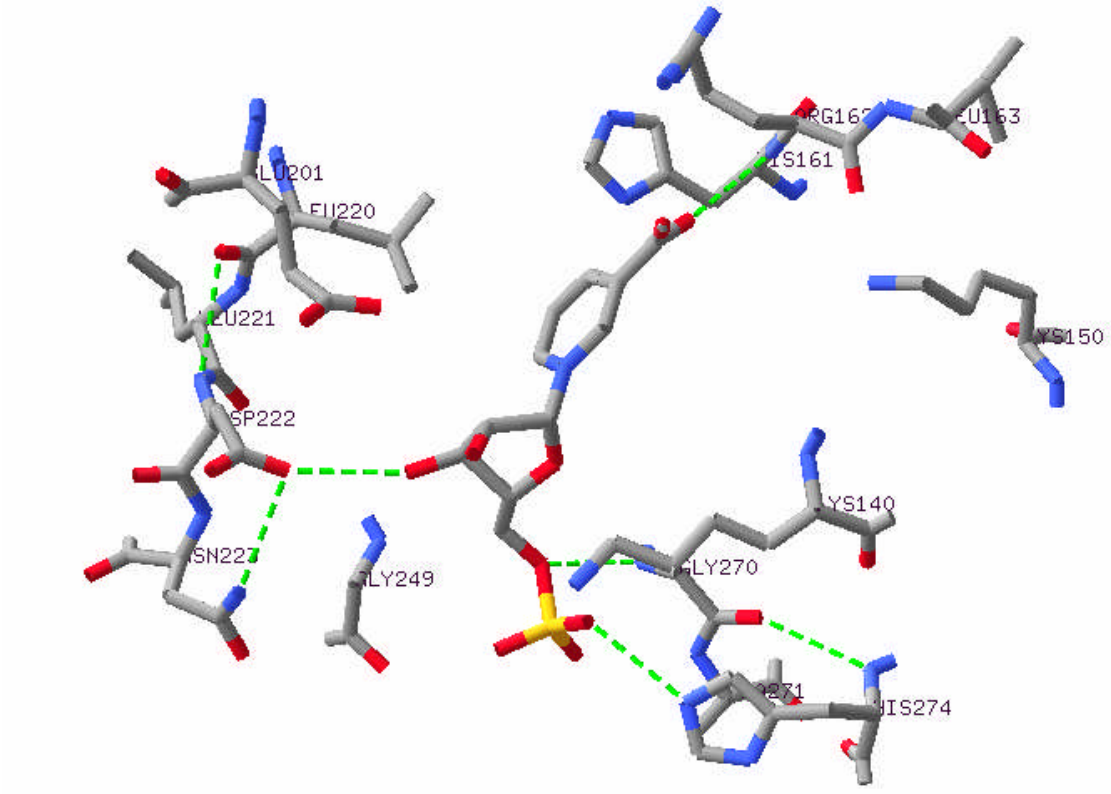

Figure 1.6: *Active site of Mycobacterium tuberculosis QPRTase with NAMN bound.*

By comparing the structures with PRPCP and NAMN in the QPRTase binding site, it was noticed that the two complexes differ substantially with respect to the position of the common phosphoribosyl moiety. In both cases the 5-phosphate is located in the phosphate binding site and forms an equal number of hydrogen bonds with the active site residues. At the ribose group, however, there is a large difference in position between the substrate and the product. In comparison to NAMN, the ribose ring of PRPCP is displaced across the binding cavity by a rotation of almost 90°.

The overall conformation of the active site in the QPRTase-NAMN complex is more similar to that of the apoenzyme and the conformational changes observed in the QPRTase-quinolinic acid complex are absent in the QPRTase-NAMN complex. It would appear, therefore, that QPRTase has two conformers: a relaxed conformer, observed in the structures of the apoenzyme and its complex with the product nicotinic acid mononucleotide, and an active conformer, seen in its complex with substrate quinolinic acid or inhibitor phthalic acid and in a non-productive ternary complex with phthalic acid and PRPCP.

1.8 References

1. J.C. Peters, *Kynurenine and Serotonin Pathways*, Ed. R. Schwarcz, Plenum, New York, 1991, 345-358.
2. D.A. Bender, *Quinolinic Acid and the Kynurenines*, Ed. T.W. Stone, CRC Press, Boca Raton, 1988, 3-38.
3. G.W. Beadle, H.K. Mitchell and J.F. Nyc, *Proc. Natl. Acad. Sci. USA*, 1947, **33**, 155-158.
4. W.E Knox, Methods in Enzymology, Vol. II, Eds. S.P. Colowick and N.O. Kaplan, Academic Press, New York, 1955, 242-254.
5. T.W. Stone and L.G. Darlington, *Nat. Rev. Drug Disc.*, 2002, **1**, 609-620.
6. J.K. Yeh and R.R. Brown, *J. Nutr.*, 1977, **107**, 261-271.
7. G. Curzon, *Acta Neurologica*, 1979, 121-131.
8. A. Freese, K.J Swartz and M.J. During, *Ann. Intern. Med.*, 1988, **108**, 312-313.
9. N.P. Botting, *Chem. Soc. Rev.*, 1995, **24**, 401-412.
10. T. W. Stone and M.N. Perkins, *Eur. J. Pharmacol.*, 1981, **72**, 411-412.
11. R. Schwarcz, W.O. Whetsell and R.M Mangano, *Science*, 1983, **219**, 316-318.
12. M.R. Castillo and J.R. Babson, *Neuroscience*, 1998, **86**, 1133-1144.
13. J.L. Farber, *Chem. Res. Toxicol.*, 1990, **3**, 503-508.
14. Figure 1.1 taken from http://medweb.bham.ac.uk/research/calcium/functions/ApopNec.html
15. P. Richelmi, F. Mirabelli, A. Salis, G. Finard, F. Berte and G. Bellomo, *Toxicology*, 1989, **57**, 29-44.
16. J. Garthwaite, G. Garthwaite, R.M.J. Palmer and S. Moncada, *Eur. J. Pharmacol.*, 1989, **172**, 413-416.
17. L. Kiedrowski, E. Costa and J.T. Wroblewski, *J. Neurochem.*, 1992, **58**, 335-341.
18. A. Guidarelli, M. Fiorani and M. Cantoni, *Free Radical Res.*, 2000, **33**, 477-487.
19. E. Rodriguez-Martinez, A. Camacho, P.D. Maldonado, J. Pedraza-Chaverri, D. Santamaria, S. Galvan-Arzate and A. Santamaria, *Brain Res.*, 2000, **858**, 436-439.
20. C. Szabo, *Toxicol. Lett.*, 2003, **140**, 105-112.

21. L. Virag, E. Szabo, P. Gergely and C. Szabo, *Toxicol. Lett.*, 2003, **140**, 113-124.
22. H. Ischiropoulos, L. Zhu, J. Chen, M. Tsai, J.C. Martin, C.D. Smith and J.S. Beckman, *Arch. Biochem. Biophys.*, 1992, **298**, 431-437.
23. M.S. Ramezanian, S. Padmaja and W.H. Koppenol, *Chem. Res. Toxicol.*, 1996, **9**, 232-237.
24. S.A. Greenacre and H. Ischiropoulos, *Free Radical Res.*, 2001, **34**, 541-581.
25. A. Santamaria, D. Santamaria, M. Diaz-Munoz, V. Espinoza-Gonzalez and C. Rios, *Toxicol. Lett.*, 1997, **93**, 117-124.
26. H. Rubbo, R. Radi, M. Trujillo, R. Telleri, B. Kalyanaraman, S. Barnes, M. Kirk and B.A Freeman, *J. Biol. Chem.*, 1994, **269**, 26066-26075.
27. V. Perez-De La Cruz, G. Gonzalez-Cortes, S.Galvan-Arzate, O.N. Medina-Campos, F. Perez-Severiano, S.F. Ali, J. Pedraza-Chaverri and A. Santamaria, *Neuroscience*, 2005, **135**, 463-474.
28. C. Szabo, B. Zingarelli, M. O'Connor and A.L. Salzman, *Proc. Natl. Acad. Sci. USA*, 1996, **93**, 1753-1758.
29. M.R. Castillo and J.R. Babson, *Neuroscience*, 1998, **86**, 1133-1144.
30. P. Nicotera, G. Bellomo and S. Orrenius, *Chem. Res. Toxicol.*, 1990, **3**, 484-494.
31. J.L. Farber and E.E. Young, *Arch. Biochem. Biophys.*, 1981, **221**, 312-320.
32. M.J. Arends, R.G. Morris and A.H. Wyllie, *Am. J. Pathol.*, 1990, **136**, 593-608.
33. A. Udvardy, P. Schedl, M. Sander and T. Hsieh, *J. Mol. Biol.*, 1986, **191**, 231-246.
34. L. Virag, G.S. Scott, S. Cuzzocrea, D. Marmer, A.L. Salzman and C. Szabo, *Immunology*, 1998, **94**, 345-355.
35. L. Tenneti, D.M. D'Emilia, C.M. Troy and S.A. Lipton, *J. Neurochem.*, 1998, **71**, 946-959.
36. L. Tenneti and S.A. Lipton, *J. Neurochem.*, 2000, **74**, 134-142.
37. M. Los, M. Mozoluk, D. Ferrari, A. Stepczynska, C. Stroh, A. Renz, Z. Herceg, Z. Wang and K. Schulze-Osthoff, *Mol. Biol. Cell*, 2002, **13**, 978-988.
38. J.P. Kim and D.W. Choi, *Neuroscience*, 1987, **23**, 423-432.
39. L. Khaspekov, E. Kida, I. Victorov and M.J. Mossakowski, *J. Neurosci. Res.*, 1989, **22**, 150-157.

40. E. Galarraga, D.J. Surmeier and S.T. Kitai, *Brain Res.*, 1990, **512**, 269-276.
41. W.O. Whetsell and R. Schwarcz, *Neurosci. Lett.*, 1989, **97**, 271-275.
42. M.F. Beal, R.J. Ferrante, K.J. Swartz and N.W. Kowall, *J. Neurosci.*, 1991, **11**, 1649-1659.
43. R. Schwarcz, *Biochem. Soc. Trans.*, 1993, **21**, 77-82.
44. P. Guidetti, G.P. Bates, R.K. Graham, M.R. Hayden, B.R. Leavitt, M.E. MacDonald, E.J. Slow, V.C. Wheeler, B. Woodman and R. Schwarcz, *Neurobiol. Dis.*, 2006, **23**, 190-197.
45. A. Freese, K.J. Swartz, M.J. During and J.B. Martin, *Neurology*, 1990, **40**, 691-695.
46. R. Schwarcz, E. Okuno, R.J. White, E.D. Bird and W.O. Whetsell, *Proc. Natl. Acad. Sci. USA*, 1988, **85**, 4079-4081.
47. A.C. Foster, W.O. Whetsell, E.D. Bird and R. Schwarcz, *Brain Res.*, 1985, **336**, 207-214.
48. M.F. Beal, W.R. Matson, E. Storey, P. Milbury, E.A. Ryan, T. Ogawa and E.D. Bird, *J. Neurol. Sci.*, 1992, **108**, 80-87.
49. D. Jauch, E.M. Urbanska, P. Guidetti, E.D. Bird, J.P.G. Vonsattel, W.O. Whetsell and R. Schwarcz, *J. Neurol. Sci.*, 1995, **130**, 39-47.
50. M.P. Heyes, K. Saito, J.S. Crowley, L.E. Davis, M.A. Demitrack, M. Der, L.A. Dilling, J. Elia, M.J.P. Kruesi, A. Lackner, S.A. Larsen, K. Lee, H.L. Leonard, S.P. Markey, A. Martin, S. Milstein, M.M. Mouradian, M.R. Pranzatelli, B.J. Quearry, A. Salazar, M. Smith, S.E. Strauss, T. Sunderland, S.W.Swedo and W.W. Tourtellotte, *Brain*, 1992, **115**, 1249-1273.
51. A.C. Foster, A. Vezzani, E.D. French and R. Schwarcz, *Neurosci. Lett.*, 1984, **48**, 273-278.
52. A.B. Young, J.T Greenamyre, Z. Hollingsworth, R. Albin, C. D'Amato, I. Shoulson and J.B. Penny, *Science*, 1988, **241**, 981-983.
53. F. Perez-Severiano, C. Rios and J. Segovia, *Brain Res.*, 2000, **862**, 234-237.
54. N. Stoy, G.M. Mackay, C.M. Forrest, J. Christofides, M. Egerton, T.W. Stone and L.G. Darlington, *J. Neurochem.*, 2005, **93**, 611-623.
55. R.J. Carter, L.A. Lione, T. Humby, L. Mangiarini, A. Mahal, G.P. Bates, S.B. Dunnett and A.J. Morton, *J. Neurosci.*, 1999, **19**, 3248-3257.
56. S.B. Tatter, W.R. Galpern, A.T. Hoogeveen and O. Isacson, *Neuroreport*, 1995, **6**, 1125-1129.

57. S. Kuemmerle, C.A. Gutekunst, A.M. Klein, X.J. Li, S.H. Li, M.F. Beal, S.M. Hersch and R.J. Ferrante, *Ann. Neurol.*, 1999, **46**, 842-849.

58. G. Bates, *Lancet*, 2003, **361**, 1642-1644.

59. I.P. Lapin, I.B. Prakhie and I.P. Kiseleva, *J. Neural Transm.*, 1982, **54**, 229-238.

60. S. Feldblum, A. Rougier, P. Loiseau, F. Cohadon, P.L. Morselli and K.G. Lloyd, *Epilepsia*, 1988, **29**, 523-529.

61. M.P. Heyes, K. Saito and S.P. Markey, *Biochem. J.*, 1992, **283**, 633-635.

62. M.P. Heyes, C.L. Achim, C.A. Wiley, E.O. Major, K. Saito and S.P. Markey, *Biochem. J.*, 1996, **320**, 595-597.

63. D. Giulian, L.J. Haverkamp, J. Li, W.L. Karshin, J. Yu, D. Tom, X. Li and J.B. Kirkpatrick, *Neurochem. Int.*, 1995, **27**, 119-137.

64. Y.M. Arends, C. Duyckaerts, J.M. Rozemuller, P. Eikelenboom and J.J. Hauw, *Neurobiol. Aging*, 2000, **21**, 39-47.

65. G.J. Guillemin, K.R. Williams, D.G. Smith, G.A. Smythe, J. Croitoru-Lamoury and B.J. Brew, *Developments in Tryptophan and Serotonin Metabolism*, Ed. G. Allegri, Plenum, New York, 2003, 167-176.

66. G.J. Guillemin, B.J. Brew, C.E. Noonan, O. Takikawa and K.M. Cullen, *Neuropathol. Appl. Neurobiol.*, 2005, **31**, 395-404.

67. T.W. Stone, *Toxicon*, 2001, **39**, 61-73.

68. M.P. Heyes, D. Rubinow, C. Lane and S.P. Markey, *Ann. Neurol.*, 1989, **26**, 275-277.

69. M.P. Heyes, K. Saito, A. Lackner, C.A. Wiley, C.L. Achim and S.P. Markey, *FASEB J.*, 1998, **12**, 881-896.

70. O. Takikawa, *Biochem. Biophys. Res. Commun.*, 2005, **338**, 12-19.

71. A.M. Sardar and G.P. Reynolds, *Neurosci. Lett.*, 1995, **187**, 9-12.

72. S.J. Kerr, P.J. Armati, L.A. Pemberton, G. Smythe, B. Tattam and B.J. Brew, *Neurology*, 1997, **49**, 1671-1681.

73. M.P. Heyes, *Biochem. Soc. Trans.*, 1993, **21**, 83-89.

74. N.H. Hunt, J. Gloenser, T. Chan-Ling, S. Parekh, C. Rae, S. Potter, I. M. Medana, J. Miu and H. J. Ball, *Int. J. Parasitol.*, 2006, **36**, 569-582.

75. I.M. Medana, N.P.J. Day, H. Salahifar-Sabet, R. Stocker, G. Smythe, L. Bwanaisa, A. Njobvu, K. Kayira, G.D.H. Turner, T.E. Taylor and N.H. Hunt, *J. Infect. Dis.*, 2003, **188**, 844-849.

76. M. Dobbie, J. Crawley, C. Waruiru, K. Marsh and R. Surtees, *Am. J. Trop. Med. Hyg.*, 2000, **62**, 284-290.
77. L.A. Sanni, S.R. Thomas and B.N. Tattam, *Am. J. Pathol.*, 1998, **152**, 611-619.
78. F. Stastny, I. Skultetyova, L. Pliss and D. Jezova, *Brain Res. Bull.*, 2000, **53**, 415-420.
79. G.E. Grau, P.F. Piguet, P. Vassalli and P.H. Lambert, *Immunol. Rev.*, 1989, **112**, 49-70.
80. M.W. Taylor and G.S. Feng, *Fed. Am. Soc. Exp. Biol. J.*, 1991, **5**, 2516-2522.
81. C.J. Clark, G.M. Mackay, G.A. Smythe, S. Bustamante, T.W. Stone and R.S. Phillips, *Infect. Immun.*, 2005, **73**, 5249-5251.
82. M.P. Heyes, K. Saito, D. Jacobowitz, S.P. Markey, O. Takikawa and J.H. Vickers, *FASEB J.*, 1992, **6**, 2977-2989.
83. J.J. Halperin and M.P. Heyes, *Neurology*, 1992, **42**, 43-50.
84. E.H. Sinz, P.M. Kochanek and M.P. Heyes, *Brain*, 1998, **121**, 610-615.
85. A.R. Blight, T.I. Cohen, K. Saito and M.P. Heyes, *Brain*, 1995, **118**, 735-752.
86. G.M. Mackay, C.M Forrest, N. Stoy, J. Christofides, M. Egerton, T.W. Stone and L.G. Darlington, *Eur. J. Neurol.*, 2006, **13**, 30-42.
87. I. Lieberman, A. Kornberg and E.S. Simms, *J. Biol. Chem.*, 1955, **215**, 403-415.
88. B.N. Ames, R.G. Martin and B.J. Garry, *J. Biol. Chem.*, 1961, **236**, 2019-2026.
89. O.H. Smith and C. Yanofsky, *J. Biol. Chem.*, 1960, **235**, 2051-2057.
90. S. Nakamura, M. Ikeda, H. Tsuji, Y. Nishizuka and O. Hayaishi, *Biochem. Biophys. Res. Commun.*, 1963, **13**, 285-290.
91. K. Iwai and H. Taguchi, *J. Nutr. Sci. Vitaminol.*, 1973, **19**, 491-499.
92. D.F. Mann and R.U. Byerrum, *J. Biol. Chem.*, 1974, **249**, 6817-6823.
93. K. Hughes, A. Dessen, P. Gray and C. Grubmeyer, *J. Bacteriol.*, 1993, **175**, 479-486.
94. R. Wagner and K.G. Wagner, *Phytochemistry*, 1984, **23**, 1881-1883.
95. H. Taguchi and K. Iwai, *Biochim. Biophys. Acta*, 1976, **422**, 29-37.
96. K. Iwai and H. Taguchi, *Biochem. Biophys. Res. Commun.*, 1974, **56**, 884-891.
97. K. Shibata and K. Iwai, *Biochim. Biophys. Acta*, 1980, **611**, 280-288.
98. K. Shibata and K. Iwai, *Agric. Biol. Chem.*, 1980, **44**, 301-308.

99. E. Okuno and R. Schwarcz, *Biochim. Biophys. Acta*, 1985, **841**, 112-119.
100. E. Okuno, R.J. White and R. Schwarcz, *J. Biochem.*, 1988, **103**, 1054-1059.
101. M. Hori and J.F. Henderson, *J. Biol. Chem.*, 1966, **241**, 3404-3408.
102 J. Victor, L.B. Greenberg and D.L. Sloan, *J. Biol. Chem.*, 1979, **254**, 2647-2655.
103. M.B. Bhatia, A. Vinitsky and C. Grubmeyer, *Biochemistry*, 1990, **29**, 10480-10487.
104. P. Natalini, S. Ruggieri, I. Santarelli, A. Vita and G. Magni, *J. Biol. Chem.*, 1979, **254**, 1558-1563.
105. L. Kalikin and K.C. Calvo, *Biochem. Biophys. Res. Commun.*, 1988, **152**, 559-564.
106. R. Bhatia and K.C. Calvo, *Arch. Biochem. Biophys.*, 1996, **325**, 270-278.
107. H. Cao, B.L. Pietrak and C. Grubmeyer, *Biochemistry*, 2002, **41**, 3520-3528.
108. V. Sharma, C. Grubmeyer and J.C. Sacchettini, *Structure*, 1998, **6**, 1587-1599.
109. W.D.L. Musick, *CRC Crit. Rev. Biochem.*, 1981, **11**, 1-34.
110. C.A. Bunton and E. Hameres, *J. Org. Chem.*, 1969, **34**, 572-576.
111. N.P. Botting, *J. Nat. Prod.*, 1994, **11**, 337-353.
112. R.K. Goitein, D. Chelsky and S.M. Parsons, *J. Biol. Chem.*, 1978, **253**, 2963-2971.
113. W. Tao, C. Grubmeyer and J.S. Blanchard, *Biochemistry*, 1996, **35**, 14-21.
114. M.R.F. Ashworth, R.P. Daffern and D.L. Hammick, *J. Chem. Soc.*, 1939, 809-812.
115. G.E. Dunn, G.K. Lee and H. Thimm, *Can. J. Chem.*, 1972, **50**, 3017-3027.
116. P. Beak and B. Siegel, *J. Am. Chem. Soc.*, 1976, **98**, 3601-3606.
117. H. L. Levine, R.S. Brody and F.H. Westheimer, *Biochemistry*, 1980, **19**, 4993-4999.
118. R.B. Silverman and M.P. Groziak, *J. Am. Chem. Soc.*, 1982, **104**, 6434-6439.
119. S.A. Acheson, J.B. Bell, M.E. Jones and R. Wolfenden, *Biochemistry*, 1990, **29**, 3198-3202.
120. J.A. Smiley, P. Paneth, M.H. O'Leary, J.B. Bell and M.E. Jones, *Biochemistry*, 1991, **30**, 6216-6223.
121. P. Harris, J.C. Navarro-Poulsen, K.F. Jensen and S. Larsen, *Biochemistry*, 2000, **39**, 4217-4224.
122. J.A. Smiley and M.E. Jones, *Biochemistry*, 1992, **31**, 12162-12168.

123. K. Iwai and H. Taguchi, *Methods Enzymol.*, 1980, **66**, 96-101.

124. G. W. Smithers and W.J. O'Sullivan, *Biochemistry*, 1984, **23**, 4767-4773.

125. S. Kunjara, C.S. Lee, G.W Smithers, K. Shibata, K. Iwai and W.J. O'Sullivan, *Int. J. Biochem.*, 1986, **18**, 489-491.

126. J. Preiss and P. Handler, *J. Biol. Chem.*, 1958, **233**, 493-500.

127. J.W. Foster and A.G. Moat, *Microbiol. Rev.*, 1980, **44**, 83-105.

128. S. Hanna, S.L Hess and D.L. Sloan, *J. Biol. Chem.*, 1983, **258**, 9745-9754.

129. J.C. Eads, D. Ozturk, T.R. Wexler, C. Grubmeyer and J.C. Sacchettini, *Structure*, 1997, **5**, 47-58.

130. G. Scapin, C. Grubmeyer, and J.C. Sacchettini, *Biochemistry*, 1994, **33**, 1287-1294.

131. A. Heroux, E.L. White, L.J. Ross, R.L. Davis and D.W. Borhani, *Biochemistry*, 1999, **38**, 14495-14506.

132. J.L. Smith, *Curr. Opin. Struct. Biol.*, 1998, **8**, 686-694.

133. M.A. Schumacher, D. Carter, D.M. Scott, D.S. Roos, B. Ullman and R.G. Brennan, *EMBO J.*, 1998, **17**, 3219-3232.

Chapter Two

Studies on Wild-type QPRTase

2.1 Introduction

To enable the study of an enzymatic reaction, it is essential to have access to good quantities of pure protein. QPRTase has been isolated from a number of sources such as shiitake mushroom,[1] castor bean endosperm[2] and mammalian liver and kidney.[3-5] However, such extractions are often very laborious, requiring several different chromatographic techniques to obtain the pure enzyme. Furthermore, isolation of sufficient protein for analysis requires access to significant quantities of the protein source. For example, 50 kg of shiitake mushroom were required to obtain sufficient QPRTase for analysis.

More recently, QPRTase from *Salmonella typhimurium*[6] and *Mycobacterium tuberculosis*[7] were obtained by cloning the QPRTase gene into a suitable vector, then expressing the target protein in bacterial host cells. However, the methods employed for the purification of the over-expressed protein were still reasonably lengthy and required a number of steps involving different chromatographic techniques. Nevertheless, good quantities of pure protein were obtained which enabled kinetic and structural studies to be undertaken. The mechanistic studies that were carried out on the bacterial enzymes were discussed in sections 1.5 and 1.7.

Despite the studies on the bacterial enzymes, there were still many unanswered questions regarding the mechanism of the QPRTase catalysed reaction. Furthermore, although interest in QPRTase had been fuelled by the involvement of quinolinic acid in CNS disease,[8] the human enzyme had yet to be studied. With this in mind, a project aimed at carrying out a thorough mechanistic study on human brain QPRTase was initiated in our laboratory in 2001.

The human QPRTase cDNA was isolated and characterised from a human brain DNA library by Fukuoka *et al*.[9] The partial amino acid sequences for purified porcine kidney QPRTase were used to design oligonucleotide probes, which were screened against the human brain cDNA library. QPRTase was isolated as a single positive clone which encodes 1182 nucleotides and has a single open reading frame of 891 base pairs (291 amino acids). Confirmation that the isolated cDNA clone encoded QPRTase came from studies of its functional expression in a bacterial host.

It was found that introduction of the human cDNA into a QPRTase defective *E. coli* strain brought about an abrupt increase in QPRTase activity and allowed the cells to grow in the absence of nicotinic acid. However, despite the enzyme being detected sufficient protein was not produced for isolation.

In our laboratory,[10] using the cDNA for human brain QPRTase which was kindly donated by Professor S.I. Fukuoka (Research Institute for Food Science, Kyoto University, Uji, Japan), the human brain QPRTase gene was amplified by PCR. The expression vector pEHISTEV-QPRTase was then constructed by ligating the QPRTase gene into the pEHISTEV plasmid. Active human brain QPRTase was then successfully over-expressed in *E. coli* strain BL21 (DE3) host cells from the pEHISTEV-QPRTase construct.

A significant advantage of using the pEHISTEV plasmid is the high expression levels of the target protein. The pEHISTEV plasmid is comprised of 5365 base pairs, which includes a gene for resistance to the antibiotic kanamycin (Appendix 1). The DNA encoding human brain QPRTase was cloned into the multiple cloning site of the plasmid downstream from a T7 promoter. The expression of the QPRTase gene is therefore under the transcriptional control of the exceptionally strong T7 promoter. The transcription of a gene encoding T7 RNA polymerase in the host is controlled by the *lac* promoter and the *lac* operator. A repressor is present which binds to the *lac* operator and blocks transcription of T7 RNA polymerase. The repressor is a variant of the *lac* repressor and binds the operator more tightly than the wild-type repressor. This helps tighten regulation of transcription so that premature expression is prevented. Once the cells have reached the mid- to late-exponential stage of growth, the inducer isopropyl-β-D-thiogalactoside (IPTG) is added to bind the *lac* repressor and induce its dissociation from the *lac* operator, allowing expression of T7 RNA polymerase in the host, *E. coli* BL21 (DE3). The T7 RNA polymerase then binds to the T7 promoter and transcribes the QPRTase gene. Thereafter, the mRNA binds to the ribosome and is translated to QPRTase. As T7 RNA polymerase is highly active and extremely promoter-selective, the desired protein can make up more than 30% of the total cell proteins.

A further advantage of using the pEHISTEV plasmid is that protein purification is simple. When the expression vector is constructed, the target gene sequence is inserted adjacent to a short sequence encoding a 6-histidine tag and a TEV protease recognition site. As a result, the target protein is expressed with a polyhistidine affinity tag on the N-terminus and the protein can be easily purified by nickel affinity chromatography. The histidine-tag can then be selectively cleaved by digestion with TEV protease. TEV protease recognises a seven amino acid sequence Glu-X-X-Tyr-X-Gln-Gly, where X can be various amino acid residues. The sequence used in this study was Glu-Asn-Leu-Tyr-Phe-Gln-Gly, which is the most commonly used TEV protease recognition sequence (Appendix 1). Cleavage occurs selectively between the glutamine and glycine residues of the sequence. TEV protease is a cysteine protease and utilises a catalytic triad of residues (Cys-Asp-His) to catalyse peptide hydrolysis. Once the histidine tag has been cleaved from the target protein, a second nickel column can be used to isolate the pure protein.

This chapter describes the expression and purification of wild-type human brain QPRTase and the kinetic and structural studies that were carried out on the purified enzyme.

2.2 Expression and purification of human brain QPRTase

Human brain QPRTase was successfully expressed in *E. coli* strain BL21 (DE3) cells from the pEHISTEV-QPRTase construct. The *E. coli* cells were grown in L-broth medium containing kanamycin to a cell density of OD_{600} 0.4 at 37 °C. The temperature was then reduced to 20 °C and the cells were grown to OD_{600} 0.6 prior to induction with IPTG. The cultures were then incubated at 20 °C for 15 hours post-induction. The expressed protein comprised human QPRTase with a 6-histidine tag separated by a TEV protease cleavage site. This was confirmed by sodium dodecyl sulfate–polyacrylamide gel electrophoresis (SDS-PAGE) which showed a large protein band at the expected mass of ~34 kDa (Figure 2.1).

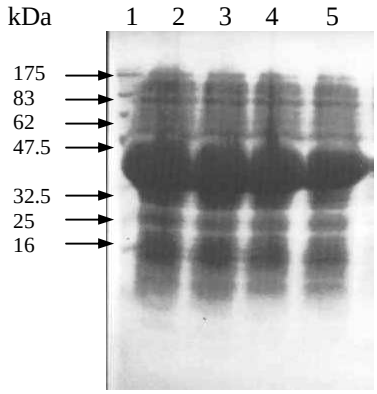

Figure 2.1: *Coomassie stained SDS-PAGE gel. Lane 1 – Molecular weight standards and Lanes 2-5 – E. coli crude extracts.*

The first stage in the purification of the protein was to separate the HISTEV-QPRTase from all the *E. coli* proteins. This was achieved by nickel affinity chromatography. Metal chelate affinity chromatography is routinely employed in the purification of proteins.[11] This technique involves immobilisation of a chelating ligand on to a polymer support. The resin bound ligand can then be charged with metal ions which are capable of coordinating to proteins. The chelating ligand employed in these studies was nitrilotriacetic acid which binds to four of the six coordination sites on nickel. The remaining sites are free to bind to exposed histidine residues in the protein (Scheme 2.1).

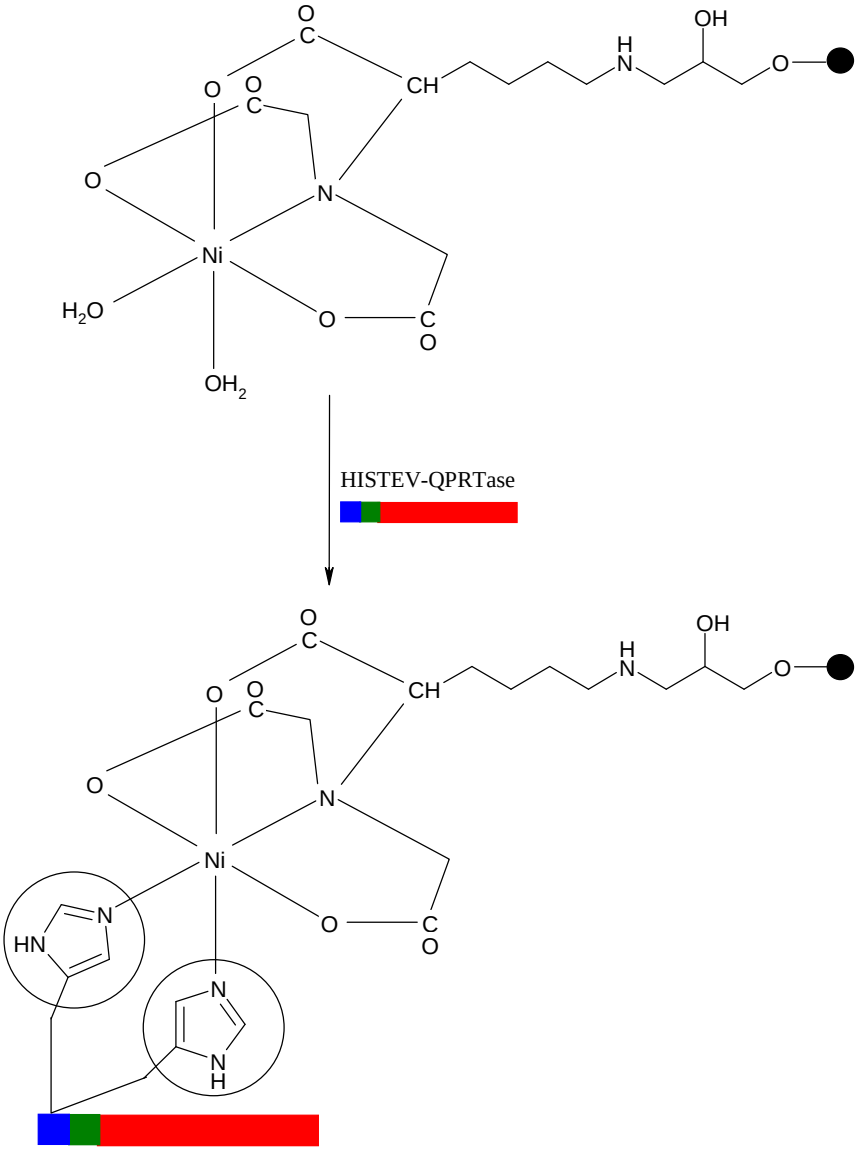

Scheme 2.1: *Binding of HISTEV-QPRTase to a nickel affinity column. (HISTEV-QPRTase is represented as blue bar: 6 x histidine affinity tag, green bar: TEV protease recognition site and red bar: QPRTase)*

It has been reported by Hochuli *et al.* that binding to a metal chelate affinity column is favoured by proteins which have two or more adjacent histidine residues.[12] Therefore, when the crude protein extract was passed through the nickel affinity column, HISTEV-QPRTase bound to nickel via the 6-histidine tag attached to the N-terminus of the protein while the *E. coli* proteins passed through relatively unhindered and were simply washed off the column. The nickel-protein interaction is reversible and the pure HISTEV-QPRTase was eluted by passing a buffer containing excess imidazole through the column.

The next stage in the purification process is the cleavage of the histidine tag. This was achieved by treating the pure HISTEV-QPRTase with TEV protease. The TEV protease used also has a histidine tag attached to the N-terminus which aids its removal in the final stage of purification.

Following digestion with TEV protease, a second nickel affinity column was used to isolate the pure QPRTase from the cleaved histidine tag and the TEV protease. Both the histidine tag and the TEV protease bound to the nickel column while the pure QPRTase passed through unhindered. The histidine tag and the TEV protease were subsequently eluted by passing a buffer containing excess imidazole through the column.

The purity of the final protein was confirmed by SDS-PAGE which showed a single protein band (Figure 2.2).

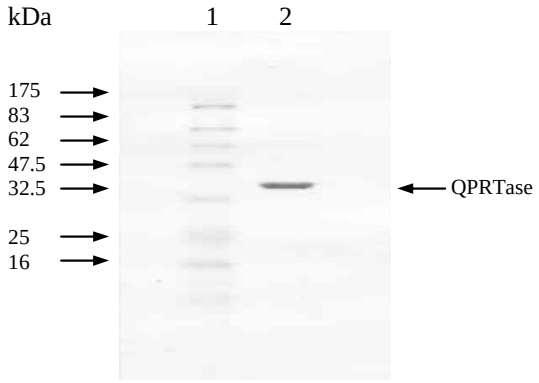

Figure 2.2: *Coomassie stained SDS-PAGE gel. Lane 1 – Molecular weight standards and Lane 2 – Pure QPRTase.*

The protein was concentrated and the final concentration was determined by performing Bradford's assay.[13] Purified human brain QPRTase was isolated in a yield of 8 mg/litre culture.

However, the overall isolated yield of pure QPRTase could have been significantly higher were it not for the problems encountered during the TEV protease digestion step of the purification process. The cleavage of the histidine tag from the pure HISTEV-QPRTase was monitored by SDS-PAGE which showed that approximately only 50% cleavage was attained, even after the addition of more TEV protease (Figure 2.3). It was found that the cleavage of the histidine tag was most successful when freshly expressed and purified TEV protease was used, but even then complete cleavage was never achieved.

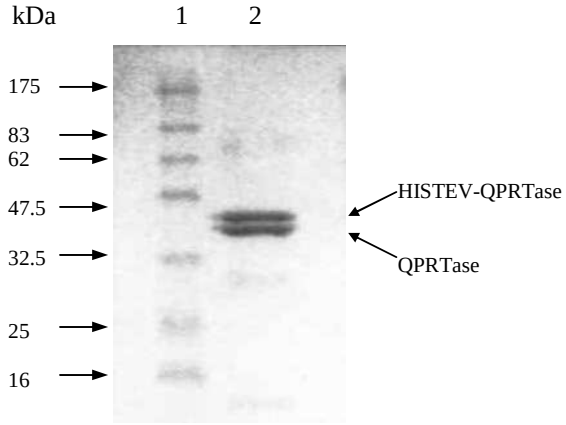

Figure 2.3: *Coomassie stained SDS-PAGE gel. Lane 1 – Molecular weight standards and Lane 2 – HISTEV-QPRTase and QPRTase.*

Since a lot of protein was being lost at this stage, it was decided to leave the histidine-tag attached to the N-terminus of QPRTase and examine whether its presence affects the function of the protein. If the histidine-tag was found to have no effect on the activity of QPRTase then this would increase the amount of protein available for kinetic studies and also reduce the time required to obtain the protein since the need for the troublesome TEV digestion step and the second nickel column would be eliminated.

2.3 Structural studies on wild-type human brain QPRTase

2.3.1 Crystal structure of human brain QPRTase

Previously in our laboratory,[10] initial crystallisation conditions were obtained with sitting-drop diffusion using Crystal Screen Kits (Hampton research) at 20 °C with a protein concentration of 10 mg/mL. Crystals appeared within 5 days in condition 29 of Hampton screen 1. Refinement of these conditions yielded a single crystal from a mixture of 2 μL of the protein (10 mg/mL, 50 mM Tris, pH 7.5) and 2 μL of precipitant (0.6 M K, Na tartrate, 0.1 M Na Hepes, pH 7.6). The crystal of native human brain QPRTase was diffracted at the European Synchrotron Radiation Facility (ESRF) to a resolution of 1.9 Å (Dr Huanting Liu, The Centre for Biomolecular Science, University of St Andrews).

Attempts to solve the structure of human brain QPRTase by molecular replacement using the bacterial enzymes as search models failed. Therefore, selenomethionine labelled QPRTase was expressed, purified and crystallised (Figure 2.4). The selenomethionine labelled QPRTase crystal was diffracted at ESRF to a resolution of 2.4 Å. The structure of human brain QPRTase was solved by a combination of multi-wavelength anomalous dispersion phasing and non-crystallographic averaging (Dr Huanting Liu, The Centre for Biomolecular Science, University of St Andrews). The crystallographic space group was identified as $P2_12_12_1$ and the unit cell dimensions were a=111.5 Å, b=179.5 Å, c=194.7 Å and $\alpha=\beta=\gamma=90°$.

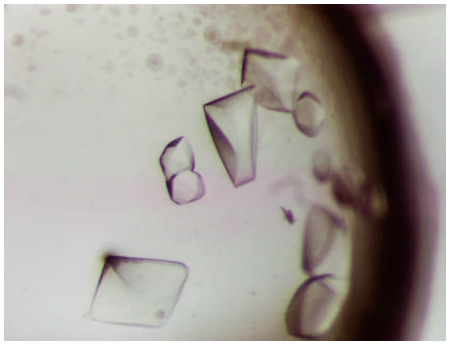

Figure 2.4: *Crystals of selenomethionine labelled QPRTase.*

Figure 2.5 shows the structure of the human brain QPRTase monomer, which comprises twelve α-helices and twelve β-strands arranged into two structural domains. The N-terminal domain (residues 1-112 and 279-291) is composed of a four-stranded (β1, β3, β5 and 12β) anti-parallel β-sheet stacked against helices α1, α2, α3, α4 and part of the 33 residue long α5. The strands β1 and β3 are followed by two short strands β2 and β4 which form a small two-stranded anti-parallel β-sheet. The C-terminal domain (residues 113-278) is an α/β-barrel structure consisting of the remaining β-strands (β6, β7, β8, β9, β10 and β11) and eight α-helices (α5, α6, α7, α8, α9, α10, α11 and α12) arranged in $(\alpha/\beta)_2\alpha(\alpha/\beta)_4\alpha$ topology. The two domains are connected by helices α5 and α12.

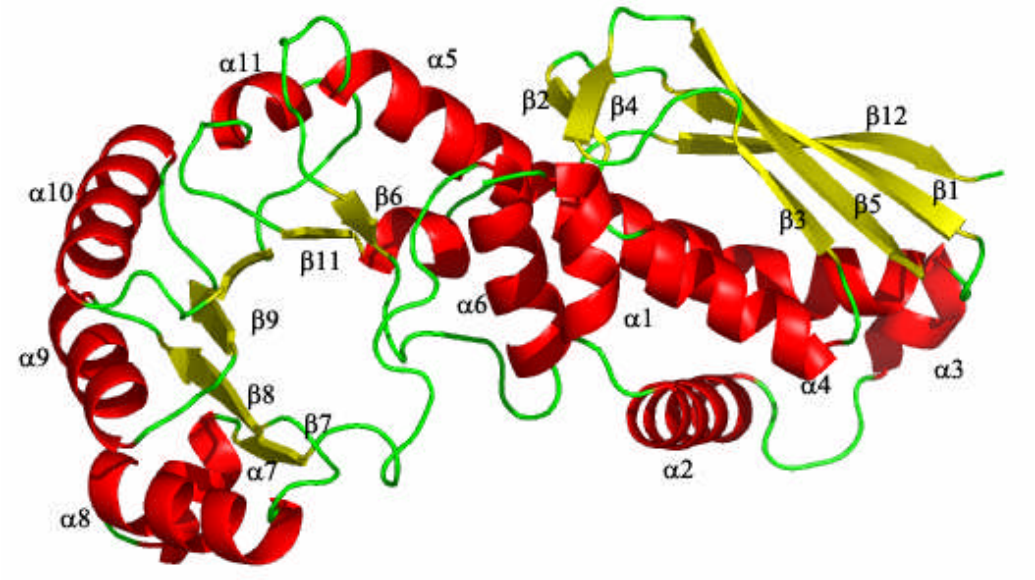

Figure 2.5: *Human brain QPRTase monomer.*

The overall structure of the human brain QPRTase monomer is very similar to that of the bacterial enzymes. The sequence alignment of the QPRTase homologues is shown in Figure 2.6 together with the secondary structure elements of human brain QPRTase and *Mycobacterium tuberculosis* QPRTase. The sequence homology of human brain QPRTase and the bacterial enzymes is quite low; 28% to *Salmonella typhimurium* QPRTase and 39% to *Mycobacterium tuberculosis* QPRTase.

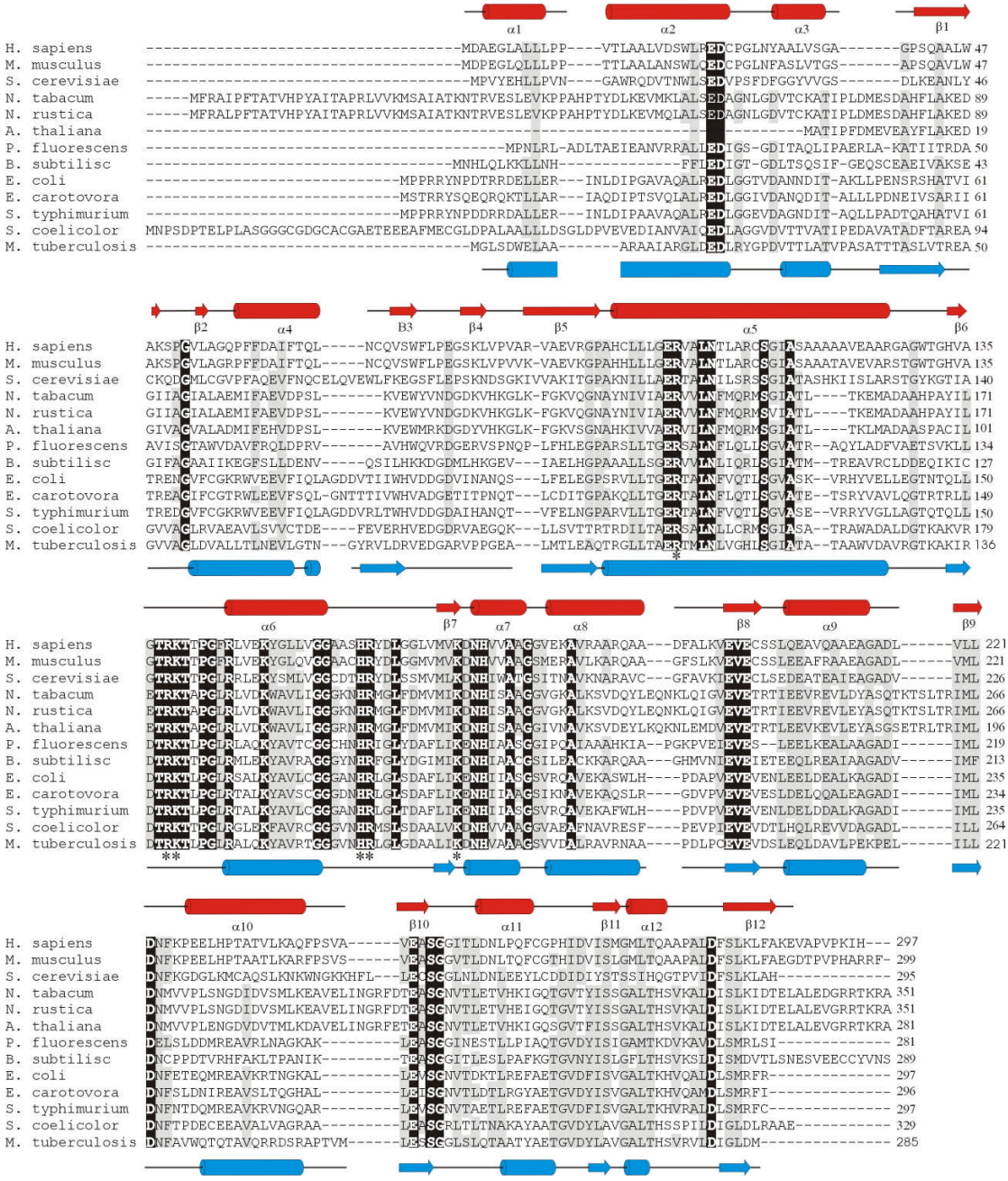

Figure 2.6: *Sequence alignment of the QPRTase homologues. Conserved residues are shown as white letters on a black background. The secondary structure elements of human brain QPRTase are shown above the alignment (red) while those of Mycobacterium tuberculosis QPRTase are shown below (blue). α-Helices are represented as rectangles and β-strands as arrows.*

In the crystalline form, the human brain QPRTase monomers associate to form a dimer (Figure 2.7). The dimer is formed by a twofold symmetry that places the N-terminal domain of one subunit next to the C-terminal domain of the other.

(a) (b)

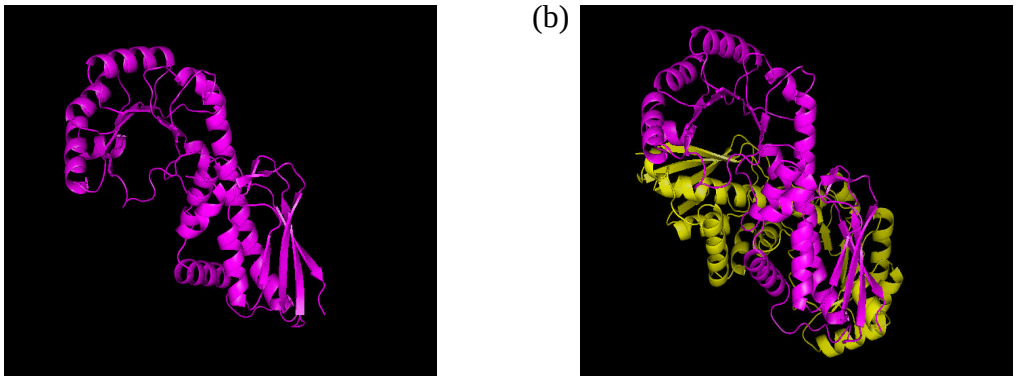

Figure 2.7: *Structure of the human brain QPRTase (a) monomer and (b) dimer.*

The two active sites are located at the interfaces between the α/β-barrel of one subunit and the β-sandwich of the second subunit and are composed of residues from both subunits. The active site is a deep pocket with a highly positive electrostatic surface (Figure 2.8). This surface is composed of three arginine residues (Arg161, Arg138, Arg102' (' denotes residues from the other subunit of the dimer)), two lysine residues (Lys139 and Lys171) and one histidine residue (His160). These residues are highly conserved among QPRTase enzymes (Figure 2.6) and adopt similar conformations in the structures of *Mycobacterium tuberculosis* QPRTase and *Salmonella typhimurium* QPRTase.

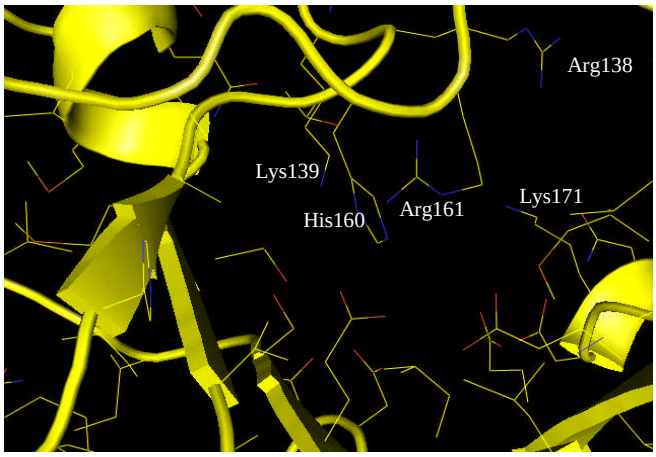

Figure 2.8: *Active site of human brain QPRTase.*

In the human brain QPRTase structure, the quinolinic acid binding site was occupied by a tartrate molecule (Figure 2.9). Tartrate **35** was present at a concentration of 0.6 M in the precipitant used to crystallise the protein. Tartrate **35** and quinolinic acid possess a similar backbone consisting of a 1,2-dicarboxylic acid functionality, which explains the binding of tartrate in the active site.

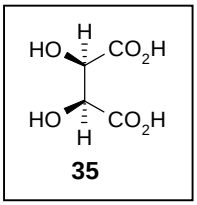

35

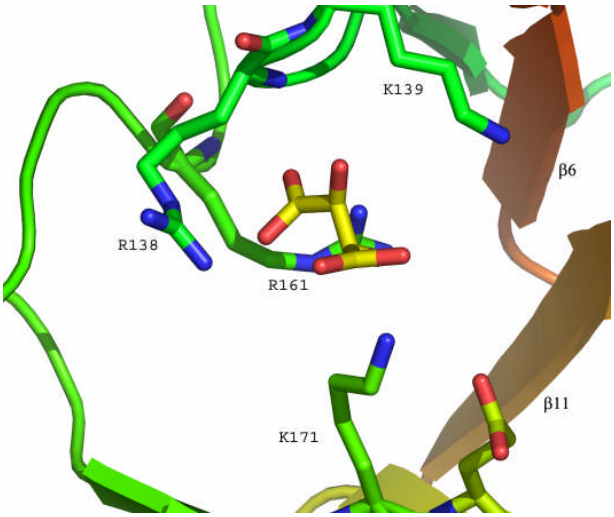

Figure 2.9: *Active site of human brain QPRTase with a tartrate molecule bound.*

The asymmetric unit of the human brain QPRTase crystal in fact contained twelve monomers of protein. Essentially the QPRTase dodecamer is an arrangement of two hexameric rings (Figure 2.10a). Each QPRTase hexamer contains three dimers which are related by a three-fold rotation axis (Figure 2.10b).

(a)

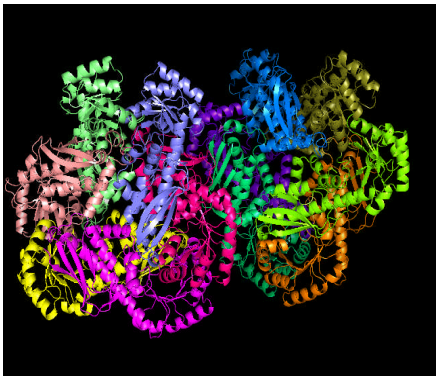

(b)

Figure 2.10: *Structure of the human brain QPRTase (a) dodecamer and (b) hexamer. Each subunit is shown in a different colour.*

In the human brain QPRTase hexamer, each subunit makes quite extensive contacts with four other monomers. Each hexamer buries in total over 26000 $Å^2$ of available surface area. Analysis of the hexamer by the program PISA confirmed the hexameric assembly is energetically stable (Dr Huanting Liu, The Centre for Biomolecular Science, University of St Andrews). The contacts between the hexamers are only of the order of 100's of $Å^2$ and the program PISA indicated the dodecameric assembly is unstable. Therefore, it would appear that human brain QPRTase is a hexamer.

The hexameric arrangement adopted by human brain QPRTase is very different from the hexameric arrangement seen in the crystal of the *Mycobacterium tuberculosis* enzyme.[7] In the bacterial enzyme, the contacts in the hexamer are much less extensive and are formed by entirely different regions of the protein compared to human brain QPRTase (Figure 2.11). Furthermore, the hexameric arrangement in *Mycobacterium tuberculosis* QPRTase was found to be energetically unstable by PISA, suggesting the bacterial enzyme is a dimer and the hexamer is simply an artefact of crystal packing.

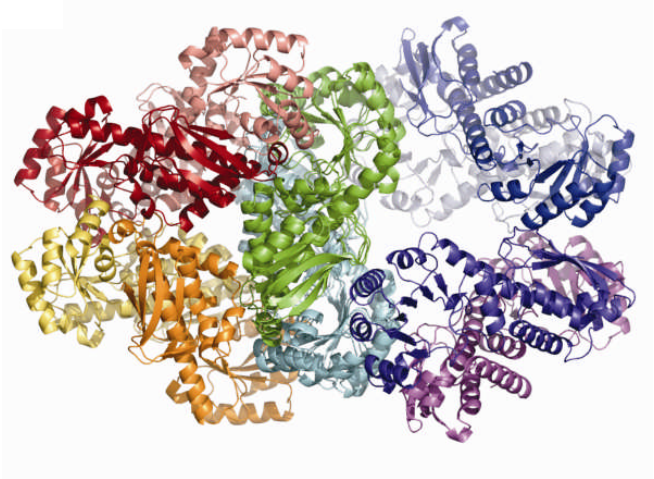

Figure 2.11: *Hexameric arrangement seen in the crystal structure of human brain QPRTase and Mycobacterium tuberculosis QPRTase. The dimer of the human QPRTase hexamer (coloured monomer A green, monomer B cyan) is superimposed with the Mycobacterium tuberculosis QPRTase dimer (also coloured monomer A green, monomer B cyan). The dimer, in the middle of the image is structurally conserved between human and bacterial enzymes. To the left are the other four subunits of the human brain QPRTase hexamer (monomers C, D, E and F are coloured deep red, salmon, yellow and orange respectively). The additional subunits of the Mycobacterium tuberculosis QPRTase "hexamer" are shown and are on the right of the dimer (monomer C light blue, monomer D deep blue, monomer E purple and monomer F indigo). As is immediately obvious, the hexameric arrangements bear no relationship to each other.*

2.3.2 Human brain QPRTase in the solution phase

Having established that human brain QPRTase adopts an energetically stable hexameric arrangement in the crystal structure, the next stage was to determine the degree of association of human brain QPRTase in solution. This was achieved by performing a series of gel filtration experiments under physiological conditions.

In gel filtration chromatography, the stationary phase consists of porous beads with a well-defined pore size. In this study a Superose column was used, which has a crossed-linked agarose matrix. The rate of movement of a molecule through the column depends on the ability of the molecule to enter the gel pores, which ultimately depends on the size of the molecule. Large molecules, which can never enter the stationary phase, move through the chromatographic bed fastest. Smaller molecules, which can enter the gel pores, move more slowly through the column, since they spend a proportion of their time in the stationary phase. The partition coefficient, K_{av}, represents the fraction of the stationary gel volume that is available for diffusion of a given species.

$$K_{av} = \frac{V_e - V_o}{V_t - V_o}$$

V_t is the total volume of the packed column (column length 30 cm, column diameter 1 cm, V_t = 23.6 mL). V_o is the void volume and is fully accessible for all molecules, independent of size. V_o was determined by passing blue dextran through the column and measuring its elution volume (V_o = 7.4 mL). Blue dextran, which is composed of the protein dextran (MW > 10^6 Da) attached to a polycyclic chromophore, is larger than the pores in the gel and is therefore only distributed in the mobile phase. V_i is the internal volume of the gel and is only accessible for smaller molecules ($V_i = V_t - V_o$ = 16.2 mL). V_e is the elution volume of the species of interest.

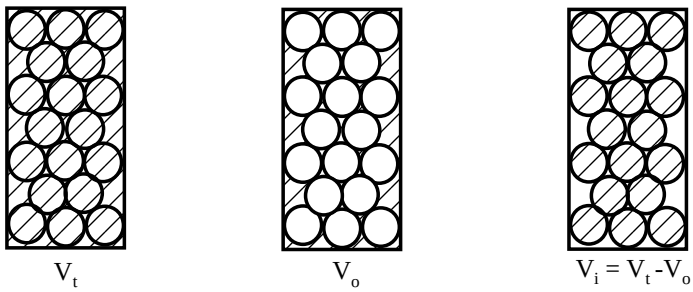

Figure 2.12: *Diagrammatic representation of V_t, V_o and V_i for a gel filtration column.*

To determine the oligomeric state of human brain QPRTase in solution, a series of protein standards of known molecular weight were passed through the gel filtration column and for each the elution volume (V_e) and hence K_{av} were determined (Table 2.1). The data were used to construct a calibration graph of K_{av} versus molecular weight (Figure 2.13).

Protein	**Molecular Weight (kDa)**	**Elution Volume (V_e, mL)**	**K_{av}**
SBTI	21	19.1	0.72
Carbonic anhydrase	29	18.7	0.70
DA	40	18.0	0.65
BSA	66	17.4	0.62
Alcohol dehydrogenase	150	16.5	0.56
β-amylase	200	15.9	0.52

Table 2.1: *Elution volume and K_{av} determined for a series of proteins of known molecular weight.*

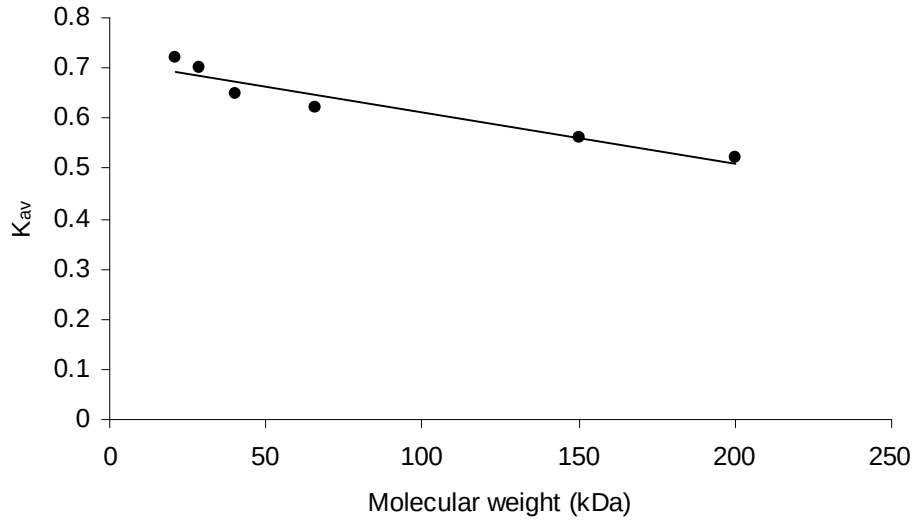

Figure 2.13: *Gel filtration calibration graph of K_{av} versus molecular weight (Protein standards: SBTI (21 kDa), carbonic anhydrase (29 kDa), DA (40 kDa), BSA (66 kDa), alcohol dehydrogenase (150 kDa) and β-amylase (200 kDa)).*

Next, a sample of pure human brain QPRTase was passed through the column in 50 mM KH_2PO_4/K_2HPO_4 buffer at pH 7.2. The resulting UV detector trace showed a single symmetrical peak, indicating human brain QPRTase exists in a single oligomeric state in solution. As before, the elution volume (V_e = 16.2 mL) and K_{av} (0.54) were determined. From the calibration graph, the K_{av} value corresponds to a protein with a molecular weight of approximately 174 kDa. This most closely resembles the molecular weight of the human brain QPRTase hexamer (Table 2.2).

QPRTase oligomer	Molecular weight (kDa)
Monomer	30.9
Dimer	61.9
Hexamer	185.6
Dodecamer	371.3

Table 2.2: *Molecular weights of possible QPRTase oligomers.*

Therefore it would appear that human brain QPRTase also exists as a hexamer in solution. This is consistent with QPRTase from other mammals, such as hog[14] and rat,[15] where hexameric QPRTase structures have also been reported. In contrast, *Mycobacterium tuberculosis* QPRTase was found to exist as a dimer during gel filtration under physiological conditions, which is consistent with the instability of the hexamer observed in the crystal structure.[7] The hexameric form observed in the crystal structure of *Mycobacterium tuberculosis* QPRTase may be a result of the high protein concentrations and ionic strengths used in crystallisation.

Human brain QPRTase however, was found to exist as a stable hexamer in both the crystal structure and during gel filtration under physiological conditions.

Similarly, HISTEV-QPRTase was found to exist as a hexamer during gel filtration under the same conditions (K_{av} = 0.51). Therefore, it can be concluded that the presence of the histidine tag does not affect the oligomeric state of the protein.

2.3.3 Characterisation of protein conformation by circular dichroism

Circular dichroism (CD) is a sensitive spectroscopic technique that can be used to characterise protein conformation. CD gives information about the unequal absorption of left- and right-handed circularly-polarised light by optically active molecules. Optical activity originates in the absorption bands of asymmetric compounds. The absorption coefficients for left and right circularly-polarised light are different if the electrons participating in the transition to the excited state sense an asymmetric environment.

Proteins are optically active because they are asymmetric. Two kinds of asymmetry are present in proteins, configurational and conformational. Amino acid residues other than glycine have intrinsic optical activity because of the L-configuration at their α-carbon atom. Threonine and isoleucine possess an additional asymmetric centre. Electronic interactions between different residues in a protein also contribute to optical activity. The right-handed screw sense of an α-helix, for example, gives rise to a large conformational contribution to optical activity.

CD has become a standard technique to measure the optical activity of proteins. CD bands of proteins occur in two spectral regions. The far-UV region (180 – 260 nm) is dominated by contributions of the peptide bonds, whereas CD bands in the near-UV region (260 – 320 nm) originate from aromatic amino acids. In addition, disulfide bonds give rise to several CD bands in the near-UV region. The two spectral regions give different kinds of information about protein structure.

The CD in the far-UV region reports on the backbone structure of a protein and is used to characterise the secondary structure and changes therein. Measurements of synthetic polypeptides and proteins of known structure have defined the CD spectra of α-helices, β-structure motifs and random coils (Figure 2.14).[16]

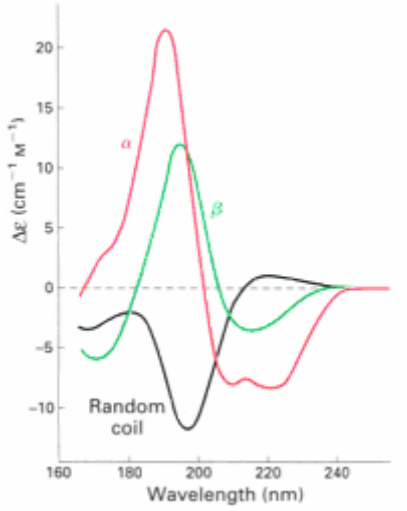

Figure 2.14: *CD spectra of an α-helix (red), β-pleated sheets (green) and random coil region (black).*[17]

CD data in the far-UV region can be used to determine the relative amounts of the different secondary structure elements of a protein. The α-helix makes a dominant contribution with negative CD bands at 208 nm and 222 nm and a positive band at 192 nm (Figure 2.14). A randomly arranged polypeptide chain, by contrast, has a negative CD band centred at 199 nm. Estimates of the α-helix content of proteins derived from CD spectra agree well with values obtained from X-ray crystallographic studies. The content of β-structures can also be estimated from CD spectra but the uncertainty is greater because β-structures are less regular than the α-helices and contribute less to the CD spectrum.

CD bands in the near-UV region (260 – 320 nm) originate from aromatic amino acids and are observed when, in a folded protein, aromatic side chains are immobilised in an asymmetric environment. The CD of the aromatic residues is virtually zero in the absence of ordered structure. The signs and wavelengths of the aromatic CD bands cannot be calculated; they depend on the immediate structure and electronic environment of the immobilised chromophores. Therefore the individual peaks in the very complex near-UV CD spectrum of a protein cannot be assigned to transitions in the vicinity of specific amino acid side chains. However, the near-UV CD spectrum represents a highly sensitive criterion for the native state of a protein. It can thus be used as a fingerprint of the correctly folded conformation.

The near-UV (260-320 nm) CD spectra of QPRTase and HISTEV-QPRTase were measured using a Jasco J-8.10 spectropolarimeter (Figure 2.15). By comparing the CD spectra of QPRTase and HISTEV-QPRTase, it can be seen that CD bands of the same sign and magnitude were observed at the same wavelengths in both spectra. Therefore, it can be concluded that the presence of the histidine tag does not cause gross changes in enzyme structure.

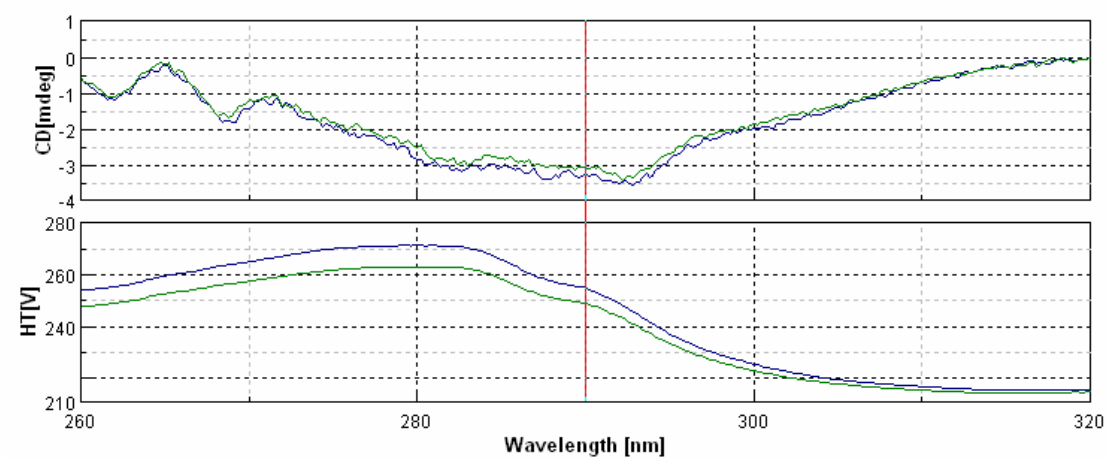

Figure 2.15: *Near-UV CD spectra of QPRTase (green) and HISTEV-QPRTase (blue) measured using a Jasco J-8.10 spectropolarimeter (Band width, 1nm; Response, 1 s; Data pitch, 0.2 nm; Scanning speed, 20 nm/min; Accumulation, 4; Cell length, 0.5 cm; Solvent, 50 mM potassium phosphate buffer; Concentration, 1 mg/mL; Temperature, room temperature).*

2.4 Kinetic studies on wild-type human brain QPRTase

2.4.1 Introduction

2.4.1.1 Assays for the measurement of QPRTase activity

QPRTase is an intriguing enzyme which appears to catalyse two distinct chemical reactions; the Mg^{2+}-dependent transfer of a phosphoribosyl moiety from PRPP **15** to the nitrogen of quinolinic acid **10** and decarboxylation at the 2-position to give nicotinic acid mononucleotide (NAMN, **11**) (Scheme 2.2).

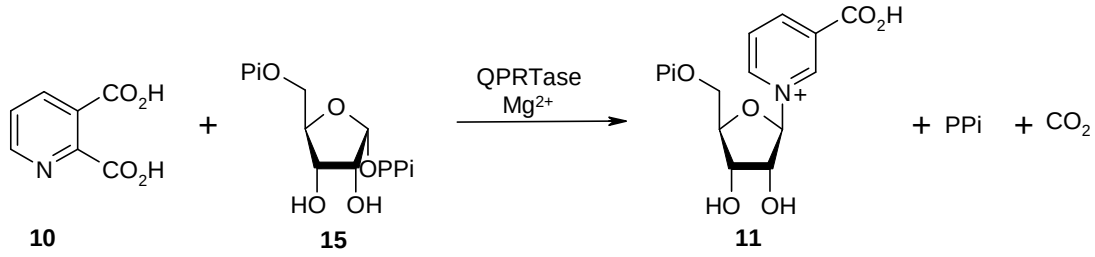

Scheme 2.2: *QPRTase catalysed reaction.*

A number of assays have been developed for the measurement of QPRTase activity including a radioactive assay which monitors the loss of ^{14}C-carbon dioxide from ^{14}C-labelled quinolinic acid,[18] an HPLC assay which measures the formation of NAMN[19] and two different spectrophotometric assays.[20,21] The first spectrophotometric assay involves the determination of a cyanide adduct formed by NAMN.[20] Following the QPRTase reaction, cyanide is added to react with NAMN **11** and generate a molecule which is more UV active and therefore easier to measure at low concentrations. However, a significant disadvantage of this assay is that the kinetic data are deduced from only single point measurements. Furthermore, the toxicity of cyanide makes the assay problematic. The second spectrophotometric assay that has been reported for the measurement of QPRTase activity is a continuous UV assay based on the difference in extinction coefficients between quinolinic acid **10** and NAMN **11** at 266 nm ($\Delta\varepsilon_{266}$ = 920 $M^{-1}cm^{-1}$).[21] This assay involves measuring the change in absorbance at this wavelength over a 30 minute period at 37 ºC and therefore allows continuous measurement of product formation.

Previously in our laboratory,[10] an HPLC assay was initially employed to confirm the over-expressed human brain QPRTase was active. Steady-state kinetic analysis was then carried out using a continuous spectrophotometric assay which monitored the appearance of product.[21] This involved measuring the change in absorbance at 266 nm over a 30 minute period, at 37 ºC. Each reaction was initiated by the addition of QPRTase. A typical UV trace for the conversion of quinolinic acid to NAMN by QPRTase is shown in Figure 2.16. From this plot, the change in absorbance, the change in concentration of NAMN and hence the rate of product formation can be determined. The slight delay in NAMN formation was observed from 0 to 3 minutes in every assay and therefore the rate of formation of NAMN was measured from this point.

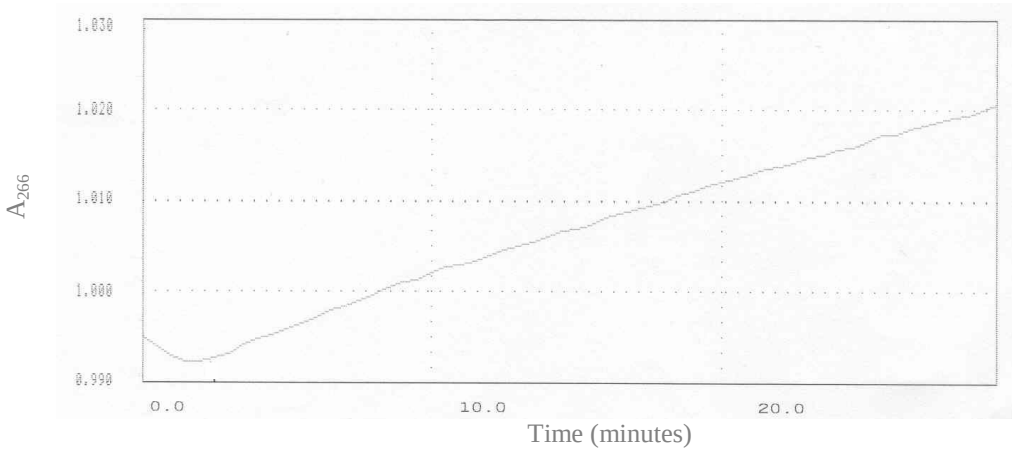

Figure 2.16: *Typical UV trace for the conversion of quinolinic acid to NAMN by QPRTase.*

The cyanide based UV assay was also examined as a way of measuring the activity of human brain QPRTase. In previous studies, the two spectrophotometric assays were found to give very similar kinetic results and the kinetic parameters determined were comparable to literature values reported for QPRTase from other sources.[10] Therefore the continuous spectrophotometric assay was selected as the assay of choice for all kinetic studies due to its simplicity and convenience.

2.4.1.2 Summary of the initial kinetic characterisation of human brain QPRTase

Previously in our laboratory,[10] the kinetic parameters K_m and V_{max} for quinolinic acid were determined at 0.1 mM PRPP and were found to be 21.6 ± 3.0 μM and 1.19 ± 0.05 μM min^{-1}, respectively. The specific activity was found to be 0.09 μmol min^{-1} mg^{-1}, which is of the same order of magnitude as data reported for other QPRTases.[21-23] The kinetic data for quinolinic acid were re-measured at different PRPP concentrations and a small decrease in K_m and a large increase in V_{max} were observed with increasing PRPP concentration up to 0.1 mM. The double reciprocal plots for these data were observed to intersect to the left of the *y*-axis, which indicated that the affinity of QPRTase for quinolinic acid is independent of the PRPP concentration (Figure 2.17). This suggested that quinolinic acid binds to QPRTase before PRPP.

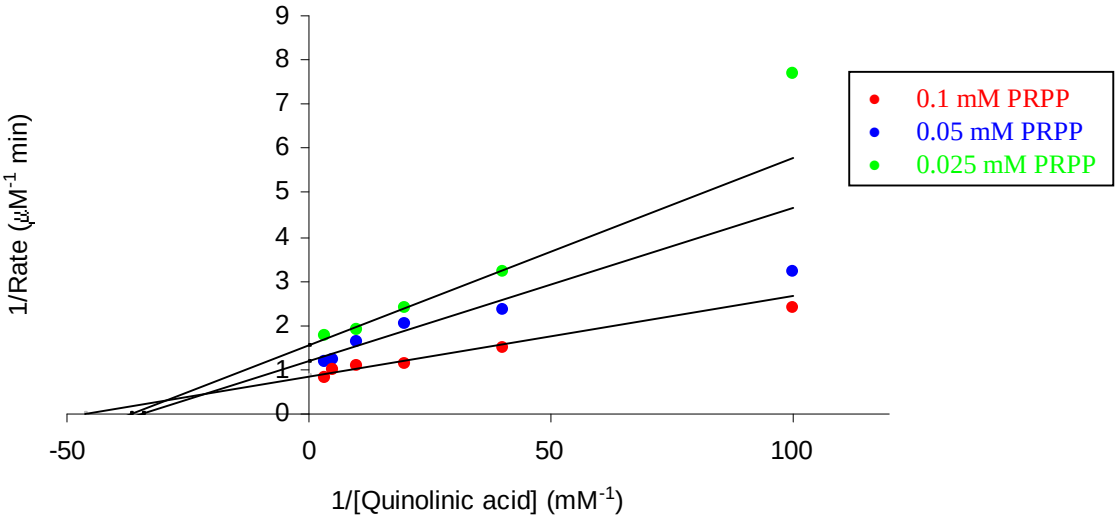

Figure 2.17: *Lineweaver-Burk plot for quinolinic acid as the variable substrate.*

Kinetic studies with PRPP as the variable substrate, with quinolinic acid fixed at 0.3 mM, showed pronounced substrate inhibition above 0.3 mM. However, taking measurements in the range 0.01 to 0.3 mM, PRPP gave a K_m of 23.2 ± 3.6 μM and V_{max} of 0.93 ± 0.03 μM min^{-1}. When the kinetic data for PRPP were re-measured at different quinolinic acid concentrations, K_m for PRPP was found to decrease as the quinolinic acid concentration was increased while V_{max} was unchanged (Figure 2.18).

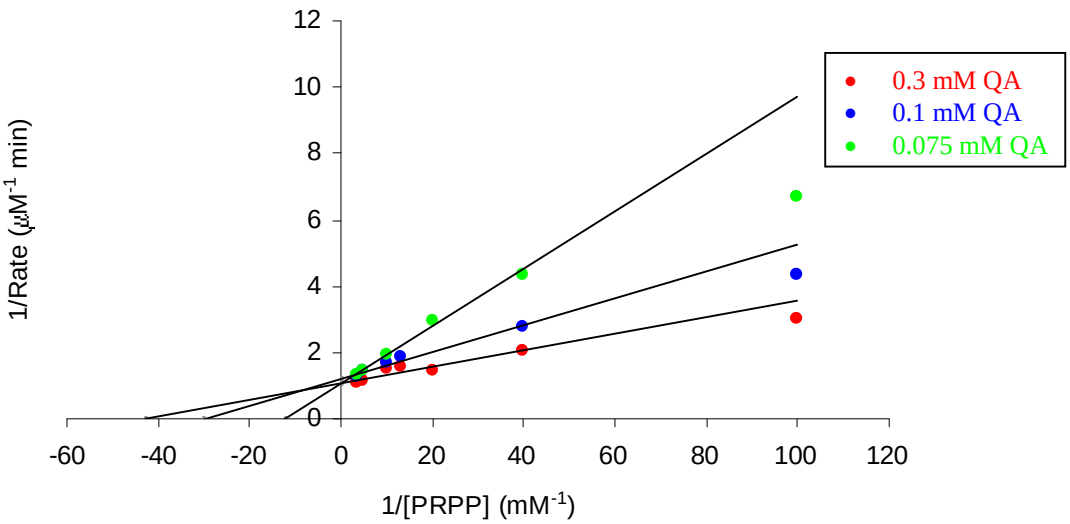

Figure 2.18: *Lineweaver-Burk plot for PRPP as the variable substrate.*

Thus, it would appear that the quinolinic acid concentration affects the distribution of enzyme species which can bind PRPP. Ultimately increased quinolinic acid concentrations lead to increased levels of the QPRTase:quinolinic acid complex. The increased affinity for PRPP observed at high quinolinic acid concentrations suggests increased affinity for PRPP for the QPRTase:quinolinic acid complex, thus implying that for human brain QPRTase the catalytic mechanism requires quinolinic acid to bind to the enzyme before PRPP. Overall, the kinetic data were clearly characteristic of an equilibrium ordered binding mechanism, which is similar to that observed for the *Salmonella typhimurium* enzyme.[21]

The substrate inhibition observed with PRPP was then investigated in more detail by determining the K_m and V_{max} for quinolinic acid at high levels of PRPP. It was found that as the PRPP concentration was increased from 0.3 mM to 5 mM, the K_m with respect to quinolinic acid increased while the V_{max} decreased. Thus, above 0.3 mM PRPP mixed inhibition was observed. Substrate inhibition by PRPP was also observed for the *Salmonella typhimurium* enzyme by Grubmeyer *et al.* and this was explained by the formation of a dead-end QPRTase:PRPP complex (section 1.5).[21] The formation of a dead-end QPRTase:PRPP complex would result in competitive inhibition, as was observed for the bacterial enzyme. However, for human QPRTase mixed inhibition was observed. The occurrence of mixed inhibition suggests that

PRPP not only binds to an active site (competitive) but also to a second site which perturbs and inhibits the active site (noncompetitive).

Thus the observed kinetics of the human enzyme[10] appear to be more complex than the kinetics of the bacterial enzymes. The hexameric structure recently established in both the solid state and in solution for human brain QPRTase offers a possible explanation for the complex kinetics this enzyme exhibits. The human QPRTase hexamer is a very intimate structure in which every subunit makes contact with four other monomers. Within the dimer, the active sites are separated by 35 Å. However, the hexameric arrangement means the active sites from different dimers are much closer to each other. The extensive contacts in the human brain QPRTase hexamer provide a structural route for information from one dimer to be transmitted to another. Changes in the active site structure in response to PRPP binding in one dimer (AB) could be transmitted across this interface to another dimer (CD). Thus when PRPP binds to the monomer A active site as well as blocking the quinolinic acid binding site in monomer A (competitive inhibition) it could additionally inhibit catalysis in monomer C (noncompetitive inhibition). This phenomenon may be the result of a regulatory mechanism for human brain QPRTase.

Although the crystal structure of the *Mycobacterium tuberculosis* enzyme reported a hexamer in the asymmetric unit, the bacterial enzymes are known to be dimeric in solution.[7] The hexamer seen in human brain QPRTase is unrelated to that seen in the crystal of *Mycobacterium tuberculosis* QPRTase. Examination of the *Mycobacterium tuberculosis* QPRTase hexamer suggested it was simply an artefact of crystal packing. The bacterial enzymes show only competitive inhibition by PRPP and show no cooperativity.[21] This reinforces the idea that the complex kinetics observed for human QPRTase are a consequence of the hexameric structure this enzyme adopts.

2.4.2 Kinetic characterisation of QPRTase and HISTEV-QPRTase

For QPRTase, the kinetic parameters K_m and V_{max} for substrate quinolinic acid were determined by employing the continuous spectrophotometric assay to measure the rate of the enzymatic reaction at a range of different quinolinic acid concentrations at a fixed concentration of PRPP (0.1 mM). The initial rate data were fitted to the Michaelis-Menten equation using non-linear regression with GraphPad Prism 3 software (Figure 2.19). K_m and V_{max} for quinolinic acid were determined as 13.4 ± 1.0 μM and 0.92 ± 0.01 μM min^{-1}, respectively, which are comparable to the values determined previously in our laboratory. The value determined for K_m is within the range of K_m values reported by Calvo *et al.* for QPRTase isolated from various sources (6 – 19 μM)[24] and in particular is comparable to the value of 12 μM reported for rat liver and rat brain.[15]

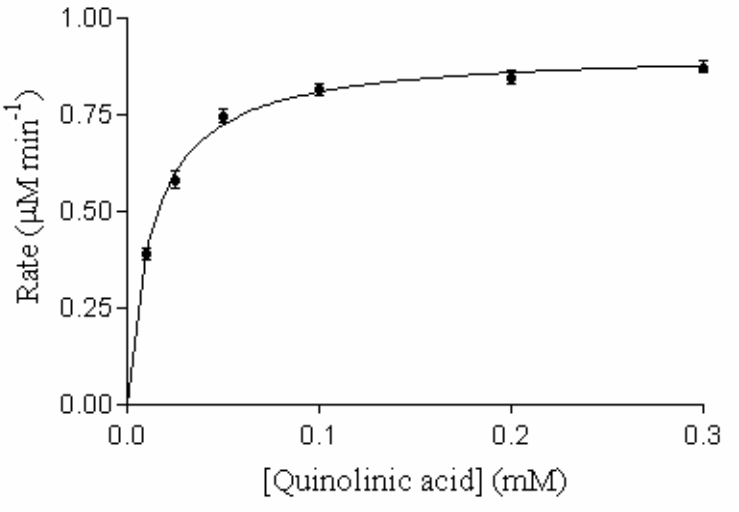

Figure 2.19: *Non-linear regression plot of QPRTase for quinolinic acid as the variable substrate.*

To determine whether the presence of the histidine tag affects the function of the protein, the kinetic parameters K_m and V_{max} for substrate quinolinic acid were also determined for pure HISTEV-QPRTase under the same conditions. The initial rate data were fitted to the Michaelis-Menten equation using non-linear regression with GraphPad Prism 3 software (Figure 2.20). K_m and V_{max} for quinolinic acid were determined as 13.1 ± 1.9 μM and 0.93 ± 0.03 μM min^{-1}, respectively.

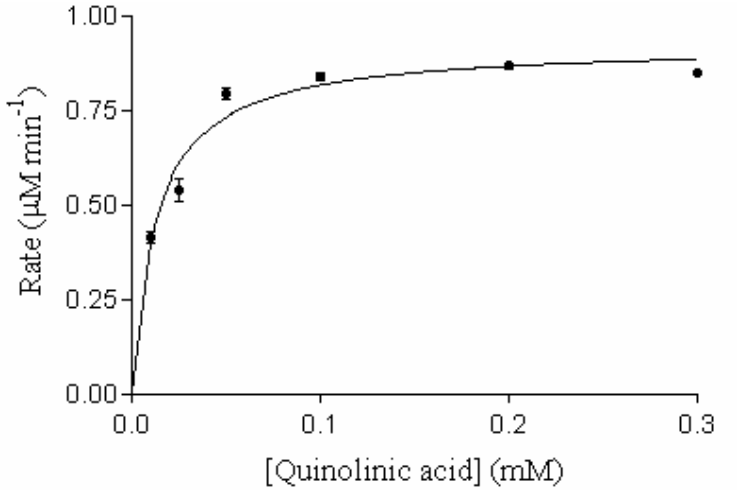

Figure 2.20: *Non-linear regression plot of HISTEV-QPRTase for quinolinic acid as the variable substrate.*

By comparing the kinetic parameters determined for QPRTase and HISTEV-QPRTase for the substrate quinolinic acid it can be concluded that the presence of the histidine tag does not affect the substrate binding or the catalytic efficiency of the enzyme (Table 2.3). It appears that the histidine tag is far enough removed from the active site such that it does not interfere with substrate binding and the subsequent reaction. Furthermore, the gel filtration and circular dichroism experiments showed the solution structure of QPRTase is unaffected by the presence of the histidine tag.

Protein	**K_m (μM)**	**V_{max} (μM min^{-1})**
QPRTase	13.4 ± 1.0	0.92 ± 0.01
HISTEV-QPRTase	13.1 ± 1.9	0.93 ± 0.03

Table 2.3: *Comparison of the kinetic parameters determined for QPRTase and HISTEV-QPRTase with respect to quinolinic acid as the variable substrate.*

The observation that the presence of the histidine tag has no effect on the enzyme kinetics means that the histidine tag does not have to be cleaved from the enzyme used in kinetic studies. This will increase the amount of protein available for kinetic studies and also reduce the time required to obtain the protein since the need for the troublesome TEV digestion step and the second nickel column will be eliminated. HISTEV-QPRTase was used in the nucleotide inhibition study described in Chapter 3.

2.4.3 Examination of cooperativity in quinolinic acid binding

Human brain QPRTase has a hexameric structure composed of six identical subunits and containing six identical active sites. As can be seen in Figure 2.21, the saturation curve for QPRTase with respect to quinolinic acid as the variable substrate is hyperbolic. This suggests that quinolinic acid does not bind cooperatively to QPRTase since, generally, if there is cooperative binding then the saturation curve will be sigmoidal rather than hyperbolic.

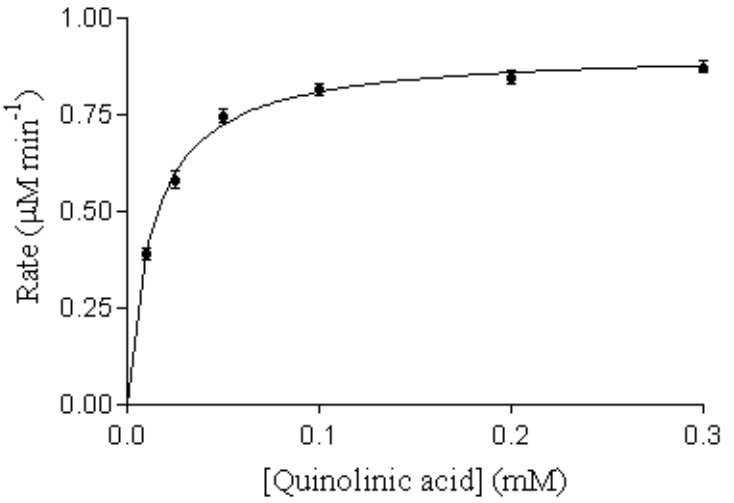

Figure 2.21: *Non-linear regression plot of QPRTase for quinolinic acid as the variable substrate.*

Construction of a Hill plot allows quantitative analysis of cooperativity.[25] The Hill plot is a logarithmic form of the Hill equation, the simplified rate equation for allosteric enzymes.

$$\log \frac{V}{V_{max} - V} = n\log[S] - \log K'$$

The Hill coefficient, n, is a central parameter in the study of ligand-protein interactions which measures the degree of cooperativity between subunits that bind the ligand in multi-subunit enzymes. A coefficient of 1 indicates completely independent binding, regardless of how many additional ligands are already bound. A coefficient of greater than 1 indicates a positively cooperative reaction. The number of n increases with the degree of cooperativity; the maximum number of n is equal to

the number of binding sites. A coefficient of less than 1 indicates a negatively cooperative reaction. The Hill constant K' comprises the intrinsic dissociation constant K_s and interaction factors and provides an estimate of the affinity of the enzyme for a particular substrate.

Hill plots can be constructed by plotting log $(V/(V_{max}-V))$ versus log [S]. The plot gives a straight line with a slope of n. Thus, the Hill coefficient, n, can be read directly from the plot. The Hill plot for QPRTase with respect to quinolinic acid as the variable substrate is shown in Figure 2.22. The plot is linear with a slope of approximately 1, which again suggests quinolinic acid does not bind cooperatively to the subunits of QPRTase.

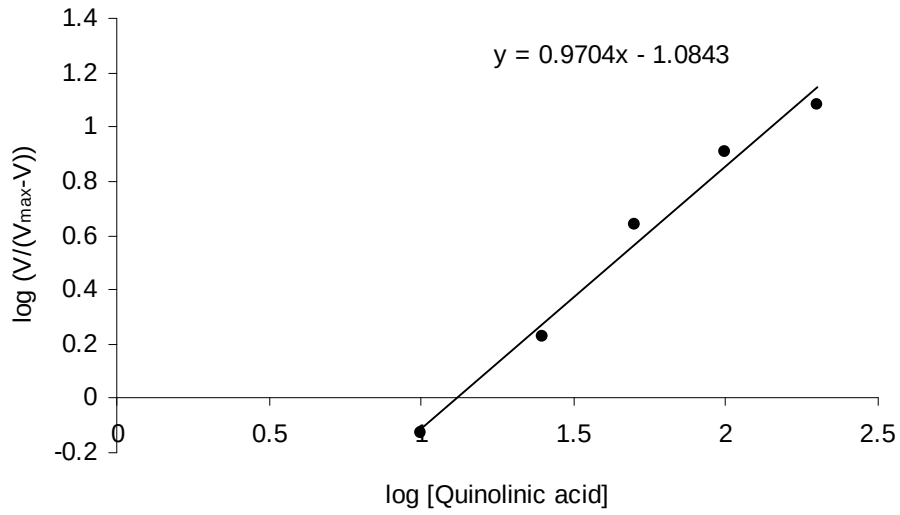

Figure 2.22: *Hill plot for QPRTase with respect to quinolinic acid as the variable substrate.*

2.4.4 pH dependency of human brain QPRTase

The pH rate profile for human brain QPRTase was determined by measuring the rate of the enzymatic reaction in a series of 50 mM K_2HPO_4/KH_2PO_4 buffers of varying pH. The pH dependency of human brain QPRTase can be seen in graphical form in Figure 2.23.

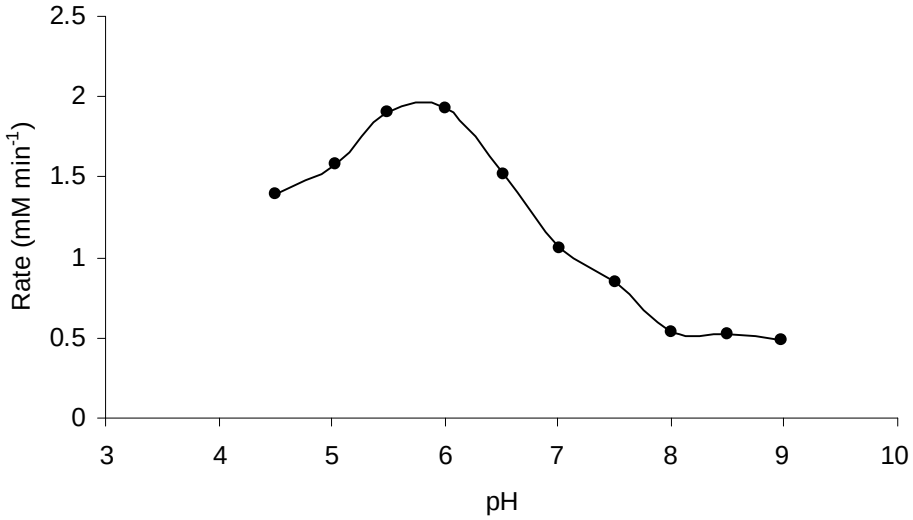

Figure 2.23: *pH dependency of purified human brain QPRTase*

From Figure 2.23, it can be seen that the activity of human brain QPRTase increases with increasing pH from pH 4.5 to a maximum activity of 1.93 μM min^{-1} at approximately pH 6. Above pH 6 the rate of the enzymatic reaction decreases fairly rapidly, and then above pH 8 the rate decrease is much slower. It is interesting that the optimum pH for enzyme activity is lower than physiological pH. However, this is consistent with human liver QPRTase which showed a maximum activity at approximately pH 6.5.[26] Similarly, the pH optimum of hog liver QPRTase was found to be pH 6.1.[27]

2.4.5 Solvent isotope effect studies

Isotope effects are caused by the substitution of a light atom for a heavier one. A kinetic isotope effect is the ratio of the reaction rates for molecules containing the light and heavy atoms, i.e. k_H/k_D. Over the last 20 years, the measurement of isotope effects has emerged as one of the most powerful techniques available for the elucidation of the chemical mechanisms of enzyme catalysed reactions.[28] The measurement of isotope effects can provide useful information regarding the identity of the rate-limiting step for a reaction. Also, it is possible to distinguish stepwise from concerted reactions, and, for stepwise reactions, the order of the steps and the nature of the intermediate can be determined. In addition, isotope effects can be used to deduce the nature of the active site catalytic residues. Furthermore, the determination of the intrinsic isotope effects gives a means of deducing the transition state structure.

In the case of QPRTase, kinetic isotope effects can be used to assess the relative kinetic importance of the two chemical steps, phosphoribosyl transfer and decarboxylation. Since reprotonation of the putative ylide intermediate **18**, that is formed immediately following decarboxylation of QAMN **16**, may be kinetically important (Scheme 2.3), solvent deuterium isotope effects were measured in order to determine if the proton transfer is rate limiting.

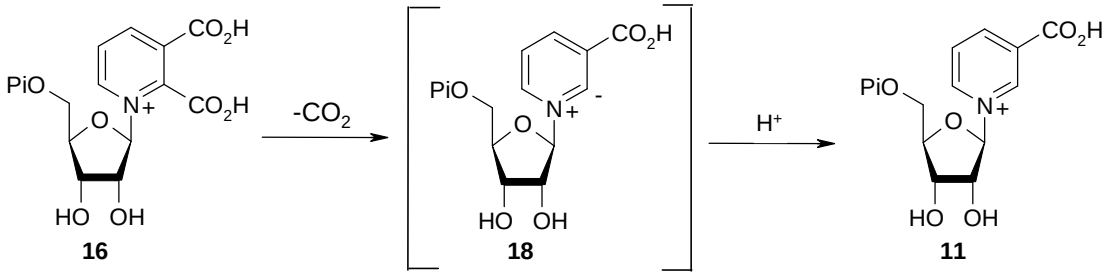

Scheme 2.3: *Decarboxylation of quinolinic acid mononucleotide.*

An important part of solvent isotope effect studies is the accurate preparation of buffers. It is essential to use equivalent buffers in H_2O and D_2O. This was achieved by keeping the concentrations of all the solutes constant, including the acid-base pair acting as the buffer and all the electrolytes. During the preparation of buffers, the D_2O solutions should not be exposed to atmospheric moisture. To avoid this, the

buffer solutions were prepared under a nitrogen atmosphere. In addition, to prevent the lowering of the % D content of the final solution the buffer solutes were lyophilised from D_2O twice to allow proton-deuterium exchange of all exchangeable protons. Measurement of the pL (L = H or D) of the solution was carried out using a normal glass pH electrode. Again, to prevent dilution of the % D in the buffer the electrode was washed in a small amount of D_2O prior to measuring the pD of the D_2O buffer solutions. As there is an actual solvent isotope effect on the electrode response,[29] the pD was then calculated using the following equation:

$$pD = \text{meter reading} + 0.4$$

In addition, the substrates, quinolinic acid and PRPP, were lyophilised from D_2O to allow the exchange of all the acidic protons for deuterium prior to preparation of the stock solutions in the freshly prepared D_2O buffer.

The isotope effects were measured at a high concentration of quinolinic acid (0.3 mM), so essentially under saturating conditions. Therefore, it is the isotope effect on V_{max} that is measured. The solvent isotope effects were determined by measuring the rate of the enzymatic reaction in equivalent 50 mM potassium phosphate buffers in H_2O and D_2O at three points on the pL rate profile (L = H or D). The rates were measured in triplicate. The results obtained at pL 7.2 indicate a small normal isotope effect (k_H/k_D = 1.16) whereas small inverse isotope effects were observed at pL 6.3 (k_H/k_D = 0.85) and pL 5.3 (k_H/k_D = 0.90). In order to confirm the small inverse isotope effects at pL 6.3 and pL 5.3, fresh buffers were prepared and the measurement of the isotope effects were repeated. As before, small inverse isotope effects were observed.

It is unclear why a normal isotope effect ($k_H/k_D > 1$) was observed at pL 7.2 while inverse isotope effects ($k_H/k_D < 1$) were measured closer to the optimum pL for enzymatic activity. However, what can be concluded from the results obtained is that the proton transfer is not rate limiting. If the reprotonation of the ylide **18** was clearly rate limiting then the magnitude of the isotope effect may be as high as 8, and even if the proton transfer was only partially rate limiting then an isotope effect of 3-4 would

be expected.[28] The results therefore suggest that the ylide intermediate **18** is unstable and is rapidly protonated to form the product, nicotinic acid mononucleotide **11**.

The observed isotope effects are small enough to be a result of small, non-specific effects on enzyme structure. Therefore, it is not possible to make any useful mechanistic conclusions from this set of data, apart from the implication the proton transfer is not rate limiting.

2.4.6 Measurement of QPRTase activity

The continuous spectrophotometric assay used in this study to measure the activity of QPRTase was found to be very reliable and provided reproducible data. However, as can be seen from the typical UV trace for the conversion of quinolinic acid to nicotinic acid mononucleotide by QPRTase (Figure 2.24), the absorbance at 266 nm does not increase linearly during the entire 30 minute period over which the assay is run. A curving of the graph is observed over the first few minutes of reaction before A_{266} increases linearly over the remainder of the time. This has always been observed in the UV trace resulting from this assay but the cause is unknown.

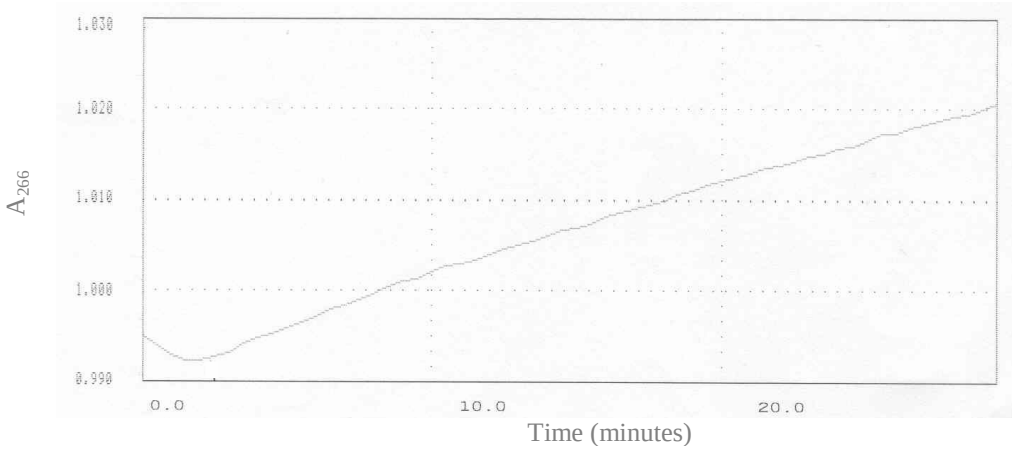

Figure 2.24: *Typical UV trace for the conversion of quinolinic acid to NAMN by QPRTase.*

To investigate the effect of enzyme concentration on the extent of the curving, the UV assay was performed at a range of different QPRTase concentrations. It was found that the extent of the curving decreased slightly as the enzyme concentration increased but was not eradicated.

In the standard UV assay, the reaction is initiated by addition of QPRTase. It was found that reversing the order of addition i.e. adding the enzyme before the substrates, had no significant effect on the resulting UV trace.

QPRTase appears to catalyse two distinct chemical reactions and one hypothetical explanation for the appearance of the UV trace was that the initial decrease in absorbance may occur as quinolinic acid undergoes rapid phosphoribosyl transfer to form the intermediate quinolinic acid mononucleotide. The linear increase in absorbance that follows could then be due to the slow decarboxylation of this intermediate to form the nicotinic acid mononucleotide. However, the initial curving of the UV trace was observed when QPRTase was incubated with the inhibitor phthalic acid in the absence of quinolinic acid, which rules out this possibility since phthalic acid **25** has no heterocyclic nitrogen atom for reaction (Figure 2.25).

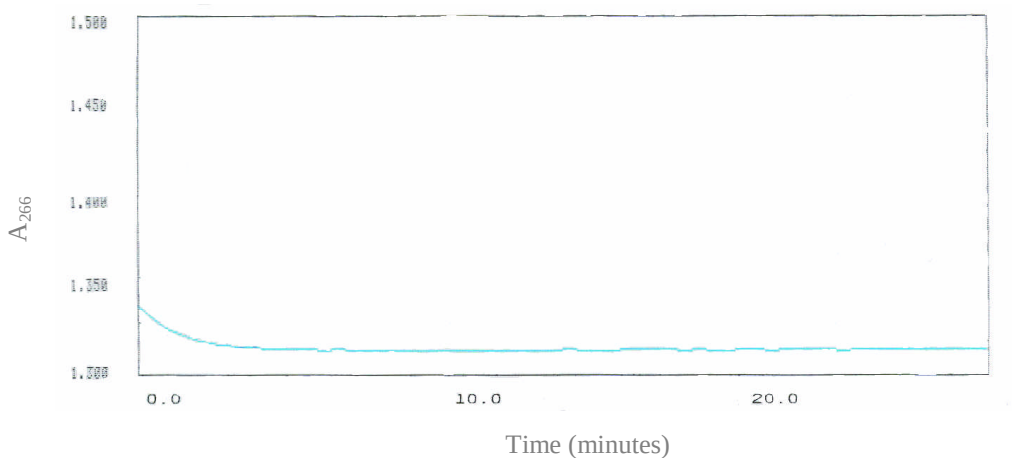

Figure 2.25: *UV trace for the incubation of phthalic acid with QPRTase.*

The cause of the initial curving of the UV trace remains unknown. It is possible that it is caused by a mixing effect or perhaps by protein reorganisation. However, the assay provides reliable and reproducible data and the kinetic parameters determined using this assay were comparable to literature values for QPRTase from other sources.

2.5 Summary

Human brain QPRTase was successfully expressed in *E. coli* BL21 (DE3) from the pEHISTEV-QPRTase construct and the protein was efficiently purified by nickel affinity chromatography. The purified protein was isolated in a yield of 8 mg per litre culture.

In the crystal structure, human brain QPRTase was found to adopt an energetically stable hexameric arrangement in which each subunit makes extensive contacts with four other monomers. The enzyme was also found to exist as a hexamer during gel filtration under physiological conditions.

The structural studies enabled identification of the active site residues. The active site is a deep pocket with a highly positive electrostatic surface composed of three arginine residues, two lysine residues and one histidine residue. The quinolinic acid binding site was occupied by a molecule of tartrate, which was present in the precipitant used to crystallise the protein.

Kinetic studies allowed the measurement of the kinetic parameters for quinolinic acid. The data gave a K_m of 13.4 ± 1.0 μM and a V_{max} of 0.92 ± 0.01 μM min^{-1}. There was no evidence for cooperative binding of quinolinic acid to the six subunits of the QPRTase hexamer. Previous kinetic studies on human brain QPRTase showed pronounced substrate inhibition by PRPP at high concentrations. The mixed inhibition observed suggested that PRPP not only binds to an active site (competitive) but also to a second site which perturbs and inhibits the active site (noncompetitive). The hexameric structure observed for human brain QPRTase offers a possible explanation for the complex kinetics this enzyme exhibits. However, no apparent cooperativity was observed between sites for quinolinic acid binding.

It was found that the presence of the histidine tag does not affect the protein folding, the oligomeric state of the protein or the enzymatic activity. The observation that the presence of the histidine tag has no effect on the enzyme kinetics means that it does not have to be cleaved from the enzyme used in kinetic studies.

2.6 Further work

Crystallisation of the QPRTase-quinolinic acid complex would provide valuable information about the active site as well as any structural changes which occur during substrate binding. Firstly, due to the presence of tartrate in the active site, crystallisation of QPRTase should be carried out using an alternative precipitant, such as acetate, propionate or possibly quinolinic acid itself. The use of quinolinic acid as the precipitant would allow direct access to the QPRTase-quinolinic acid complex. Acetate or propionate should not bind as tightly in the active site as tartrate since they lack the 1,2-dicarboxylic acid functionality. If crystals were generated under these conditions then soaking experiments could be undertaken to access the complexes of QPRTase with the substrates, products and inhibitors. If acetate or propionate molecules did bind to the active site, displacement by substrate or inhibitor should be easier due to the lower affinity for the enzyme. The availability of the crystal structures of QPRTase with and without its substrates and products would provide a detailed perspective for the active site interactions in pre-catalytic, catalytic and post-catalytic stages of the enzyme.

Further kinetic isotope effect studies should be undertaken to examine the ^{13}C isotope effect for the decarboxylation step. This would not require the synthesis of labelled substrates and could be measured using natural abundance material.[30] From measurements of the variation in the $^{13}C/^{12}C$ ratio of the carbon dioxide produced as the reaction proceeds, using dual-isotope ratio mass spectrometry, the ^{13}C isotope effect can be measured with a high degree of accuracy. In addition, measurement of the ^{13}C isotope effect in D_2O could be used to investigate the relative timing of O-H and C-C bond cleavage during decarboxylation.

2.7 References

1. K. Iwai and H. Taguchi, *J. Nutr. Sci. Vitaminol.*, 1973, **19**, 491-499.
2. D.F. Mann and R.U. Byerrum, *J. Biol. Chem.*, 1974, **249**, 6817-6823.
3. H. Taguchi and K. Iwai, *Biochim. Biophys. Acta*, 1976, **422**, 29-37.
4. K. Shibata and K. Iwai, *Biochim. Biophys. Acta*, 1980, **611**, 280-288.
5. K. Shibata and K. Iwai, *Agric. Biol. Chem.*, 1980, **44**, 301-308.
6. K. Hughes, A. Dessen, P. Gray and C. Grubmeyer, *J. Bacteriol.*, 1993, **175**, 479-486.
7. V. Sharma, C. Grubmeyer and J.C. Sacchettini, *Structure*, 1998, **6**, 1587-1599.
8. T. W. Stone and M.N. Perkins, *Eur. J. Pharmacol.*, 1981, **72**, 411-412.
9. S.I. Fukuoka, C.M. Nyaruhucha and K. Shibata, *Biochim. Biophys. Acta*, 1998, **1395**, 192-201.
10. K. Woznica, *PhD Thesis*, University of St Andrews, St Andrews, 2004.
11. J. Porath, J. Carlsson, I. Olsson and G. Belfrage, *Nature*, 1975, **258**, 598-599.
12. E. Hochuli, H. Dobeli and A. Schacher, *J. Chromatogr.*, 1987, **411**, 177-184.
13. M.M. Bradford, *Anal. Biochem.*, 1976, **72**, 248-254.
14. K. Iwai and H. Taguchi, *Biochem. Biophys. Res. Commun.*, 1974, **56**, 884-891.
15. E. Okuno and R. Schwarcz, *Biochim. Biophys. Acta*, 1985, **841**, 112-119.
16. W.C. Johnson, *Protein Struct. Funct. Genet.*, 1990, **7**, 205-214.
17. L. Stryer, *Biochemistry*, Fourth Edition, W.H. Freeman and Company, New York, 1995, 63.
18. A.C. Foster, W.C. Zinkand and R. Schwarz, *J. Neurochem.*, 1985, **44**, 446-453.
19. K. Shibata, T. Fukuwatari and E. Sugimoto, *J. Chromatogr. B*, 2000, **749**, 281-285.
20. L. Kalikin and K.C. Calvo, *Biochem. Biophys. Res. Commun.*, 1988, **152**, 559-564.
21. H. Cao, B.L. Pietrak and C. Grubmeyer, *Biochemistry*, 2002, **41**, 3520-3528.
22. C. Kohler, L.G. Eriksson, P.R. Flood, J.A. Hardie, E. Okuno and R. Schwarcz, *J. Neurosci.*, 1988, **8**, 975-987.

23. J.C. Eads, D. Ozturk, T.R. Wexler, C. Grubmeyer and J.C. Sacchettini, *Structure*, 1997, **5**, 47-58.
24. R. Bhatia and K.C. Calvo, *Arch. Biochem. Biophys.*, 1996, **325**, 270-278.
25. A.V. Hill, *J. Physiol.*, 1910, **40**, 4-7.
26. E. Okuno, R.J. White and R. Schwartz, *J. Biochem.*, 1988, **103**, 1054-1059.
27. K. Iwai, K. Shibata, H. Taguchi and T. Ikatura, *Agric. Biol. Chem.*, 1979, **43**, 345-350.
28. N.P. Botting, *Nat. Prod. Rep.*, 1994, **11**, 337-353.
29. Q.H. Gibson, B.E.P. Swoboda and V. Massey, *J. Biol. Chem.*, 1964, **239**, 3927-3934.
30. M.H. O'Leary, *Methods Enzymol.*, 1980, **64**, 83-104.

Chapter Three

Inhibitor Synthesis and Inhibition Studies

3.1 Introduction

Investigation into the inhibition of an enzyme system is an extremely important part of understanding the enzyme. The use of inhibitors is vital, not just to prevent the enzyme from functioning, but also to examine possible mechanisms for the catalysed reaction.

As discussed in section 1.6, inhibitors of QPRTase may have many important roles. They may be useful mechanistic tools for identifying important interactions in the active site and therefore assisting in the elucidation of the chemical mechanism of the QPRTase catalysed reaction. They may also be useful biological tools for the evaluation of QPRTase and its importance *in vivo*. Inhibitors of QPRTase may allow the neurological effects of quinolinic acid to be investigated by blocking the active site of the enzyme, inhibiting its action and therefore artificially raising quinolinic acid levels. The biological effect of this increase could be investigated and compared with neurological disorders. In addition, inhibitors of QPRTase may possess anti-mycobacterial and anti-fungal activity.

Several inhibition studies on QPRTase have been reported, mostly using analogues of quinolinic acid although some analogues of PRPP have also been examined as inhibitors of QPRTase. Phthalic acid **25** and picolinic acid **26** are both potent inhibitors of QPRTase from most sources.[1-4] However, the methyl esters of these compounds do not inhibit QPRTase, implying that the free acid is required at the 2-position for binding in the active site.[5]

Inhibition studies on QPRTase from ATCC strain 23269 carried out by Calvo *et al.* also highlighted the importance of an acidic group at the 2-position for binding in the active site.[6] In this study it was found that analogues of nicotinic acid with a hydroxyl **28** or thiol **29** group at the 2-position were good competitive inhibitors of QPRTase, while the corresponding 3-nitro derivatives **30** and **31** were even more effective. The results therefore suggested that the effectiveness of an inhibitor correlates with the degree of ionisation of the acidic group at the 2-position, implying that negative charge on the 2-substituent is an important contributor to tight binding to the enzyme.

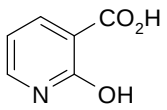

28

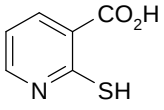

29

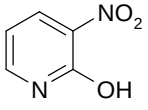

30

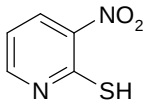

31

Previously in our laboratory, two of these compounds were tested as inhibitors of human brain QPRTase.[7] A preliminary inhibition screen showed 2-mercaptonicotinic acid **29** and 2-hydroxy-3-nitropyridine **30** were very good inhibitors, even when present at a concentration of 1 μM. Detailed inhibition studies then showed 2-mercaptonicotinic acid **29** was a very effective competitive inhibitor (K_i 3.55 μM).

In addition, two new compounds were synthesised and tested as inhibitors of human brain QPRTase. 2-Sulfonicotinic acid **36** was found to be a reasonable competitive inhibitor (K_i 146 μM) although was not as effective as 2-mercaptonicotinic acid **29**. This suggests that the presence of the larger sulfonate group at the 2-position leads to weaker binding in the active site. The size effect was further highlighted by the poor inhibitory properties of 2-phosphonomethylnicotinic acid **37** (K_i 1.32 mM), which has an additional carbon between the ring and the acidic group at the 2-position. Furthermore, the results suggest that the closer the anion at the 2-position is to the pyridine ring, the more effective the inhibitor.

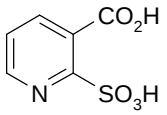

36

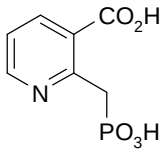

37

Previous work on the synthesis of quinolinic acid analogues has therefore focused mainly on replacing the carboxylic acid group at the 2-position with an alternative acidic group. The aim now was to begin investigating the effect of substituents at different positions of the ring with a view to probing binding interactions in the active site of human brain QPRTase.

3.2 Synthesis of potential inhibitors of human brain QPRTase

3.2.1 Synthesis of N-substituted compounds

3.2.1.1 Synthesis of N-methyl and N-ethylquinolinic acid

The first position of quinolinic acid selected for functionalisation was the ring nitrogen. The rationale behind introducing substituents at this position was that the resulting compounds would bear some resemblance to the putative reaction intermediate, quinolinic acid mononucleotide **16**, and might therefore prove to be effective inhibitors of QPRTase. In addition, compounds of this type might be useful as substrates for enzymatic decarboxylation studies (Chapter 4).

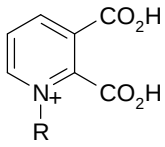

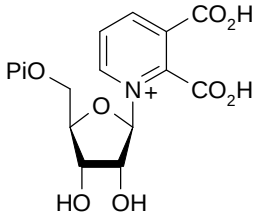

16

The first two synthetic targets were simple *N*-alkylquinolinic acid derivatives. The synthetic route to *N*-methyl and *N*-ethylquinolinic acid is outlined in Scheme 3.1.

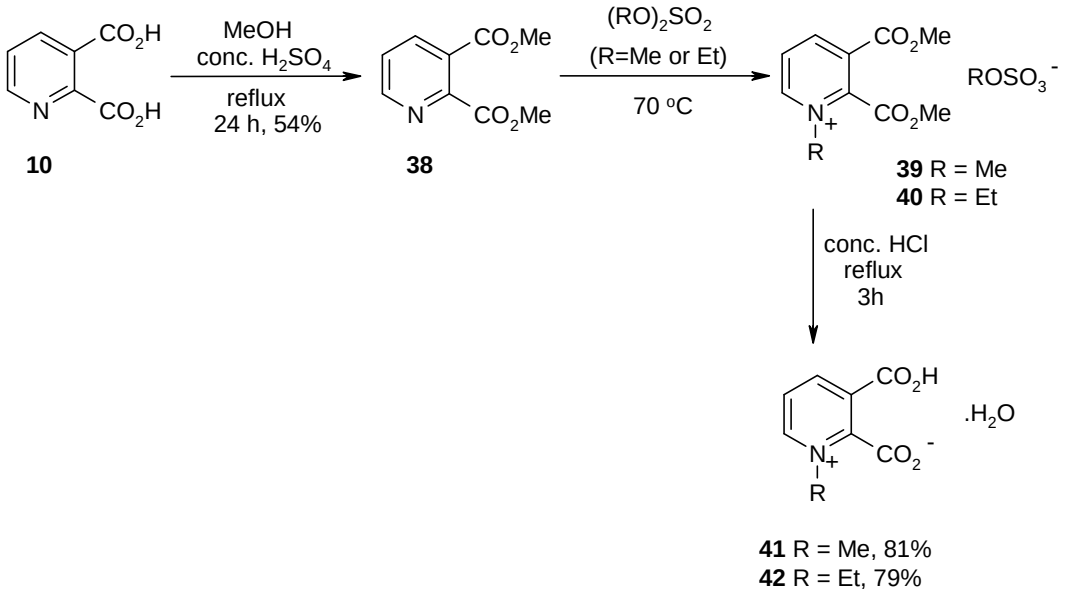

Scheme 3.1: *Synthetic route to N-alkylquinolinic acids.*

Firstly, dimethyl quinolinate **38** was prepared by acid catalysed esterification of quinolinic acid **10** in boiling methanol (Scheme 3.1). The product was obtained as a white solid in reasonable yield (54%). The ^{1}H NMR spectrum was consistent with the expected product. Two singlets were observed at 3.94 and 4.01 ppm corresponding to the protons of the two methyl groups. The aromatic protons were observed between 7.50 and 8.77 ppm. The identity of the product was also confirmed by electrospray mass spectrometry (ES^{+}) which showed a signal corresponding to the $(M+H)^{+}$ molecular ion at *m/z* 196.

The next step was to introduce the *N*-substituent (Scheme 3.1). The *N*-alkylation reaction was achieved by treating dimethyl quinolinate **38** with one equivalent of the appropriate dialkyl sulfate and heating the resulting mixture at 70 °C.

In the case of the *N*-methylation reaction, ^{1}H and ^{13}C NMR spectroscopy showed the reaction had reached completion after 2 hours. The signal corresponding to the protons of the *N*-methyl group was observed as a singlet at 4.50 ppm in the ^{1}H NMR spectrum. In the ^{13}C NMR spectrum, the signal for the *N*-methyl group was observed at 58.0 ppm. The NMR spectra suggest the counterion for the positively charged dimethyl *N*-methylquinolinate **39** is the methyl sulfate anion ($CH_3OSO_3^{-}$). The signal for the methyl protons of the counterion was observed as a singlet at 3.60 ppm in the ^{1}H NMR spectrum. The corresponding signal was observed in the ^{13}C NMR spectrum at 50.2 ppm.

It was found that the reaction of dimethyl quinolinate **38** with diethyl sulfate was slower, reaching completion after 12 hours. ^{1}H and ^{13}C NMR spectroscopy confirmed the desired product **40** had been formed exclusively. The signals corresponding to the protons of the *N*-ethyl group were observed as a triplet at 1.71 ppm (CH_3) and a quartet at 4.78 ppm (CH_2) in the ^{1}H NMR spectrum. In the ^{13}C NMR spectrum, the signals for *N*-ethyl group were observed at 17.6 ppm (CH_3) and 65.6 ppm (CH_2). The NMR spectra suggest the counterion is the ethyl sulfate anion ($CH_3CH_2OSO_3^{-}$). The signals corresponding to the protons of the counterion were observed as a triplet at 1.26 ppm (CH_3) and a quartet at 4.10 ppm (CH_2) in the ^{1}H NMR spectrum.

In the final step, acid catalysed hydrolysis of the diester produced the desired *N*-alkylquinolinic acid (Scheme 3.1). Following recrystallisation from water, both *N*-methyl and *N*-ethylquinolinic acid were obtained as white crystalline solids in high yields of 81% and 79%, respectively. The *N*-alkylquinolinic acids were fully characterised. In the ^{1}H NMR spectrum of *N*-methylquinolinic acid **41**, the signal for the protons of the *N*-methyl group was observed as a singlet at 4.36 ppm. The identity of the product was also confirmed by electrospray mass spectrometry (ES^+) which showed a signal corresponding to the molecular ion at *m/z* 182. Similarly for *N*-ethylquinolinic acid **42**, a signal corresponding to the molecular ion was observed at *m/z* 196. In the ^{1}H NMR spectrum of *N*-ethylquinolinic acid, the signals corresponding to the protons of the *N*-ethyl group were observed as a triplet at 1.50 ppm (CH_3) and a quartet at 4.53 ppm (CH_2). CHN microanalysis showed that both *N*-methyl and *N*-ethylquinolinic acid exist in the zwitterionic monohydrate form shown in Scheme 3.1. CHN microanalysis showed both compounds were pure and are therefore suitable for biological testing.

3.2.1.2 Synthesis of 5-ethyl–N-methylquinolinic acid

5-Ethylquinolinic acid **43** is commercially available and it was decided to synthesise the *N*-methyl derivative and test both compounds as inhibitors of human brain QPRTase to further investigate the effect of the *N*-substituent on the inhibitory properties. This inhibition study would also enable the effect of the substituent at the 5-position on the binding in the active site to be examined. The synthetic route to 5-ethyl-*N*-methylquinolinic acid **46** is outlined in Scheme 3.2.

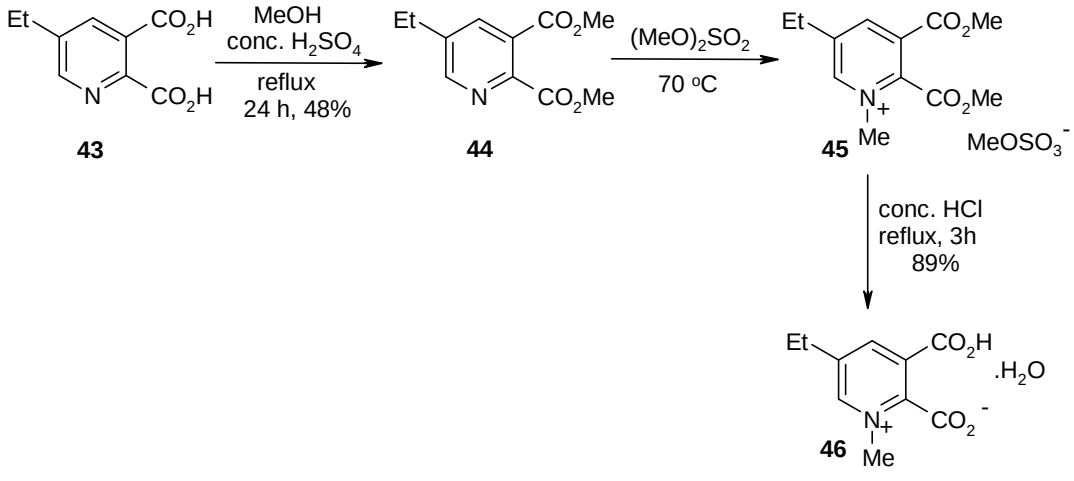

Scheme 3.2: *Synthesis of 5-ethyl-N-methylquinolinic acid.*

The synthetic route was successfully followed and after recrystallisation from water, 5-ethyl-*N*-methylquinolinic acid **46** was obtained as a white solid in high yield (89%). The ^{1}H NMR spectrum of the final product was consistent with the desired product. The signal for the protons of the *N*-methyl group was observed as a singlet at 4.14 ppm. The identity of the product was also confirmed by electrospray mass spectrometry (ES^{+}) which showed a signal corresponding to the molecular ion at *m/z* 210. CHN microanalysis showed 5-ethyl-*N*-methylquinolinic acid was pure and exists in the zwitterionic monohydrate form shown in Scheme 3.2.

3.2.1.3 Synthesis of N-alkylpicolinic acids

To investigate the relative importance of the carboxylic acid group at the 3-position and the presence of the *N*-substituent on binding in the active site of QPRTase, it was decided to synthesise *N*-methyl and *N*-ethylpicolinic acid and test these compounds, as well as picolinic acid **26**, as inhibitors of QPRTase (Scheme 3.3).

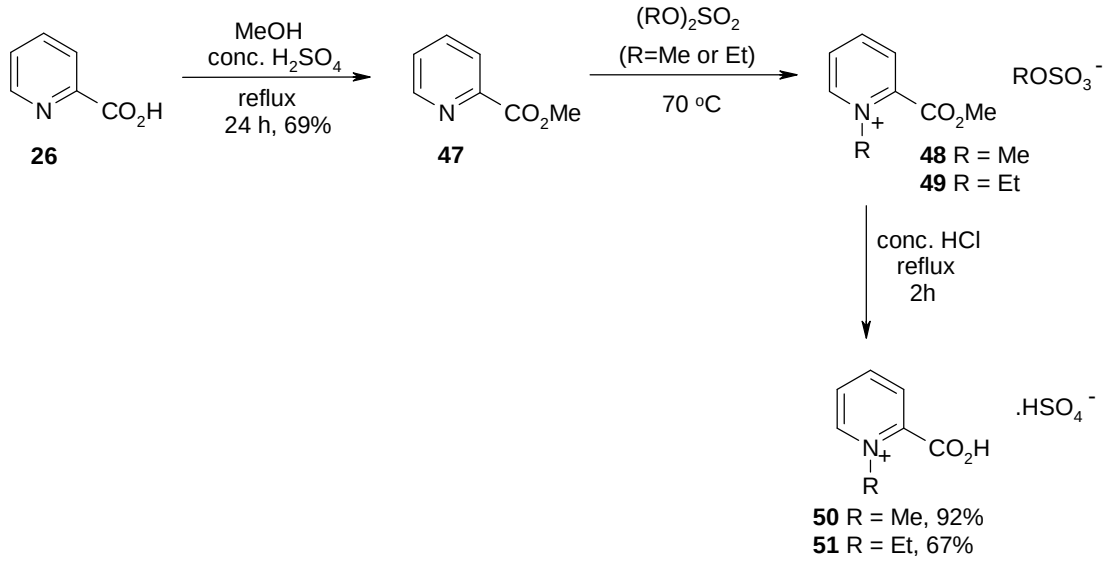

Scheme 3.3: *Synthetic route to N-alkylpicolinic acids.*

By following this route *N*-methyl and *N*-ethylpicolinic acid were obtained as white crystalline solids in good yields of 92% and 67%, respectively. The *N*-alkylpicolinic acids were fully characterised. In the ^{1}H NMR spectrum of *N*-methylpicolinic acid **50**, the signal for the protons of the *N*-methyl group was observed as a singlet at 4.24 ppm. The identity of the product was also confirmed by electrospray mass

spectrometry (ES^+) which showed a signal corresponding to the molecular ion at *m/z* 138. Similarly for *N*-ethylpicolinic acid **51**, a signal corresponding to the molecular ion was observed at *m/z* 152. In the ^1H NMR spectrum of *N*-ethylpicolinic acid, the signals corresponding to the protons of the *N*-ethyl group were observed as a triplet at 1.42 ppm (CH_3) and a quartet at 4.58 ppm (CH_2). CHN microanalysis showed that both *N*-methyl and *N*-ethylpicolinic acid were pure and exist as the hydrogen sulfate salts shown in Scheme 3.3.

3.2.1.4 Synthesis of N-methylquinoline-2-carboxylic acid

Quinoline-2-carboxylic acid **52** is commercially available and it was decided to synthesise the *N*-methyl derivative and test both compounds as inhibitors of human brain QPRTase to further investigate the effect of the *N*-substituent on the inhibitory properties. This inhibition study would also enable the effect of the larger bicyclic structure on the binding in the active site to be examined. The synthetic route to *N*-methylquinoline-2-carboxylic acid **55** is outlined in Scheme 3.4.

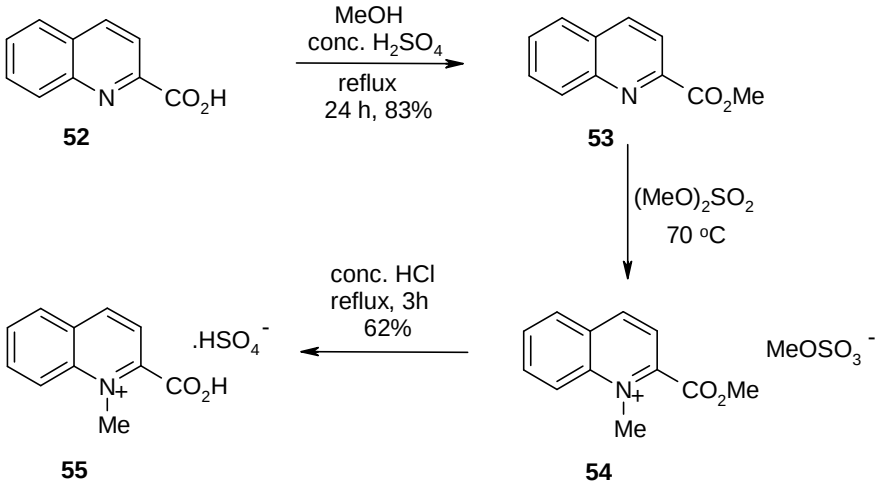

Scheme 3.4: *Synthesis of N-methylquinoline-2-carboxylic acid.*

The synthetic route was successfully followed and after recrystallisation from methanol, *N*-methylquinoline-2-carboxylic acid **55** was obtained as a white solid in good yield (62%). The ^1H NMR spectrum of the final product was consistent with the desired product. The signal for the protons of the *N*-methyl group was observed as a singlet at 4.35 ppm. The identity of the product was also confirmed by electrospray

mass spectrometry (ES^+) which showed a signal corresponding to the molecular ion at *m/z* 188. CHN microanalysis showed *N*-methylquinoline-2-carboxylic acid was pure and exists as the hydrogen sulfate salt shown in Scheme 3.4.

3.2.1.5 Synthesis of N-alkylnicotinic acids

To investigate the relative importance of the carboxylic acid group at the 2-position and the presence of the *N*-substituent on binding in the active site of QPRTase, it was decided to synthesise *N*-methyl and *N*-ethylnicotinic acid and test these compounds, as well as nicotinic acid **27**, as inhibitors of QPRTase (Scheme 3.5).

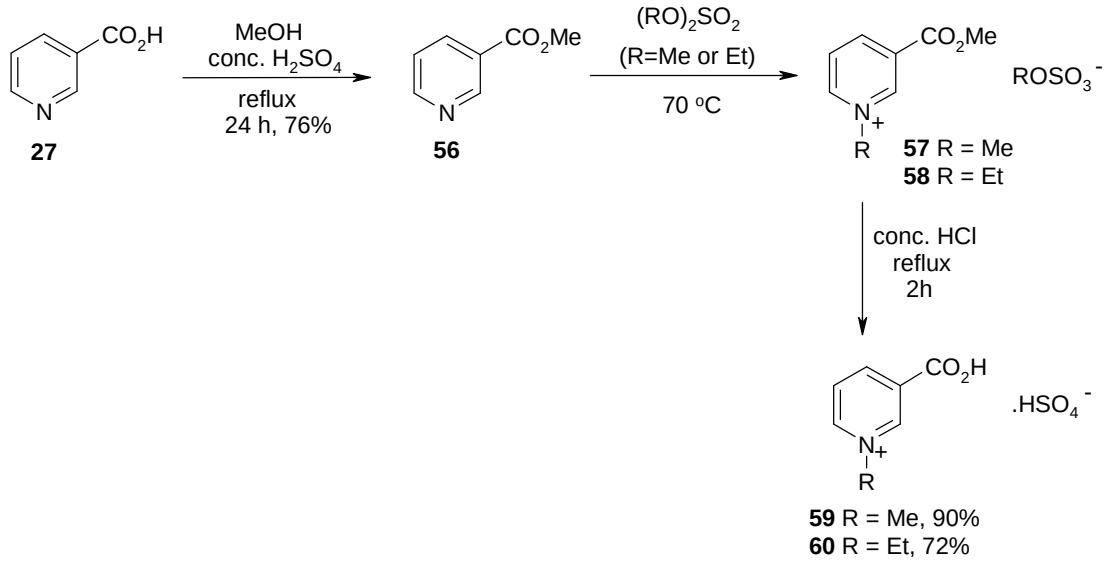

Scheme 3.5: *Synthetic route to N-alkylnicotinic acids.*

N-Methyl and *N*-ethylnicotinic acid were obtained as white crystalline solids in good yields of 90% and 72%, respectively. The *N*-alkylnicotinic acids were fully characterised. In the ^1H NMR spectrum of *N*-methylnicotinic acid **59**, the signal for the protons of the *N*-methyl group was observed as a singlet at 4.32 ppm. The identity of the product was also confirmed by electrospray mass spectrometry (ES^+) which showed a signal corresponding to the molecular ion at *m/z* 138. Similarly for *N*-ethylnicotinic acid **60**, a signal corresponding to the molecular ion was observed at *m/z* 152. In the ^1H NMR spectrum of *N*-ethylnicotinic acid, the signals corresponding to the protons of the *N*-ethyl group were observed as a triplet at 1.49 ppm (CH_3) and a quartet at 4.54 ppm (CH_2). CHN microanalysis showed that both *N*-methyl and *N*-ethylnicotinic acid exist as the hydrogen sulfate salts shown in Scheme 3.5.

3.2.1.6 Synthesis of quinolinic acid N-oxide

Having prepared a series of *N*-alkyl compounds, it was decided to change the nature of the *N*-substituent and examine the effect this has on the binding in the active site of QPRTase. The initial synthetic route to quinolinic acid *N*-oxide **62** is outlined in Scheme 3.6.

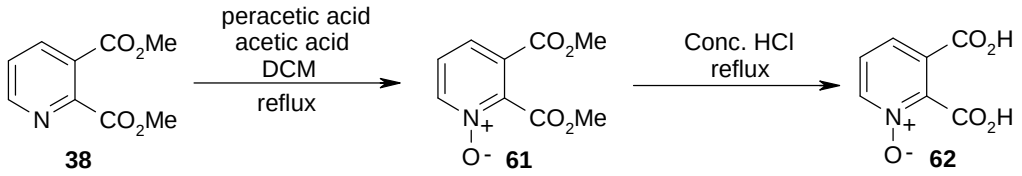

Scheme 3.6: *Proposed synthetic route to quinolinic acid N-oxide.*

Firstly, formation of the *N*-oxide was achieved by treating dimethyl quinolinate **38** with excess peracetic acid in dichloromethane and heating under reflux for 6 hours (Scheme 3.6). Analysis of the crude product by TLC and ^{1}H NMR spectroscopy showed there was still a small amount of unreacted dimethyl quinolinate remaining. Recrystallisation from methanol gave the desired product **61** as a white solid in 24% yield. In the ^{1}H NMR spectrum of the product, the signals for the aromatic protons were shifted upfield compared to the corresponding signals of the starting material and were observed at 7.35 ppm (H-5), 7.82 ppm (H-4) and 8.30 ppm (H-6). The identity of the product was confirmed by electrospray mass spectrometry (ES^{+}) which showed a signal corresponding to the $(M+H)^{+}$ molecular ion at *m/z* 212.

In the next step, an attempt was made to hydrolyse the diester **61** under acidic conditions to give the desired *N*-substituted quinolinic acid derivative **62** (Scheme 3.6). The ^{1}H NMR spectrum of the crude product showed hydrolysis of the dimethyl ester had been achieved. However, the desired product, quinolinic acid *N*-oxide **62**, has only 3 aromatic protons but 4 signals were observed in the ^{1}H NMR spectrum at 7.62 ppm, 8.18 ppm, 8.42 ppm and 8.75 ppm. In addition, the ^{13}C NMR spectrum showed only one signal corresponding to a carbonyl carbon at 164.2 ppm. Therefore, it would appear that under the conditions employed, decarboxylation at the 2-position has occurred to form nicotinic acid *N*-oxide **63** (Scheme 3.7). This was confirmed by electrospray mass spectrometry (ES^{+}) which showed a signal corresponding to the $(M+H)^{+}$ molecular ion at *m/z* 140.

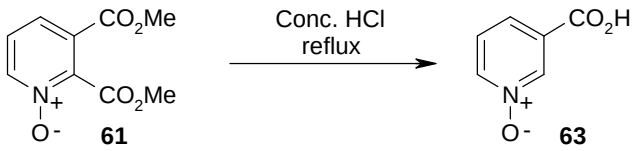

Scheme 3.7: *Formation of nicotinic acid N-oxide from dimethyl quinolinate N-oxide.*

The initial route to quinolinic acid *N*-oxide **62**, starting from dimethyl quinolinate **38**, was selected due to the poor solubility of quinolinic acid **10** in dichloromethane and also because the diester moiety would make the product less polar and would therefore aid purification. However, with the observation that decarboxylation occurs at the 2-position when heated under reflux in concentrated hydrochloric acid, it was decided to avoid the hydrolysis step and try to obtain quinolinic acid *N*-oxide **62** by direct oxidation of quinolinic acid **10** with excess peracetic acid (Scheme 3.8).

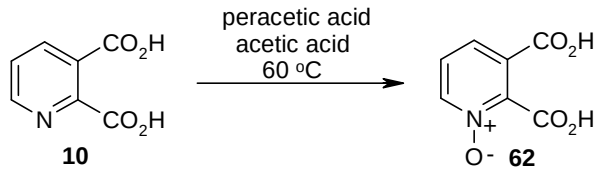

Scheme 3.8: *Synthesis of quinolinic acid N-oxide.*

The reaction was heated gently until solution of quinolinic acid **10** was complete and then heating was maintained at 60 °C. After 4 hours, a white solid began to precipitate. Heating at 60 °C was continued for a further 2 hours then the product was collected by suction filtration. Recrystallisation from water gave quinolinic acid *N*-oxide **62** as a white solid in 30% yield. The identity of the product was confirmed by electrospray mass spectrometry (ES^+) which showed a signal corresponding to the $(M+H)^+$ molecular ion at *m/z* 184 (relative intensity 100%). The ^1H and ^{13}C NMR spectra were also consistent with the desired product.

In the ^1H NMR spectrum of the filtrate, there was evidence for a small amount of nicotinic acid *N*-oxide **63** in addition to quinolinic acid *N*-oxide **62** and unreacted quinolinic acid **10**, which explains the low yield. A series of pyridine dicarboxylic acid *N*-oxides have previously been prepared by treatment with aqueous acetic acid and 30% hydrogen peroxide and the *N*-oxides were separated from unreacted starting material as Pb^{2+} complexes which were subsequently decomposed with H_2S.[8] The yield of quinolinic acid *N*-oxide (21%) was considerably lower than the other pyridine

dicarboxylic acid *N*-oxides. In this reaction, decarboxylation was also observed and some nicotinic acid *N*-oxide was isolated.

3.2.1.7 Attempted synthesis of N-(2-hydroxyethyl)quinolinic acid

Increasing the similarity of the *N*-substituent to that in the putative reaction intermediate, quinolinic acid mononucleotide **16,** might provide additional binding interactions in the active site of human brain QPRTase and might therefore lead to increased inhibition of the enzyme. Therefore, it was decided to attempt the synthesis of *N*-(2-hydroxyethyl)quinolinic acid **64**.

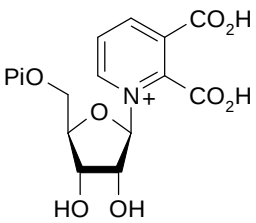

16

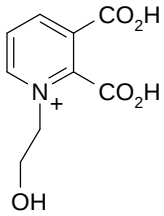

64

The proposed synthetic route to *N*-(2-hydroxyethyl)quinolinic acid **64** is outlined in Scheme 3.9.

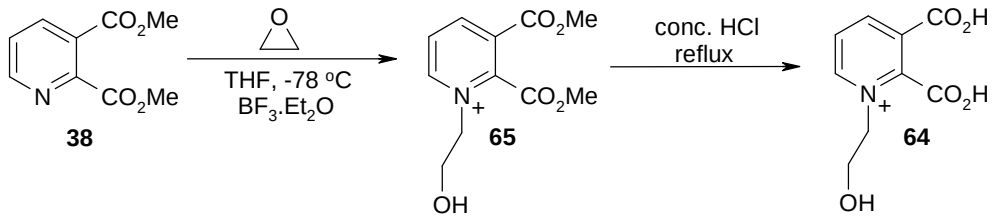

38 **65** **64**

Scheme 3.9: *Proposed route to N-(2-hydroxyethyl)quinolinic acid.*

The key reaction to introduce the *N*-substituent was achieved by reacting dimethyl quinolinate **38** with excess ethylene oxide in the presence of boron trifluoride diethyl etherate ($BF_3.Et_2O$). In the absence of boron trifluoride no reaction occurred indicating that the Lewis acid is required to activate the ethylene oxide towards nucleophilic attack by dimethyl quinolinate. It was found that the best results were achieved when 3 equivalents of the Lewis acid catalyst were used. Under these conditions, TLC and ^{1}H NMR analysis of the crude product showed there was no unreacted dimethyl quinolinate remaining. The ^{1}H NMR spectrum of the crude product was consistent with the desired product **65** and showed two triplets at 3.38 ppm and 4.05 ppm corresponding to the protons of the methylene groups of the

N-substituent. However, an additional large signal was observed at 3.65 ppm. It was thought that this might be due to polyethylene glycol, formed by the polymerisation of ethylene oxide under the reaction conditions. This would also explain the high yield and appearance of the crude product, which was a thick white semi-solid material.

Dimethyl *N*-(2-hydroxyethyl)quinolinate **65** was successfully extracted by washing the crude material with water. The ^{1}H NMR spectrum of the insoluble white solid showed only a single signal at 3.45 ppm. The ^{1}H NMR spectrum of the extracted material however was consistent with the desired product **65** and the absence of the large signal at 3.65 ppm showed the impurity had successfully been removed. The identity of the product was also confirmed by electrospray mass spectrometry (ES^{+}) which showed a signal corresponding to the molecular ion at *m/z* 240 (relative intensity 100%).

In the final step, an attempt was made to hydrolyse the diester **65** under acidic conditions to give the desired *N*-substituted quinolinic acid derivative **64**. The ^{1}H NMR spectrum of the crude product showed hydrolysis of the dimethyl ester had been achieved. However, analysis of the crude material by electrospray mass spectrometry (ES^{+}) indicated that the desired product had not been formed. A signal was observed at *m/z* 194. Therefore, it would appear that under the acidic conditions, the hydroxyl group of the *N*-substituent has reacted with the ester group at the 2-position resulting in the formation of a six membered ring (Scheme 3.10).

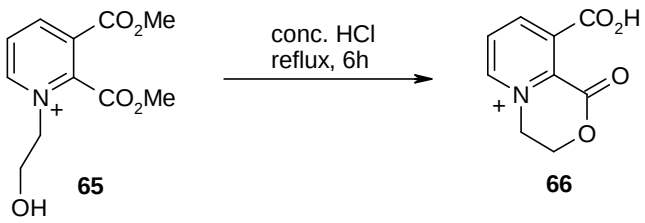

65 **66**

Scheme 3.10: *Hydrolysis of dimethyl N-(2-hydroxyethyl)quinolinate.*

While it was not the target compound, **66** would also be an interesting compound to test as an inhibitor of QPRTase. Unfortunately, due to the polarity of the compound, purification proved very difficult. All attempts at recrystallisation failed. However, the compound appeared to be pure by NMR analysis so it was decided to perform a preliminary inhibition screen to provide an indication of its inhibitory properties.

3.2.2 Routes to 4-substituted quinolinic acid derivatives

The second group of synthetic target compounds were derivatives of quinolinic acid substituted at the 4-position. These compounds were of interest as tools to probe binding interactions in the active site of human brain QPRTase.

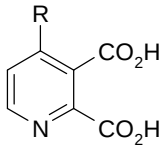

3.2.2.1 Route 1 - Directed ortho-metalation

The initial route to 4-substituted quinolinic acid derivatives was planned involving directed *ortho*-metalation to guide the substitution of quinolinic acid.[9] Directed *ortho*-metalation involves the deprotonation of a site *ortho* to a heteroatom-containing substituent (directed metalation group, DMG) by a strong base, normally an alkyl lithium reagent, leading to an *ortho*-lithiated species. This species, upon treatment with electrophilic reagents, yields 1,2-disubstituted products. This process can be viewed, albeit rather simplistically, as a three step sequence: coordination of the alkyllithium aggregate to the DMG heteroatom; deprotonation to give the coordinated *ortho*-lithiated species; and reaction with an electrophile to yield the disubstituted product (Scheme 3.11).

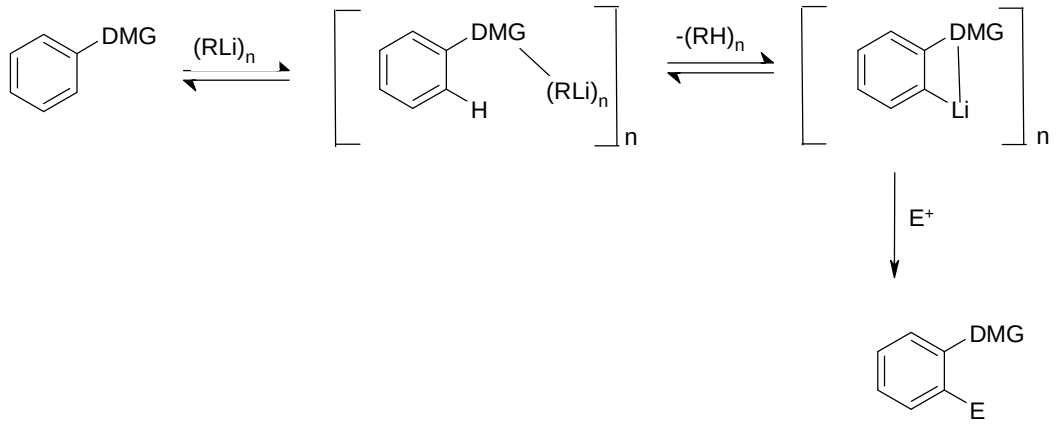

Scheme 3.11: *The directed ortho-metalation process.*

An attempt was made to functionalise the 4-position of dimethyl quinolinate **38** by employing an *in situ* trapping method of directed *ortho*-metalation.[10] The hindered, non-nucleophilic base lithium diisopropylamide (LDA) was generated in dry tetrahydrofuran. The electrophilic trap, trimethylsilyl chloride, was then added just prior to the addition of dimethyl quinolinate **38**. The idea is that removal of the pyridyllithium **67** by reaction with the electrophilic trap drives forward the otherwise unfavourable equilibrium between dimethyl quinolinate **38** and the pyridyllithium **67** (Scheme 3.12). For the first attempts at the directed *ortho*-metalation reaction, trimethylsilyl chloride was selected as the electrophilic trap simply because the trimethylsilyl group is easily observed by ^{1}H NMR spectroscopy and the low shift of this signal means that it does not obscure any of the other signals making it easy to establish whether or not the reaction was successful.

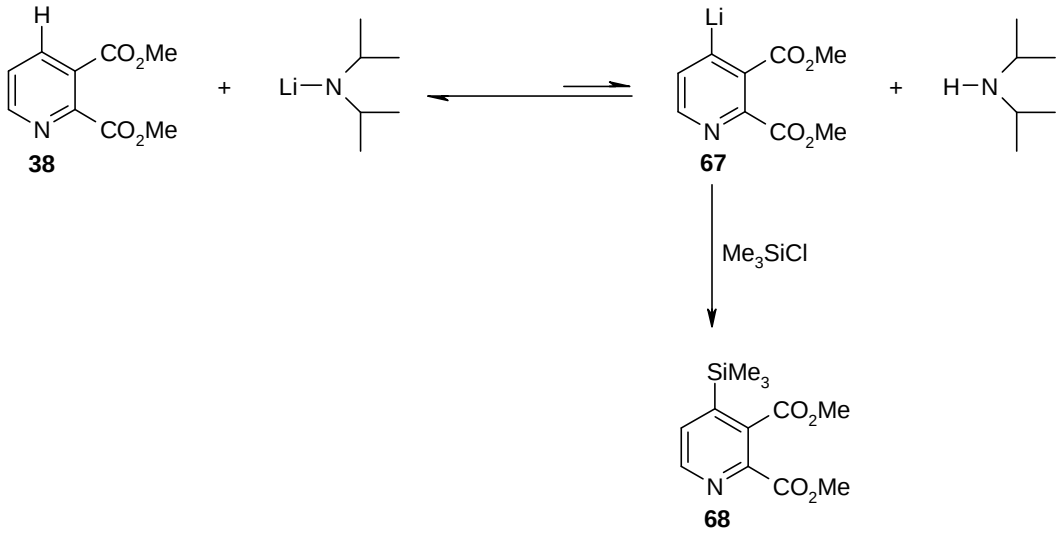

Scheme 3.12: *The in situ trapping method.*

TLC analysis of the crude product showed there was no unreacted dimethyl quinolinate **38** remaining. However, the ^{1}H NMR spectrum of the crude material was not very clean and showed no sign of the desired product, dimethyl 4-trimethylsilylquinolinate **68**. While it can not be concluded from the spectral data, it is possible that a self-condensation reaction is competing with the trapping with trimethylsilyl chloride. In a study of the *in situ* trapping of *ortho*-lithiated alkyl benzoates by Krizan *et al*, it was found that the reaction worked best with isopropyl benzoate, while the less sterically hindered ethyl ester had a tendency to self-condense.[11]

Therefore it was decided to synthesise diisopropyl quinolinate **69** for use in the directed *ortho*-metalation reaction. This involved a simple esterification of quinolinic acid **10** with isopropanol in the presence of acid (Scheme 3.13). Purification of the crude product by column chromatography on silica gave the desired product as a colourless oil in 40% yield. The ^{1}H NMR spectrum was consistent with the expected product. Two doublets were observed at 1.36 and 1.39 ppm corresponding to the methyl protons from the two isopropyl groups. The corresponding methine protons were both observed in a complex multiplet that spanned 5.17 to 5.31 ppm. The aromatic protons were observed between 7.63 and 8.72 ppm. The identity of the product was also confirmed by electrospray mass spectrometry (ES^{+}) which showed a signal corresponding to the $(M+H)^{+}$ molecular ion at *m/z* 252.

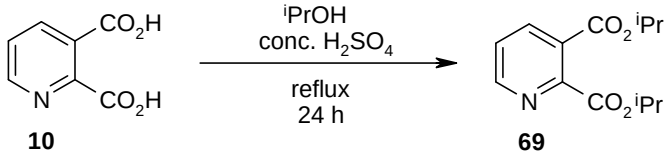

10 **69**

Scheme 3.13: *Synthesis of diisopropyl quinolinate.*

The next step was to attempt the directed *ortho*-metalation reaction with diisopropyl quinolinate **69** as the substrate. As before, trimethylsilyl chloride was used as the electrophilic trap, but lithium 2,2,6,6-tetramethylpiperidine (LiTMP), which is a very sterically encumbered base, was used instead of LDA (Scheme 3.14). A 1:2:10 ratio of substrate, base and electrophilic trap was used.

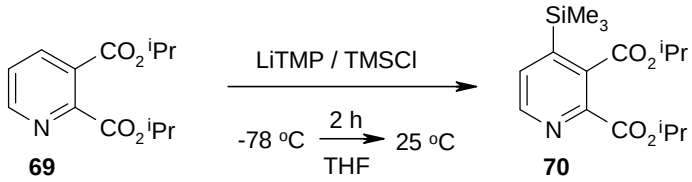

69 **70**

Scheme 3.14: *Attempted synthesis of diisopropyl 4-trimethylsilylquinolinate.*

TLC analysis of the crude material showed the reaction was not clean and a number of products had been produced. An attempt was made to separate the different components of the crude product by column chromatography on silica. The least polar component was the major product and was isolated as a pure white solid in 15%

yield. In the ^{1}H NMR spectrum of this solid there were two singlets at 0.25 and 0.27 ppm and in the aromatic region there was only one singlet at 7.66 ppm. This suggested that this compound contained two trimethylsilyl groups. This was confirmed by electrospray mass spectrometry (ES^+), which showed a signal corresponding to a $(M+H)^+$ molecular ion at *m/z* 396 (relative intensity 25%) and also $(M+Na)^+$ at *m/z* 418 (relative intensity 100%). The shift of the aromatic signal in the ^{1}H NMR spectrum is consistent with H-5 and therefore the disubstituted product appears to be diisopropyl 4,6-di(trimethylsilyl)quinolinate **71**.

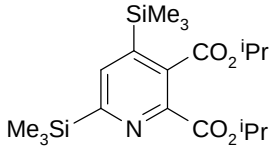

71

Isolation of the second least polar component of the crude product in pure form by column chromatography proved difficult but it was isolated in a mixture with the identified 4,6-disubstituted derivative. The ^{1}H NMR spectrum of this mixture showed, in addition to the signals for the disubstituted derivative, a pair of doublets in the aromatic region at 7.42 ppm (*J* 5 Hz) and 8.48 ppm (*J* 5 Hz). This suggested the possible presence of the desired diisopropyl 4-trimethylsilylquinolinate **70** in the product mixture. However, the electrospray mass spectrum of the mixture was identical to that for the pure disubstituted derivative and showed no sign of the desired product. Due to the lack of material no further purification attempt was made to separate the two components of this mixture.

In this directed *ortho*-metalation reaction, a second lithiation at the 6-position *ortho* to the ring nitrogen occurred leading to a complex mixture of mono- and disubstituted products that proved difficult to separate. This is often seen with pyridines. However, in this reaction 2 equivalents of LiTMP were used and it was therefore decided to try and optimise the reaction by using less base in the hope that this would prevent the formation of the disubstituted derivative. The reaction was repeated using the same substrate, base, electrophilic trap and reaction conditions but reducing the amount of base added to just 1.1 equivalents. However, this reaction was unsuccessful. The ^{1}H NMR spectrum of the crude product showed only unreacted starting material.

Replacing trimethylsilyl chloride with different electrophiles gave similar negative results. Firstly, diisopropyl quinolinate was treated with 1.1 equivalents of LiTMP in the presence of 3 equivalents of benzyl bromide as the electrophilic trap. However, the ^{1}H NMR spectrum of the crude product showed only unreacted starting material. It was therefore decided to increase the reactivity of the electrophile, but the reaction with benzaldehyde under the same conditions was also unsuccessful. The attempted reactions are summarised in Table 3.1.

Substrate	**Base**	**Electrophilic trap**	**Substrate:base:trap**	**Outcome**
Diisopropyl quinolinate	LiTMP	Trimethylsilyl chloride	1:2:10	Complex mixture of products
Diisopropyl quinolinate	LiTMP	Trimethylsilyl chloride	1:1.1:10	No reaction
Diisopropyl quinolinate	LiTMP	Benzyl bromide	1:1.1:3	No reaction
Diisopropyl quinolinate	LiTMP	Benzaldehyde	1:1.1:3	No reaction

Table 3.1: *Reaction summary.*

It is possible that the latter reactions failed because the deprotonation of diisopropyl quinolinate **69** was unsuccessful when only 1.1 equivalents of the base were used. However, it was shown that using a larger excess of the base leads to the formation of a complex mixture of products including mono- and disubstituted derivatives that are difficult to separate. With the failure of the directed *ortho*-metalation reaction, an alternative route to 4-substituted quinolinic acid derivatives was sought.

3.2.2.2 Route 2 - Addition of organometallic reagents to 1-acylpyridinium salts

Many investigations have been reported on the reaction of organometallic reagents with pyridines to introduce substituents directly to the pyridine ring. The synthesis of substituted pyridines by the reaction of Grignard reagents and pyridine is not a practical method due to the strenuous conditions required for addition, the low yields obtained and frequent lack of regioselectivity. Therefore to obtain high yields of addition with Grignard reagents, activation of the pyridine ring is necessary. Fraenkel *et al.* reported that the pyridine ring could be readily attacked by Grignard reagents in the presence of ethyl chloroformate to produce 2-substituted 1-(ethoxycarbonyl)-1,2-dihydropyridines **73** (Scheme 3.15).[12] Lyle *et al.* elaborated on this method by demonstrating that acid chlorides are also effective in activating the pyridine ring towards nucleophilic attack by Grignard reagents.[13] It was shown that the intermediate 1,2-dihydropyridines **73** could then be readily oxidised by heating with sulfur to produce the 2-substituted pyridines **74** in good yield (Scheme 3.15).[14]

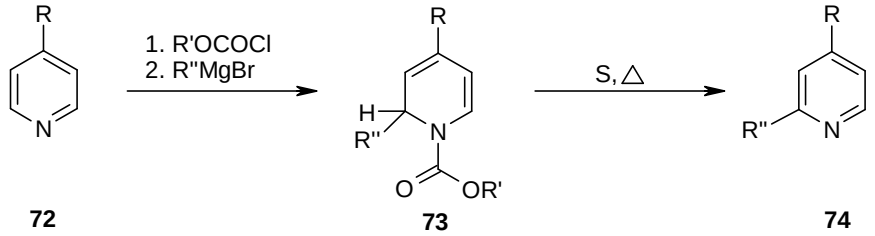

Scheme 3.15: *Grignard addition to 1-acylpyridinium salts followed by rearomatisation.*

However, the degree of regioselectivity of the addition (1,2- versus 1,4-addition) of the Grignard reagents to the 1-acylpyridinium salts was unclear from this study since in most of the reactions examined, 4-alkylpyridines **72**, in which the 4-position is blocked, were used as the starting material and hence nucleophilic attack occurred preferentially at the 2-position (Scheme 3.15).

In a study by Comins *et al*., the regioselectivity of this reaction with regard to how the structures of the acyl halide and Grignard reagent influence the degree of 1,2- versus 1,4-addition to unsubstituted pyridine was investigated.[15] It was found that the amount of attack at the 4-position is dependent upon the degree of steric hindrance at the 2-position. The larger the *N*-substituent and the Grignard reagent, the more 1,4-addition occurs. The nitrogen substituent must sterically shield the 2-position while activating the 4-position to nucleophilic attack.

In the same study, the effect of adding a catalytic amount of cuprous iodide on the regioselectivity of the Grignard addition step was investigated. The Grignard reagent was added dropwise to the preformed acylpyridinium salt and CuI in tetrahydrofuran, allowing the organocopper intermediate to react with the substrate as soon as it was formed. This procedure gave good yields and the added catalytic amount of CuI had a major effect on the regioselectivity, causing nearly exclusive attack at the 4-position (Scheme 3.16). Similarly, Piers *et al.* reported that lithium dialkylcuprates react with pyridine in the presence of methyl chloroformate to give mainly 1,4-dihydropyridines, which were readily oxidised to the corresponding 4-alkylpyridines.[16]

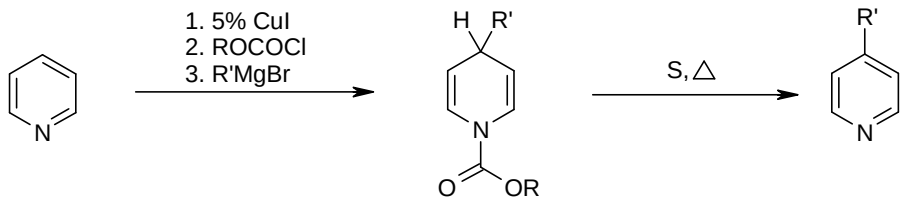

75 **76** **77**

Scheme 3.16: *Regioselective synthesis of 4-substituted pyridines.*

The previous studies have therefore demonstrated a highly efficient and practical synthesis of 4-substituted pyridines. In addition, it has been shown that the pyridine ring is so activated that addition to the ring will occur in the presence of other reactive functional groups such as ketones and esters.[13] It was therefore decided to attempt the synthesis of 4-substituted quinolinic acid derivatives utilising this methodology.

The previous studies had shown that nucleophilic attack occurs preferentially at the 4-position of 1-acylpyridinium salts when soft, bulky nucleophiles and large *N*-substituents are used. An attempt was therefore made to synthesise 5-phenylquinolinic acid by first reacting diisopropyl quinolinate **69** with phenyl magnesium bromide in presence of ethyl chloroformate and catalytic CuI, following the procedure reported by Comins *et al.* (Scheme 3.17).[15]

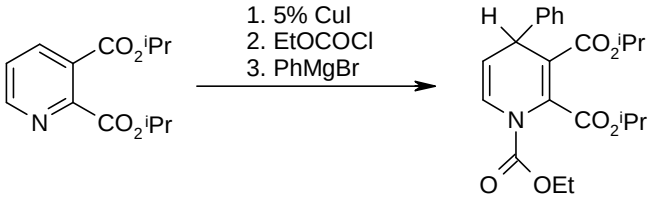

69 **78**

Scheme 3.17: *Attempted functionalisation of diisopropyl quinolinate.*

However, analysis of the crude product by TLC and ^{1}H NMR spectroscopy showed the reaction had been unsuccessful. If the desired product had been formed it was expected that, in the ^{1}H NMR spectrum, the signals corresponding to the three protons in the ring would be shifted upfield relative to the starting material. However, the signals for the ring protons were observed at 7.60 (H-5), 8.20 (H-4) and 8.75 (H-6), which are almost identical to the shifts observed for diisopropyl quinolinate **69**. Signals corresponding to the protons of the two isopropyl groups were observed showing the diester moiety was still intact and no side reactions had occurred. In addition, signals corresponding to unreacted ethyl chloroformate (1.20 ppm and 4.25 ppm) and the quenched organometallic reagent (7.05-7.40 ppm) were observed in the ^{1}H NMR spectrum of the crude product. Therefore it would appear that no reaction occurred.

It is possible that this reaction failed due to steric factors. The combination of using a large organometallic reagent (phenyl magnesium bromide (5% CuI)) and the bulky diisopropyl ester of quinolinic acid may make nucleophilic attack at the 4-position very difficult. It was therefore decided to repeat the reaction using a smaller nucleophile, methyl magnesium bromide in the presence of 5% CuI. However, this reaction was also unsuccessful. The reaction was then carried out using the less bulky dimethyl ester of quinolinic acid, the idea being that reducing the size of the ester

group might make the 4-position more accessible for nucleophilic attack. However, the reaction between dimethyl quinolinate **38** and phenyl magnesium bromide in the presence of 5% CuI and ethyl chloroformate was also unsuccessful. The attempted reactions are summarised in Table 3.2.

Starting material	Organometallic reagent	Alkyl chloroformate	Outcome
Diisopropyl quinolinate	PhMgBr (5% CuI)	Ethyl chloroformate	No reaction
Diisopropyl quinolinate	MeMgBr (5% CuI)	Ethyl chloroformate	No reaction
Dimethyl quinolinate	PhMgBr (5% CuI)	Ethyl chloroformate	No reaction

Table 3.2: *Reaction summary.*

It is possible that, rather than steric factors preventing nucleophilic attack on the *N*-acylpyridinium salt **80**, the failure of these reactions could be due to a combination of steric and electronic factors preventing the formation of the *N*-acylpyridinium salt **80** in the first place. Firstly, the steric bulk of the ester group at the 2-position may prevent the reaction between the dialkyl quinolinate **79** and ethyl chloroformate taking place, as this would leave the nitrogen very congested. Furthermore, the two ester groups will have an electron withdrawing effect on the pyridine ring and as a result the ring nitrogen might be a reasonably poor nucleophile, which could prevent the reaction with ethyl chloroformate taking place. *N*-Acylation is required to activate the ring towards nucleophilic attack and hence if the *N*-acylpyridinium salt **80** does not form, the subsequent reaction with the organometallic reagent will not occur (Scheme 3.18).

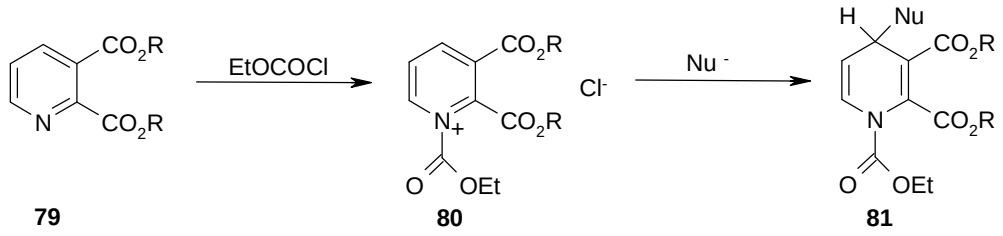

79 **80** **81**

Scheme 3.18: *Formation of the N-acylpyridinium salt followed by nucleophilic attack.*

3.2.2.3 Route 3 - Oxidation of substituted quinolines

Due to the problems with the initial synthetic strategy, an alternative route to 4-substituted quinolinic acid derivatives was sought. A literature search revealed that oxidation of 4-substituted quinolines **82** could be an attractive route to the corresponding substituted quinolinic acids **83** (Scheme 3.19). There are several reports of different methods for the oxidation of quinolines to the corresponding quinolinic acids, with varying degrees of success. These include potassium permanganate oxidation,[17-20] oxidation with hydrogen peroxide in the presence of cupric acetate,[21] ruthenium tetroxide catalysed oxidation using sodium periodate, periodic acid or sodium hypochlorite as the oxidant,[22-25] ozone oxidation[22,26] and electrolytic oxidation.[27,28]

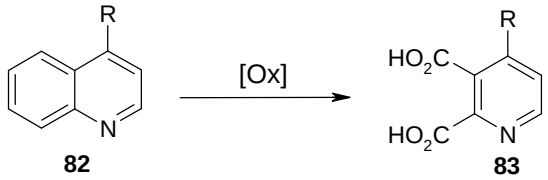

82 **83**

Scheme 3.19: *Preparation of 4-substituted quinolinic acids by oxidation of the corresponding quinolines.*

Access to a series of quinolinic acid analogues substituted at the 4-position would require the availability of the corresponding series of substituted quinolines. Starting from 4-methylquinoline **84**, it is possible to modify and extend the side chain at the 4-position to access a range of substituted quinolines. Methyl groups at the C-2 and C-4 positions of quinoline are easily deprotonated. This is because the resultant carbanion **85** is resonance stabilised and the negative charge can be delocalised onto the electronegative nitrogen atom (Scheme 3.20). The stabilised anion can then be alkylated, acylated or condensed with aldehydes to extend the quinoline side chain. Oxidation of the substituted quinolines **86** will lead to the corresponding quinolinic acid derivatives.

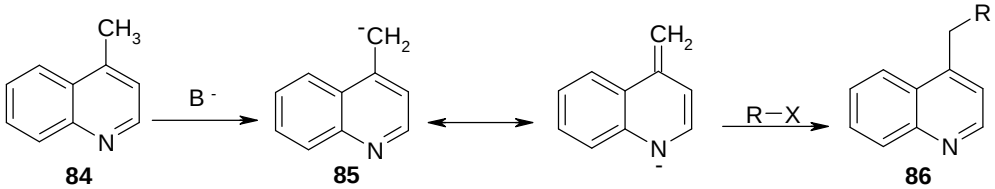

84 **85** **86**

Scheme 3.20: *Deprotonation and alkylation of 4-methylquinoline.*

An initial attempt was made to prepare 4-isobutylquinoline **87** from 4-methylquinoline **84**, n-butyllithium and isopropyl bromide following the procedure reported by Osuch *et al.* (Scheme 3.21).[29] A 2:2:1 molar ratio of substrate, organolithium compound and alkyl halide was used.

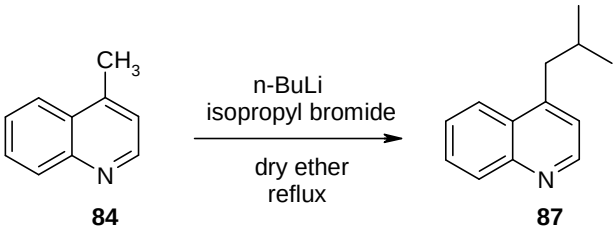

84 **87**

Scheme 3.21: *Attempted synthesis of 4-isobutylquinoline.*

TLC analysis showed there was no starting material remaining and indicated the presence of two new, less polar compounds. The ^{1}H NMR spectrum of the crude product was not consistent with the desired product but did confirm the presence of two new compounds. The minor product was identified as 2-butyl-4-methylquinoline **89**. This conclusion was reached because in the aromatic region of the ^{1}H NMR spectrum (Figure 3.1), the signal corresponding to H-2 was absent and the signal corresponding to H-3 was observed as a singlet at 7.06 ppm. The signals corresponding to the protons of the butyl group were observed at 0.88 ppm (CH_3), 1.13 ppm, 1.35 ppm and 1.69 ppm ($3 \times CH_2$). In addition, the presence of the singlet at 2.59 ppm indicated the methyl group at the 4-position was still intact. Similarly, the major product was identified as 2-butyl-4-methyl-1,2-dihydroquinoline **88**. The key evidence for this product from the ^{1}H NMR spectrum (Figure 3.1) was the presence of only 4 signals in the aromatic region and a signal corresponding to an alkene proton (H-3) at 5.31 ppm. Also, a signal corresponding to the remaining H-2 was observed at 4.07 ppm and a broad signal was observed at 3.56-3.80 ppm due to the presence of the NH. Again, the signals for the protons of the butyl group were present and the singlet at 1.90 ppm confirmed the methyl group at the 4-position was still intact. The identity of the two products was confirmed by mass spectrometry which showed a signal corresponding to the $(M+H)^+$ molecular ion for 2-butyl-4-methylquinoline **89** at *m/z* 200 (relative intensity 100%) and also the $(M+H)^+$ molecular ion for 2-butyl-4-methyl-1,2-dihydroquinoline **88** at *m/z* 202 (relative intensity 10%).

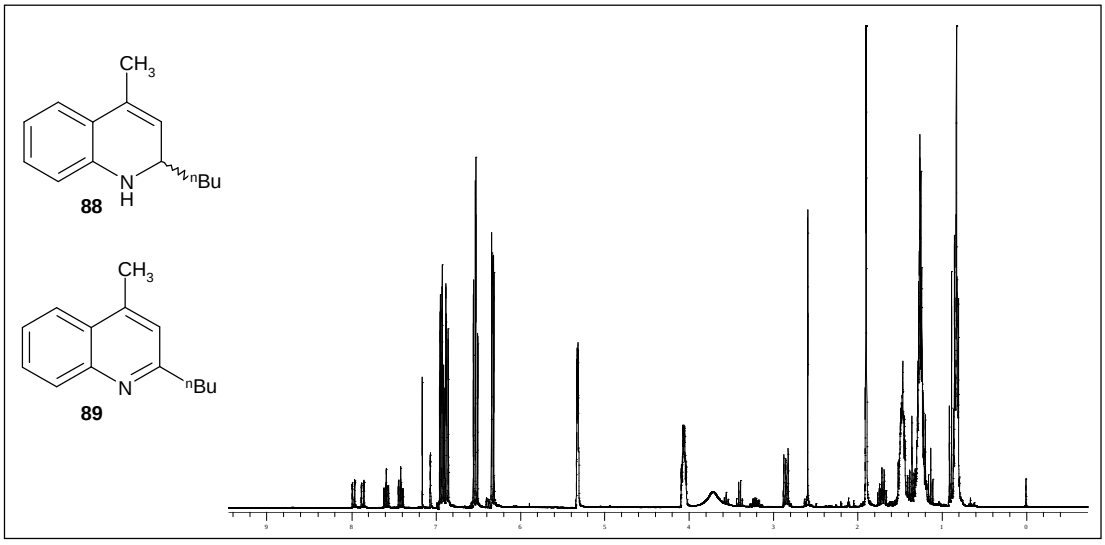

Figure 3.1: *^{1}H NMR spectrum of the crude product mixture from the attempted alkylation reaction.*

The spectral data are therefore consistent with nucleophilic addition of n-butyllithium to form the major product, 2-butyl-4-methyl-1,2-dihydroquinoline **88**, followed by some adventitious oxidation to give the minor product, 2-butyl-4-methylquinoline **89** (Scheme 3.22).

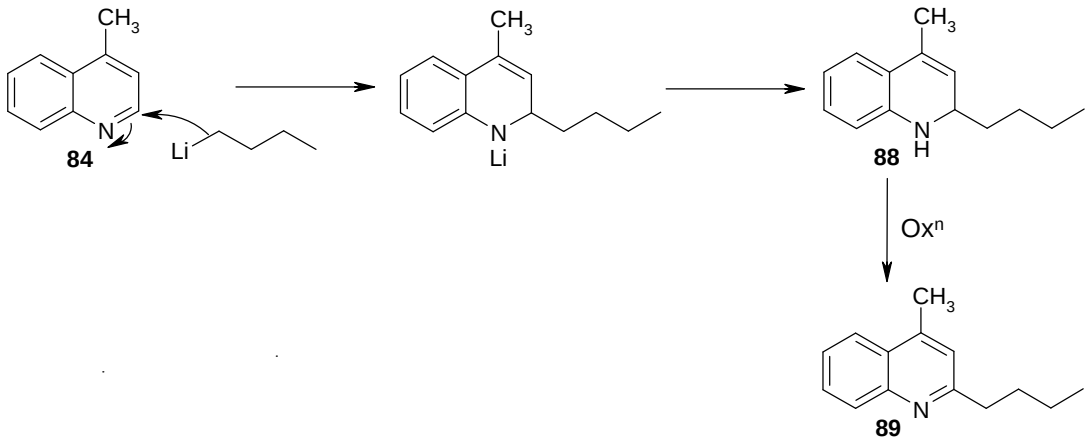

Scheme 3.22: *Formation of 2-butyl-4-methyl-1,2-dihydroquinoline and 2-butyl-4-methylquinoline by reaction of 4-methylquinoline with n-butyllithium.*

Therefore, apparently n-butyllithium is not an effective reagent for the deprotonation of the methyl group of 4-methylquinoline **84** under the conditions employed. It has been reported that phenyllithium also adds to the azomethine linkage of 4-methylquinoline to give a mixture of 2-phenyl-4-methylquinoline and 2,2-diphenyl-4-methyl-1,2-dihydroquinoline.[30] However, it has been claimed that the desired alkylated product was produced when methyllithium was used as the base. [29]

An attempt was therefore made to prepare 4-isobutylquinoline **87** from 4-methylquinoline **84** and isopropyl bromide using methyllithium in place of n-butyllithium. As before, a 2:2:1 molar ratio of substrate, organolithium compound and alkyl halide was used. However, this reaction was also unsuccessful. Both the ^{1}H NMR data and the mass spectrometry data showed addition of methyllithium at the 2-position had occurred to give 2,4-dimethyl-1,2-dihydroquinoline **90** (Scheme 3.23).

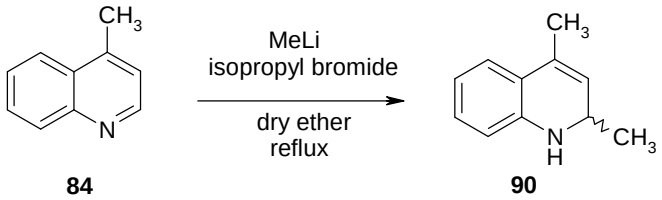

84 **90**

Scheme 3.23: *Nucleophilic addition of methyllithium to 4-methylquinoline.*

An attempt was then made to prepare 4-isobutylquinoline **87** by treating 4-methylquinoline **84** with the sterically hindered, non-nucleophilic base, lithium diisopropylamide and then reacting the resulting anion with isopropyl bromide (Scheme 3.24). However, both TLC and ^{1}H NMR analysis of the crude product showed only the two intact starting materials were present, indicating no reaction had occurred.

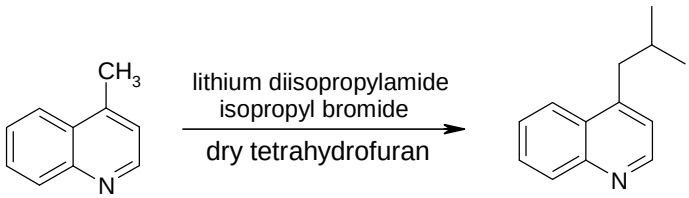

84 **87**

Scheme 3.24: *Attempted synthesis of 4-isobutylquinoline.*

Attention therefore turned to the alkylation of 4-methylquinoline using sodium amide as the base, a method that has greater literature precedent.[31-36] An initial attempt was made to prepare 4-isobutylquinoline **87** by treating 4-methylquinoline **84** with 1.1 equivalents of sodium amide, generated *in situ* from metallic sodium, liquid ammonia and iron (III) nitrate, and then reacting the resulting anion with 1.1 equivalents of the alkylating agent, isopropyl bromide (Scheme 3.25).[31,32]

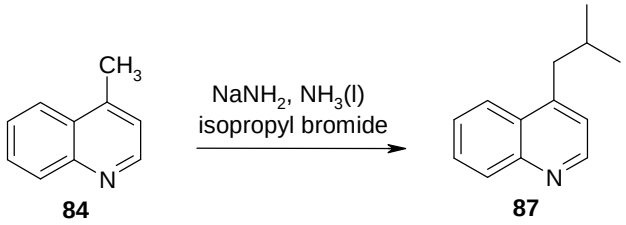

84 **87**

Scheme 3.25: *Synthesis of 4-isobutylquinoline.*

TLC analysis indicated the presence of a new less polar compound in addition to unreacted 4-methylquinoline **84**. The product was successfully purified by column chromatography on silica. The ^{1}H NMR spectrum of the pure product was consistent with the desired product, 4-isobutylquinoline **87**. The signal corresponding to the new CH_2 group was observed as a doublet at 2.84 ppm. The identity of the product was confirmed by electrospray mass spectrometry (ES^+) which showed a signal corresponding to the $(M+H)^+$ molecular ion at *m/z* 186 (relative intensity 100%).

However, the yield of 4-isobutylquinoline was low (20%). Since a lot of unreacted starting material was recovered, it was decided to try and push the reaction closer to completion by using 1.5 equivalents of base and alkylating agent and increasing the reaction time. An improved yield of pure 4-isobutylquinoline **87** (43%) was achieved, but there was still unreacted starting material present in the crude product.

Using the same method, two further 4-substituted quinolines were successfully synthesised. 4-Benzylquinoline **91** was prepared by treating 4-methylquinoline **84** with 1.5 equivalents of sodium amide and then reacting the resulting anion with 1.5 equivalents of bromobenzene (Scheme 3.26).[31,32]

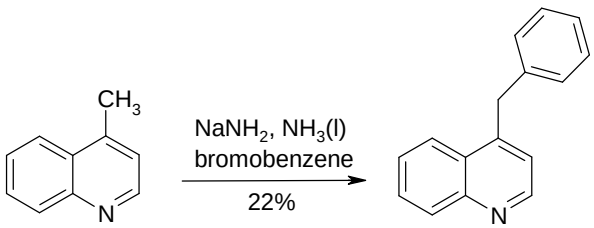

84 **91**

Scheme 3.26: *Synthesis of 4-benzylquinoline.*

TLC analysis showed there was unreacted 4-methylquinoline **84** present. Purification of the crude product by column chromatography on silica gave the desired product in 22% yield. The ^{1}H NMR spectrum was consistent with the expected product, 4-benzylquinoline **91**. The signal for the CH_2 group that links the two aromatic rings was observed as a singlet at 4.44 ppm. The identity of the product was confirmed by electrospray mass spectrometry (ES^+), which showed a signal corresponding to the $(M+H)^+$ molecular ion at *m/z* 220 (relative intensity 100%).

It is thought that this reaction proceeds via an elimination-addition mechanism (Scheme 3.27). This would involve removal of a proton *ortho* to the bromo substituent of bromobenzene **92** by sodium amide, followed by loss of the bromide ion in an elimination reaction to form benzyne **93**. The next step would then involve addition of the nucleophilic anion **85**, formed by deprotonation of 4-methylquinoline **84** by sodium amide, to the triple bond of benzyne. Finally, protonation of the benzene ring would give the product.

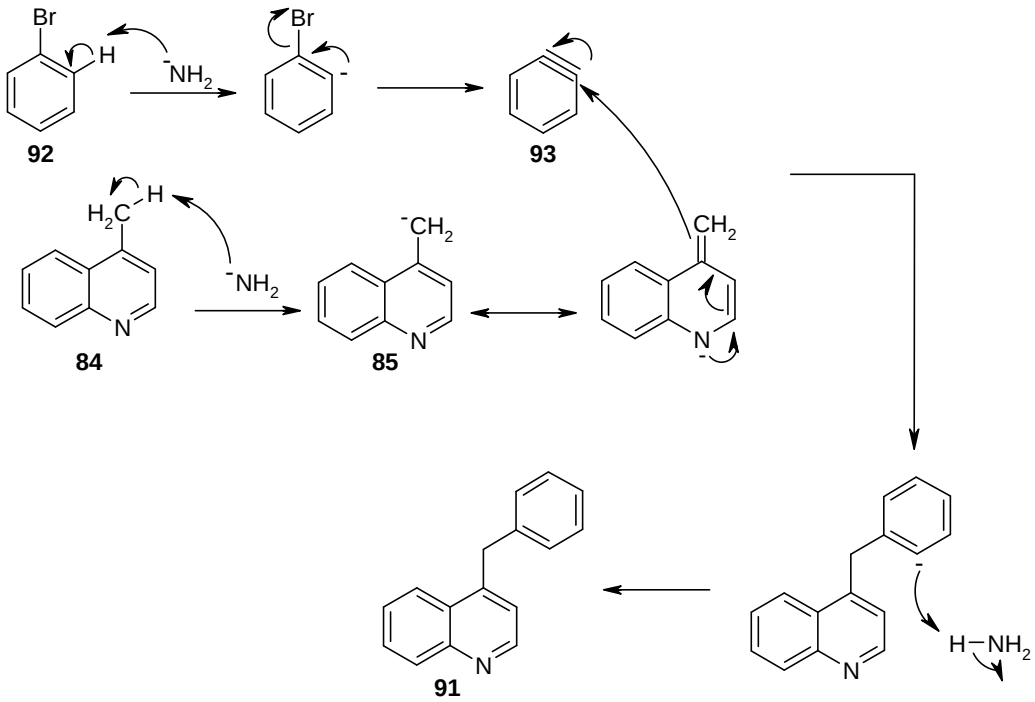

Scheme 3.27: *Possible mechanism for the formation of 4-benzylquinoline.*

Finally, 4-phenethylquinoline **94** was prepared by treating 4-methylquinoline **84** with 1.5 equivalents of sodium amide and then reacting the resulting anion with 1.5 equivalents of benzyl bromide (Scheme 3.28).[31,32]

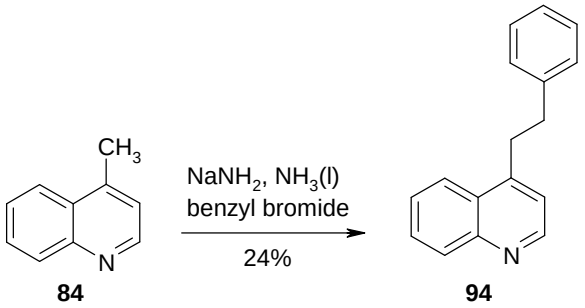

84 **94**

Scheme 3.28: *Synthesis of 4-phenethylquinoline.*

TLC analysis showed there was unreacted 4-methylquinoline **84** present. Purification of the crude product by column chromatography on silica gave the desired product in 24% yield. The ^{1}H NMR spectrum was consistent with the expected product, 4-phenethylquinoline **94**. The signals for the two CH_2 groups that link the two aromatic rings were observed as a pair of triplets at 3.01 ppm and 3.32 ppm. The identity of the product was confirmed by mass spectrometry, which showed a signal corresponding to the $(M+H)^+$ molecular ion at *m/z* 234 (relative intensity 100%).

Although 4-isobutylquinoline **87**, 4-benzylquinoline **91** and 4-phenethylquinoline **94** were successfully prepared by the sodium amide mediated alkylation of 4-methylquinoline **84**, the yield of pure product in each case was rather low. A lot of unreacted starting material was recovered indicating incomplete conversion. In addition, the low crude yield of each product suggested material was being lost during the work-up procedure. However, sufficient product had been obtained in each case to attempt the oxidation reaction to produce the corresponding quinolinic acid derivatives.

There are several reports of different methods for the oxidation of quinolines to the corresponding quinolinic acid derivatives.[17-28] An initial attempt was made to oxidise 4-methylquinoline **84** using potassium permanganate as the oxidising agent (Scheme 3.29).[19] This involved heating a mixture of 4-methylquinoline **84** and water under reflux while slowly adding an aqueous solution of potassium permanganate. Upon addition, the potassium permanganate decolourised and a brown precipitate formed. The addition of the potassium permanganate solution was continued until the decolourisation became much slower. After six hours, approximately 6.5 equivalents of potassium permanganate had been added. The brown precipitate of manganese dioxide was removed by filtration and the filtrate was concentrated. The product did not precipitate upon addition of acid, so the remainder of the water was removed under reduced pressure to give a yellow solid.

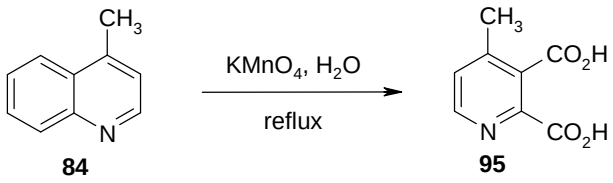

84 **95**

Scheme 3.29: *Attempted potassium permanganate oxidation of 4-methylquinoline.*

The ^{1}H NMR spectrum of the desired product, 4-methylquinolinic acid **95**, would be expected to show a pair of doublets corresponding to the two aromatic protons and a singlet upfield corresponding to the methyl group protons. Interestingly, the ^{1}H NMR spectrum of the crude product showed a pair of doublets in the aromatic region at 7.76 and 8.37 ppm with a corresponding singlet for a methyl group at 2.45 ppm, but also a lower intensity pair of doublets at 7.51 and 8.45 ppm, also with a corresponding singlet for a methyl group at 2.25 ppm. Also observed were small signals corresponding to unreacted 4-methylquinoline **84**. TLC analysis confirmed the presence of the unreacted starting material and also showed a spot on the baseline.

The mechanism of the oxidation reaction may provide a clue as to the identity of the two products from the initial oxidation attempt. The reaction proceeds in two stages; oxidative cleavage of the aromatic ring to form a dialdehyde **96** followed by oxidation of the intermediate dialdehyde to give the desired diacid **95** (Scheme 3.30). It is possible that the desired reaction has not reached completion and an intermediate

from incomplete oxidation may be present in addition to the desired diacid. The absence of a signal in the ^{1}H NMR spectrum in the region 9-10 ppm corresponding to an aldehyde proton suggests that the dialdehyde **96** is not present. It is possible that the product is a cyclised adduct **99, 100** formed from an intermediate containing one aldehyde group and one carboxylic acid group **97, 98** (Scheme 3.30).

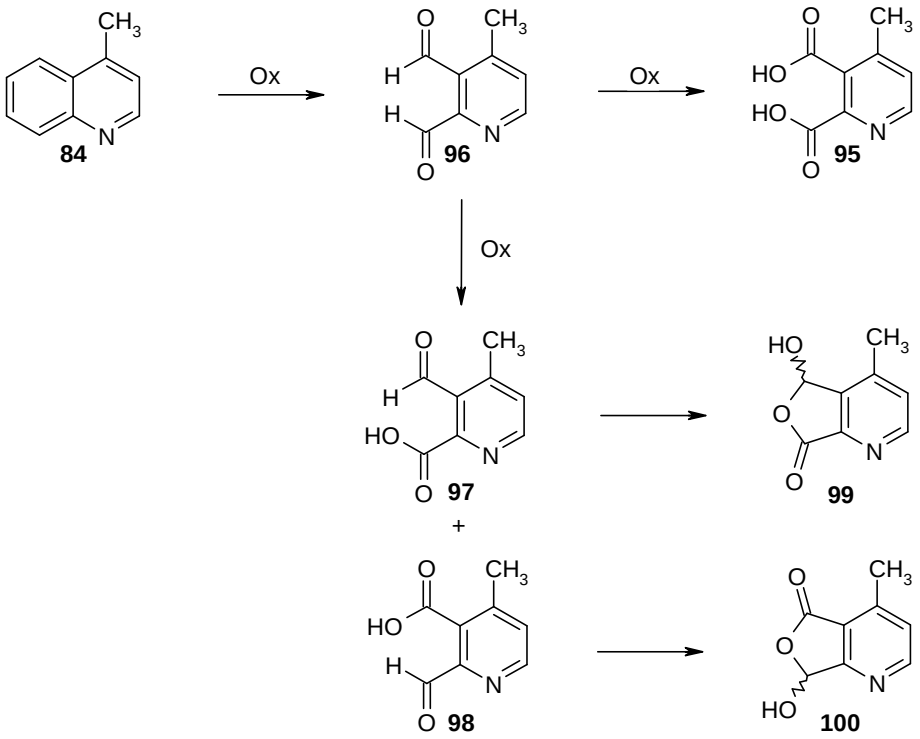

Scheme 3.30: *Oxidation of 4-methylquinoline.*

In an attempt to push the oxidation reaction closer to completion, the oxidation of 4-methylquinoline **84** was repeated using a greater excess of potassium permanganate and a longer reaction time. Over a period of six hours, approximately 8 equivalents of the oxidising agent were added and then heating under reflux was continued overnight. The ^{1}H NMR spectrum of the crude material showed 4 products had been produced. The same two pairs of doublets in the aromatic region and corresponding singlets upfield were observed. However, two new pairs of doublets were also observed in the aromatic region. This would suggest that further reaction has occurred, probably oxidation of the methyl group to the carboxylic acid. The crude mixture was analysed by electrospray mass spectrometry (ES^+), which showed a signal corresponding to a $(M+H)^+$ molecular ion at *m/z* 182 (relative intensity 100%)

and also $(M+K)^+$ at *m/z* 220 (relative intensity 20%) corresponding to the desired product, 4-methylquinolinic acid **95**. Also observed was a signal at *m/z* 250 (relative intensity 25%), which is consistent with an $(M+K)^+$ ion for the fully oxidised pyridine-2,3,4-tricarboxylic acid **101**. The identity of the remaining two products is still unknown.

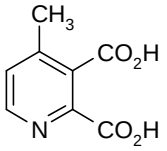

95

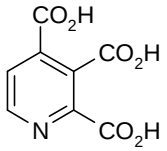

101

Since the separation of the desired product from the mixture of oxidation products is very difficult, a more efficient oxidation method was sought. Attention turned to the ruthenium tetroxide (RuO_4) catalysed oxidation of quinolines using sodium hypochlorite as the stoichiometric co-oxidant, a method of interest because of its simplicity and convenience.[22] Such reactions are carried out in an aqueous / organic biphasic solvent system. Scheme 3.31 represents the processes that occur within the biphasic system. Initially, ruthenium tetroxide (RuO_4) is generated *in situ* by the oxidation of the ruthenium (IV) oxide by the hypochlorite in the aqueous phase. The RuO_4 then partitions between the two phases, strongly favouring the organic phase where it oxidises the water-insoluble organic substrate. In doing so, the RuO_4 is reduced to an insoluble Ru (IV) species and when this species is transferred into the aqueous phase it is reoxidised to RuO_4 by the excess hypochlorite present. The RuO_4 then partitions into the organic phase and the catalytic cycle involving RuO_4 mediating the oxidation of the organic substrate by the strong oxidising agent continues. It is crucial to have the maximum degree of mixing of the two phases in order that there should be rapid transfer of RuO_4 from the aqueous phase into the organic phase and, upon reduction, return of RuO_2 back into the aqueous phase. This will aid the fast and efficient oxidation of the organic substrate.

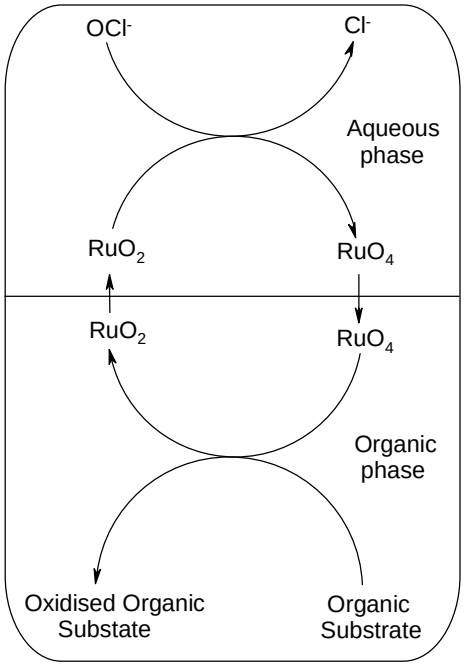

Scheme 3.31: *Schematic diagram illustrating the processes which occur in the biphasic system during the oxidation of a water-insoluble organic substrate using an oxidising agent (OCl^-) mediated by RuO_4, generated in situ.*

The oxidation of 4-methylquinoline **84** was attempted using this ruthenium tetroxide catalysed method (Scheme 3.32).[22]

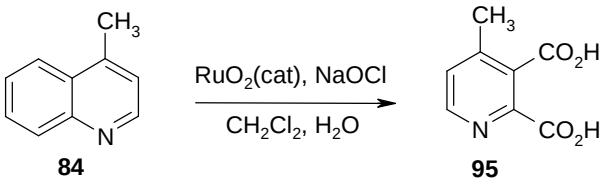

84 **95**

Scheme 3.32: *Ruthenium tetroxide catalysed oxidation of 4-methylquinoline.*

The progress of the reaction was monitored by TLC using samples taken from both the aqueous phase and the organic phase at regular intervals. The reaction was continued until TLC analysis showed there was no 4-methylquinoline **84** remaining in the organic phase. TLC analysis showed the product was present in the aqueous phase. The two phases were separated and the aqueous phase was acidified and evaporated to dryness to give the crude product. The ^{1}H NMR spectrum of the crude product was consistent with the expected product, 4-methylquinolinic acid **95**, showing a pair of doublets at 7.91 ppm and 8.49 ppm for the two aromatic protons and a corresponding singlet at 2.52 ppm for the protons of the methyl group.

While the ^{1}H NMR spectrum showed there were no organic impurities present, it was evident from the high crude yield that there were some inorganic impurities present. Also, the crude product smelled strongly of bleach. The crude product was obtained from the aqueous phase and since the reaction uses a large excess of sodium hypochlorite as the co-oxidant, evaporation to dryness gives the product mixed with the excess solid sodium hypochlorite salt. Hence the product required desalinisation. However, the product was too polar for purification by column chromatography on silica or alumina. The product also proved to be too polar for chromatography on a C-18 reverse phase column and passed through unhindered. Attention therefore turned to ion exchange chromatography, a technique commonly used to purify amino acids. This technique achieves separation based on the charges carried by a molecule. At pH 1, 4-methylquinolinic acid **95** will exist in the fully protonated cationic form **102** (Scheme 3.33) and an attempt was made to purify the product by cation exchange chromatography using an aliphatic sulfonic acid resin. However, this was unsuccessful. At pH 10, 4-methylquinolinic acid **95** will exist in the fully deprotonated anionic form **103** (Scheme 3.33). However, an attempt to purify the product by anion exchange chromatography using a quaternary amine resin was also unsuccessful.

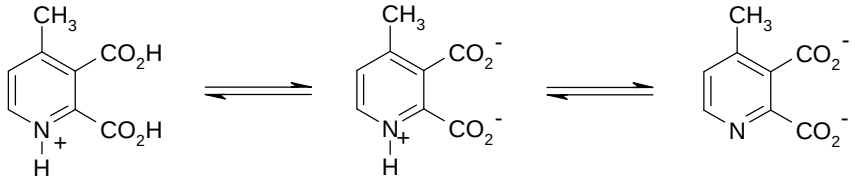

102 **103**

Scheme 3.33: *Different protonated forms of 4-methylquinolinic acid.*

It was therefore decided to try and separate the product from the excess sodium hypochlorite by utilising their different chemical properties, in particular solubility. *N*,*N*-Dimethylformamide was added to dissolve the product and the insoluble sodium hypochlorite salt was removed by filtration. The filtrate was evaporated to dryness and the resulting orange solid was washed repeatedly with toluene followed by chloroform and the product was recrystallised from ethanol. Spectroscopic characterisation of the product confirmed its identity as the desired 4-methylquinolinic acid **95**. Analysis of the product by electrospray mass spectrometry (ES^{+}) showed a signal corresponding to the $(M+H)^{+}$ molecular ion at

m/z 182 (relative intensity 100%). The ^{1}H NMR spectrum showed signals corresponding to the two aromatic protons at 7.91 ppm and 8.49 ppm, with a corresponding singlet at 2.52 ppm for the protons of the methyl group. The ^{13}C NMR spectrum showed two quaternary carbon signals at 167.5 ppm and 171.4 ppm, confirming the presence of the two carboxylic acid groups. This was also confirmed by infrared spectroscopy. However, the slightly low melting point and the UV data (λ_{max} 276 nm log ε 1.96, cf. lit.[37] λ_{max} 276 log ε 3.69) suggested the product was not entirely pure. Also, the product still smelled slightly of bleach. Therefore, while this appears to be a simpler and more efficient oxidation method than the potassium permanganate oxidation, there are still problems with purification.

Using this ruthenium tetroxide catalysed method, attempts were also made to oxidise the other 4-substituted quinoline derivatives that had been prepared. In all the attempts to oxidise 4-isobutylquinoline **87** two products were produced. In the ^{1}H NMR spectrum of the crude product, two doublets were observed at 8.09 and 8.67 ppm and two lower intensity doublets were observed at 7.97 and 8.75 ppm. For each pair of doublets there were signals corresponding to the protons of an isobutyl group, indicating the side chain was intact in both products. It is possible that the desired product was present in addition to an intermediate from incomplete oxidation. Since the polarity of the two products would make separation by column chromatography impossible, it was decided to try to esterify the desired 4-isobutylquinolinic acid in the crude material to make it less polar and therefore separable from the crude mixture. The crude mixture was thus heated in refluxing methanol in the presence of acid overnight. However, the ^{1}H NMR spectrum of the crude material showed no sign of the desired product, showing the reaction had been unsuccessful.

Similarly for 4-benzylquinoline **91** and 4-phenethylquinoline **94** the oxidation reaction produced a mixture of products that proved difficult to separate. Therefore, this route also failed to produce pure 4-substituted quinolinic acid derivatives that could be tested as inhibitors of QPRTase.

3.3 Inhibition studies on human brain QPRTase

3.3.1 Introduction

In 1913, Michaelis and Menten described a simple model for a single substrate enzyme that accounts for the kinetic properties of enzyme catalysed reactions.[38] Although the QPRTase catalysed reaction is bimolecular, if kinetic studies are carried out under pseudo-first order conditions then the Michaelis-Menten model can be employed. The Michaelis-Menten model describes an enzymatic reaction as a two-step process (Scheme 3.34). Firstly, an enzyme E combines with substrate S to form an enzyme-substrate complex (ES). The ES complex has two possible fates; it can dissociate to E and S or can proceed to form product P. It is assumed that product formation is irreversible. A further assumption implicit in this model is that there is only one kinetically significant step between the ES complex and product formation. The product formation step is first order, with the rate constant k_{cat}. The kinetic constant k_{cat} represents the number of substrate molecules turned over by one molecule of enzyme per second and therefore provides an indication of how quickly an enzyme is operating.

$$E + S \underset{}{\overset{K_m}{\rightleftharpoons}} ES \xrightarrow{k_{cat}} P$$

Scheme 3.34: *General reaction described by the Michaelis-Menten equation.*

The Michaelis-Menten equation quantitatively describes the rate of an enzyme catalysed reaction. V_{max} is the maximum rate of an enzyme catalysed reaction and is attained when the catalytic sites on the enzyme are saturated with substrate. The Michaelis constant, K_m, is equal to the substrate concentration at which the reaction rate is half its maximal value and reflects the affinity of an enzyme for its substrate. The lower the value of K_m the greater the affinity of the enzyme for its substrate. The kinetic parameters K_m and V_{max} can be readily derived from rates of catalysis measured at different substrate concentrations:

$$V = \frac{V_{max}[S]}{K_m + [S]}$$

Addition of an inhibitor to this system makes the reaction slightly more complicated. The enzyme can now exist as four possible species; the free enzyme E, the enzyme-substrate complex (ES), the enzyme-inhibitor complex (EI) or the enzyme-substrate-inhibitor complex (ESI) depending on the type of inhibition observed.

In reversible competitive inhibition, an inhibitor I binds at the same site as the substrate S and therefore competes with the enzyme's substrate for binding to the active site (Scheme 3.35).

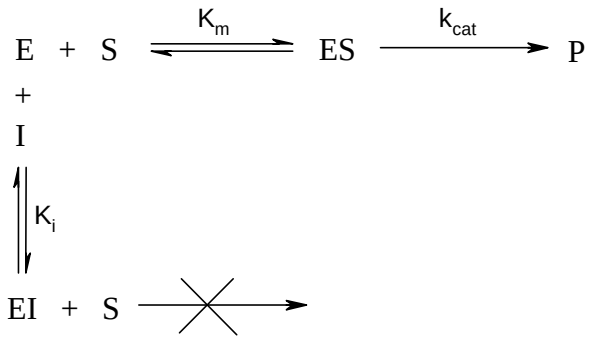

Scheme 3.35: *Competitive inhibition.*

This results in an apparent increase in K_m (i.e. an apparent decrease in the affinity of the enzyme for its substrate). V_{max} is unaffected by competitive inhibition since at high substrate concentrations the substrate can competitively displace the inhibitor. The rate equation for an enzymatic reaction in the presence of a competitive inhibitor then becomes:

$$V = \frac{V_{max}[S]}{K_{m(app)} + [S]} \qquad \text{where } K_{m(app)} = K_m (1 + [I] / K_i)$$

K_i is the dissociation constant for the enzyme-inhibitor complex. The lower the value of K_i, the greater the affinity of the enzyme for the inhibitor i.e. the better the compound is at inhibiting the enzyme.

In reversible noncompetitive inhibition, the substrate and inhibitor can bind simultaneously to the enzyme. They are not competing for the same binding site and therefore the inhibitor can interact with both the free enzyme and the enzyme-substrate complex (Scheme 3.36).

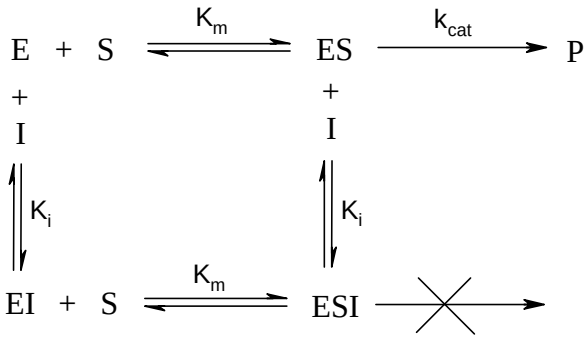

Scheme 3.36: *Noncompetitive inhibition.*

A noncompetitive inhibitor acts by decreasing the turnover number rather than by diminishing the proportion of enzyme molecules that are bound to substrate. Noncompetitive inhibition cannot be overcome by increasing the substrate concentration. Therefore in noncompetitive inhibition an apparent decrease in V_{max} is observed, while K_m remains unaffected. The rate equation for an enzymatic reaction in the presence of a noncompetitive inhibitor then becomes:

$$V = \frac{V_{max(app)}\,[S]}{K_m + [S]} \qquad \text{where } V_{max(app)} = V_{max} / (1 + [I] / K_i)$$

In reversible uncompetitive inhibition, the inhibitor interacts with the enzyme-substrate complex at a site other than the active site (Scheme 3.37).

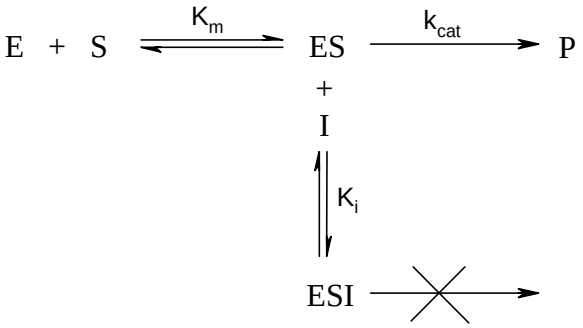

Scheme 3.37: *Uncompetitive inhibition.*

This results in an apparent decrease in both V_{max} and K_m. The apparent increase in affinity of the enzyme for substrate is due to unproductive substrate binding, resulting in a decrease in free enzyme concentration. Half-maximum rate, or half-maximal saturation, will therefore be attained at a relatively lower substrate concentration. The rate equation for an enzymatic reaction in the presence of an uncompetitive inhibitor then becomes:

$$V = \frac{V_{max(app)}\,[S]}{K_{m(app)} + [S]} \qquad \text{where } V_{max(app)} = V_{max} / (1 + [I] / K_i)$$
$$K_{m(app)} = K_m / (1 + [I] / K_i)$$

The different types of reversible inhibition are therefore kinetically distinguishable. A summary of the effects of reversible inhibitors on the kinetic parameters K_m and V_{max} is presented in Table 3.3.

Type of inhibition	**$K_{m(app)}$**	**$V_{max(app)}$**
Competitive	Increase $K_m (1+ [I]/K_i)$	No effect V_{max}
Noncompetitive	No effect K_m	Decrease $V_{max}/(1+ [I]/K_i)$
Uncompetitive	Decrease $K_m/(1+ [I]/K_i)$	Decrease $V_{max}/(1+ [I]/K_i)$

Table 3.3: *Summary of the effects of reversible inhibitors on the kinetic parameters K_m and V_{max}.*

A useful way to illustrate the type of inhibition observed is to display the kinetic data as a Lineweaver-Burk plot. The Lineweaver-Burk plot is a linear transform obtained by inverting the Michaelis-Menten equation:

$$\frac{1}{V} = \frac{K_m}{V_{max}} \cdot \frac{1}{[S]} + \frac{1}{V_{max}}$$

A plot of 1/V versus 1/[S] is linear with a slope equal to K_m/V_{max}. The *y*-intercept represents $1/V_{max}$ and the *x*-intercept represents $-1/K_m$. Therefore this plot can be used to illustrate the effect of an inhibitor on the kinetic parameters K_m and V_{max}. Although linear regression is effective for illustrative purposes, it is a poor model for

calculating kinetic parameters accurately. Since it is a double reciprocal plot, errors at low concentration are overemphasised while errors at high concentration are underemphasised. Therefore the best way to analyse enzyme kinetic data is to fit the data directly to the Michaelis-Menten equation using nonlinear regression. A Lineweaver-Burk plot can then be employed to illustrate the results.

3.3.2 Inhibition studies using quinolinic acid analogues

The following quinolinic acid analogues, which were either commercially available or were prepared in the laboratory, were all tested as inhibitors of human brain QPRTase.

2,3-Dicarboxylic acid derivatives:

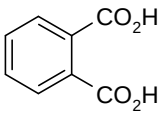

25

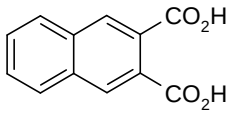

104

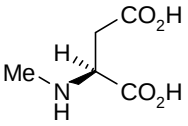

14

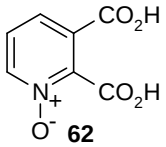

62

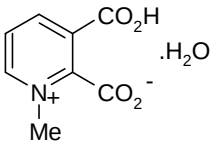

41

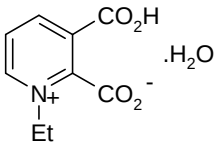

42

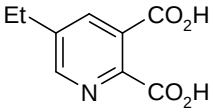

43

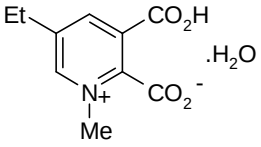

46

2-Carboxylic acid derivatives:

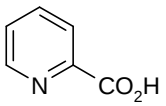

26

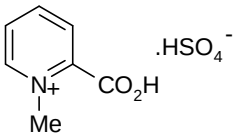

50

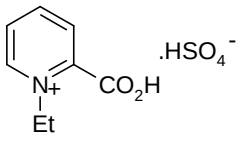

51

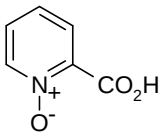

105

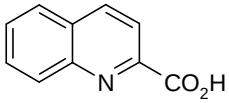

52

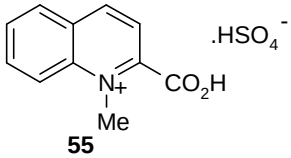

55

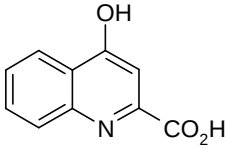

7

3-Carboxylic acid derivatives:

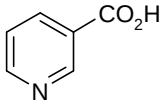

27

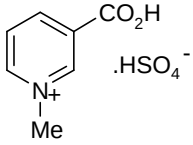

59

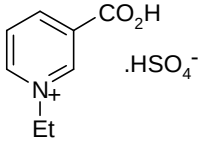

60

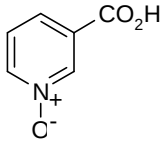

63

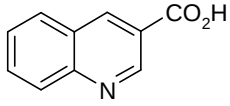

106

Firstly, a preliminary inhibition screen of the compounds was carried out by assessing the percentage inhibition of QPRTase activity at a fixed concentration of quinolinic acid (0.1 mM) and PRPP (0.1 mM). Detailed inhibition studies were then carried out on the compounds that were found to inhibit QPRTase. In order to determine the inhibitory properties of the compounds, the K_m and V_{max} values for the QPRTase reaction with respect to quinolinic acid as the variable substrate were determined at various fixed inhibitor concentrations. The effect on the kinetic parameters gave a measure of inhibition and also identified the type of inhibition observed. Lineweaver-Burk plots were constructed to illustrate the type of inhibition exhibited by each inhibitor, although these were used for illustrative purposes only and not for calculating kinetic parameters. Note that in all the Lineweaver-Burk plots, the line was constructed to fit the $K_{m(app)}$ and $V_{max(app)}$ values determined from non-linear regression. K_i values were determined using linear regression plots of $K_{m(app)}$ versus inhibitor concentration.

3.3.2.1 2,3-Dicarboxylic acid derivatives

The results of the preliminary inhibition screen of the 2,3-dicarboxylic acid derivatives are summarised in Table 3.4 and displayed in Figure 3.2.

Inhibitor	**% Inhibition with**			
	0.01 mM inhibitor	**0.1 mM inhibitor**	**1 mM inhibitor**	**10 mM inhibitor**
N-Methylquinolinic acid **41**	0	28	93	100
N-Ethylquinolinic acid **42**	0	24	96	100
5-Ethylquinolinic acid **43**	0	5	43	95
5-Ethyl-*N*-methylquinolinic acid **46**	0	0	30	90
Quinolinic acid *N*-oxide **62**	0	40	100	100
Phthalic acid **25**	6	45	100	100
2,3-Naphthalene dicarboxylic acid **104**	0	11	59	100
NMDA **14**	0	0	0	18

Table 3.4: *Percentage inhibition at varied inhibitor concentrations.*

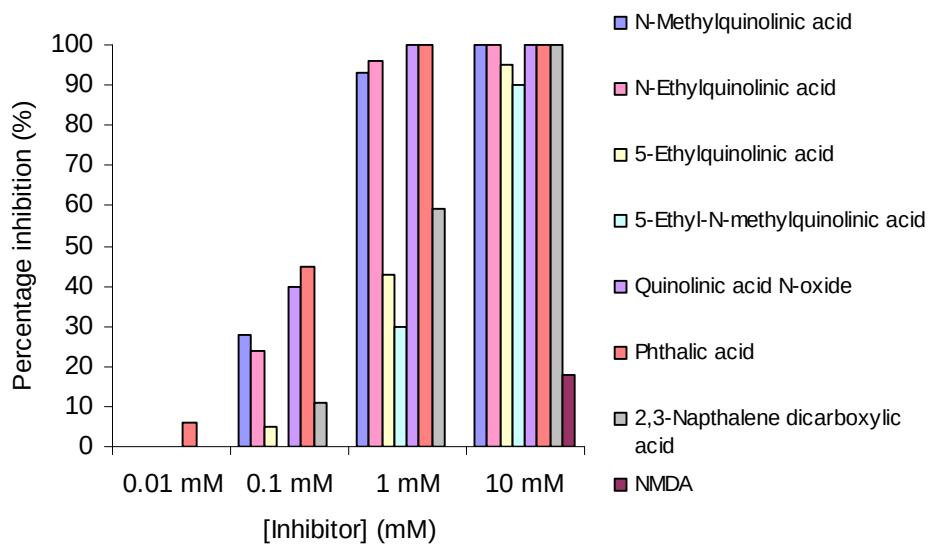

Figure 3.2: *Preliminary inhibition screen of the 2,3-dicarboxylic acid derivatives.*

Phthalic acid **25** was the only compound tested that inhibited QPRTase when present at a concentration of 0.01 mM. *N*-Methylquinolinic acid **41**, *N*-ethylquinolinic acid **42**, quinolinic acid *N*-oxide **62** and 2,3-naphthalene dicarboxylic acid **104** showed good levels of inhibition when present at concentrations above 0.1 mM. 5-Ethylquinolinic acid **43** and 5-ethyl-*N*-methylquinolinic acid **46** were effective inhibitors of QPRTase at higher concentrations.

NMDA **14**, however, showed only a low level of inhibition at high concentrations (18%, 10 mM). Quinolinic acid exerts its neurotoxic activity by overstimulating NMDA receptors.[39] Quinolinic acid is able to interact with the NMDA receptor since quinolinic acid and NMDA possess a similar backbone consisting of a 1,2-dicarboxylic acid functionality. The apparent lack of binding of NMDA to the active site of QPRTase at low concentrations may therefore be due to the absence of aromaticity. Structural studies on QPRTase have highlighted residues that are within Van der Waals distance of the substrate and in human brain QPRTase the sidechain of His160 could form an important interaction with the aromatic ring of quinolinic acid.

However, in the structural studies on human brain QPRTase, tartaric acid was found bound in the active site (section 2.3.1). Tartaric acid was present at a concentration of 0.6 M in the precipitant used to crystallise the protein. The 1,2-dicarboxylic acid functionality present in quinolinic acid is also present in tartaric acid and hence

tartaric acid is able to bind in the active site of QPRTase. Therefore, it seems that despite the lack of aromaticity, simple dicarboxylic acids are able to bind to QPRTase when present at high concentrations. Similarly, previous inhibition studies have found that maleic acid, malic acid, oxaloacetic acid, citric acid and succinic acid show low levels of inhibition of QPRTase when present at concentrations above 10 mM.[40,41]

Due to the low level of inhibition observed, it was decided not to carry out any further inhibition studies on NMDA. The inhibitory properties of all the other 2,3-dicarboxylic acid derivatives were examined in detail by performing careful kinetic analysis of the QPRTase catalysed reaction in the presence of different concentrations of the inhibitors.

3.3.2.1.1 N-Methylquinolinic acid

N-Methylquinolinic acid **41** was found to be a competitive inhibitor of QPRTase with respect to quinolinic acid. This was observed by an increase in K_m with increasing inhibitor concentration, while V_{max} remained relatively unchanged within the experimental error (Table 3.5). The competitive inhibition pattern is illustrated with a Lineweaver-Burk plot, which shows a series of straight lines intersecting on the *y*-axis (Figure 3.3).

[Inhibitor] (μM)	**$K_{m(app)}$ (μM)**	**$V_{max(app)}$ (μM min^{-1})**
0	13.6 ± 1.2	0.94 ± 0.02
100	42.4 ± 4.1	0.93 ± 0.03
200	74.1 ± 6.7	0.99 ± 0.04
300	106.8 ± 8.6	1.02 ± 0.04

Table 3.5: *Effect of N-methylquinolinic acid on kinetic parameters.*

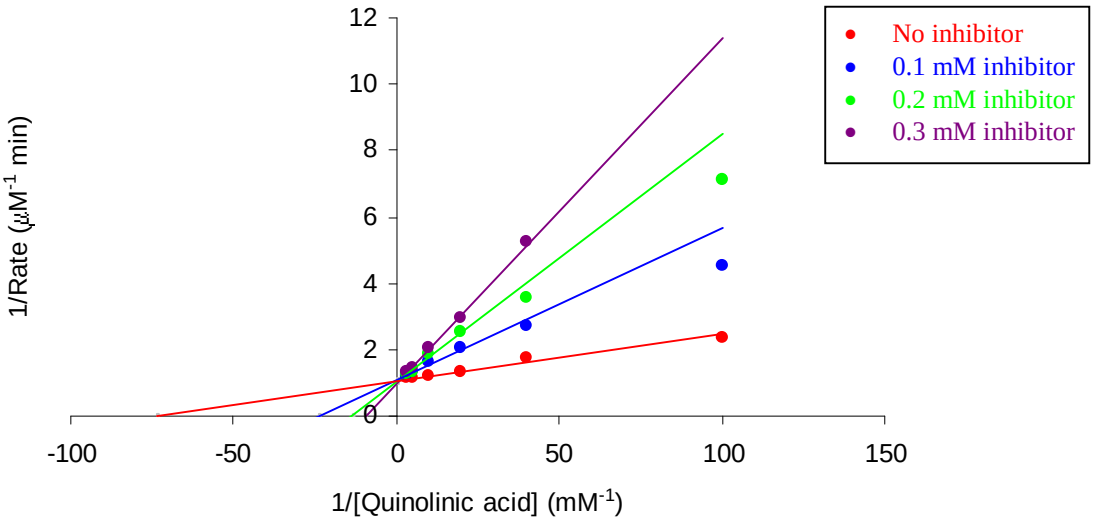

Figure 3.3: *Lineweaver-Burk plot for inhibition with N-methylquinolinic acid.*

In the presence of a competitive inhibitor, K_m increases by a factor of $(1 + [I]/K_i)$. The inhibition constant K_i can therefore be determined from a plot of $K_{m(app)}$ versus inhibitor concentration. This plot is linear and the slope is equal to K_m/K_i.

$$K_{m(app)} = K_m (1 + [I] / K_i)$$

$$K_{m(app)} = \frac{K_m}{K_i} . [I] + K_m$$

By performing this analysis, the K_i value for *N*-methylquinolinic acid was determined as 40 ± 2 μM with respect to quinolinic acid as the variable substrate (Figure 3.4).

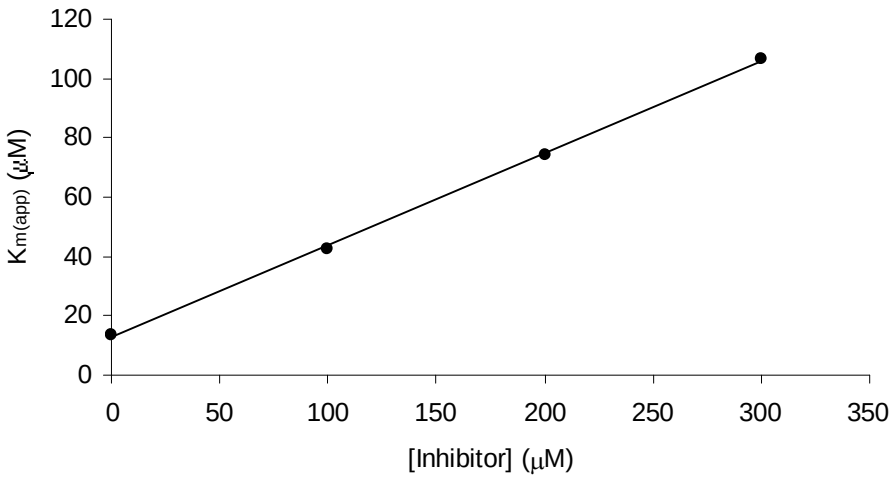

Figure 3.4: *Plot of $K_{m(app)}$ versus [N-methylquinolinic acid].*

3.3.2.1.2 N-Ethylquinolinic acid

Similarly, *N*-ethylquinolinic acid **42** was found to be a competitive inhibitor of QPRTase with respect to quinolinic acid (Table 3.6). The competitive inhibition pattern is illustrated with a Lineweaver-Burk plot (Figure 3.5).

[Inhibitor] (μM)	$K_{m(app)}$ (μM)	$V_{max(app)}$ (μM min^{-1})
0	13.6 ± 2.3	0.89 ± 0.05
100	32.1 ± 3.2	0.87 ± 0.03
200	70.5 ± 6.9	0.91 ± 0.04
300	98.0 ± 9.8	0.83 ± 0.08

Table 3.6: *Effect of N-ethylquinolinic acid on kinetic parameters.*

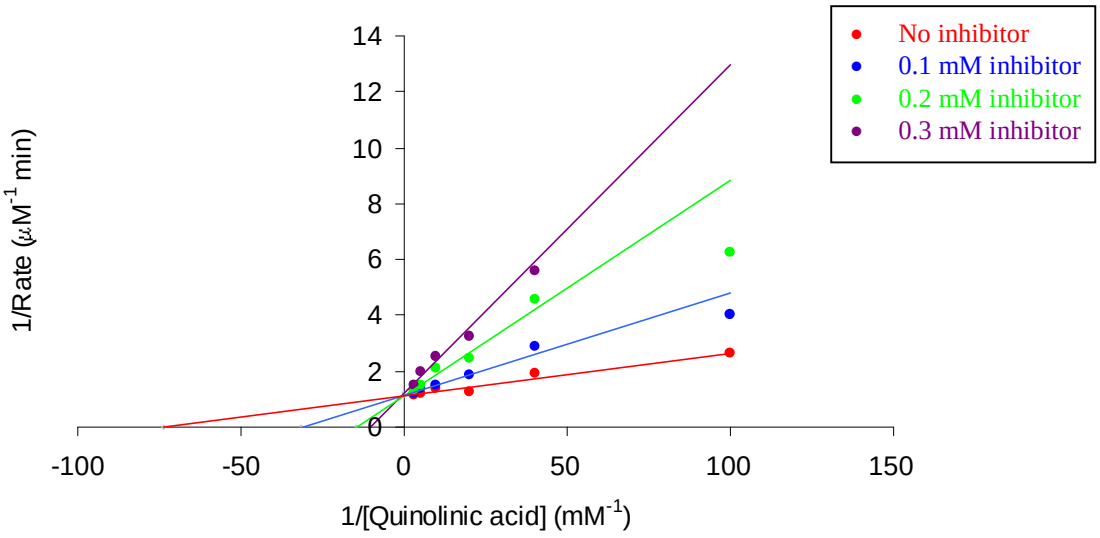

Figure 3.5: *Lineweaver-Burk plot for inhibition with N-ethylquinolinic acid.*

From a plot of $K_{m(app)}$ versus inhibitor concentration, the K_i value for *N*-ethylquinolinic acid **42** was determined as 34 ± 4 μM with respect to quinolinic acid as the variable substrate (Figure 3.6). This is very similar to the value of 40 μM determined for *N*-methylquinolinic acid **41** which suggests that increasing the size of the *N*-substituent from a methyl group to an ethyl group does not significantly affect the binding in the QPRTase active site.

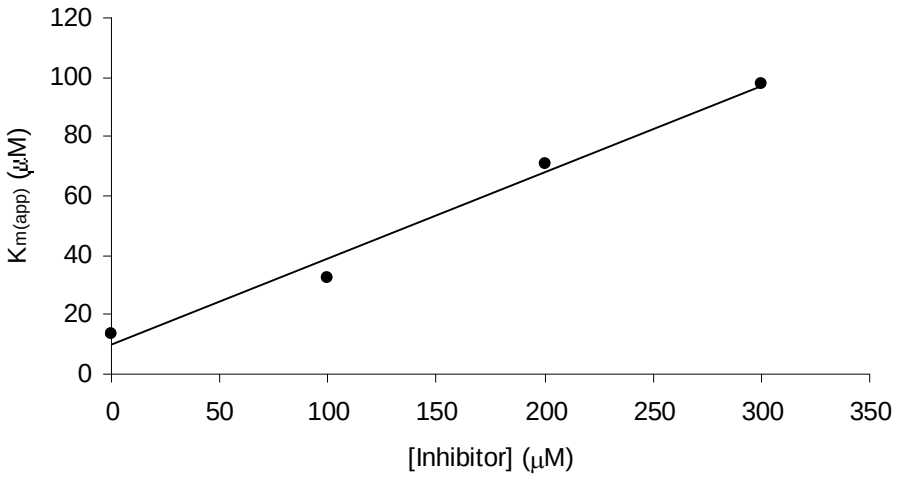

Figure 3.6: *Plot of $K_{m(app)}$ versus [N-ethylquinolinic acid]*.

The effectiveness of *N*-methyl and *N*-ethylquinolinic acid as inhibitors of QPRTase could be explained by their resemblance to the putative reaction intermediate, QAMN **16**. These compounds could be viewed as simple mimics of QAMN.

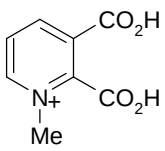

41

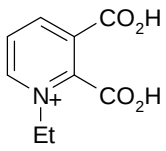

42

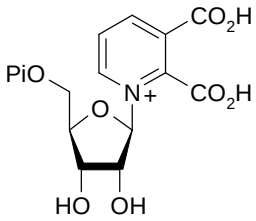

16

3.3.2.1.3 5-Ethylquinolinic acid

5-Ethylquinolinic acid **43** was found to be a competitive inhibitor of QPRTase with respect to quinolinic acid. This was observed by an increase in K_m with increasing inhibitor concentration, while V_{max} remained relatively unchanged within the experimental error (Table 3.7). The competitive inhibition pattern is illustrated with a Lineweaver-Burk plot (Figure 3.7).

[Inhibitor] (μM)	**$K_{m(app)}$ (μM)**	**$V_{max(app)}$ (μM min^{-1})**
0	13.4 ± 1.0	0.92 ± 0.01
600	33.2 ± 2.9	0.98 ± 0.04
800	44.9 ± 5.9	0.90 ± 0.06
1000	74.1 ± 12.1	0.86 ± 0.07

Table 3.7: *Effect of 5-ethylquinolinic acid on kinetic parameters.*

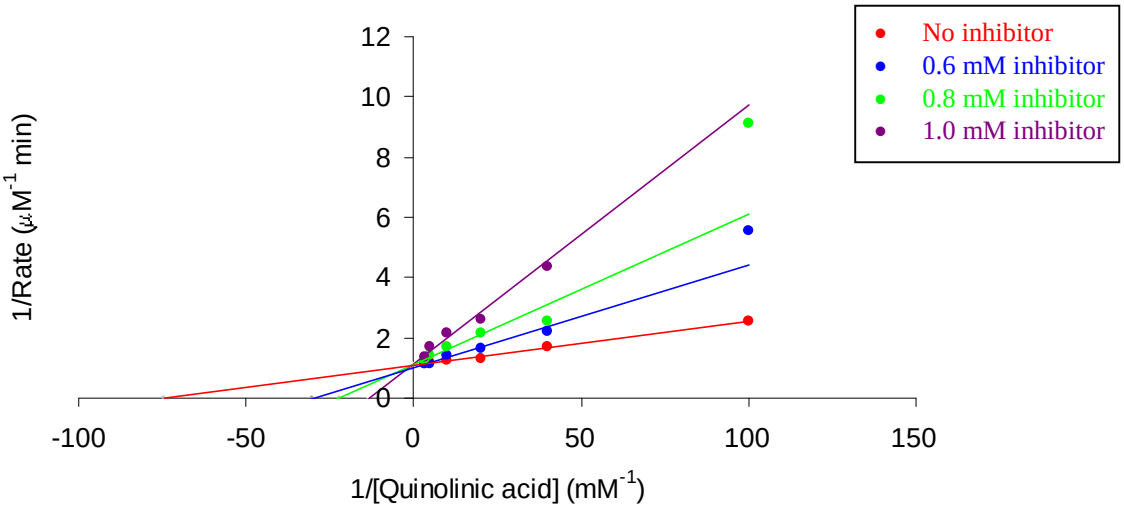

Figure 3.7: *Lineweaver-Burk plot for inhibition with 5-ethylquinolinic acid.*

From a plot of $K_{m(app)}$ versus inhibitor concentration, the K_i value for 5-ethylquinolinic acid **43** was determined as 158 ± 21 μM with respect to quinolinic acid as the variable substrate (Figure 3.8). 5-Ethylquinolinic acid is therefore an effective inhibitor of QPRTase.

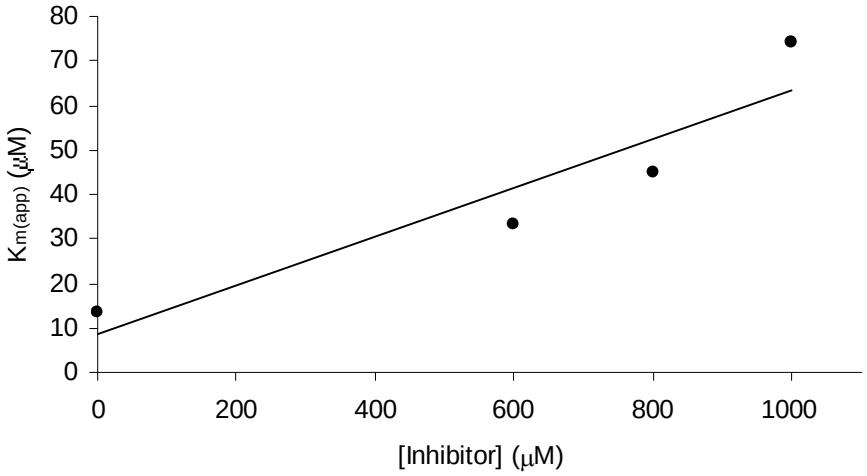

Figure 3.8: *Plot of $K_{m(app)}$ versus [5-ethylquinolinic acid].*

3.3.2.1.4 5-Ethyl-N-methylquinolinic acid

Similarly, 5-ethyl-*N*-methylquinolinic acid **46** was found to be a competitive inhibitor of QPRTase with respect to quinolinic acid (Table 3.8). The competitive inhibition pattern is illustrated with a Lineweaver-Burk plot (Figure 3.9).

[Inhibitor] (μM)	$K_{m(app)}$ (μM)	$V_{max(app)}$ (μM min^{-1})
0	13.4 ± 1.0	0.92 ± 0.01
600	26.8 ± 2.5	0.97 ± 0.02
800	37.5 ± 3.3	0.93 ± 0.02
1000	54.6 ± 8.4	0.88 ± 0.04

Table 3.8: *Effect of 5-ethyl-N-methylquinolinic acid on kinetic parameters.*

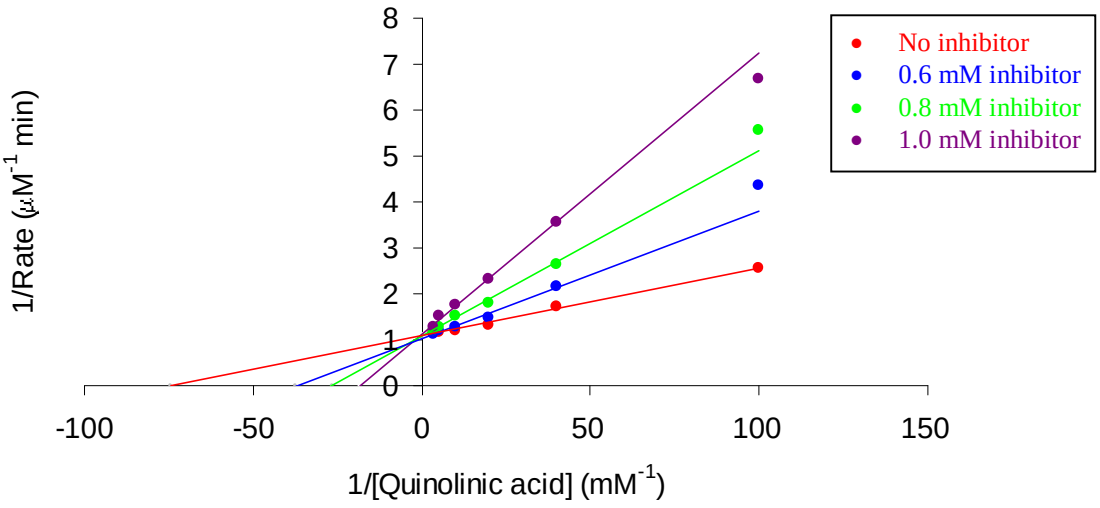

Figure 3.9: *Lineweaver-Burk plot for inhibition with 5-ethyl-N-methylquinolinic acid.*

The K_i value for 5-ethyl-*N*-methylquinolinic acid **46** was determined as 270 ± 29 μM with respect to quinolinic acid as the variable substrate (Figure 3.10). 5-Ethyl-*N*-methylquinolinic acid **46** is therefore a weaker inhibitor than the non-methylated derivative **43**. It would appear therefore that the presence of the *N*-substituent causes unfavourable interactions in the active site, leading to weaker binding. Furthermore, by comparing the K_i values determined for 5-ethyl-*N*-methylquinolinic acid **46** (270 ± 29 μM) and *N*-methylquinolinic acid

41 (40 ± 2 μM), it can be seen that 5-ethyl-*N*-methylquinolinic acid is a less effective inhibitor of QPRTase. Thus it would appear that, rather than providing additional binding interactions, the increased steric bulk resulting from the presence of the ethyl group at the 5-position of the pyridine ring leads to weaker binding in the active site.

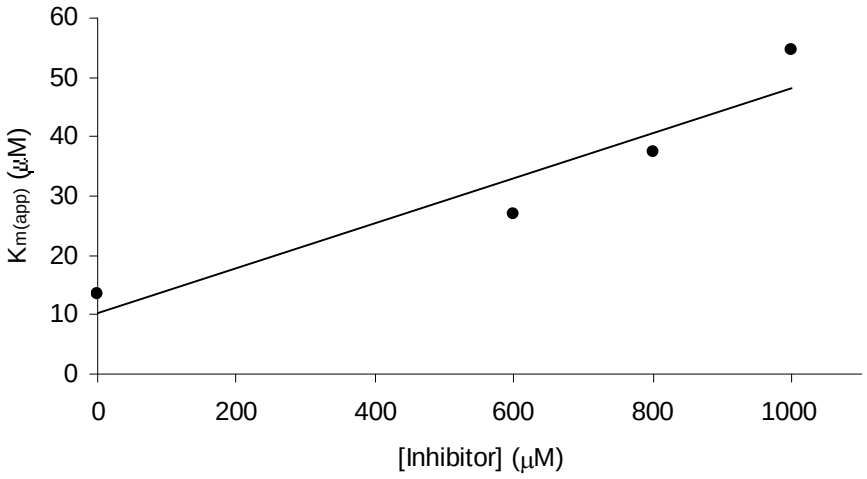

Figure 3.10: *Plot of $K_{m(app)}$ versus [5-ethyl-N-methylquinolinic acid].*

3.3.2.1.5 Quinolinic acid N-oxide

Quinolinic acid *N*-oxide **62** was found to be a competitive inhibitor of QPRTase with respect to quinolinic acid (Table 3.9). The competitive inhibition pattern is illustrated with a Lineweaver-Burk plot (Figure 3.11).

[Inhibitor] (μM)	**$K_{m(app)}$ (μM)**	**$V_{max(app)}$ (μM min^{-1})**
0	13.5 ± 1.6	0.94 ± 0.02
50	35.7 ± 3.5	0.94 ± 0.03
100	60.7 ± 5.1	1.00 ± 0.03
200	111.0 ± 10.0	1.07 ± 0.04

Table 3.9: *Effect of quinolinic acid N-oxide on kinetic parameters.*

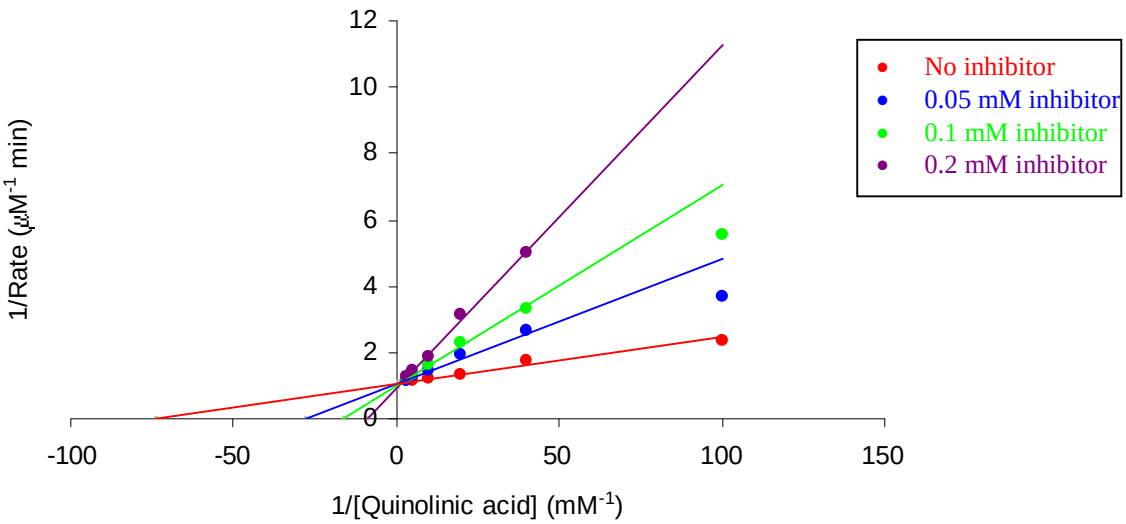

Figure 3.11: *Lineweaver-Burk plot for inhibition with quinolinic acid N-oxide.*

The K_i value for quinolinic acid *N*-oxide was determined as 25 ± 2 μM with respect to quinolinic acid as the variable substrate (Figure 3.12). Quinolinic acid *N*-oxide is therefore a potent competitive inhibitor of human brain QPRTase and appears to bind more tightly in the active site than the *N*-alkyl quinolinic acid derivatives. This could be due to electrostatic interactions between the negatively charged oxygen of the *N*-oxide and the highly positive electrostatic surface of the QPRTase active site.

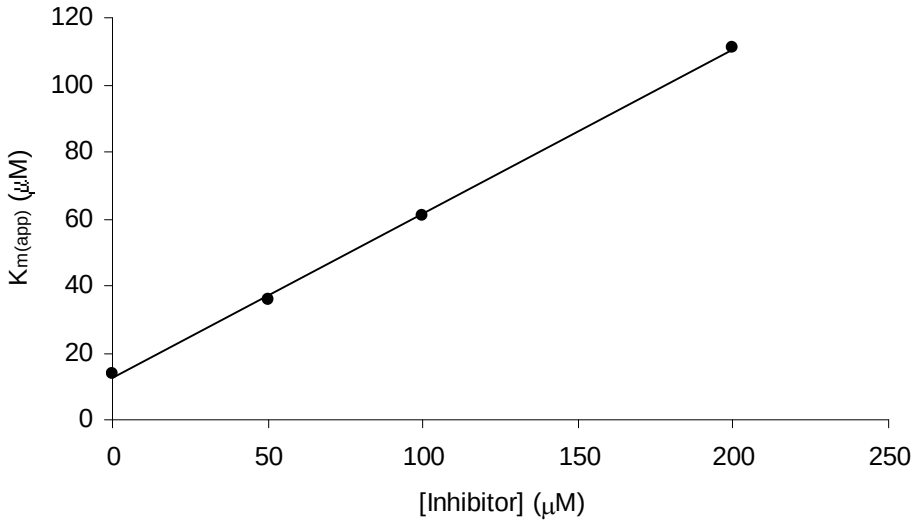

Figure 3.12: *Plot of $K_{m(app)}$ versus [quinolinic acid N-oxide].*

3.3.2.1.6 Phthalic acid

Phthalic acid **25** was found to be a competitive inhibitor of QPRTase with respect to quinolinic acid. This was observed by an increase in K_m with increasing inhibitor concentration, while V_{max} remained relatively unchanged within the experimental error (Table 3.10). The competitive inhibition pattern is illustrated with a Lineweaver-Burk plot (Figure 3.13).

[Inhibitor] (μM)	**$K_{m(app)}$ (μM)**	**$V_{max(app)}$ (μM min^{-1})**
0	13.5 ± 1.4	0.96 ± 0.02
50	74.0 ± 7.4	1.03 ± 0.04
100	109.7 ± 11.2	1.06 ± 0.06
200	203.0 ± 28.9	1.17 ± 0.09

Table 3.10: *Effect of phthalic acid on kinetic parameters.*

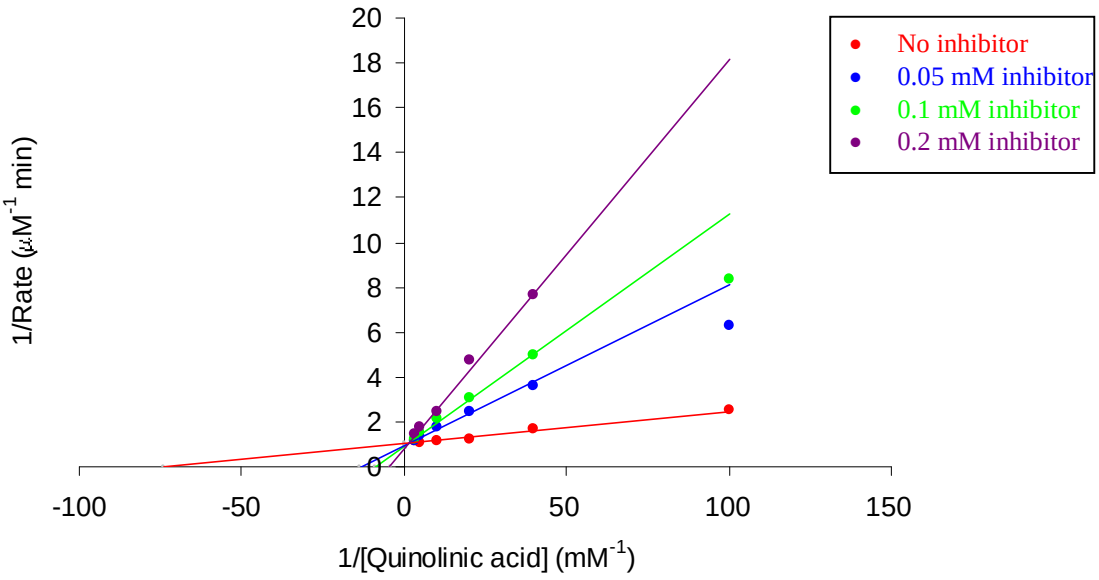

Figure 3.13: *Lineweaver-Burk plot for inhibition with phthalic acid.*

From a plot of $K_{m(app)}$ versus inhibitor concentration, the K_i value for phthalic acid was determined as 21 ± 3 μM with respect to quinolinic acid as the variable substrate (Figure 3.14).

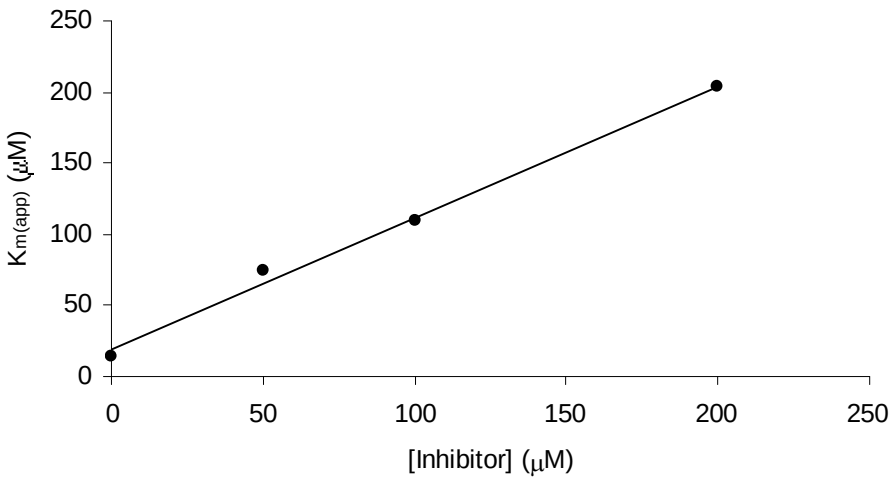

Figure 3.14: *Plot of $K_{m(app)}$ versus [phthalic acid].*

Phthalic acid **25** is therefore a potent competitive inhibitor of human brain QPRTase. This suggests that the ring nitrogen is not essential for binding. Consistent with this observation, previous structural studies on bacterial QPRTase did not highlight any binding interactions between the ring nitrogen of quinolinic acid and the active site residues.[42]

3.3.2.1.7 2,3-Naphthalene dicarboxylic acid

2,3-Naphthalene dicarboxylic acid **104** was found to be a competitive inhibitor of QPRTase with respect to quinolinic acid (Table 3.11). The competitive inhibition pattern is illustrated with a Lineweaver-Burk plot (Figure 3.15).

[Inhibitor] (μM)	**$K_{m(app)}$ (μM)**	**$V_{max(app)}$ (μM min^{-1})**
0	13.5 ± 1.4	0.96 ± 0.02
100	25.4 ± 2.0	0.95 ± 0.02
200	37.8 ± 3.2	0.94 ± 0.02
300	55.1 ± 4.3	0.98 ± 0.03

Table 3.11: *Effect of 2,3-naphthalene dicarboxylic acid on kinetic parameters.*

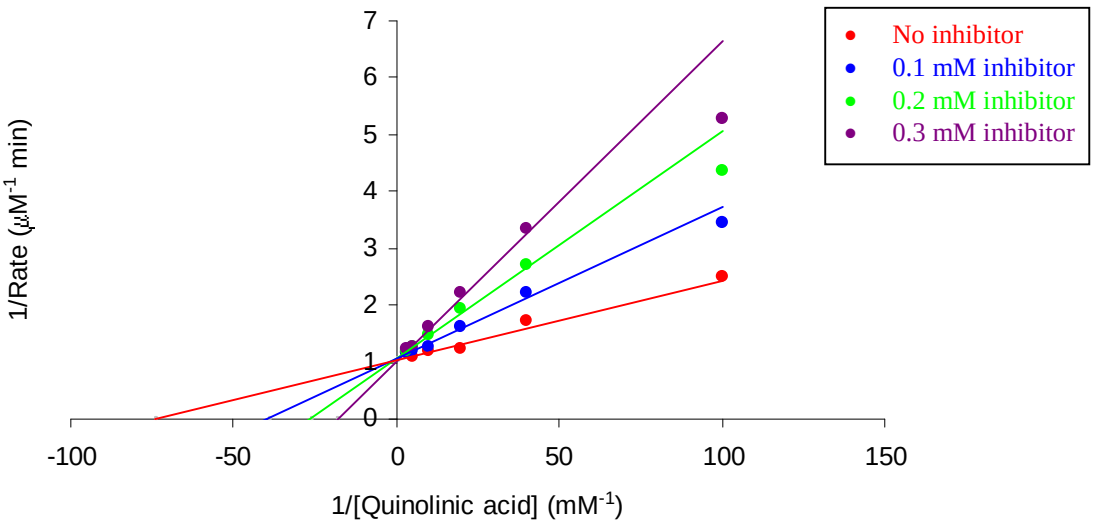

Figure 3.15: *Lineweaver-Burk plot for inhibition with 2,3-naphthalene dicarboxylic acid.*

The K_i value for 2,3-naphthalene dicarboxylic acid **104** was determined as 90 ± 4 μM with respect to quinolinic acid as the variable substrate (Figure 3.16). 2,3-Naphthalene dicarboxylic acid is therefore an effective inhibitor of QPRTase. This again suggests that the ring nitrogen is not essential for binding. However, this compound does not bind as tightly as phthalic acid **25**. This may be due to steric interference as a result of the larger bicyclic structure of 2,3-naphthalene dicarboxylic acid.

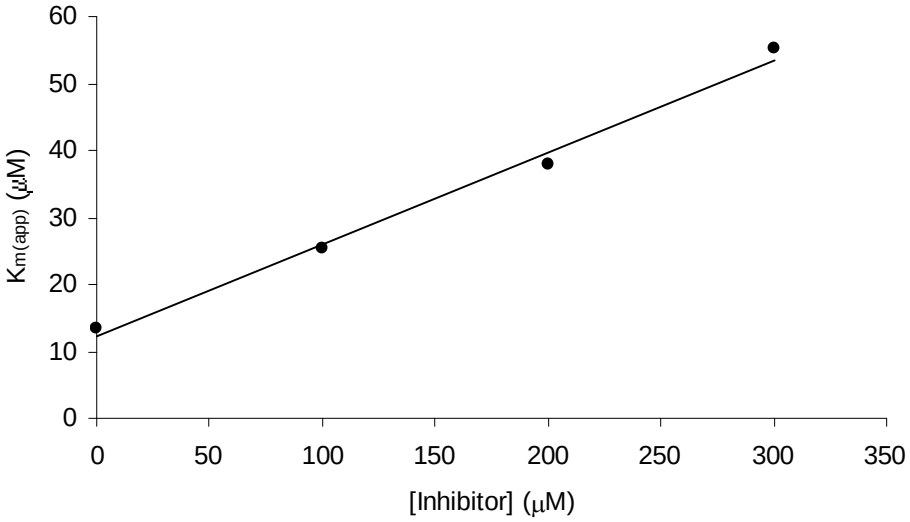

Figure 3.16: *Plot of $K_{m(app)}$ versus [2,3-naphthalene dicarboxylic acid].*

3.3.2.2 2-Carboxylic acid derivatives

The results of the preliminary inhibition screen of the 2-carboxylic acid derivatives are summarised in Table 3.12 and displayed in Figure 3.17.

Inhibitor	**% Inhibition with**			
	0.01 mM inhibitor	**0.1 mM inhibitor**	**1 mM inhibitor**	**10 mM inhibitor**
Picolinic acid **26**	0	14	75	100
N-Methylpicolinic acid **50**	0	8	60	100
N-Ethylpicolinic acid **51**	0	10	63	100
Picolinic acid *N*-oxide **105**	0	10	68	100
Quinoline-2-carboxylic acid **52**	0	5	47	95
N-Methylquinoline-2-caboxylic acid **55**	0	0	32	85
Kynurenic acid **7**	0	0	5	26

Table 3.12: *Percentage inhibition at varied inhibitor concentrations.*

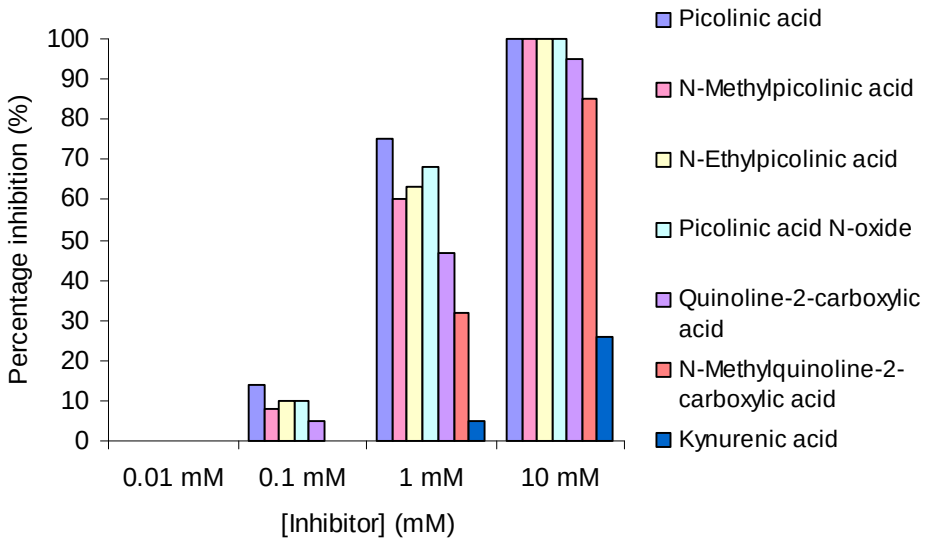

Figure 3.17: *Preliminary inhibition screen of the 2-carboxylic acid derivatives.*

Picolinic acid, the *N*-methyl and *N*-ethyl derivatives and picolinic acid *N*-oxide showed good levels of inhibition of QPRTase when present at concentrations above 0.1 mM, inhibiting the enzyme completely at 10 mM. Similarly, quinoline-2-carboxylic acid and the *N*-methyl derivative were effective inhibitors of

the enzymatic reaction at concentrations above 1 mM. Kynurenic acid, however, showed only a low level of inhibition at high concentrations (26%, 10 mM).

The rationale behind testing kynurenic acid as an inhibitor of QPRTase was that quinolinic acid and kynurenic acid are neurologically important co-metabolites, both acting on the NMDA receptor. Kynurenic acid is an NMDA receptor antagonist and is therefore able to block neuronal damage induced by quinolinic acid, which is an agonist.[43]

The structure of kynurenic acid **7** differs from the structure of quinoline-2-carboxylic acid **52** only by the presence of an hydroxyl group at the 4-position. This suggests there might be a certain degree of steric interference at the 4-position preventing kynurenic acid from binding tightly in the active site. Due to the low level of inhibition observed, it was decided not to carry out any further inhibition studies on this compound.

The inhibitory properties of all the other 2-carboxylic acid derivatives were examined in detail by performing careful kinetic analysis of the QPRTase catalysed reaction in the presence of different concentrations of the inhibitors.

3.3.2.2.1 Picolinic acid

Picolinic acid **26** was found to be a competitive inhibitor of QPRTase with respect to quinolinic acid. This was observed by an increase in K_m with increasing inhibitor concentration, while V_{max} remained unchanged within the experimental error (Table 3.13). The competitive inhibition pattern is illustrated with a Lineweaver-Burk plot, which shows a series of straight lines intersecting on the *y*-axis (Figure 3.18).

[Inhibitor] (μM)	**$K_{m(app)}$ (μM)**	**$V_{max(app)}$ (μM min^{-1})**
0	13.5 ± 1.1	0.94 ± 0.02
100	30.6 ± 2.5	0.96 ± 0.02
200	51.4 ± 6.1	0.99 ± 0.04
300	69.8 ± 8.9	0.99 ± 0.05

Table 3.13: *Effect of picolinic acid on kinetic parameters.*

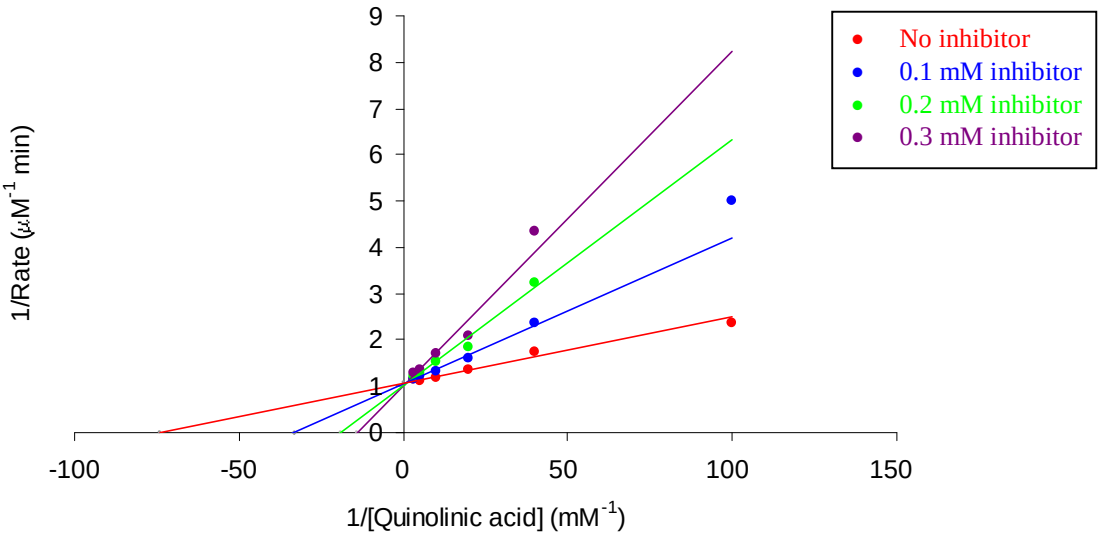

Figure 3.18: *Lineweaver-Burk plot for inhibition with picolinic acid.*

From a plot of $K_{m(app)}$ versus inhibitor concentration, the K_i value for picolinic acid was determined as 68 ± 2 μM with respect to quinolinic acid as the variable substrate (Figure 3.19). The observation that picolinic acid is an effective competitive inhibitor of QPRTase suggests that the carboxylic acid group at the 3-position is not essential for binding.

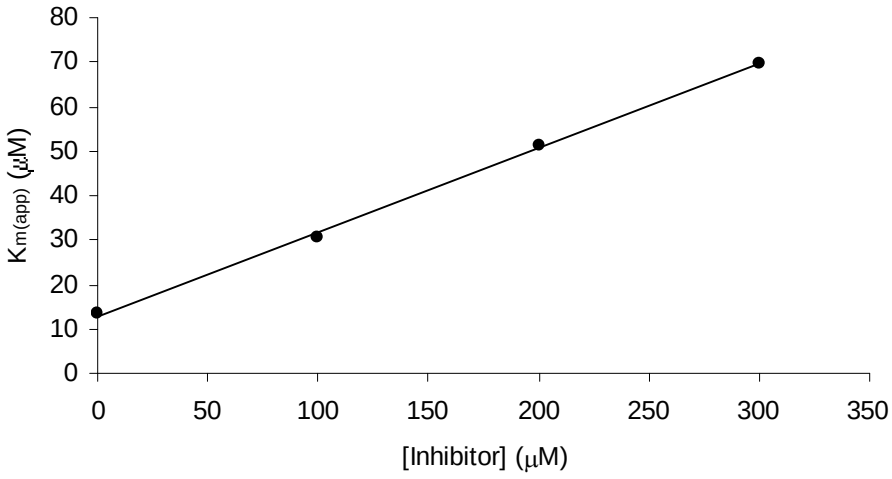

Figure 3.19: *Plot of $K_{m(app)}$ versus [picolinic acid].*

3.3.2.2.2 N-Methylpicolinic acid

N-Methylpicolinic acid **50** was found to be a competitive inhibitor of QPRTase with respect to quinolinic acid (Table 3.14). The competitive inhibition pattern is illustrated with a Lineweaver-Burk plot (Figure 3.20).

[Inhibitor] (μM)	$K_{m(app)}$ (μM)	$V_{max(app)}$ (μM min^{-1})
0	13.5 ± 1.1	0.94 ± 0.02
100	22.4 ± 1.3	0.96 ± 0.01
200	30.6 ± 2.5	0.95 ± 0.02
300	43.4 ± 4.4	0.98 ± 0.04

Table 3.14: *Effect of N-methylpicolinic acid on kinetic parameters.*

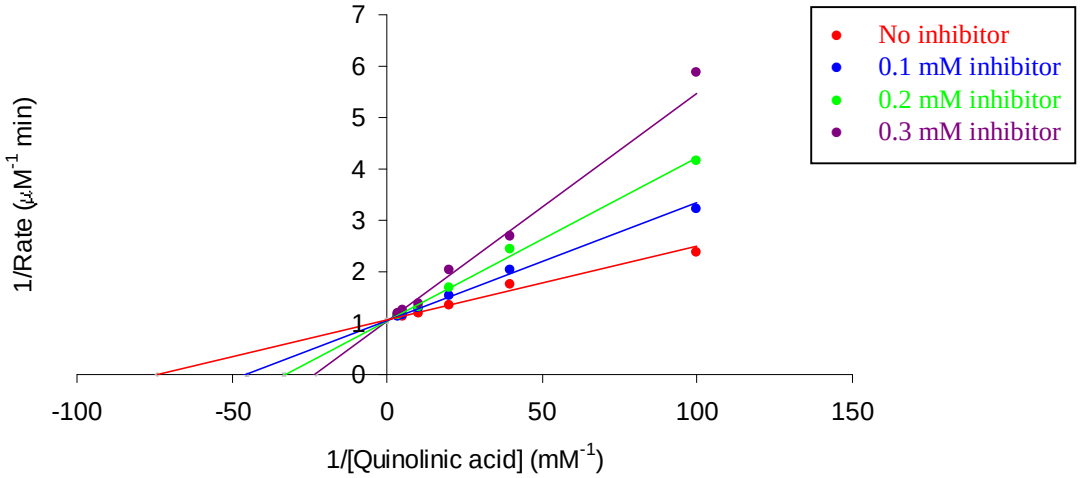

Figure 3.20: *Lineweaver-Burk plot for inhibition with N-methylpicolinic acid.*

The K_i value for *N*-methylpicolinic acid was determined as 131 ± 4 μM with respect to quinolinic acid as the variable substrate (Figure 3.21). *N*-Methylpicolinic acid **50** is therefore a weaker inhibitor than the non-methylated derivative **26**. It would appear therefore that the presence of the *N*-substituent causes unfavourable interactions in the active site, leading to weaker binding. Furthermore, by comparing the K_i values determined for *N*-methylpicolinic acid **50** (131 μM) and *N*-methylquinolinic acid **41** (40 μM), it can be seen that affinity is lost when the carboxylic acid group is absent at the 3-position. This suggests that the carboxylic acid group at the 3-position is important, but not essential, for binding.

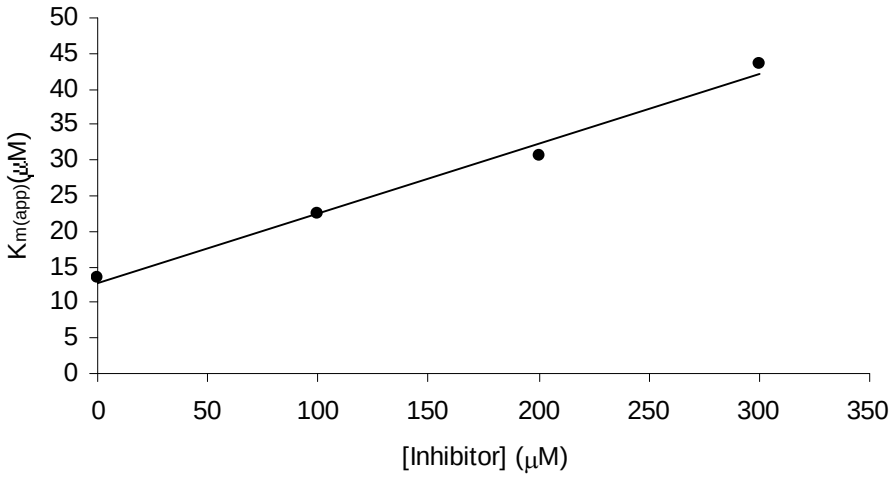

Figure 3.21: *Plot of $K_{m(app)}$ versus [N-methylpicolinic acid].*

3.3.2.2.3 N-Ethylpicolinic acid

N-Ethylpicolinic acid **51** was found to be a competitive inhibitor of QPRTase with respect to quinolinic acid (Table 3.15). The competitive inhibition pattern is illustrated with a Lineweaver-Burk plot (Figure 3.22).

[Inhibitor] (μM)	**$K_{m(app)}$ (μM)**	**$V_{max(app)}$ (μM min^{-1})**
0	13.5 ± 1.1	0.94 ± 0.02
100	22.5 ± 1.5	0.94 ± 0.02
200	29.7 ± 2.2	0.95 ± 0.03
300	44.6 ± 3.8	0.99 ± 0.03

Table 3.15: *Effect of N-ethylpicolinic acid on kinetic parameters.*

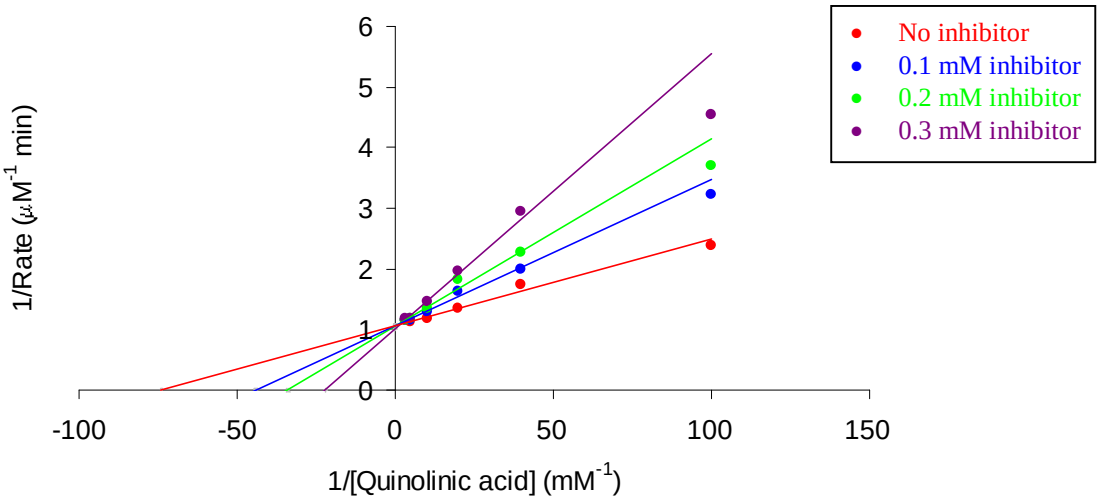

Figure 3.22: *Lineweaver-Burk plot for inhibition with N-ethylpicolinic acid.*

From a plot of $K_{m(app)}$ versus inhibitor concentration, the K_i value for *N*-ethylpicolinic acid **51** was determined as 124 ± 6 μM with respect to quinolinic acid as the variable substrate (Figure 3.23). This is very similar to the value of 131 μM obtained for *N*-methylpicolinic acid **50** which again suggests that increasing the size of the *N*-substituent from a methyl group to an ethyl group does not significantly affect the binding in the QPRTase active site.

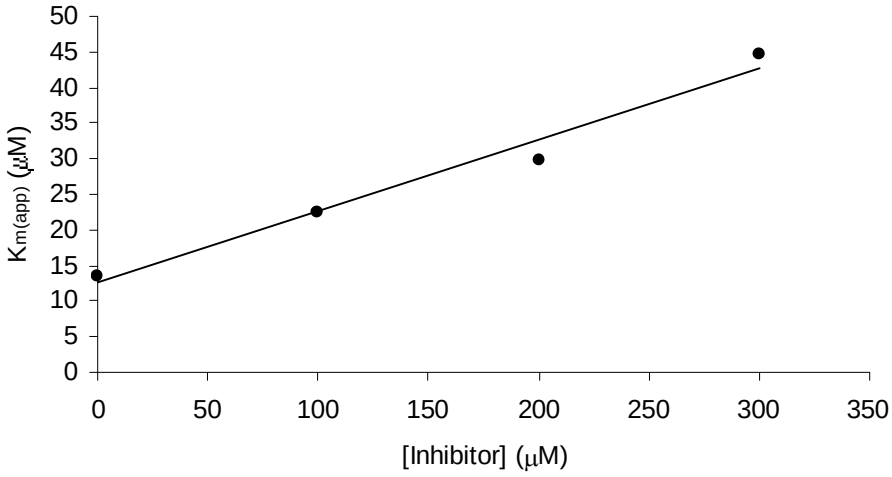

Figure 3.23: *Plot of $K_{m(app)}$ versus [N-ethylpicolinic acid].*

3.3.2.2.4 Picolinic acid N-oxide

Picolinic acid *N*-oxide **105** was found to be a competitive inhibitor of QPRTase with respect to quinolinic acid (Table 3.16). The competitive inhibition pattern is illustrated with a Lineweaver-Burk plot (Figure 3.24).

[Inhibitor] (μM)	$K_{m(app)}$ (μM)	$V_{max(app)}$ (μM min^{-1})
0	13.5 ± 1.6	0.94 ± 0.02
100	22.6 ± 2.1	0.95 ± 0.02
200	35.6 ± 2.4	0.91 ± 0.02
300	47.0 ± 4.6	0.89 ± 0.03

Table 3.16: *Effect of picolinic acid N-oxide on kinetic parameters.*

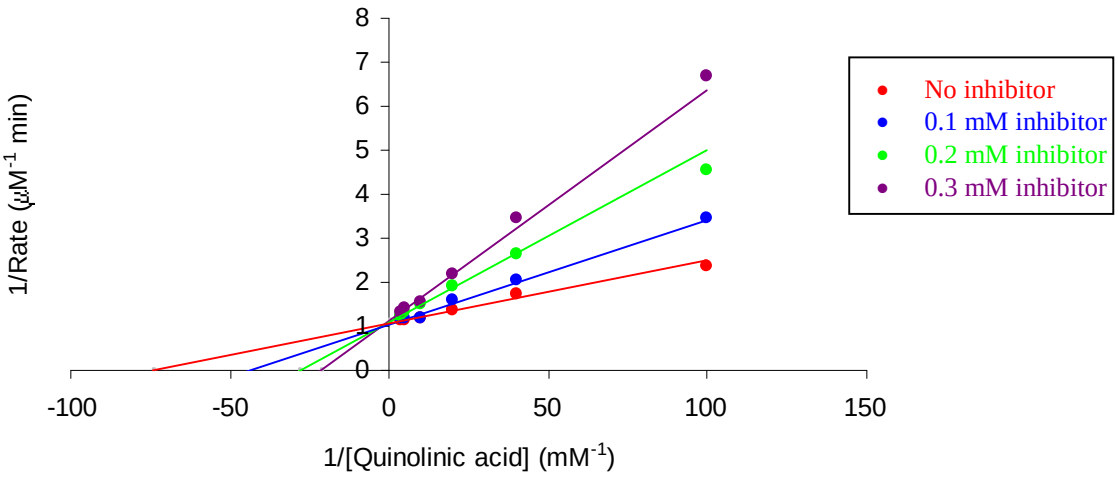

Figure 3.24: *Lineweaver-Burk plot for inhibition with picolinic acid N-oxide.*

The K_i value for picolinic acid *N*-oxide was determined as 111 ± 4 μM with respect to quinolinic acid as the variable substrate (Figure 3.25). Picolinic acid *N*-oxide is therefore a good competitive inhibitor of human brain QPRTase and appears to bind more tightly in the active site than the *N*-alkyl picolinic acid derivatives. Again, this could be due to electrostatic interactions between the negatively charged oxygen of the *N*-oxide and the highly positive electrostatic surface of the QPRTase active site.

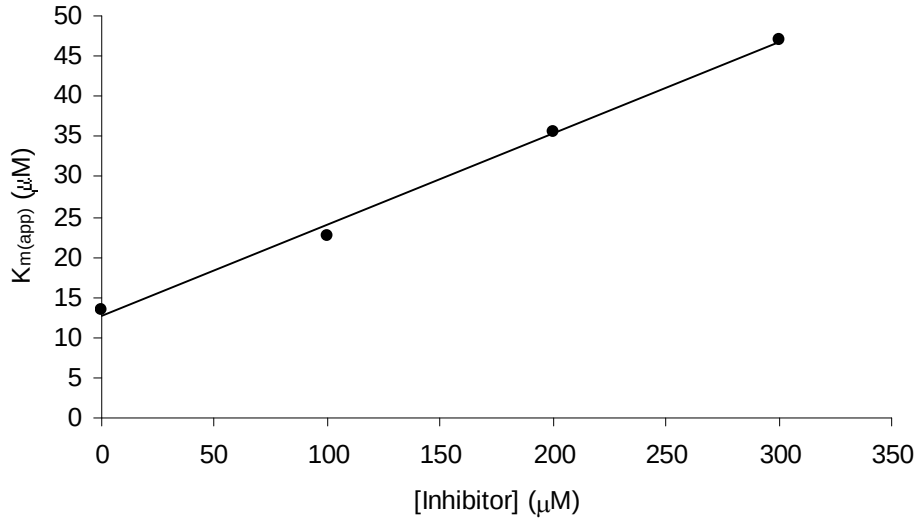

Figure 3.25: *Plot of $K_{m(app)}$ versus [picolinic acid N-oxide].*

3.3.2.2.5 Quinoline-2-carboxylic acid

Quinoline-2-carboxylic acid **52** was found to be a competitive inhibitor of QPRTase with respect to quinolinic acid. This was observed by an increase in K_m with increasing inhibitor concentration, while V_{max} remained relatively unchanged within the experimental error (Table 3.17). The competitive inhibition pattern is illustrated with a Lineweaver-Burk plot (Figure 3.26).

[Inhibitor] (μM)	**$K_{m(app)}$ (μM)**	**$V_{max(app)}$ (μM min^{-1})**
0	13.5 ± 1.4	0.96 ± 0.02
300	35.2 ± 2.6	1.04 ± 0.02
500	56.3 ± 5.6	1.09 ± 0.05
700	76.4 ± 6.8	1.10 ± 0.08

Table 3.17: *Effect of quinoline-2-carboxylic acid on kinetic parameters.*

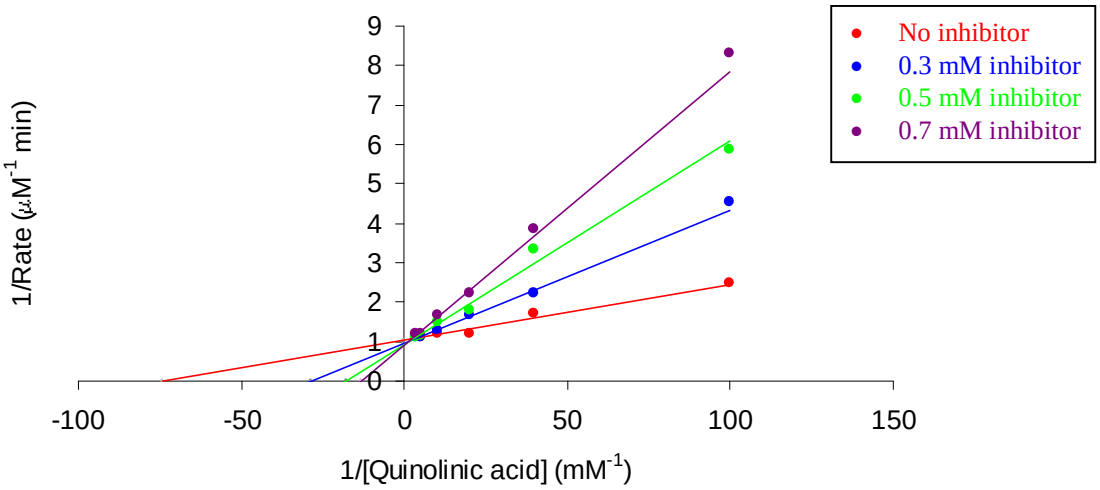

Figure 3.26: *Lineweaver-Burk plot for inhibition with quinoline-2-carboxylic acid.*

From a plot of $K_{m(app)}$ versus inhibitor concentration, the K_i value for quinoline-2-carboxylic acid **52** was determined as 127 ± 4 μM with respect to quinolinic acid as the variable substrate (Figure 3.27). Quinoline-2-carboxylic acid is therefore a good competitive inhibitor of QPRTase. However, this compound does not bind as tightly as picolinic acid **26**. This may be due to steric interference as a result of the larger bicyclic structure of quinoline-2-carboxylic acid.

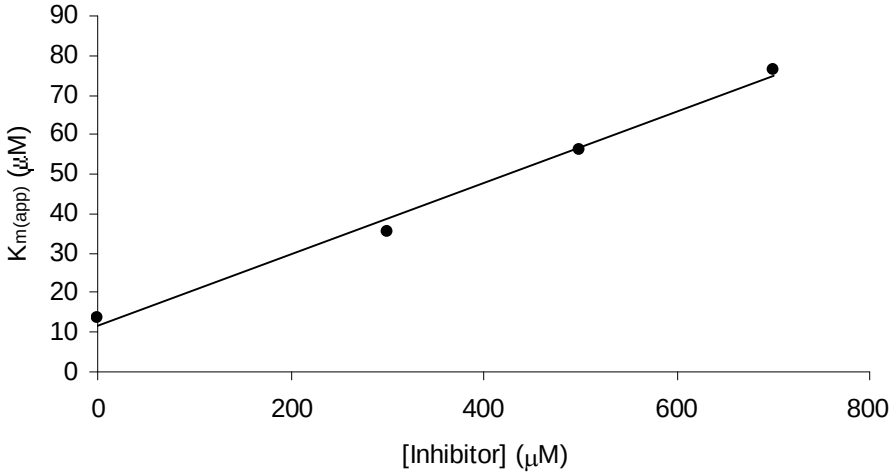

Figure 3.27: *Plot of $K_{m(app)}$ versus [quinoline-2-carboxylic acid].*

3.3.2.2.6 N-Methylquinoline-2-carboxylic acid

N-Methylquinoline-2-carboxylic acid **55** was found to be a competitive inhibitor of QPRTase with respect to quinolinic acid (Table 3.18). The competitive inhibition pattern is illustrated with a Lineweaver-Burk plot (Figure 3.28).

[Inhibitor] (μM)	$K_{m(app)}$ (μM)	$V_{max(app)}$ (μM min^{-1})
0	13.5 ± 1.4	0.96 ± 0.02
300	25.5 ± 1.7	1.00 ± 0.02
500	35.5 ± 2.7	1.01 ± 0.03
700	49.0 ± 4.0	1.02 ± 0.03

Table 3.18: *Effect of N-methylquinoline-2-carboxylic acid on kinetic parameters.*

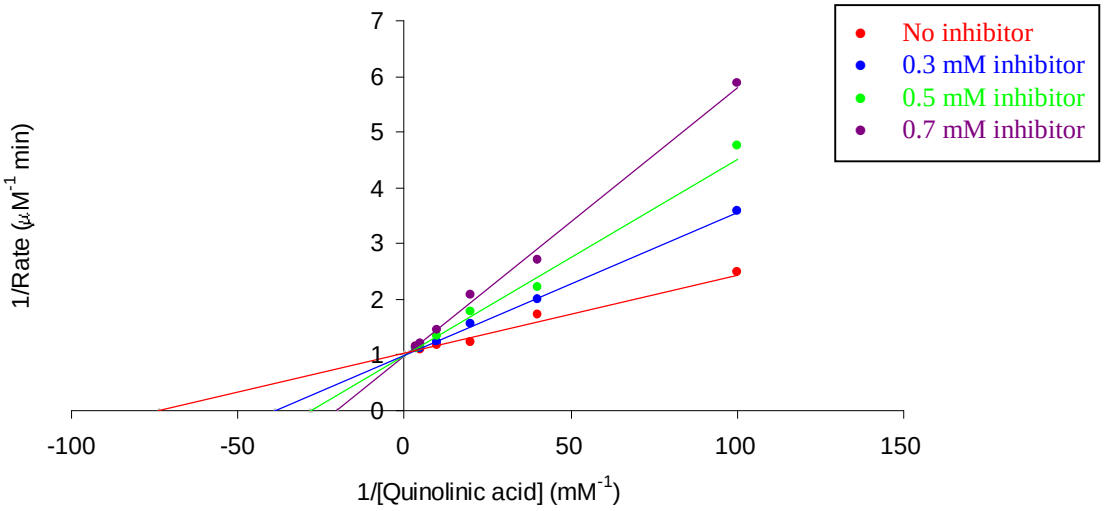

Figure 3.28: *Lineweaver-Burk plot for inhibition with N-methylquinoline-2-carboxylic acid.*

From a plot of $K_{m(app)}$ versus inhibitor concentration, the K_i value for *N*-methylquinoline-2-carboxylic acid **55** was determined as 242 ± 7 μM with respect to quinolinic acid as the variable substrate (Figure 3.29). *N*-Methylquinoline-2-carboxylic acid **55** is therefore a less effective inhibitor than the non-methylated derivative **52**. Again, it would appear that the presence of the *N*-substituent causes unfavourable interactions in the active site, leading to weaker binding.

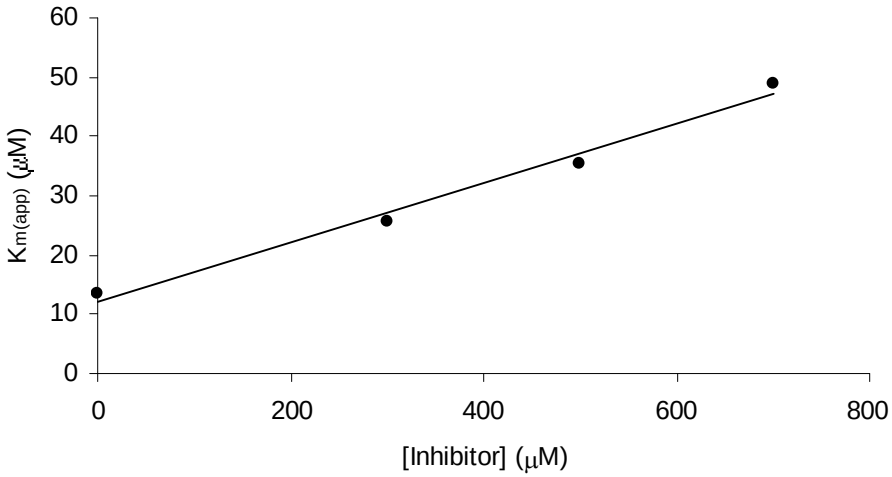

Figure 3.29: *Plot of $K_{m(app)}$ versus [N-methylquinoline-2-carboxylic acid].*

3.3.2.3 3-Carboxylic acid derivatives

A preliminary inhibition screen of nicotinic acid **27**, *N*-methylnicotinic acid **59**, *N*-ethylnicotinic acid **60**, nicotinic acid *N*-oxide **63** and quinoline-3-carboxylic acid **106** showed that these compounds do not inhibit the QPRTase catalysed reaction when present at a concentration of 0.01 mM, 0.1 mM, 1 mM or 10 mM. This suggests that the carboxylic acid group at the 2-position is essential for binding. This is consistent with previous inhibition studies carried out on QPRTase from other sources.[5] In addition, it would appear that the presence of a small, hydrophobic *N*-substituent, the *N*-oxide functionality or an additional aromatic ring does not compensate for the interactions lost when the carboxylic acid group at the 2-position is absent, suggesting the carboxylic acid group at the 2-position is most important for binding to the enzyme.

3.3.2.4 Summary of the quinolinic acid analogues inhibition study

The results of this study on the inhibition of human brain QPRTase by quinolinic acid analogues are summarised in Table 3.19.

Inhibitor	Variable Substrate	Type of Inhibition	K_i (μM)
N-Methylquinolinic acid **41**	Quinolinic acid	Competitive	40 ± 2
N-Ethylquinolinic acid **42**	Quinolinic acid	Competitive	34 ± 4
5-Ethylquinolinic acid **43**	Quinolinic acid	Competitive	158 ± 21
5-Ethyl-*N*-methyl quinolinic acid **46**	Quinolinic acid	Competitive	270 ± 29
Quinolinic acid *N*-oxide **62**	Quinolinic acid	Competitive	25 ± 2
Phthalic acid **25**	Quinolinic acid	Competitive	21 ± 3
2,3-Napthalene dicarboxylic acid **104**	Quinolinic acid	Competitive	90 ± 4
NMDA **14**	Quinolinic acid	Preliminary screen showed low inhibition at high concentrations	
Picolinic acid **26**	Quinolinic acid	Competitive	68 ± 2
N-Methylpicolinic acid **50**	Quinolinic acid	Competitive	131 ± 4
N-Ethylpicolinic acid **51**	Quinolinic acid	Competitive	124 ± 6
Picolinic acid *N*-oxide **105**	Quinolinic acid	Competitive	111 ± 4
Quinoline-2-carboxylic acid **52**	Quinolinic acid	Competitive	127 ± 4
N-Methylquinoline-2-carboxylic acid **55**	Quinolinic acid	Competitive	242 ± 7
Kynurenic acid **7**	Quinolinic acid	Preliminary screen showed low inhibition at high concentrations	
Nicotinic acid **27**	Quinolinic acid	Preliminary screen showed no inhibition	
N-Methylnicotinic acid **59**	Quinolinic acid	Preliminary screen showed no inhibition	
N-Ethylnicotinic acid **66**	Quinolinic acid	Preliminary screen showed no inhibition	
Nicotinic acid *N*-oxide **63**	Quinolinic acid	Preliminary screen showed no inhibition	
Quinoline-3-carboxylic acid **106**	Quinolinic acid	Preliminary screen showed no inhibition	

Table 3.19: *Summary of the quinolinic acid analogues inhibition study. The K_m for quinolinic acid under these conditions is 13.5 μM.*

Some general conclusions can be drawn from the results of this inhibition study:-

- It would appear that the ring nitrogen is not essential for binding. Of the compounds tested, phthalic acid **25** proved to be the most effective competitive inhibitor.

- The 3-carboxylic acid group is somewhat important for substrate interaction with the enzyme because when this group was absent, the compounds became less effective as inhibitors.

- The carboxylic acid group at the 2-position appears to be essential for binding. This conclusion was most clearly indicated by the fact that nicotinic acid **27** did not inhibit the enzymatic reaction, whereas picolinic acid **26** did.

- Small, hydrophobic *N*-substituents do not provide additional binding. Instead it would appear that the presence of such subsituents leads to weaker binding. It was found that the size of the *N*-alkyl group does not significantly affect the binding. *N*-Ethylquinolinic acid **42** and *N*-ethylpicolinic acid **51** were found to be slightly better inhibitors than the corresponding *N*-methyl derivatives, although the difference between the K_i values determined for these compounds was just within experimental error.

- The *N*-oxide compounds appear to bind more tightly than the corresponding *N*-alkyl compounds. This could be due to electrostatic interactions between the negatively charged oxygen of the *N*-oxide and the highly positive electrostatic surface of the QPRTase active site.

- It would appear that aromaticity is important for tight binding. However, increasing the size of the aromatic ring system to a bicyclic structure leads to weaker binding. This is most likely due to steric interference in the active site.

- Similarly, there appears to be a certain degree of steric hindrance at the 4- and 5-positions of the pyridine ring. This was indicated by the observation that 5-ethylquinolinic acid **43** and especially kynurenic acid **7**, which has a hydroxyl group at the 4-position, were weaker inhibitors of QPRTase.

3.3.3 Inhibition studies using nucleotides

Nucleotides of adenine, cytosine, guanine, thymine and uracil have all previously been tested as inhibitors of QPRTase from hog liver.[4,44] In the preliminary inhibition screens, the purine and pyrimidine nucleotide mono-, di- and triphosphates were all shown to inhibit QPRTase. However, detailed inhibition studies to determine the type of inhibition and the inhibition constants (K_i) for these compounds were not carried out.

In this study, a detailed investigation of the inhibitory properties of adenosine 5'-monophosphate (AMP, **107**), guanosine 5'-monophosphate (GMP, **108**), cytidine 5'-monophosphate (CMP, **109**) and thymidine 5'-monophosphate (TMP, **110**) was undertaken.

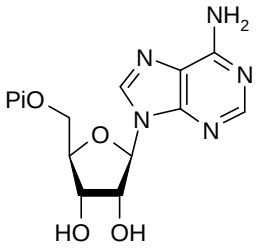

107

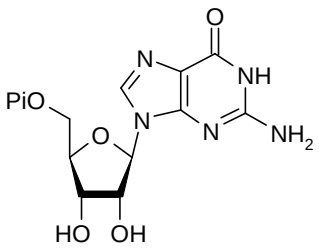

108

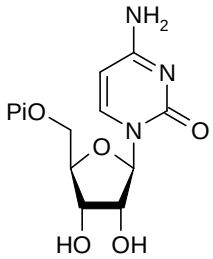

109

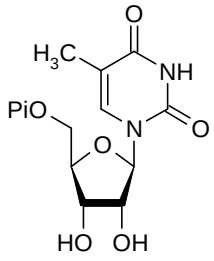

110

Firstly, to determine a suitable inhibitor concentration range for the inhibition studies, a preliminary inhibition screen of the nucleotides was carried out by assessing the percentage inhibition of QPRTase activity at a fixed concentration of quinolinic acid (0.1 mM) and PRPP (0.1 mM). When present at a concentration of 0.01 mM, the nucleotides did not inhibit QPRTase. However, when present at higher concentrations (0.1 mM and 1 mM) the four nucleotides were found to inhibit QPRTase to a similar extent (Table 3.20 and Figure 3.30).

Inhibitor	% Inhibition with		
	0.01 mM inhibitor	**0.1 mM inhibitor**	**1 mM inhibitor**
AMP **107**	0	19	60
GMP **108**	0	18	57
CMP **109**	0	24	65
TMP **110**	0	26	68

Table 3.20: *Percentage inhibition at varied inhibitor concentrations.*

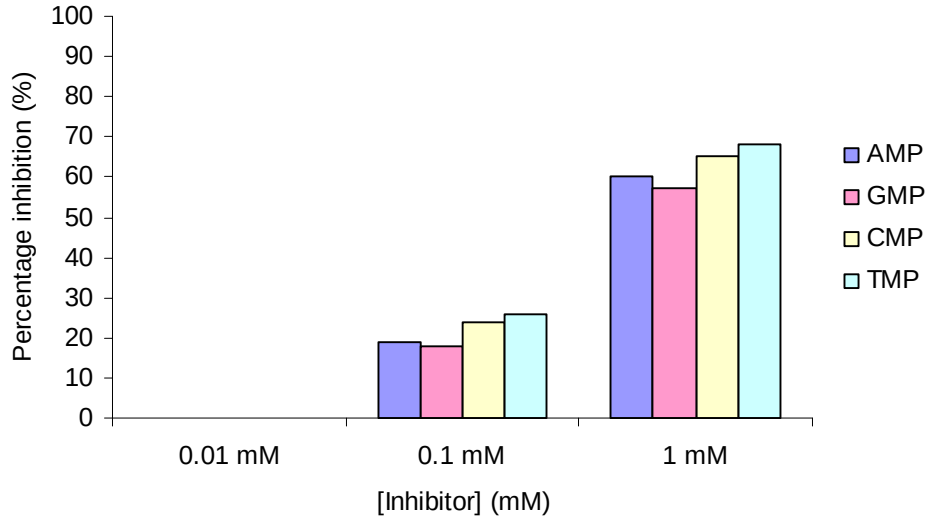

Figure 3.30: *Preliminary inhibition screen.*

In order to determine the inhibitory properties of the four nucleotides, the K_m and V_{max} values for the QPRTase reaction, with respect to both quinolinic acid and PRPP, were then determined at various fixed inhibitor concentrations. The effect on the kinetic parameters gave a measure of inhibition and also identified the type of inhibition observed. Lineweaver-Burk plots were constructed to illustrate the type of inhibition exhibited by each inhibitor, although these were used for illustrative purposes only and not for calculating kinetic parameters. Note that in all the Lineweaver-Burk plots, the line was constructed to fit the $K_{m(app)}$ and $V_{max(app)}$ values determined from non-linear regression. K_i values were determined using linear regression plots of $K_{m(app)}$ versus inhibitor concentration (competitive inhibition) or $1/V_{max(app)}$ versus inhibitor concentration (noncompetitive inhibition).

3.3.3.1 Adenosine 5'-monophosphate (inhibition with respect to quinolinic acid)

Adenosine 5'-monophosphate **107** was found to be a noncompetitive inhibitor of QPRTase with respect to quinolinic acid. This was observed by a decrease in V_{max} with increasing inhibitor concentration, while K_m remained unchanged within the experimental error (Table 3.21). The noncompetitive inhibition pattern is illustrated with a Lineweaver-Burk plot, which shows a series of straight lines intersecting, approximately, on the *x*-axis (Figure 3.31).

[Inhibitor] (μM)	**$K_{m(app)}$ (μM)**	**$V_{max(app)}$ (μM min^{-1})**
0	13.5 ± 1.4	0.96 ± 0.02
100	13.7 ± 1.8	0.80 ± 0.02
200	13.9 ± 1.4	0.71 ± 0.02
300	15.3 ± 3.3	0.62 ± 0.03

Table 3.21: *Effect of adenosine 5'-monophosphate on kinetic parameters.*

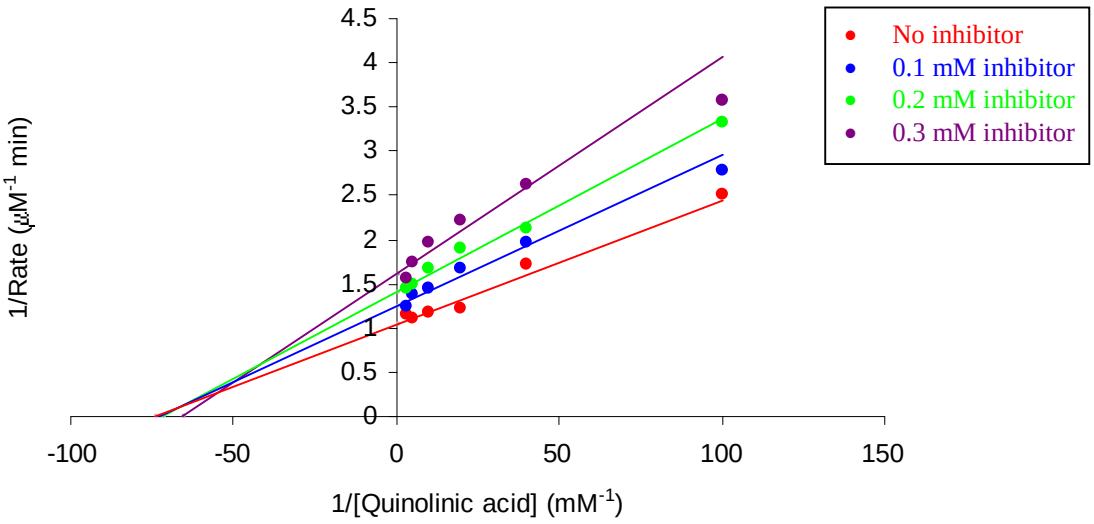

Figure 3.31: *Lineweaver-Burk plot for inhibition with adenosine 5'-monophosphate.*

In the presence of a noncompetitive inhibitor, V_{max} decreases by a factor of $(1 + [I]/K_i)$. The inhibition constant K_i can therefore be determined from a plot of $1/V_{max(app)}$ versus inhibitor concentration. This plot is linear and the slope is equal to $1/V_{max}.K_i$.

$$V_{max(app)} = V_{max} / (1 + [I] / K_i)$$

$$\frac{1}{V_{max(app)}} = \frac{1}{V_{max}.K_i} . [I] + \frac{1}{V_{max}}$$

By performing this analysis, the K_i value for adenosine 5'-monophosphate **107** was determined as 551 ± 5 μM with respect to quinolinic acid as the variable substrate (Figure 3.32).

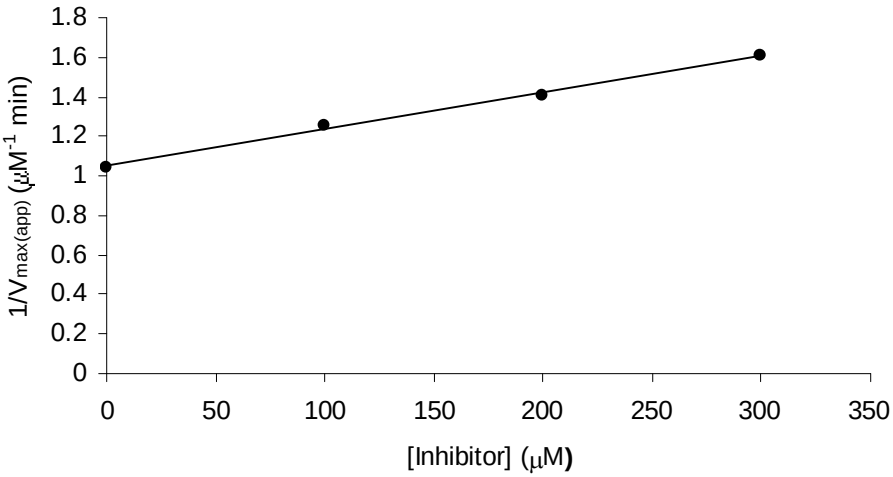

Figure 3.32: *Plot of $1/V_{max(app)}$ versus [adenosine 5'-monophosphate]*.

3.3.3.2 Adenosine 5'-monophosphate (inhibition with respect to PRPP)

Adenosine 5'-monophosphate **107** was found to be a competitive inhibitor of QPRTase with respect to PRPP. This was observed by an increase in K_m with increasing inhibitor concentration, while V_{max} remained unchanged within the experimental error (Table 3.22). The competitive inhibition pattern is illustrated with a Lineweaver-Burk plot, which shows a series of straight lines intersecting on the *y*-axis (Figure 3.33).

[Inhibitor] (μM)	$K_{m(app)}$ (μM)	$V_{max(app)}$ (μM min^{-1})
0	22.1 ± 2.3	0.99 ± 0.03
300	44.9 ± 4.0	0.98 ± 0.04
500	58.2 ± 5.9	0.97 ± 0.04
700	73.7 ± 7.6	0.92 ± 0.04

Table 3.22: *Effect of adenosine 5'-monophosphate on kinetic parameters.*

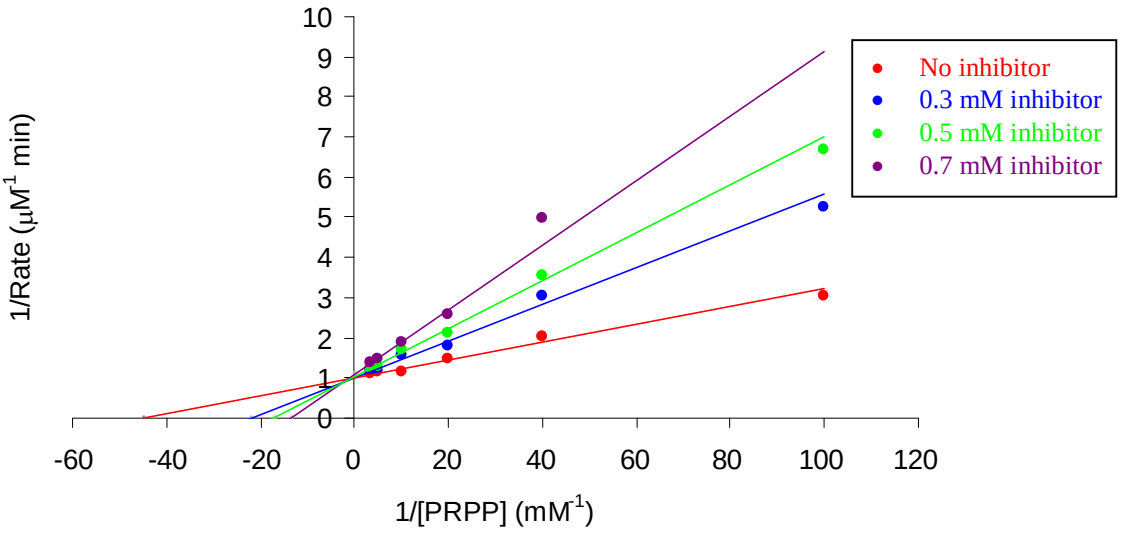

Figure 3.33: *Lineweaver-Burk plot for inhibition with adenosine 5'-monophosphate.*

From a plot of $K_{m(app)}$ versus inhibitor concentration, the K_i value for adenosine 5'-monophosphate **107** was determined as 304 ± 4 μM with respect to PRPP as the variable substrate (Figure 3.34).

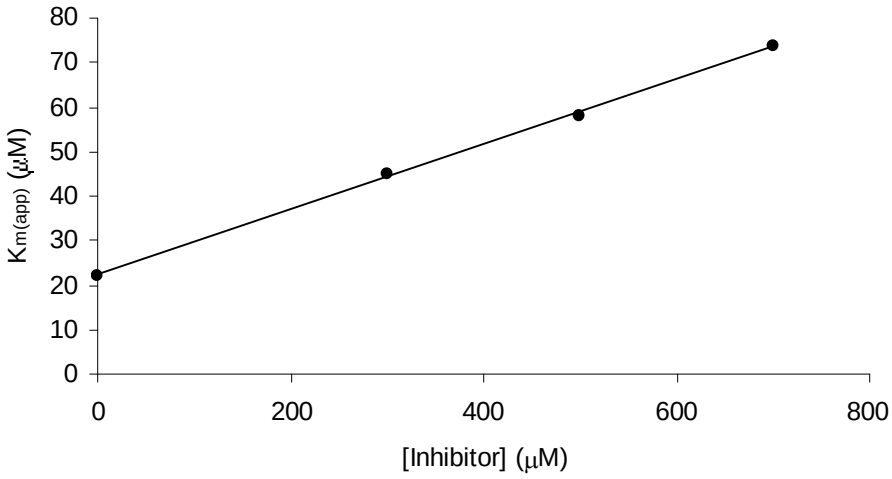

Figure 3.34: *Plot of $K_{m(app)}$ versus [adenosine 5'-monophosphate].*

3.3.3.3 Guanosine 5'-monophosphate (inhibition with respect to quinolinic acid)

Guanosine 5'-monophosphate **108** was found to be a noncompetitive inhibitor of QPRTase with respect to quinolinic acid (Table 3.23). The noncompetitive inhibition pattern is illustrated with a Lineweaver-Burk plot (Figure 3.35).

[Inhibitor] (μM)	**$K_{m(app)}$ (μM)**	**$V_{max(app)}$ (μM min^{-1})**
0	13.5 ± 1.4	0.96 ± 0.02
100	13.0 ± 1.6	0.82 ± 0.02
200	13.1 ± 1.3	0.72 ± 0.02
300	14.9 ± 2.0	0.63 ± 0.03

Table 3.23: *Effect of guanosine 5'-monophosphate on kinetic parameters.*

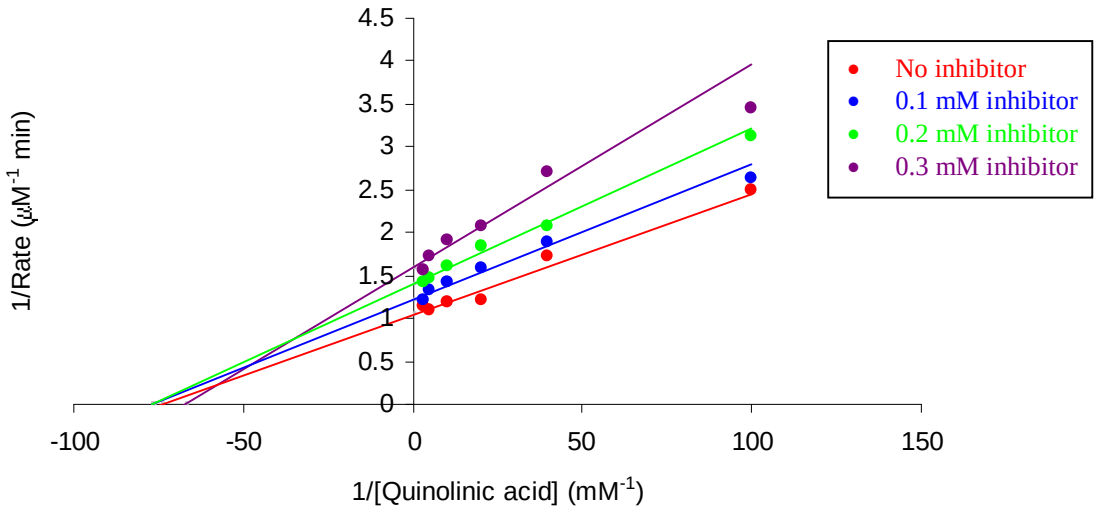

Figure 3.35: *Lineweaver-Burk plot for inhibition with guanosine 5'-monophosphate.*

From a plot of $1/V_{max(app)}$ versus inhibitor concentration, the K_i value for guanosine 5'-monophosphate **108** was determined as 576 ± 4 μM with respect to quinolinic acid as the variable substrate (Figure 3.36).

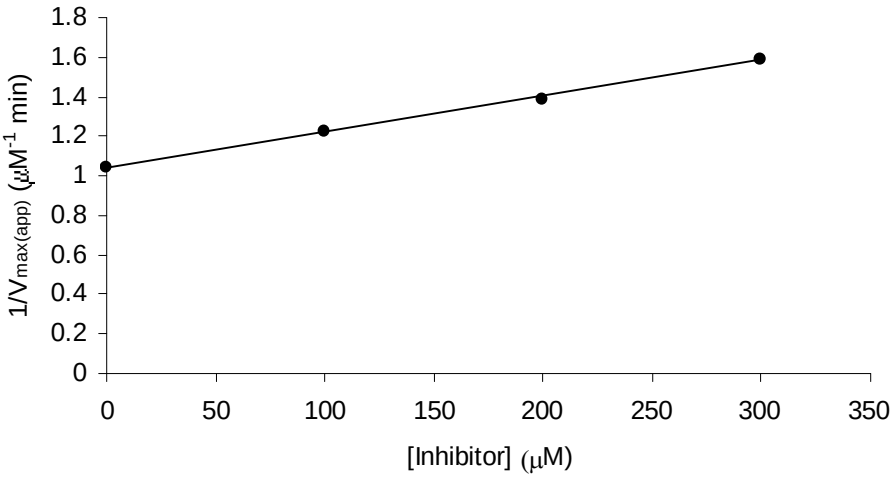

Figure 3.36: *Plot of $1/V_{max(app)}$ versus [guanosine 5'-monophosphate].*

3.3.3.4 Guanosine 5'-monophosphate (inhibition with respect to PRPP)

Guanosine 5'-monophosphate **108** was found to be a competitive inhibitor of QPRTase with respect to PRPP (Table 3.24). The competitive inhibition pattern is illustrated with a Lineweaver-Burk plot (Figure 3.37).

[Inhibitor] (μM)	**$K_{m(app)}$ (μM)**	**$V_{max(app)}$ (μM min^{-1})**
0	22.1 ± 2.3	0.99 ± 0.03
300	39.6 ± 2.1	0.98 ± 0.02
500	53.2 ± 3.4	0.98 ± 0.02
700	69.7 ± 5.7	0.97 ± 0.04

Table 3.24: *Effect of guanosine 5'-monophosphate on kinetic parameters.*

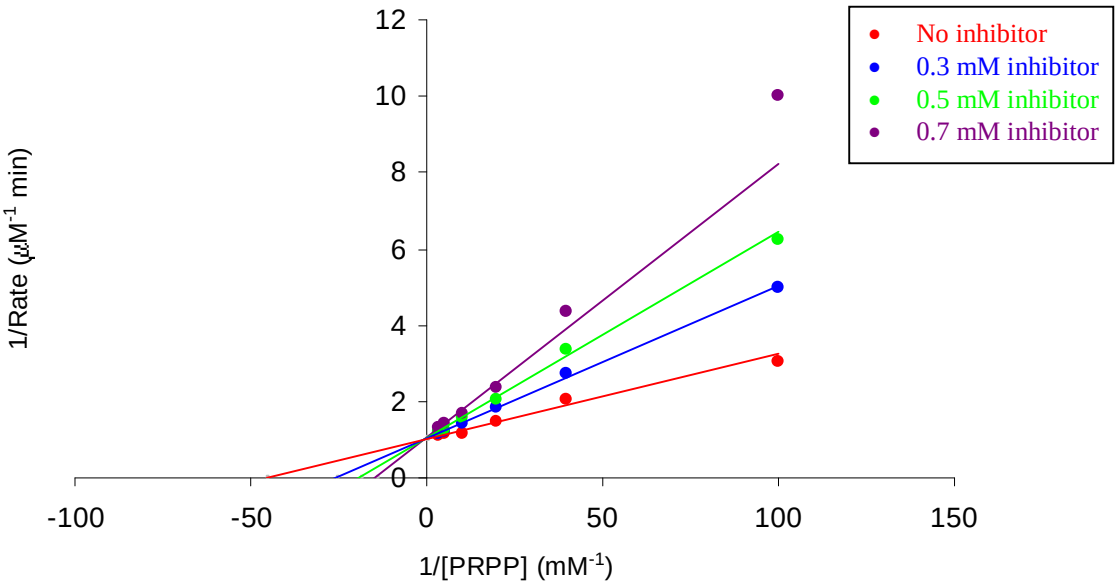

Figure 3.37: *Lineweaver-Burk plot for inhibition with guanosine 5'-monophosphate.*

From a plot of $K_{m(app)}$ versus inhibitor concentration, the K_i value for guanosine 5'-monophosphate **108** was determined as 309 ± 6 μM with respect to PRPP as the variable substrate (Figure 3.38).

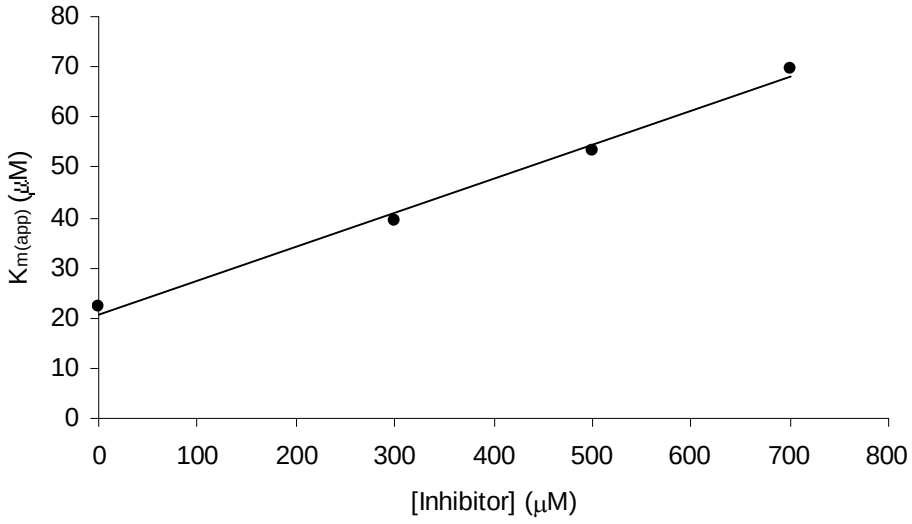

Figure 3.38: *Plot of $K_{m(app)}$ versus [guanosine 5'-monophosphate].*

3.3.3.5 Cytidine 5'-monophosphate (inhibition with respect to quinolinic acid)

Cytidine 5'-monophosphate **109** was found to be a noncompetitive inhibitor of QPRTase with respect to quinolinic acid (Table 3.25). The noncompetitive inhibition pattern is illustrated with a Lineweaver-Burk plot (Figure 3.39).

[Inhibitor] (μM)	**$K_{m(app)}$ (μM)**	**$V_{max(app)}$ (μM min^{-1})**
0	13.5 ± 1.4	0.96 ± 0.02
100	13.9 ± 2.6	0.76 ± 0.03
200	12.3 ± 2.1	0.63 ± 0.02
300	13.4 ± 2.6	0.56 ± 0.02

Table 3.25: *Effect of cytidine 5'-monophosphate on kinetic parameters.*

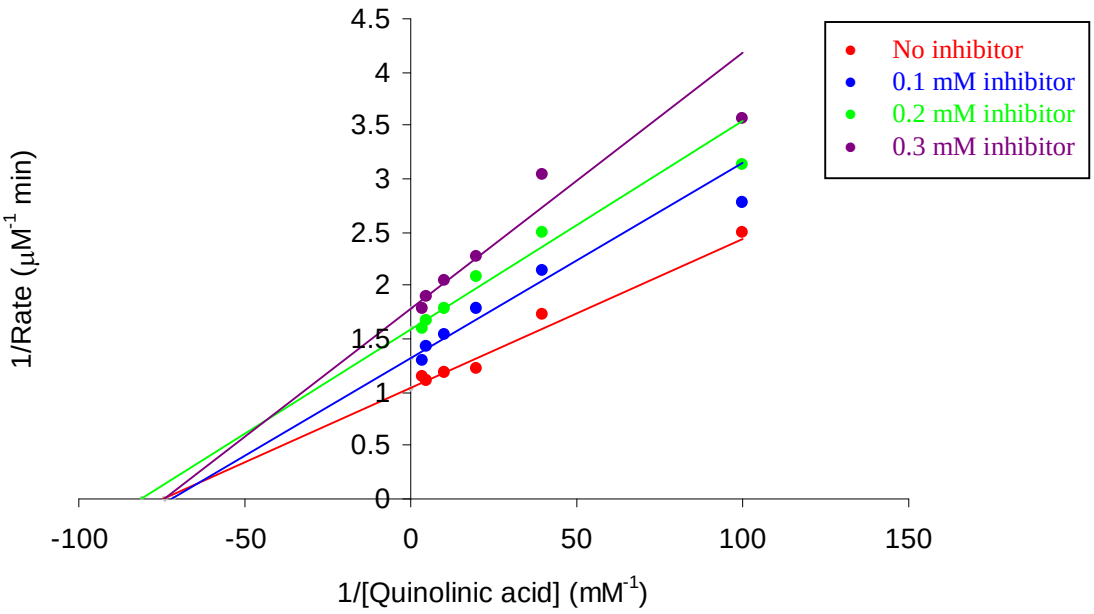

Figure 3.39: *Lineweaver-Burk plot for inhibition with cytidine 5'-monophosphate.*

The K_i value for cytidine 5'-monophosphate **109** was determined as 423 ± 6 μM with respect to quinolinic acid as the variable substrate (Figure 3.40).

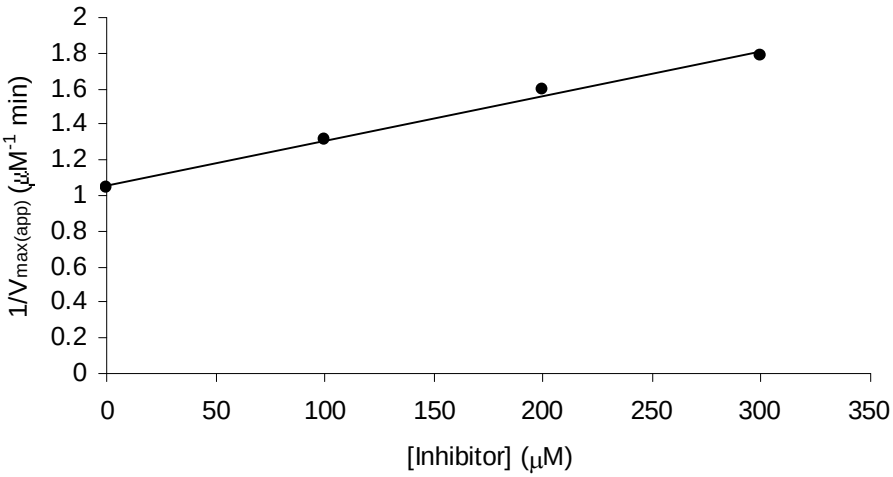

Figure 3.40: *Plot of $1/V_{max(app)}$ versus [cytidine 5'-monophosphate].*

3.3.3.6 Cytidine 5'-monophosphate (inhibition with respect to PRPP)

Cytidine 5'-monophosphate **109** was found to be a competitive inhibitor of QPRTase with respect to PRPP (Table 3.26). The competitive inhibition pattern is illustrated with a Lineweaver-Burk plot (Figure 3.41).

[Inhibitor] (μM)	**$K_{m(app)}$ (μM)**	**$V_{max(app)}$ (μM min^{-1})**
0	22.1 ± 2.3	0.99 ± 0.03
300	48.3 ± 4.4	0.98 ± 0.04
500	70.0 ± 6.0	1.00 ± 0.03
700	88.6 ± 9.0	0.98 ± 0.04

Table 3.26: *Effect of cytidine 5'-monophosphate on kinetic parameters.*

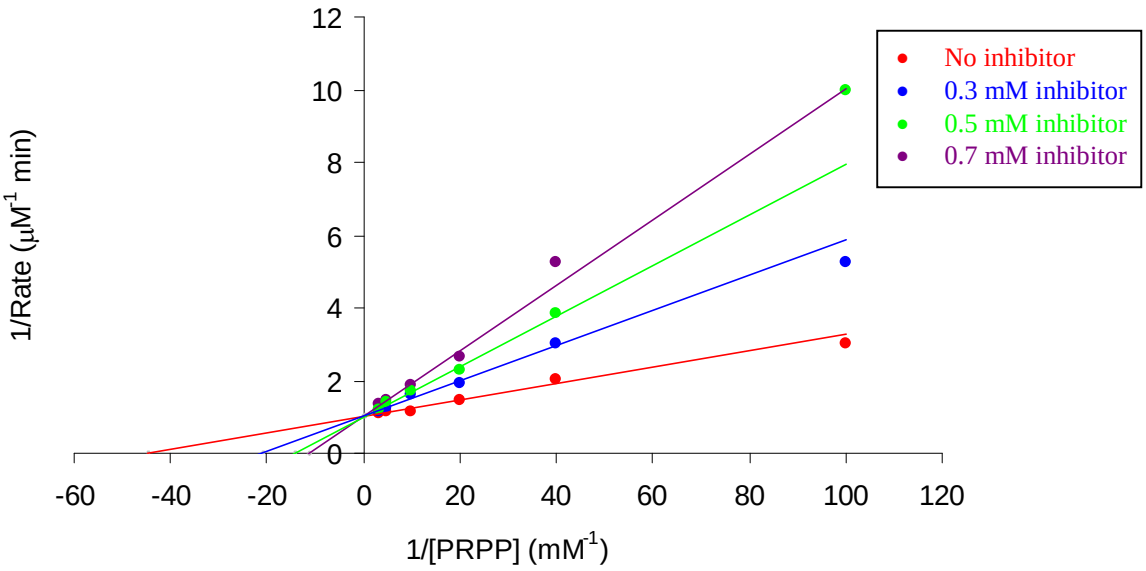

Figure 3.41: *Lineweaver-Burk plot for inhibition with cytidine 5'-monophosphate.*

The K_i value for cytidine 5'-monophosphate **109** was determined as 222 ± 4 μM with respect to PRPP as the variable substrate (Figure 3.42).

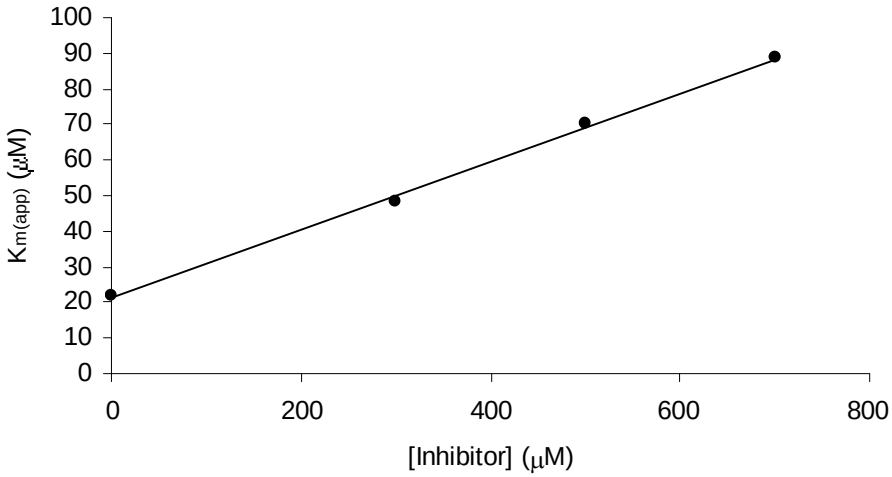

Figure 3.42: *Plot of $K_{m(app)}$ versus [cytidine 5'-monophosphate].*

3.3.3.7 Thymidine 5'-monophosphate (inhibition with respect to quinolinic acid)

Thymidine 5'-monophosphate **110** was found to be a noncompetitive inhibitor of QPRTase with respect to quinolinic acid (Table 3.27). The noncompetitive inhibition pattern is illustrated with a Lineweaver-Burk plot (Figure 3.43).

[Inhibitor] (μM)	**$K_{m(app)}$ (μM)**	**$V_{max(app)}$ (μM min^{-1})**
0	13.5 ± 1.4	0.96 ± 0.02
100	15.6 ± 2.7	0.73 ± 0.02
200	15.9 ± 2.8	0.64 ± 0.02
300	15.6 ± 3.5	0.55 ± 0.03

Table 3.27: *Effect of thymidine 5'-monophosphate on kinetic parameters.*

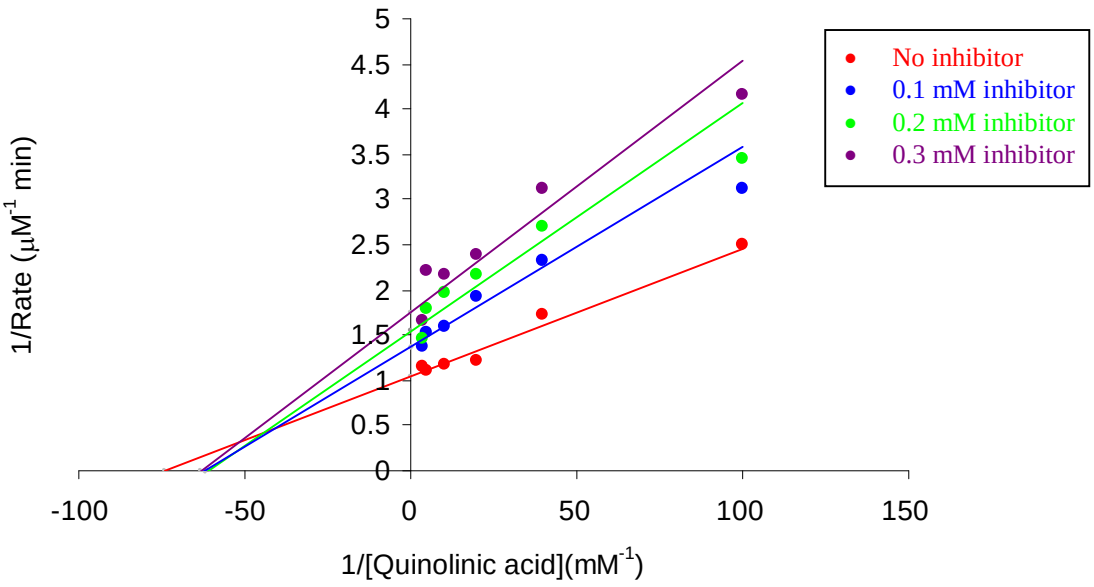

Figure 3.43: *Lineweaver-Burk plot for inhibition with thymidine 5'-monophosphate.*

The K_i value for thymidine 5'-monophosphate **110** was determined as 427 ± 8 μM with respect to quinolinic acid as the variable substrate (Figure 3.44).

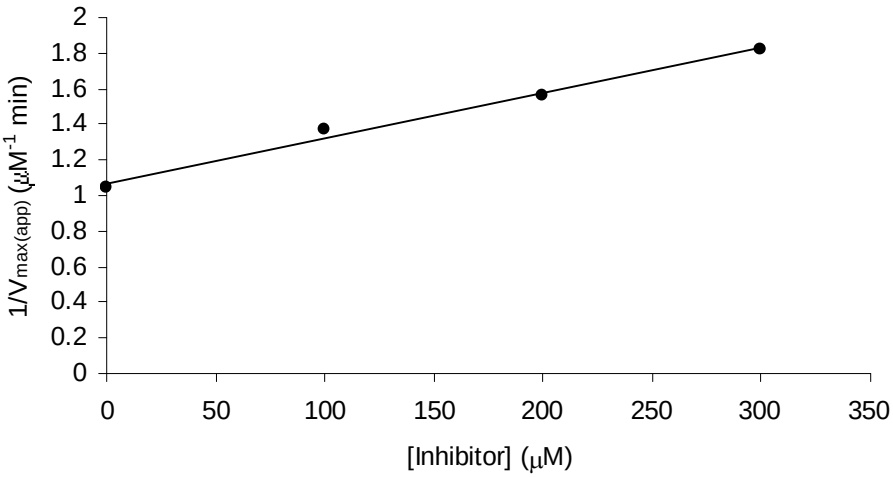

Figure 3.44: *Plot of $1/V_{max(app)}$ versus [thymidine 5'-monophosphate].*

3.3.3.8 Thymidine 5'-monophosphate (inhibition with respect to PRPP)

Thymidine 5'-monophosphate **110** was found to be a competitive inhibitor of QPRTase with respect to PRPP (Table 3.28). The competitive inhibition pattern is illustrated with a Lineweaver-Burk plot (Figure 3.45).

[Inhibitor] (μM)	**$K_{m(app)}$ (μM)**	**$V_{max(app)}$ (μM min^{-1})**
0	22.1 ± 2.3	0.99 ± 0.04
300	51.2 ± 5.5	1.00 ± 0.03
500	68.6 ± 4.9	1.02 ± 0.03
700	88.8 ± 7.6	1.00 ± 0.03

Table 3.28: *Effect of thymidine 5'-monophosphate on kinetic parameters.*

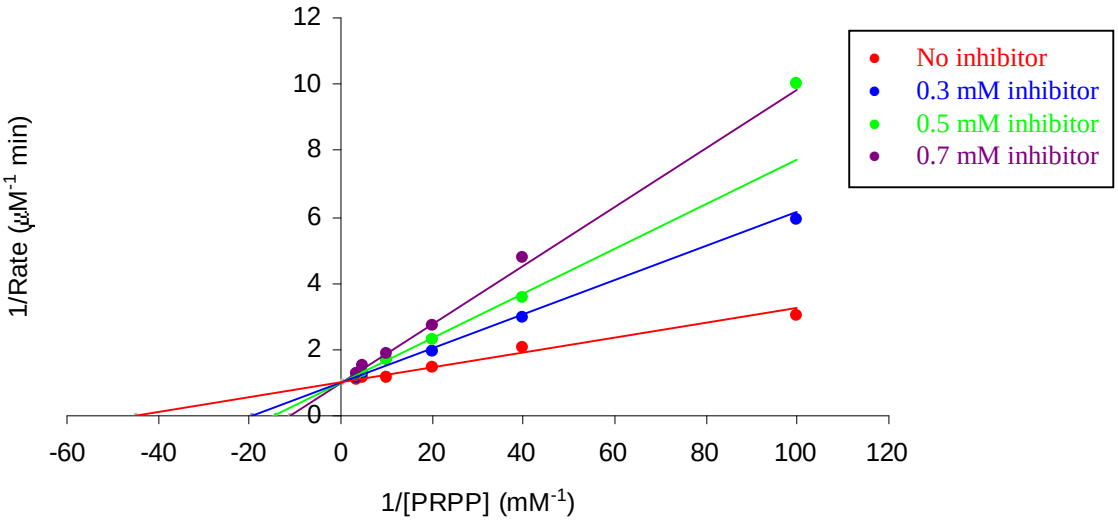

Figure 3.45: *Lineweaver-Burk plot for inhibition with thymidine 5'-monophosphate.*

From a plot of $K_{m(app)}$ versus inhibitor concentration, the K_i value for thymidine 5'-monophosphate **110** was determined as 235 ± 4 μM with respect to PRPP as the variable substrate (Figure 3.46).

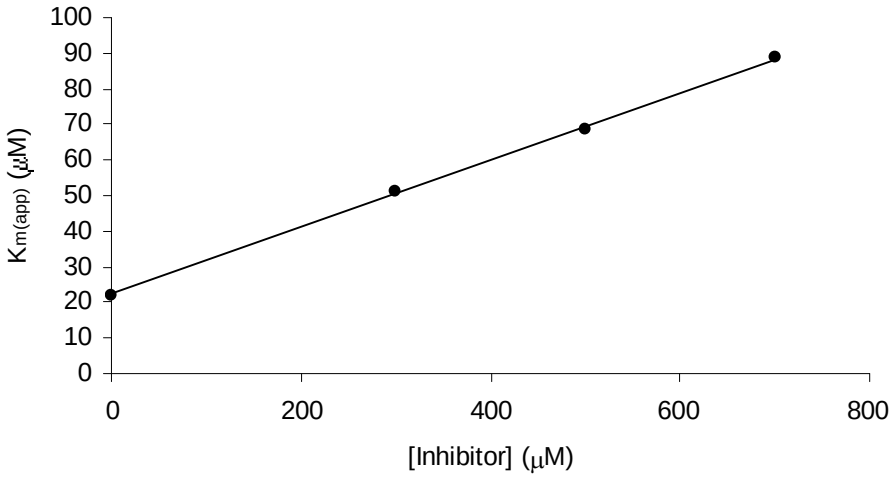

Figure 3.46: *Plot of $K_{m(app)}$ versus [thymidine 5'-monophosphate].*

3.3.3.9 Summary of the nucleotide inhibition study

The four nucleotides investigated in this study were all found to be competitive inhibitors of human brain QPRTase with respect to PRPP as the variable substrate and noncompetitive inhibitors with respect to quinolinic acid as the variable substrate (Table 3.29).

Variable Substrate	Inhibitor	Type of Inhibition	K_i (μM)
Quinolinic acid	AMP **107**	Noncompetitive	551 ± 5
Quinolinic acid	GMP **108**	Noncompetitive	576 ± 4
Quinolinic acid	CMP **109**	Noncompetitive	423 ± 6
Quinolinic acid	TMP **110**	Noncompetitive	427 ± 8
PRPP	AMP **107**	Competitive	304 ± 4
PRPP	GMP **108**	Competitive	309 ± 6
PRPP	CMP **109**	Competitive	222 ± 4
PRPP	TMP **110**	Competitive	235 ± 4

Table 3.29: *Summary of the nucleotide inhibition study.*

The results therefore demonstrate that the nucleotides bind to the PRPP binding site of QPRTase. This result can be explained by the structural similarity between the 5-phosphoribosyl moiety of the nucleotides and the substrate PRPP **15**, meaning the nucleotides can form similar hydrogen bonding interactions in the PRPP binding site of QPRTase. The results appear to suggest that the nucleotides do not mimic the putative reaction intermediate, quinolinic acid mononucleotide **16** or the product, nicotinic acid mononucleotide **11**, since if this was the case then it might be expected that quinolinic acid binding could also be affected by the presence of the inhibitors. The purine and pyrimidine nucleotides therefore appear to be acting as PRPP mimics.

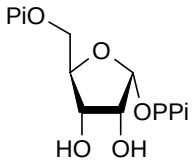

15

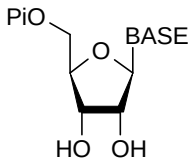

It was found that, with respect to PRPP as the variable substrate, the pyrimidine nucleotides, CMP **109** and TMP **110**, were better competitive inhibitors of QPRTase than the purine nucleotides, AMP **107** and GMP **108** (Table 3.29). It is possible that as a result of the greater steric bulk of the purine ring, AMP **107** and GMP **108** cannot adopt a position in the active site to enable the 5-phosphoribosyl moiety to form the hydrogen bonding interactions with the PRPP binding site as effectively as CMP **109** and TMP **110**, which have a relatively smaller pyrimidine ring. Hence, CMP and TMP are able to bind more tightly to the PRPP binding site of QPRTase, as is reflected in the lower K_i values for these inhibitors with respect to PRPP (Table 3.29).

The observation that the nucleotides bind to the PRPP binding site of QPRTase is consistent with results from previous inhibition studies. Both Calvo *et al.* and Grubmeyer *et al.* have shown that NAMN **11**, the product of the QPRTase reaction, is a competitive inhibitor with respect to PRPP as the variable substrate.[2,3] Furthermore, structural studies have shown that NAMN adopts a conformation in the active site such that both the 5-phosphate group and the ribose hydroxyl group oxygen atoms of NAMN form similar hydrogen bonding interactions with the active site residues as PRPP.[42]

The inhibition pattern of NAMN with respect to quinolinic acid has not previously been determined. However, Calvo *et al.* found that the PRPP analogue fructose-1,6-bisphosphate **32** was a weak noncompetitive inhibitor versus quinolinic acid (K_i 10.9 mM).[2] The four nucleotides examined in this study were all found to be more effective noncompetitive inhibitors of QPRTase with respect to quinolinic acid as the variable substrate.

3.3.4 Potential irreversible inhibitors

Irreversible inhibition occurs when an inhibitor first binds at the active site, then reacts with an active site group to form a covalent bond (Scheme 3.38). The active site is then irreversibly blocked by the inhibitor and is permanently inactivated.

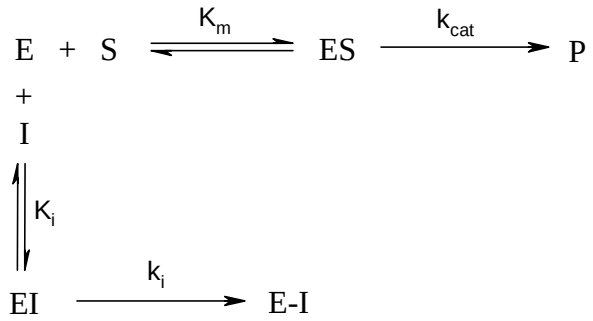

Scheme 3.38: *Irreversible inhibition.*

The kinetic characteristic associated with irreversible inhibition is that it is time-dependent. This is because as time goes by more and more enzyme will be blocked irreversibly by conversion of the reversible EI complex to E-I. If enzyme activity is plotted versus time, an exponential decrease of activity is observed (Figure 3.47a). This is in contrast to reversible inhibition where the enzyme activity is reduced, but is constant with time (Figure 3.47b).

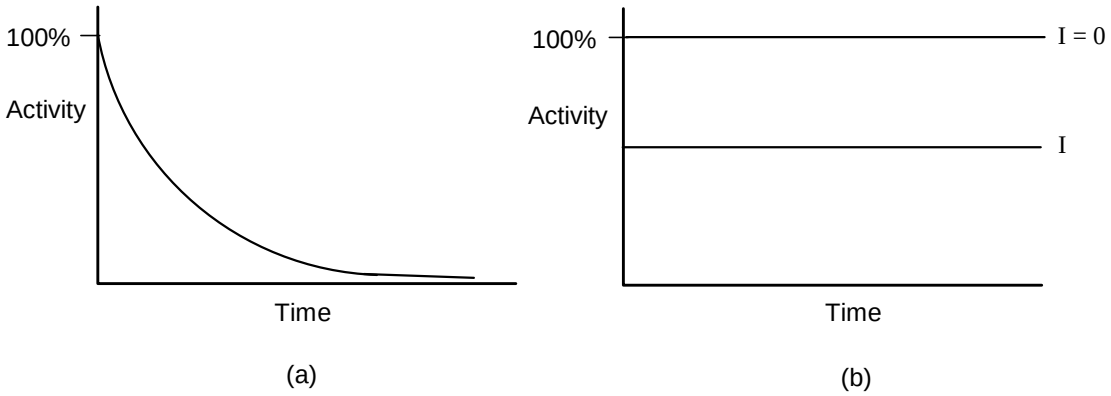

Figure 3.47: *(a) Time-dependence of irreversible inhibition (b) Time-independence of reversible inhibition.*

Irreversible inhibitors usually contain electrophilic functional groups, such as halogen substituents or epoxides that are capable of reacting with nucleophilic residues in the enzyme active site. It was decided to examine two compounds as potential irreversible inhibitors of QPRTase, pyridine 2,3-dicarboxylic acid anhydride **111** and the bicyclic compound **66**, which had been prepared in the laboratory (section 3.2.1.7).

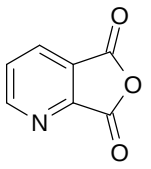

111

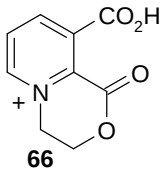

66

Firstly, a preliminary inhibition screen of the compounds was carried out by assessing the percentage inhibition of QPRTase activity at a fixed concentration of quinolinic acid (0.1 mM) and PRPP (0.1 mM). In this inhibition screen, the enzyme was not preincubated with the compounds prior to addition of the substrates. It was found that neither compound inhibited the QPRTase catalysed reaction when present at a concentration of 0.01 mM, 0.1 mM, 1 mM or 10 mM. This observation is consistent with previous studies which have shown that the free carboxylic acid group at the 2-position is required for binding.[5] Therefore if these compounds are to inhibit QPRTase, they must do so by reacting with an active site residue. Structural studies on human brain QPRTase have identified a lysine residue (Lys171) in the active site that might react with the electrophilic groups in these molecules, leading to irreversible inhibition of the enzyme (Scheme 3.39).

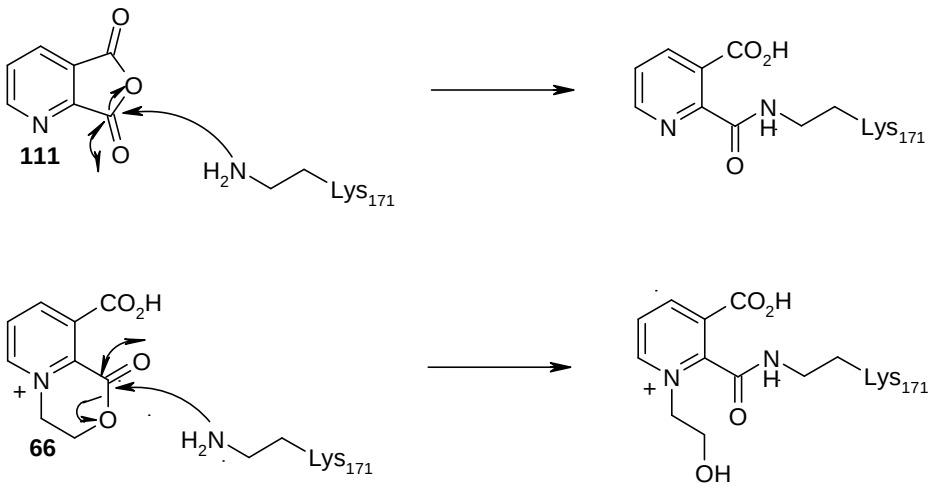

Scheme 3.39: *Potential irreversible inhibition of QPRTase.*

In order to probe this possibility, it was decided to carry out time-dependent inhibition studies. To this end, QPRTase was incubated with each compound (0.5 mM) at 37 °C for a fixed length of time prior to adding the substrates and measuring the enzyme activity. For each compound and set of reaction conditions, the rates were measured in triplicate. The results are summarised in Table 3.30.

Compound	**Length of incubation (h)**	**Average rate (μM min^{-1})**
Pyridine-2,3-dicarboxylic acid anhydride **111**	0	0.84
Pyridine-2,3-dicarboxylic acid anhydride **111**	2	0.70
Pyridine-2,3-dicarboxylic acid anhydride **111**	4	0.60
66	0	0.81
66	2	0.68
66	4	0.61
None present	0	0.82
None present	2	0.73
None present	4	0.58

Table 3.30: *Results from the time-dependent inhibition study.*

The observed time dependence of the decrease in enzyme activity may be indicative of irreversible inhibition. However, it was found that the decrease in rate following enzyme incubation at 37 °C in the presence of the compounds was approximately the same as the decrease in rate observed when the enzyme was incubated at the same temperature for the same length of time but in the absence of the compounds (Table 3.30). It would appear therefore that the observed reduction in enzyme activity is a consequence of the effect the temperature has on the enzyme rather than the compounds binding irreversibly in the active site.

3.4 Overall summary and further work

The four nucleotides (AMP **107**, GMP **108**, CMP **109** and TMP **110**) investigated in this study were all found to be competitive inhibitors of human brain QPRTase with respect to PRPP as the variable substrate and noncompetitive inhibitors with respect to quinolinic acid as the variable substrate. The results therefore demonstrated that the nucleotides act as PRPP mimics and bind to the PRPP binding site of QPRTase.

The study of the inhibition of human brain QPRTase by quinolinic acid analogues highlighted some structural features that are required for potent competitive inhibition and can thus be incorporated into future inhibitor design. Pyridine 2,3-dicarboxylic acid anhydride **111** did not show any inhibition of QPRTase suggesting the free carboxylic acid groups are required for binding. The carboxylic acid group at the 3-position is somewhat important for interaction with the enzyme because when this group was absent, the compounds became less effective as inhibitors. The carboxylic acid group at the 2-position appears to be essential for binding. This conclusion was most clearly indicated by the fact that nicotinic acid **27** did not inhibit the enzymatic reaction, whereas picolinic acid **26** did.

The studies showed that aromaticity is important for tight binding. However, the aromatic ring does not have to be a pyridine ring as is present in the substrate quinolinic acid. Of the compounds tested, phthalic acid **25** proved to be the most effective competitive inhibitor and therefore it would appear that the ring nitrogen is not essential for binding. It might therefore be interesting to examine the inhibitory properties of 2-hydroxybenzoic acid **112** and 2-mercaptobenzoic acid **113** since the corresponding pyridine derivatives have previously been shown to be potent inhibitors of QPRTase.

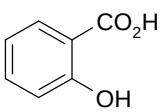

112

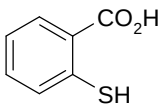

113

It was found that increasing the size of the aromatic ring system to a bicyclic structure leads to weaker binding. This is most likely due to steric interference in the active site. Similarly, there appears to be a certain degree of steric hindrance at the 4- and 5-positions of the pyridine ring. This was indicated by the observation that 5-ethylquinolinic acid **43** and especially kynurenic acid **7**, which has a hydroxyl group at the 4-position, were weaker inhibitors of QPRTase.

Unfortunately, the attempts to synthesise 4-substituted quinolinic acid derivatives, which could be used to further probe interactions at this position, were unsuccessful. Both the directed *ortho*-metalation route and the route involving addition of organometallic reagents to *N*-acylpyridinium salts failed to produce the desired product. While the route involving the oxidation of 4-substituted quinolines looked more promising, there were separation and purification problems and therefore this route also failed to produce pure 4-subtituted quinolinic acid derivatives that could be tested as inhibitors of human brain QPRTase.

In order to further probe the structural requirements for potent inhibition, a future strategy might be to examine the inhibitory properties of substituted phthalic acid derivatives.

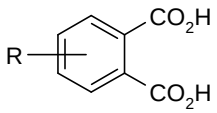

Finally, a series of *N*-substituted compounds were successfully synthesised and tested as inhibitors of human brain QPRTase. This study showed that the presence of small, hydrophobic *N*-substituents leads to weaker binding. It was found that the size of the *N*-alkyl group does not significantly affect the binding. The *N*-oxide compounds appeared to bind more tightly than the corresponding *N*-alkyl compounds. Quinolinic acid *N*-oxide was found to be a potent competitive inhibitor of human brain QPRTase, with a K_i comparable to phthalic acid.

3.5 References

1. E. Okuno and R. Schwarcz, *Biochim. Biophys. Acta*, 1985, **841**, 112-119.
2. R. Bhatia and K.C. Calvo, *Arch. Biochem. Biophys.*, 1996, **325**, 270-278.
3. H. Cao, B.L. Pietrak and C. Grubmeyer, *Biochemistry*, 2002, **41**, 3520-3528.
4. K. Iwai and H. Taguchi, *Methods Enzymol.*, 1980, **66**, 96-101.
5. D.F. Mann and R.U. Byerrum, *J. Biol. Chem.*, 1974, **249**, 6817-6823.
6. L. Kalikin and K.C. Calvo, *Biochem. Biophys. Res. Commun.*, 1988, **152**, 559-564.
7. K. Woznica, *PhD Thesis*, University of St Andrews, St Andrews, 2004.
8. B. Brzezinski and M. Szafran, *Roczniki Chemii*, 1972, **46**, 1887-1889.
9. V. Snieckus, *Chem. Rev.*, 1990, **90**, 879-933.
10. D.L. Comins and D.H. LaMunyon, *Tetrahedron Lett.*, 1988, **29**, 773-776.
11. T.D. Krizan and J.C. Martin, *J. Am. Chem. Soc.*, 1983, **105**, 6155-6157.
12. G. Fraenkel, J.W. Cooper and C.M. Fink, *Angew. Chem. Int. Ed.*, 1970, **9**, 523.
13. R.E. Lyle, J.L. Marshall and D.L. Comins, *Tetrahedron Lett.*, 1977, **18**, 1015-1018.
14. R.E. Lyle and D.L. Comins, *J. Org. Chem.*, 1976, **41**, 3250-3252.
15. D.L. Comins and A.H. Abdullah, *J. Org. Chem.*, 1982, **47**, 4315-4319.
16. E. Piers and M. Soucy, *Can. J. Chem.*, 1974, **52**, 3563-3564.
17. S. Hoogewerff and W.A. Van Dorp, *Chem. Ber.*, 1880, **13**, 1639-1640.
18. W.M. Lauer, C.J. Claus, R.W. Von Korff and S.A. Sundet, *J. Am. Chem. Soc.*, 1952, **74**, 2080-2082.
19. C.F. Koelsch and A.F. Steinhauer, *J. Org. Chem.*, 1953, **18**, 1516-1522.
20. S.M. Gadekar, J.L. Frederick, J. Semb, and J.R. Vaughan, *J. Org. Chem.*, 1961, **26**, 468-473.
21. R.K. Gholson, I. Ueda, N. Ogasawara and L.M. Henderson, *J. Biol. Chem.*, 1964, **239**, 1208-1214.
22. M.D. La Bas, C. Guéret, C. Perrio, M.C. Lasne and L. Barré, *Synthesis*, 2001, **16**, 2495-2499.
23. K.N. Cho, M.S. Park, Y.K. Shim and K.I. Lee, *Bull. Korean. Chem. Soc.*, 2002, **23**, 1830-1832.
24. D.C. Ayers and A.M.M Hossain, *J. Chem. Soc., Perkin Trans. I*, 1975, 707-710.

25. M.T. Nunez and V.S. Martin, *J. Org. Chem.*, 1990, **55**, 1928-1932.
26. A.F. Lindenstruth and C.A. Vanderwerf, *J. Am. Chem. Soc.*, 1949, **71**, 3020-3021.
27. M. Kulka, *J. Am. Chem. Soc.*, 1946, **68**, 2472-2473.
28. J.C. Cochran and W.F Little, *J. Org. Chem.*, 1961, **26**, 808-811.
29. C. Osuch and R. Levine, *J. Am. Chem. Soc.*, 1956, **78**, 1723-1725.
30. N.N. Goldberg and R. Levine, *J. Am. Chem. Soc.*, 1955, **77**, 3647-3648.
31. B.S. Furniss, A.J. Hannaford, P.W.G Smith and A.R. Tatchell, *Vogel's Textbook of Practical Organic Chemistry*, 5th Edition, Longman Scientific and Technical, 1989, 1171-1172.
32. M.J. Weiss and C.H. Hauser, *J. Am. Chem. Soc.*, 1949, **71**, 2023-2026.
33. P.H. Dirstine and F.W. Bergstrom, *J. Org. Chem.*, 1946, **11**, 55-59.
34. R.A. Seibert and F.W. Bergstrom, *J. Org. Chem.*, 1945, **10**, 544-550.
35. M.J. Weiss and C.H. Hauser, *J. Am. Chem. Soc.*, 1949, **71**, 2026-2027.
36. F.W. Bergstrom, *J. Am. Chem. Soc.*, 1931, **53**, 4065-4076.
37. C. O'Murchu, *Synthesis*, 1989, 880-882.
38. L. Michaelis and M. Menten, *Biochem. Z.*, 1913, **49**, 333-369.
39. T. W. Stone and M.N. Perkins, *Eur. J. Pharmacol.*, 1981, **72**, 411-412.
40. K. Iwai, K. Shibata and H. Taguchi, *Agric. Biol. Chem.*, 1979, **43**, 351-355.
41. K. Shibata and K. Iwai, *Biochim. Biophys. Acta*, 1980, **611**, 280-288.
42. V. Sharma, C. Grubmeyer and J.C. Sacchettini, *Structure*, 1998, **6**, 1587-1599.
43. A.C. Foster, A. Vezzani, E.D. French and R. Schwarcz, *Neurosci. Lett.*, 1984, **48**, 273-278.
44. H. Taguchi and K. Iwai, *Agric. Biol. Chem.*, 1976, **40**, 385-389.

Chapter Four

Enzymatic Decarboxylation Studies

4.1 Introduction

QPRTase is an unusual PRTase enzyme in that it appears to catalyse a second reaction, decarboxylation of the quinolinic acid mononucleotide **16** to form the corresponding nicotinic acid mononucleotide **11**. This decarboxylation reaction is considered to have an analogous mechanism to that observed for the decarboxylation of pyridine carboxylic acids in chemical studies. The mechanism proposed by Hammick *et al.* involves loss of carbon dioxide to form a nitrogen ylide, which is then protonated to give the product (Scheme 4.1).[1]

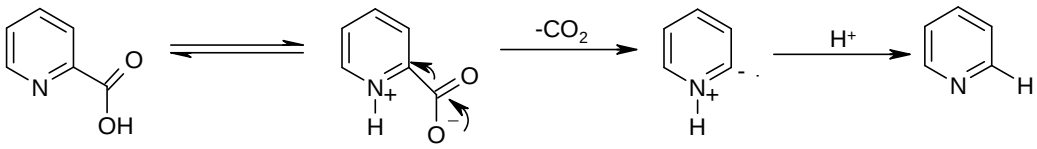

Scheme 4.1: *Mechanism for the decarboxylation of pyridine carboxylic acids.*

An analogous mechanism can be envisaged for the decarboxylation of quinolinic acid mononucleotide **16**, proceeding via the nitrogen ylide **18** (Scheme 4.2).

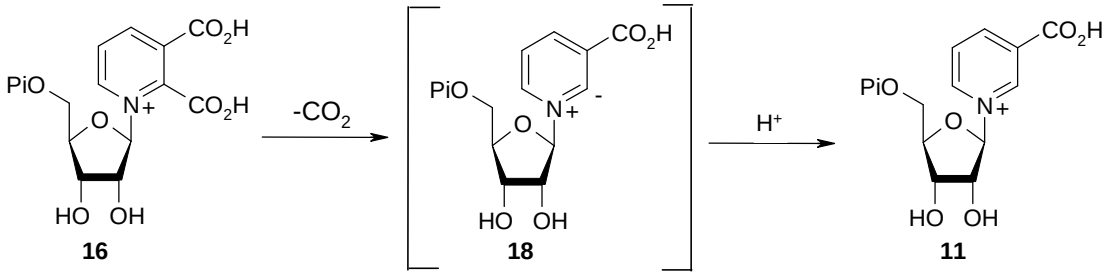

Scheme 4.2: *Decarboxylation of quinolinic acid mononucleotide.*

However, enzymatic involvement in the decarboxylation step is yet to be conclusively proven. As similar reactions were observed to occur spontaneously, it was suggested that QPRTase played no part in the decarboxylation step and it occurred after the mononucleotide had been released from the active site. In order to test this theory, experiments were conducted involving the non-enzymatic decarboxylation of pyridine carboxylic acids.[2-4] Quinolinic acid was the most rapidly decarboxylated of all the pyridine carboxylic acids studied, but the reaction was still very slow and required harsh conditions. Quinolinic acid was shown to decarboxylate in aqueous

hydrochloric acid (pH 1) at 95 °C, with a half life of *ca.* 3 days.[2] Clearly the harsh conditions whereby decarboxylation was observed are quite remote from the physiological conditions (pH 7.2 and 37 °C) under which the QPRTase catalysed reaction takes place. Some enzymatic involvement would therefore seem to be necessary. Ideally, examination of the non-enzymatic decarboxylation of quinolinic acid mononucleotide **16** would solve this problem.

Previously in our laboratory, considerable effort was made towards the synthesis of quinolinic acid mononucleotide **16** for use in decarboxylation studies.[5] The initial proposed synthetic route involved direct coupling to form the *N*-glycosidic bond (Scheme 4.3).

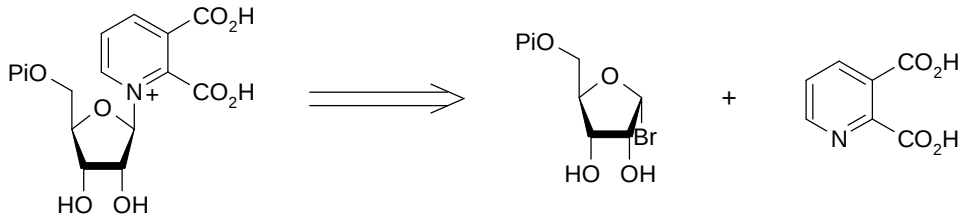

Scheme 4.3: *Disconnection of quinolinic acid mononucleotide.*

To investigate this route, a series of model reactions involving the coupling of 2,3-disubstituted pyridine derivatives to acetobromoglucose **114** were carried out (Scheme 4.4). Similar coupling reactions involving acetobromoglucose are well documented.[6-8]

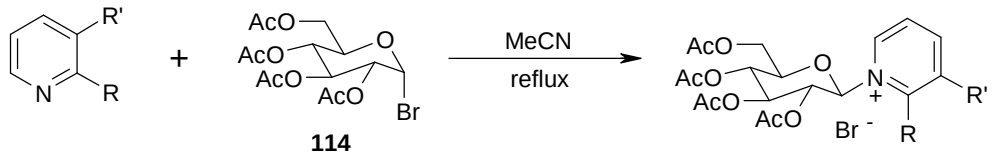

Scheme 4.4: *Coupling of substituted pyridine derivatives to acetobromoglucose.*

The coupling of dimethyl quinolinate (R=R'=CO_2Me) and acetobromoglucose failed. It is possible this was due to the steric bulk of the ester group at the 2-position of the pyridine ring since coupling reactions between nicotinamide (R=H, R'=$CONH_2$) and either acetobromoglucose or 2,3,5-triacetylribofuranosyl bromide were successful.

The coupling of pyridine 2,3-dicarboxylic acid anhydride and acetobromoglucose was then attempted. The reason for using pyridine 2,3-dicarboxylic acid anhydride was that in this molecule the acidic substituents at C-2 and C-3 are tied together to form the anhydride and it was hoped this would reduce steric congestion around the nitrogen atom, enabling the coupling reaction to occur. Subsequent hydrolysis would generate the desired diacid functionality. However, the coupling reaction failed. It is possible that the anhydride has a substantial electron withdrawing effect on the pyridine ring. As a result the ring nitrogen is a very poor nucleophile, which prevents the coupling reaction taking place.

The reaction of pyridine-2,3-dicarbinol (R=R'=CH_2OH) with acetobromoglucose was then attempted. It was hoped the use of pyridine-2,3-dicarbinol might eliminate the steric and electronic problems, enabling the coupling reaction to occur. Subsequent oxidation would generate the desired diacid functionality. However, this coupling reaction was also unsuccessful.

Therefore, due to a combination of steric and electronic effects, direct coupling of 2,3-disubstituted pyridines to sugar groups is not an effective method for the synthesis of quinolinic acid mononucleotide.

An alternative synthetic route to quinolinic acid mononucleotide **16**, involving reacting an amino sugar with a 1,5-diketo compound to construct the pyridine ring, was then investigated (Scheme 4.5). However, this route was also unsuccessful.

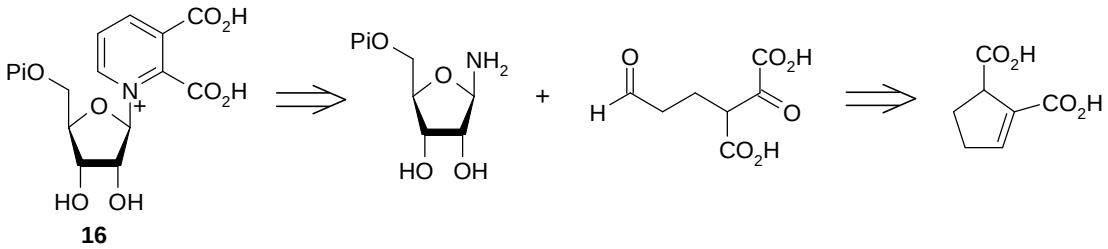

16

Scheme 4.5: *Alternative disconnection of quinolinic acid mononucleotide.*

Thus previous studies have shown quinolinic acid mononucleotide is a very difficult compound to synthesise.[5] Therefore, it has not been possible to determine the role of QPRTase in the decarboxylation reaction. However, simple mimics of quinolinic acid

mononucleotide would be easier to synthesise and might be useful as substrates for enzymatic and non-enzymatic decarboxylation studies. The decarboxylation studies might provide some information that can be translated to the quinolinic acid mononucleotide system.

4.2 Non-enzymatic decarboxylation studies

Previously in our laboratory, two simple mimics of quinolinic acid mononucleotide, *N*-methyl and *N*-ethylquinolinic acid, were synthesised and non-enzymatic decarboxylation studies were carried out on these compounds.[9]

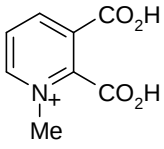

41

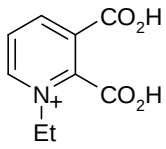

42

Dunn *et al.* found that quinolinic acid decarboxylates in aqueous hydrochloric acid (pH 1) at 95 °C, with a half life of *ca.* 3 days.[2] The non-enzymatic decarboxylation studies on the *N*-alkylquinolinic acid derivatives showed that *N*-substitution increases the rate of decarboxylation and the bulkier the *N*-substituent the greater the observed increase in rate (*N*-methylquinolinic acid **41**, $t_{1/2}$ 6.7 hours and *N*-ethylquinolinic acid **42**, $t_{1/2}$ 4.6 hours).[9] However, the actual rate was still quite slow when compared to an enzymatic reaction. Furthermore, the harsh conditions required for decarboxylation (pH 1 and 95 °C) are quite remote from physiological conditions (pH 7.2 and 37 °C). Presumably, the larger *N*-substituent increases steric congestion around the 2-carboxylic acid group which is released upon decarboxylation. This effect would be even greater in the case of quinolinic acid mononucleotide **16**. However, it cannot yet be deduced whether there would be sufficient rate increase to make this reaction as rapid as an enzymatic reaction under physiological temperature and pH. Therefore, it is still likely that the decarboxylation reaction is catalysed by QPRTase. It is possible that the enzyme is involved in reducing the effective pH at the active site, therefore ensuring that the quinolinic acid mononucleotide is in a monoprotonated form, allowing efficient decarboxylation.

4.3 Enzymatic decarboxylation studies

Now that QPRTase is available in our laboratory, the aim was to undertake enzymatic decarboxylation studies to determine whether QPRTase can catalyse the decarboxylation of the simple *N*-alkylquinolinic acids under physiological conditions (Scheme 4.6).

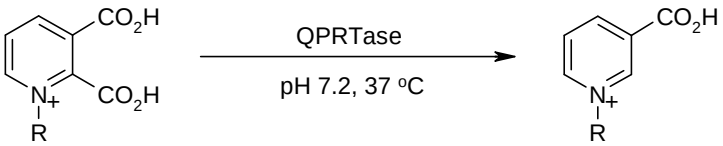

41 R = Me
42 R = Et

59 R = Me
60 R = Et

Scheme 4.6: *Possible decarboxylation of N-alkylquinolinic acids.*

Firstly, the substrates for the decarboxylation studies, *N*-methyl and *N*-ethylquinolinic acid **41** and **42**, were synthesised as described in section 3.2.1. The authentic decarboxylation products, *N*-methyl and *N*-ethylnicotinic acid **59** and **60**, were also synthesised in an identical manner.

A UV scan for each compound was then carried out which revealed it is possible to monitor the decarboxylation reaction by measuring the decrease in absorbance at 280 nm over time as the substrate is converted to product. The UV absorbance spectra for *N*-methylquinolinic acid **41** and *N*-methylnicotinic acid **59** are shown in Figure 4.1.

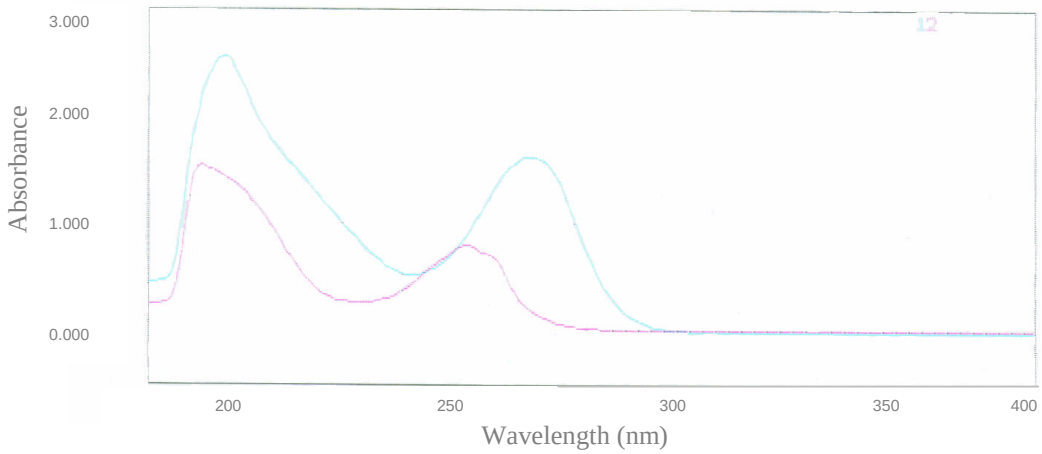

Figure 4.1: *UV absorbance spectra for N-methylquinolinic acid (turquoise) and N-methylnicotinic acid (pink) at 37 ℃, pH 7.2.*

For the decarboxylation studies, the assay mixtures contained 0.3 mM *N*-alkylquinolinic acid in 50 mM K_2HPO_4/KH_2PO_4 buffer (pH 7.2). Each assay was initiated by the addition of QPRTase (14 μg). The absorbance at 280 nm was then measured continuously over a 30 minute period at 37 °C. For comparison, control experiments in which the *N*-alkylquinolinic acids were incubated under the same conditions but in the absence of QPRTase were also set up so that if decarboxylation was observed, the role of the enzyme would be apparent. However, for both the *N*-methyl and *N*-ethyl compounds, A_{280} remained constant with time suggesting no decarboxylation occurred, either in the presence or absence of the enzyme. A series of assays were then set up to monitor the reaction continuously over a longer period of time (2 h, 5 h and 8 h) under the same conditions. However, no significant change in absorbance was observed, again suggesting no decarboxylation occurred.

The initial decarboxylation studies were performed in the absence of the second QPRTase substrate, PRPP. Since it is possible that binding of both substrates may lead to structural changes in the active site causing the enzyme to adopt a reactive conformation, it was decided to repeat the decarboxylation studies on the *N*-alkylquinolinic acid derivatives in the presence of PRPP. However, as before no change in absorbance at 280 nm was observed suggesting no decarboxylation occurred.

It was therefore decided to set up a longer incubation of the *N*-alkylquinolinic acid derivatives with QPRTase at 37 °C and pH 7.2. Rather than monitor the reactions continuously at 280 nm, the UV absorbance scan of the incubated reactions were recorded after 48 hours and compared to the UV spectra of the pure starting material (*N*-alkylquinolinic acid) and authentic decarboxylation product (*N*-alkylnicotinic acid). For both the *N*-methyl and *N*-ethyl compounds, the UV spectra recorded after 48 hours were identical to the UV spectra of the *N*-alkylquinolinic acid derivatives suggesting no decarboxylation occurred under the enzymatic conditions examined (Figure 4.2).

(a)

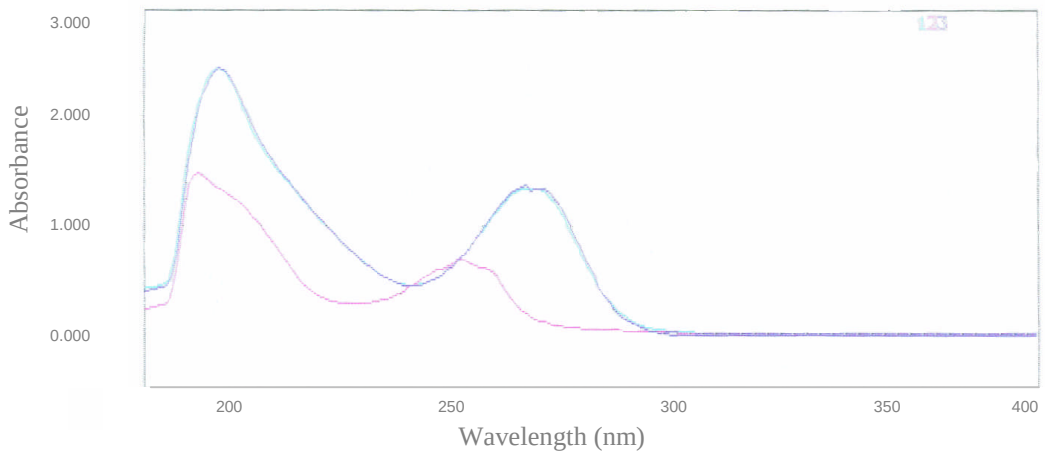

(b)

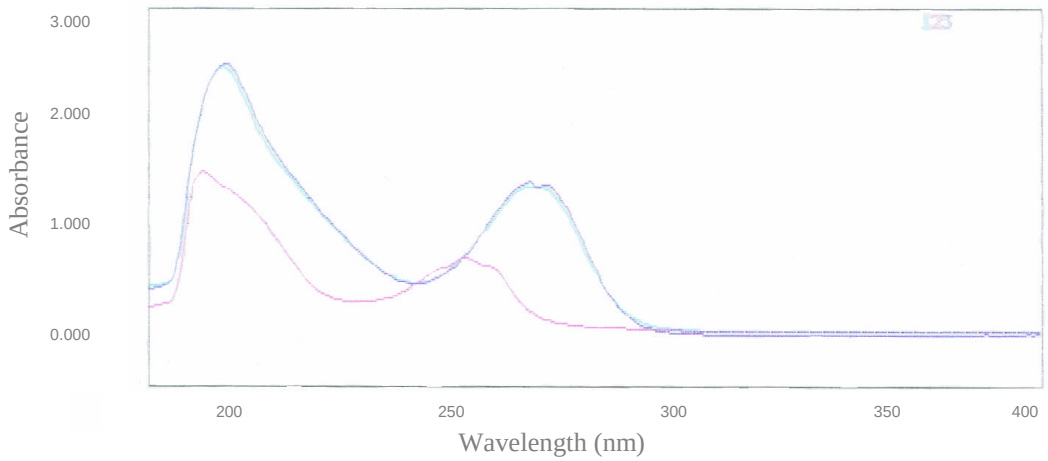

Figure 4.2: *(a) UV absorbance spectra for N-methylquinolinic acid (turquoise), N-methylnicotinic acid (pink) and the reaction incubated for 48 hours (dark blue) at 37 ℃, pH 7.2. (b) UV absorbance spectra for N-ethylquinolinic acid (turquoise), N-ethylnicotinic acid (pink) and the reaction incubated for 48 hours (dark blue) at 37 ℃, pH 7.2.*

4.4 Summary and further work

Previous non-enzymatic decarboxylation studies showed *N*-methyl and *N*-ethylquinolinic acid undergo spontaneous decarboxylation but the reactions were slow and required harsh conditions.[9] The model studies suggested some enzymatic involvement in the decarboxylation of quinolinic acid mononucleotide would seem to be necessary.

However, the enzymatic decarboxylation experiments undertaken in this study suggested QPRTase is unable to catalyse the decarboxylation of *N*-methyl and *N*-ethylquinolinic acid under physiological conditions. The inhibition studies had shown that both *N*-methyl and *N*-ethylquinolinic acid are potent competitive inhibitors of QPRTase with respect to quinolinic acid as the variable substrate, confirming they do bind to the quinolinic acid binding site (section 3.3.2). However, the inhibition studies also showed that the presence of the *N*-alkyl substituent leads to weaker binding. It is therefore possible that the small hydrophobic *N*-substituent cannot position the molecules correctly in the active site to allow catalysis of the decarboxylation. Structural studies on QPRTase with the *N*-alkylquinolinic acid derivatives bound in the active site are required to probe the interactions between these compounds and the enzyme.

Thus the involvement of QPRTase in the decarboxylation of quinolinic acid mononucleotide remains unclear from these studies. Increasing the similarity of the *N*-substituent to that in quinolinic acid mononucleotide might lead to more useful substrates for enzymatic decarboxylation studies. Quinolinic acid mononucleotide itself remains a key synthetic target since access to this compound would enable the unambiguous determination of the enzymatic involvement in the decarboxylation reaction.

4.5 References

1. M.R.F. Ashworth, R.P. Daffern and D.L. Hammick, *J. Chem. Soc.*, 1939, 809-812.
2. G.E. Dunn, G.K. Lee and H. Thimm, *Can. J. Chem.*, 1972, **50**, 3017-3027.
3. G.E. Dunn and G.K. Lee, *Can. J. Chem.*, 1971, **49**, 1032-1035.
4. G.E. Dunn, E.A. Lawler and A.B. Yamashito, *Can. J. Chem.*, 1977, **55**, 2478-2481.
5. K. Woznica, *PhD Thesis*, University of St Andrews, St Andrews, 2004.
6. R.W. Johnson, T.M. Marschner and N.J. Oppenheimer, *J. Am. Chem. Soc.*, 1988, **110**, 2257-2263.
7. J. Lee, H. Churchil, W-B. Choi, J.E. Lynch, F.E. Roberts, R.P. Volante and P.J. Reider, *J. Chem. Soc., Chem. Commun.*, 1999, 729-730.
8. I.A. Mikhailopulo, T.I. Pricota, V.A. Timoshuck and A.A Akhrem, *Synthesis*, 1981, 388-389.
9. A.M. Allsebrook, *PhD Thesis*, University of St Andrews, St Andrews, 1998.

Chapter Five

Site-directed Mutagenesis Studies

5.1 Introduction

5.1.1 Chemical modifications of amino acids

Chemical reagents that react specifically with a given amino acid side chain can be used to identify the presence of the amino acid in an unknown protein. In addition, by examination of the effect that chemical modification of different classes of amino acid side chains has on the activity of the enzyme, it is possible to determine which amino acids are critical for the structure or function of the protein. For example, if a reagent that covalently interacts with only lysine residues is found to inhibit the function of the protein, a lysine might be considered to be important for the catalytic activity of the protein. A list of some reagents used for the modification of specific amino acids is shown in Table 5.1.

Amino acid	**Group modified**	**Reagent**	**Modification reaction**
Cysteine	SH	Iodoacetate Iodoacetamide DTNB *p*-Hydroxymercuribenzoate	Alkylation Alkylation Disulfide formation Metal complexation
Histidine	NH	Diethyl pyrocarbonate	Acylation
Lysine	NH_2	Succinic anhydride	Acylation
Arginine	Guanidine	Phenylglyoxal	Heterocycle formation
Aspartate Glutamate	CO_2H	EDC + amine	Amide formation
Tyrosine	Phenol	Tetranitromethane	Nitration
Tryptophan	Indole	*N*-Bromosuccinimide	Oxidation

Table 5.1: *Group specific reagents used for amino acid modification. (DTNB 5,5'-dithiobis-(2-nitrobenzoic acid); EDC 1-ethyl-3-(3-dimethylaminopropyl) carbodiimide)*

The effects of various chemical modification agents on the activity of hog liver QPRTase have been investigated.[1] β-Naphthoquinone-4-sulfonic acid and 2,4,6-trinitrobenzene sulfonic acid are known to react with lysine residues. Histidine residues can be modified by reaction with diethylpyrocarbonate or *p*-diazobenzene sulfonic acid. Arginine residues can be modified by reaction with glyoxal. All of these reagents showed inhibitory effects at fairly low concentrations, which implied that lysine, histidine and arginine residues may be involved in the active site of QPRTase. Inhibition with β-naphthoquinone-4-sulfonic acid and *p*-diazobenzene sulfonic acid was suppressed by the presence of the substrate, although reaction with glyoxal was not. Chemical modifications of hog liver QPRTase therefore demonstrated that arginine, lysine and histidine residues are necessary for activity, with lysine and histidine residues closely associated with the quinolinic acid binding site.

Diisopropylfluorophosphate, 2-hydroxy-5-nitrobenzyl bromide and acetylimidazole are chemical modification agents for serine, tryptophan and tyrosine residues respectively. These reagents did not inhibit QPRTase to any degree, which suggested that these residues are not present in the active site of hog liver QPRTase.

It was found that QPRTase from hog liver was strongly inhibited by reagents that react specifically with thiol groups, such as *p*-chloromercuribenzoic acid, *N*-ethylmaleimide, 5,5'-dithiobis-(2-nitrobenzoic acid) and monoiodoacetic acid.[2] This suggested that thiol groups have an important role in determining the enzymatic activity of the hog liver enzyme. This is in contrast to the shiitake mushroom enzyme, the activity of which was unaffected by treatment with such reagents.[3]

The effects of various chemical modification agents on the activity of hog kidney QPRTase have also been investigated.[4] It was found that acetylimidazole, 2-hydroxy-5-nitrobenzyl bromide and 1,2-cyclohexanedione did not affect the enzyme activity. These results suggested that tryptophan, tyrosine and arginine residues are not present in the active site of the enzyme. However, it was found that enzymatic activity was significantly reduced when treated with thiol group modifying reagents (*p*-chloromercuribenzoic acid and 5,5'-dithiobis-(2-nitrobenzoic acid)), amino group

modifying reagents (trinitrobenzenesulfonate) and imidazole group modifying reagents (diethyl pyrocarbonate). In addition, it was found that inhibition by these chemical modification reagents was suppressed by preincubation with the substrates. The results therefore suggested that thiol, amino and imidazole groups exist in the binding sites of quinolinic acid and PRPP in hog kidney QPRTase.

In a recent study by Gaur *et al.*, QPRTase from *E. coli* was examined for susceptibility to different chemical modification reagents.[5] Loss of enzyme activity with trinitrobenzenesulfonate (TNBS) occurred when 1.1 lysines per subunit were modified. Tryptic digestion of the modified enzyme followed by HPLC-MS analysis of the peptides showed Lys70 reacts with TNBS. This lysine is not conserved in the sequence of the enzyme from all sources, nor is the amino acid part of the active site according to the X-ray structures of QPRTase from *Salmonella typhimurium* and *Mycobacterium tuberculosis*. Based on X-ray studies, it was found that this amino acid residue participates in a conformational change distant from the active site. The Lys70 modified enzyme is no longer functional, which suggested that chemical modification hinders a catalytically critical movement.

In the same study, the modification of cysteine residues was investigated with several reagents; iodoacetic acid, iodoacetamide, 5,5'-dithiobis-(2-nitrobenzoic acid) and *N*-ethylmaleimide. No significant loss of activity of QPRTase was observed with any of these reagents. Similarly, arginine modifying reagents such as butanedione and phenylglyoxal did not lead to loss of enzyme activity.

In summary, the chemical modification experiments performed on QPRTase from various sources have demonstrated that lysine and histidine residues are present in the active site and are essential for enzymatic activity. It would appear that arginine and cysteine residues have an important role in determining the enzymatic activity of QPRTase from some sources. Tryptophan, tyrosine and serine residues do not appear to be present in the active site of any of the QPRTases investigated.

5.1.2 Site-directed mutagenesis

A useful way to obtain information regarding the importance of specific active site residues in binding and catalysis is to perform site-directed mutagenesis studies. The genetic code programmed into DNA determines the number and sequence of amino acids in a protein, and thus also the functional properties of the protein. Site-directed mutagenesis, first reported by Smith *et al*. in 1982, makes it possible to reprogramme the genetic code and in this way replace specific amino acids in proteins.[6]

This technique requires that the wild-type gene sequence is known. The key to the mutation is the preparation of an oligonucleotide primer that is complementary to the wild-type gene but contains a mismatched nucleotide (Figure 5.1). Oligonucleotide primers are usually 20-30 bases in length and are synthesised chemically exactly according to the designed sequence. Since a small number of mismatches (1-3 bp) are tolerable for primer binding to the template wild-type DNA, mismatches can be precisely incorporated as mutations in the newly synthesised DNA. In general, mismatches are placed in the middle of a primer rather than at the 5'- or 3'-ends, enabling the wild-type template to bind the primer by both stretches of sequence surrounding the mismatch. By using a specific mutagenic primer, a specific mutant with a predetermined site and type of mutation will be produced.

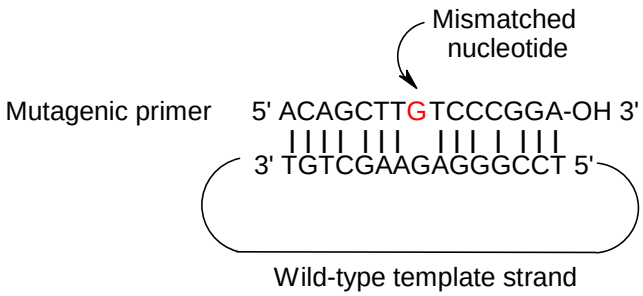

Figure 5.1: *Oligonucleotide-directed mutagenesis reported by Smith et al. A primer containing a mismatched nucleotide is used to produce a desired point mutation.*

Following wild-type strand separation, the specifically designed mutagenic primer is annealed to the complementary sequence on the wild-type template strand (Figure 5.1). The primer is then elongated by DNA polymerase and the double stranded circle is closed by adding DNA ligase. Other than the mismatches introduced through the primer, the mutant DNA is reproduced exactly according to the wild-type DNA template. The mutant DNA sequence is then replicated in a suitable host organism.

Expression of the plasmid containing the specific codon change (e.g. TCT to TGT) will produce a protein with the desired amino acid substitution (e.g. Ser to Cys) at a unique position. The biological activity of the mutated protein can then be compared to that of the wild-type protein. In this way, the functional and structural roles of amino acid residues in a protein of interest can be studied. By making one amino acid substitution at a time, it is possible to build up a picture of the importance of each active site residue in binding and catalysis.

Since its invention, there have been continual improvements in the basic methodologies and versatility of site-directed mutagenesis, in particular the employment of the polymerase chain reaction (PCR) to amplify the mutant DNA sequence.[7] So central has this technique become to all of biochemistry and molecular biology that Michael Smith, its pioneer, shared the Nobel Prize in Chemistry in 1993 with Kary B. Mullis who developed PCR.

To date, no site-directed mutagenesis studies on QPRTase have been reported.

5.2 Site-directed mutagenesis studies on human brain QPRTase

5.2.1 Introduction

Structural studies carried out on human brain QPRTase have enabled the identity and spatial positioning of the active site residues to be determined (Figure 5.2). The active site of human brain QPRTase is located at the centre of the α/β-barrel and is a deep pocket with a highly positive electrostatic surface. This surface is composed of three arginine residues (Arg161, Arg138, Arg102' (' denotes residues from the other subunit of the dimer)), two lysine residues (Lys139 and Lys171) and one histidine residue (His160). These residues are highly conserved among QPRTase enzymes (section 2.3.1) and adopt similar conformations in the structures of *Mycobacterium tuberculosis* QPRTase and *Salmonella typhimurium* QPRTase. These residues are therefore ideal targets for site-directed mutagenesis studies to probe the mechanism of QPRTase.

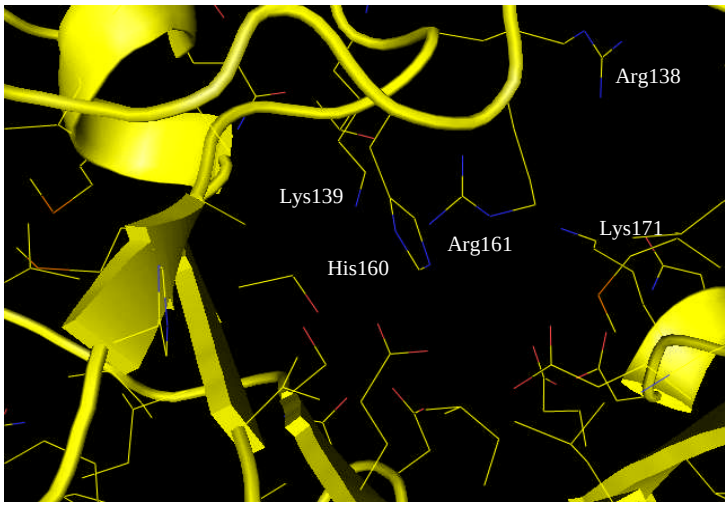

Figure 5.2: *Active site of human brain QPRTase.*

The role of these residues is unclear from the structural studies on human brain QPRTase since currently only the structure of the apoenzyme has been determined. However, detailed structural studies have been carried out on *Mycobacterium tuberculosis* QPRTase and various complex structures with substrates, products and inhibitors bound in the active site are available.[8] The structure of *Mycobacterium tuberculosis* QPRTase with the inhibitor phthalic acid bound in the active site is

shown in Figure 5.3. From this structure the possible interactions between the enzyme and the substrate become clearer and hence more informed decisions can be made regarding the choice of mutations. Sequence alignment has shown that the target residues in human brain QPRTase, Arg161, Arg138, Arg102', Lys171 and Lys139, correspond to residues Arg162, Arg139, Arg105', Lys172 and Lys140, respectively, in *Mycobacterium tuberculosis* QPRTase (section 2.3.1).

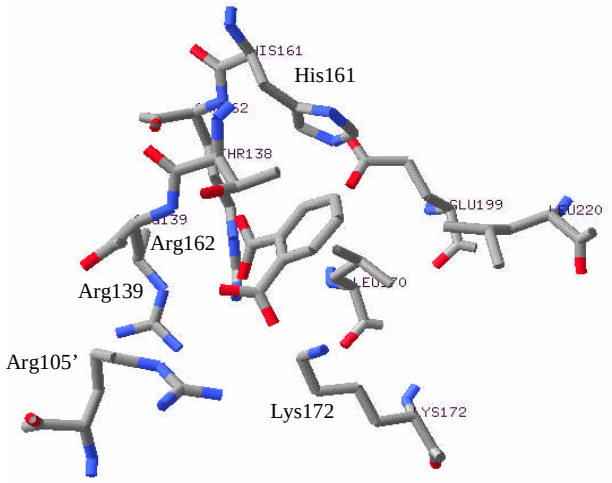

Figure 5.3: *Active site of Mycobacterium tuberculosis QPRTase with inhibitor phthalic acid bound [Protein Data Bank 1QPQ].*

The three arginine residues in the active site might be involved in electrostatic interactions with the carboxylate groups of the substrate quinolinic acid. Therefore, to probe binding interactions, it was decided to change the nature of the amino acid side chain and examine the effect of replacing each individual arginine residue with alanine and also with glutamine, since a glutamine residue would still be of reasonable size and polarity but not positively charged like arginine.

The side chain of residue Lys172 (*Mycobacterium tuberculosis* QPRTase numbering) appears to be close to the C-2 carboxylate group and might therefore play an important role in binding and/or catalysis (Figure 5.3). It was decided to replace this lysine residue in human brain QPRTase (Lys171) with alanine and also serine, which is a bit bigger and more polar but still uncharged, and examine the effect this has on the enzymatic reaction. Similarly, it was decided to replace residue Lys139 in human brain QPRTase with alanine and serine. This residue looks important in the active site of human brain QPRTase although its role was unclear from the structures of *Mycobacterium tuberculosis* QPRTase.

5.2.2 Generation of the mutant proteins

5.2.2.1 Cloning and amplification of the mutant QPRTase genes

Site-directed mutagenesis makes it possible to replace specific amino acids in proteins by reprogramming the genetic code. The target mutations in human brain QPRTase were:

Arg102Gln	Arg102Ala	Lys139Ala	Lys139Ser
Arg161Gln	Arg161Ala	Lys171Ala	Lys171Ser
Arg138Gln			

Site-directed mutagenesis was performed on a pEHISTEV-QPRTase clone based on the megaprimer PCR method[9] by Dr Huanting Liu (The Centre for Biomolecular Science, University of St Andrews).

The principle of the megaprimer method for PCR site-directed mutagenesis is outlined in Figure 5.4. For this method two flanking primers (primers A and C), one internal mutagenic primer (primer B) and wild-type templates are needed. The first round of PCR uses one flanking primer (primer A) and the internal mutagenic primer (primer B), containing the desired base substitution(s), to generate a double stranded megaprimer containing the mutations introduced by the mutagenic primer. Both the original template and the product become further templates for subsequent rounds of DNA synthesis and the mutant DNA predominates over the original template after several PCR cycles. The pure megaprimer is isolated by extraction from an agarose gel. In the second round of PCR, the purified megaprimer is then used together with the second flanking primer (primer C) to generate the complete mutant DNA sequence for subsequent purification and cloning into the appropriate expression vector.

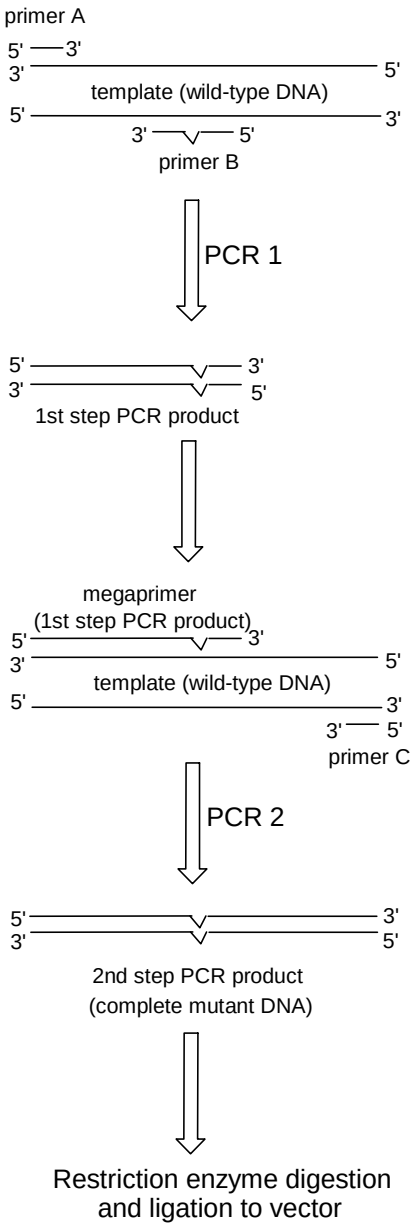

Figure 5.4: *Schematic outline of the mutagenesis protocol used in this study.*

In this study, the template DNA was a pEHISTEV-QPRTase clone, which contains a full length DNA sequence encoding wild-type human brain QPRTase. All the primers used were synthesised by Eurogentic. Specific internal mutagenic primers (primer B) were designed to introduce the desired mutations at the correct position in the QPRTase gene. The two flanking primers (primers A and C) were designed to bind to the two ends of the target sequence (the wild-type QPRTase gene). To enable the subsequent cloning of the mutant QPRTase gene into the pEHISTEV expression vector, the 5' primer (primer A) contained a BspHI recognition site and the 3' primer (primer C) contained a BamHI recognition site just after the QPRTase stop codon.

The final DNA product from each mutagenesis reaction was digested with the appropriate restriction enzymes. The expression vector pEHISTEV-QPRTase was then constructed by ligating the BspHI/BamHI digested mutant QPRTase gene into the compatible NcoI/BamHI digested pEHISTEV vector. The constructed expression vector is shown in Figure 5.5.

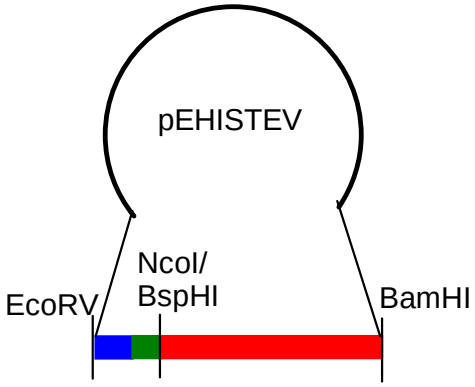

Figure 5.5: *Construction of the pEHISTEV-QPRTase expression vector. The partial circle represents the pEHISTEV plasmid. The transcription/expression region encompasses the mutant QPRTase gene (red bar), a TEV protease recognition site (green bar) and a 6 x histidine tag (blue bar).*

The resulting ligation mixture was used to transform competent *E. coli* cells. Several colonies from each mutagenesis reaction were selected and the plasmid DNA was isolated. The pure plasmid DNA was isolated by firstly lysing the bacterial cells under alkaline conditions. The lysate was then neutralised and adjusted to high-salt binding conditions. The DNA was adsorbed onto a silica column, washed and then the pure plasmid DNA was eluted. The purified plasmids from each mutagenesis reaction were screened for the presence of the desired mutation by DNA sequencing.

All the mutations and the sequence integrity of the QPRTase gene were confirmed by automated DNA sequencing (The Sequencing Service, School of Life Sciences, University of Dundee). T7 promoter and terminator primers were employed to read the DNA sequence from 5' to 3' and 3' to 5' respectively. The DNA sequences were transformed to give the protein sequence using the program DNAMAN. Short segments of the DNA and protein sequences showing the mutations present in the nine QPRTase mutants are shown in Figure 5.6. No additional secondary mutations were observed in any of the sequences.

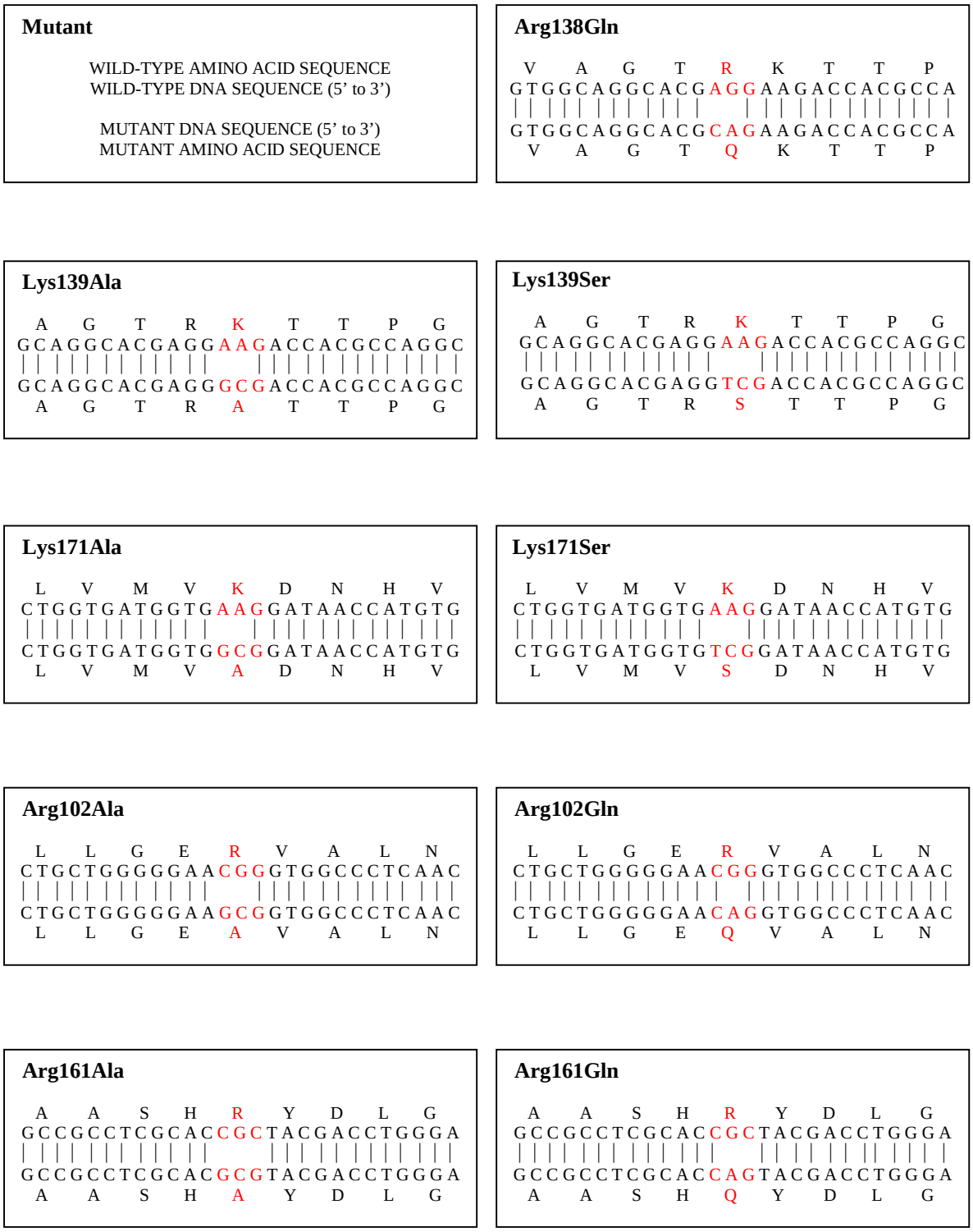

Figure 5.6: *Partial DNA and amino acid sequences for the QPRTase mutants. The mutations are highlighted in red.*

5.2.2.2 Expression and purification of the mutant proteins (HISTEV-QPRTase)*

To express the QPRTase mutants, the purified plasmids containing the human brain QPRTase gene with the designed mutations (pEHISTEV-QPRTase*) were transformed into *E. coli* strain BL21 (DE3). Small scale expression trials showed all the QPRTase mutants expressed well under the same conditions used for the expression of the wild-type enzyme. Each QPRTase mutant was then expressed on a large scale under these conditions. The transformed *E. coli* were grown in L-broth medium (1 L) containing kanamycin to a cell density of OD_{600} 0.4 at 37 °C. The temperature was then reduced to 20 °C and the cells were grown to OD_{600} 0.6 prior to induction with IPTG. The cultures were then incubated at 20 °C for 15 hours post-induction.

Since it had been shown for wild-type QPRTase that the presence of the histidine tag does not affect the protein folding, the oligomeric state of the protein or the enzymatic activity (Chapter 2), it was decided to leave the histidine tag attached to all the mutant QPRTase proteins. Therefore, the over-expressed mutant HISTEV-QPRTase proteins were purified by a single nickel affinity column followed by gel filtration. The purified proteins were dialysed then concentrated to 10 mg/mL. The purity of the HISTEV-QPRTase mutants was confirmed by SDS-PAGE (Figure 5.7).

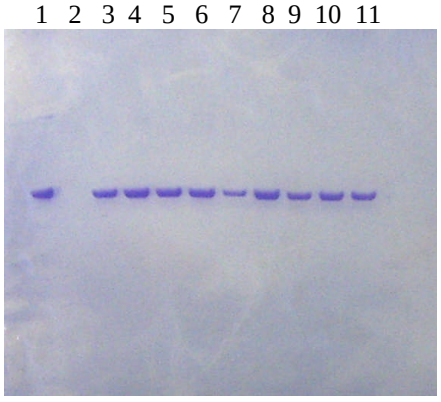

Figure 5.7: *Coomassie stained SDS-PAGE gel of the purified HISTEV-QPRTase proteins; Lane 1 wild-type QPRTase, lane 2 empty, lane 3 Lys139Ala QPRTase, lane 4 Lys139Ser QPRTase, lane 5 Lys171Ala QPRTase, lane 6 Lys171Ser QPRTase, lane 7 Arg138Gln QPRTase, lane 8 Arg102Ala QPRTase, lane 9 Arg102Gln QPRTase, lane 10 Arg161Ala QPRTase and lane 11 Arg161Gln QPRTase.*

5.2.3 Characterisation of the mutant proteins

5.2.3.1 Analysis of the mutant proteins by mass spectrometry

The molecular weight of an intact protein is a key physiocochemical characteristic because it reflects the amino acid composition and the modifications of a polypeptide. Analysis of the intact QPRTase mutants by electrospray mass spectrometry suggested the desired amino acid substitutions were present in the proteins (Table 5.2).

Protein	**Molecular weight (Da)**	
	Expected	**Found**
Arg102Ala QPRTase	33695.9	33696.6
Arg102Gln QPRTase	33752.9	33751.0
Arg161Ala QPRTase	33695.9	33678.8
Arg161Gln QPRTase	33752.9	33749.7
Arg138Gln QPRTase	33752.9	33750.0
Lys139Ala QPRTase	33723.9	33730.1
Lys139Ser QPRTase	33739.9	33743.7
Lys171Ala QPRTase	33723.9	33722.8
Lys171Ser QPRTase	33739.9	33746.0

Table 5.2: *Molecular weights of the HISTEV-QPRTase mutants.*

Furthermore, digestion of the modified proteins with trypsin, a proteolytic enzyme which cleaves selectively at the carboxyl side of lysine and arginine residues, followed by MALDI-MS or nanoLC ESI-MS/MS analysis of the resulting peptides confirmed the desired amino acid substitutions in the QPRTase mutants.

The tryptic peptides aa92-102 (1165.6 Da) and aa87-102 (1719.9 Da) were observed for the wild-type enzyme but not for Arg102Ala QPRTase and Arg102Gln QPRTase, confirming residue Arg102 has been replaced in these proteins. Furthermore, for Arg102Ala QPRTase, peptides corresponding to aa92-110 (1976.1 Da) and aa87-110 (2530.4 Da) were observed. The molecular weights of these peptides are consistent with the replacement of Arg102 with alanine and therefore confirm the desired amino acid substitution. Similarly, for Arg102Gln QPRTase, the desired amino acid substitution was confirmed by the observation of peptides aa92-110 (2033.1 Da) and aa87-110 (2582.4 Da).

The tryptic peptide aa139-145 (806.5 Da) was observed for the wild-type enzyme but not for Arg138Gln QPRTase, confirming residue Arg138 has been replaced in this protein. The replacement of this arginine residue by glutamine was confirmed the observation of the peptide aa127-139 (1269.6 Da).

The tryptic peptide aa127-139 (1297.7 Da) was observed for the wild-type enzyme but not for Lys139Ala QPRTase and Lys139Ser QPRTase, confirming residue Lys139 has been replaced in these proteins. Furthermore, for Lys139Ala QPRTase, a peptide corresponding to aa139-145 (749.4 Da) was observed. The molecular weight of this peptide is consistent with the replacement of Lys139 with alanine and therefore confirms the desired amino acid substitution. Similarly, for Lys139Ser QPRTase, the desired amino acid substitution was confirmed by the observation of the peptide aa139-145 (765.4 Da).

The tryptic peptides aa150-161 (1200.7 Da) and aa146-161 (1669.9 Da) were observed for the wild-type enzyme but not for Arg161Ala QPRTase and Arg161Gln QPRTase, confirming residue Arg161 has been replaced in these proteins. Furthermore, for Arg161Ala QPRTase, peptides corresponding to aa150-171 (2191.2 Da) and aa146-171 (2660.4 Da) were observed. The molecular weights of these peptides are consistent with the replacement of Arg161 with alanine and therefore confirm the desired amino acid substitution. Similarly, for Arg161Gln QPRTase, the desired amino acid substitution was confirmed by the observation of the peptide aa150-171 (2248.2 Da).

The tryptic peptide aa172-183 (1195.6 Da) was observed for the wild-type enzyme but not for Lys171Ala QPRTase and Lys171Ser QPRTase, confirming residue Lys171 has been replaced in these proteins. Furthermore, for Lys171Ala QPRTase, a peptide corresponding to aa162-183 (2214.1 Da) was observed. The molecular weight of this peptide is consistent with the replacement of Lys171 with alanine and therefore confirms the desired amino acid substitution. Similarly, for Lys171Ser QPRTase, the desired amino acid substitution was confirmed by the observation of the peptide aa162-183 (2230.1 Da).

5.2.3.2 Analysis of the mutant proteins by circular dichroism

As discussed in section 2.3.3, the near-UV CD spectrum of a protein represents a highly sensitive criterion for the native state of a protein and can thus be used as a fingerprint of the correctly folded conformation. Therefore this technique is useful for comparing wild-type and mutant proteins to see if the mutation causes any significant changes in protein conformation. The near-UV (260-320 nm) CD spectra of wild-type QPRTase and the QPRTase mutants were measured using a Jasco J-8.10 spectropolarimeter (Figure 5.8).

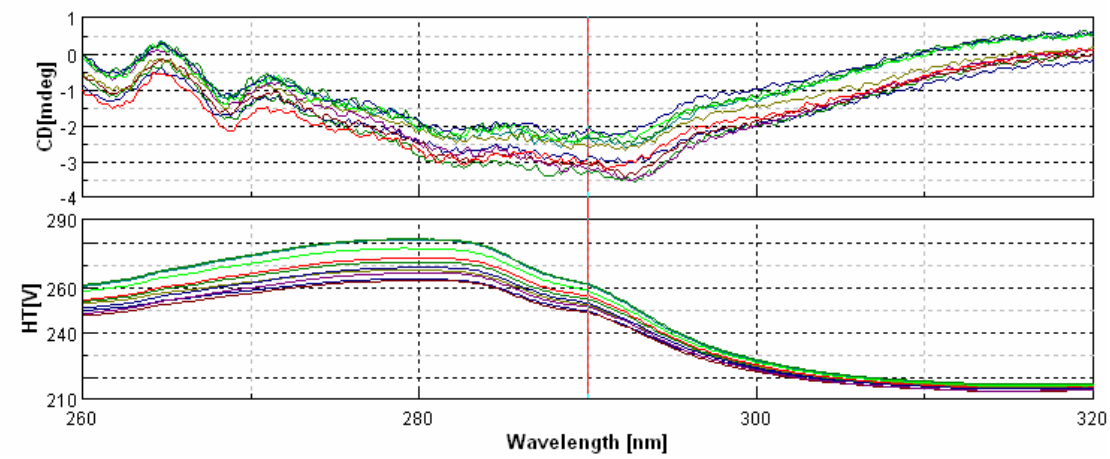

Figure 5.8: *Near-UV CD spectra of Wild-type QPRTase, Arg102Ala QPRTase, Arg102Gln QPRTase, Arg138Gln QPRTase, Arg161Ala QPRTase, Arg161Gln QPRTase, Lys139Ala QPRTase, Lys139Ser QPRTase, Lys171Ala QPRTase, and Lys171Ser QPRTase measured using a Jasco J-8.10 spectropolarimeter (Band width, 1nm; Response, 1 s; Data pitch, 0.2 nm; Scanning speed, 20 nm/min; Accumulation, 4; Cell length, 0.5 cm; Solvent, 50 mM potassium phosphate buffer; Concentration, ~1 mg/mL; Temperature, room temperature).*

By comparing the CD spectra of wild-type QPRTase and the nine QPRTase mutants, it can be concluded that all the proteins are folded correctly. If the proteins were not folded then the aromatic CD would be virtually zero. Instead, CD bands of comparable magnitude were observed at the same wavelengths in all the spectra. The slight differences between the spectra are due to small differences in the concentration of the protein samples.

5.2.3.3 Kinetic analysis of the mutant proteins

The activity of each QPRTase mutant was determined using a continuous spectrophotometric assay based on the difference in extinction coefficients between quinolinic acid and nicotinic acid mononucleotide at 266 nm ($\Delta\varepsilon_{266}$ = 920 $M^{-1}cm^{-1}$). This involved measuring the change in absorbance at this wavelength over a 30 minute period, at 37 ºC. The assay mixtures contained 0.3 mM quinolinic acid, 0.1 mM PRPP and 6 mM $MgCl_2$ in 50 mM K_2HPO_4/KH_2PO_4 buffer (pH 7.2). Each assay was initiated by the addition of the mutant QPRTase (14 μg). The rates were measured in triplicate for each QPRTase mutant and were compared to a standard assay for wild-type QPRTase. The results are shown in Table 5.3 and are displayed in graphical form in Figure 5.9.

QPRTase mutant	**Percentage activity (compared to wild-type enzyme)**
Arg161Ala	20%
Arg161Gln	Inactive
Lys171Ala	Inactive
Lys171Ser	Inactive
Arg102Ala	11%
Arg102Gln	11%
Arg138Gln	Inactive
Lys139Ala	Inactive
Lys139Ser	Inactive

Table 5.3: *Activity of the QPRTase mutants.*

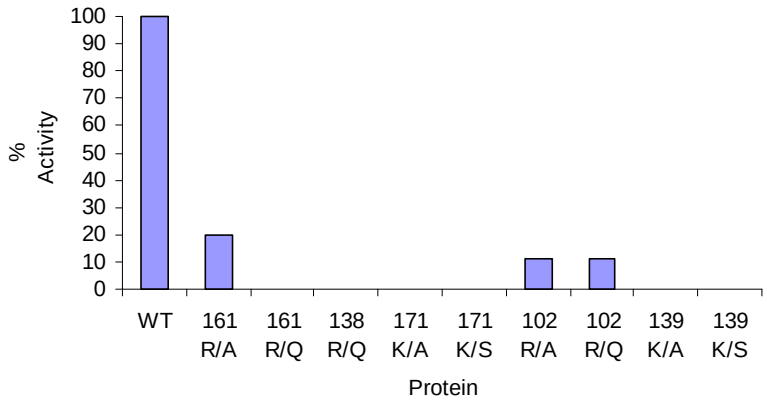

Figure 5.9: *Activity of the QPRTase mutants.*

It was found that when Arg161 was replaced with alanine, the protein retained 20% activity relative to the wild-type enzyme. However, when the same residue was changed to glutamine, all activity was lost. The two Arg102 mutants (Arg102Ala and Arg102Gln) were found to retain just over 10% of the activity of the wild-type enzyme. All the other QPRTase mutants were found to be inactive.

The activities of Arg102Ala QPRTase and Arg102Gln QPRTase were too low to accurately determine the kinetic parameters K_m and V_{max} for the substrates. However, for Arg161Ala QPRTase, the kinetic parameters K_m and V_{max} with respect to quinolinic acid were determined by measuring the rate of the enzymatic reaction at a range of different quinolinic acid concentrations at a fixed concentration of PRPP (0.1 mM). The initial rate data were fitted to the Michaelis-Menten equation using non-linear regression with GraphPad Prism 3 software (Figure 5.10). K_m and V_{max} for quinolinic acid were determined as 319 ± 60 μM and 0.71 ± 0.06 μM min^{-1}, respectively.

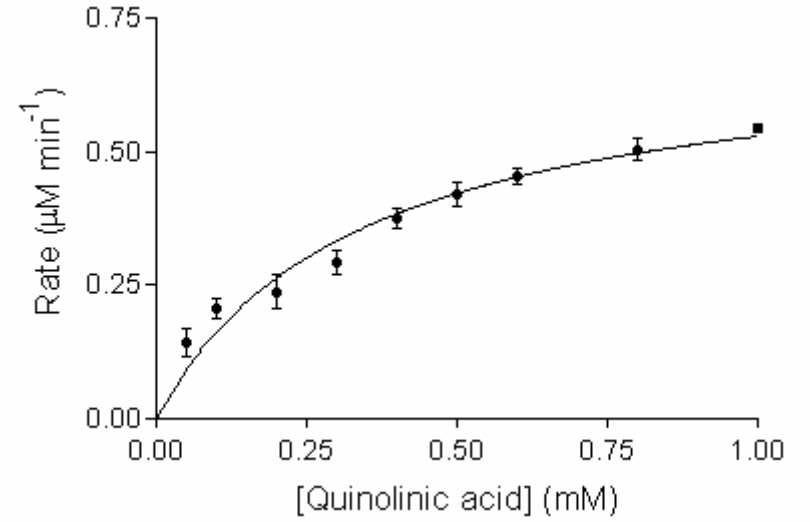

Figure 5.10: *Non-linear regression plot of Arg161Ala QPRTase for quinolinic acid as the variable substrate.*

5.2.4 Discussion

From the results of the kinetic studies on the QPRTase mutants, it would appear that all the residues that were targeted in the site-directed mutagenesis studies are important for binding and/or catalysis. The active site residues targeted in the mutagenesis studies are all highly conserved among QPRTase enzymes (section 2.3.1) and adopt similar conformations in the active sites of human brain QPRTase and QPRTase from bacterial sources. Sequence alignment has shown that the target residues in human brain QPRTase, Arg161, Arg138, Arg102', Lys171 and Lys139, correspond to residues Arg162, Arg139, Arg105', Lys172 and Lys140, respectively, in *Mycobacterium tuberculosis* QPRTase (section 2.3.1). From the schematic diagram of the interactions of *Mycobacterium tuberculosis* QPRTase with quinolinic acid **10** and PRPP **15**, it can be seen that all the residues targeted in the mutagenesis studies appear to form binding interactions with the substrates (Figure 5.11). By mutating these residues and changing the nature of the amino acid side chain, key interactions between the enzyme and substrates are lost, which explains the significant reduction or complete loss of activity observed for the QPRTase mutants. A more detailed discussion of the information gained from the individual mutations follows.

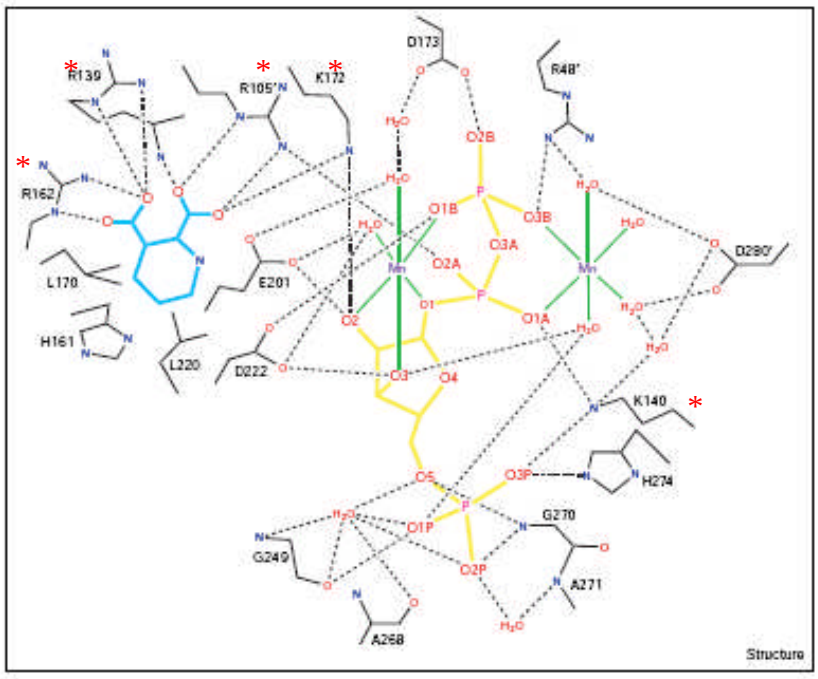

Figure 5.11: *Schematic diagram of the interactions of Mycobacterium tuberculosis QPRTase with quinolinic acid and PRPP (target residues are highlighted with *).*[8]

5.2.4.1 Mutation of Arg161

Mutation of residue Arg161 to alanine was found to result in significant reduction in the enzymatic activity. Careful kinetic analysis of the enzymatic reaction enabled determination of the kinetic parameters K_m and V_{max} for quinolinic acid (Table 5.4). Comparison with the kinetic parameters for the wild-type enzyme shows a significant increase in K_m for the mutant enzyme. This indicates loss of binding, suggesting Arg161 must form an important binding interaction with quinolinic acid. The observed decrease in V_{max} indicates loss of catalytic efficiency.

Protein	**K_m (μM)**	**V_{max} (μM min^{-1})**
Wild-type QPRTase	13.1 ± 1.9	0.93 ± 0.03
Arg161Ala QPRTase	319 ± 60	0.71 ± 0.06

Table 5.4: *Comparison of the kinetic parameters for wild-type QPRTase and Arg161Ala QPRTase.*

Structural studies on *Mycobacterium tuberculosis* QPRTase suggested this arginine residue binds to the C-3 carboxylate group of quinolinic acid (Figure 5.11). Arg161Ala QPRTase does retain some enzymatic activity and shows some affinity for quinolinic acid which indicates that this interaction is important but not essential for binding in the active site. This is consistent with results from the inhibition of human brain QPRTase by picolinic acid derivatives (Chapter 3). It was found that while the compounds inhibited QPRTase, affinity was lost when the carboxylate group was absent at the 3-position suggesting this carboxylate group is important, but not essential, for binding in the active site of QPRTase.

When Arg161 was mutated to glutamine, however, the resulting protein was found to be inactive. It is unlikely the differences between the two Arg161 mutants are due to a size effect, since the glutamine side chain is still smaller than the arginine side chain. It is possible that the glutamine residue introduced at this position makes new interactions with the neighbouring arginine residue (Arg 138) and this disturbs the normal interactions. Structural studies on this QPRTase mutant are required to probe this further.

5.2.4.2 Mutation of Arg138

It was found that mutation of residue Arg138 to glutamine results in complete loss of enzymatic activity suggesting the positively charged arginine side chain is involved in essential interactions between the enzyme and substrate. From structural studies on *Mycobacterium tuberculosis* QPRTase, it would appear that this arginine residue binds to both the C-2 and C-3 carboxylate groups of quinolinic acid (Figure 5.11).

5.2.4.3 Mutation of Lys139

The kinetic studies on the QPRTase mutants showed that when Lys139 was replaced with the uncharged residues alanine or serine, all enzymatic activity was lost suggesting this lysine residue is key to the catalytic activity of the enzyme. From structural studies on *Mycobacterium tuberculosis* QPRTase, it would appear that this lysine residue is involved in binding to the phosphate groups of PRPP (Figure 5.11).

It has been proposed that the QPRTase catalysed phosphoribosyl transfer reaction proceeds via a two step S_N1-type mechanism involving an oxocarbonium ion intermediate **17** (Scheme 5.1).[10] The active site residue Lys139 may participate in the stabilisation of the excess negative charge on the leaving pyrophosphate group. Subsequently, the nucleophilic N1 of quinolinic acid **10** combines with the oxocarbonium ion **17** to form quinolinic acid mononucleotide **16**. It is possible that a large positive electrostatic potential due to the side chain of Lys139 guides the movement of the oxocarbonium ion intermediate **17** towards quinolinic acid **10** by repulsion of the positively charged C1-O4 bond.

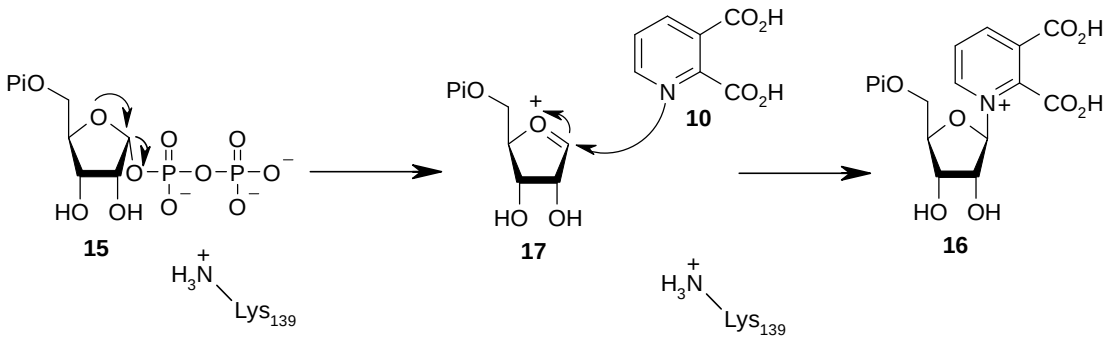

Scheme 5.1: *S_N1 mechanism for phosphoribosyl transfer step.*

5.2.4.4 Mutation of Arg102'

In the site-directed mutagenesis studies it was found that replacing residue Arg102' in human brain QPRTase with either alanine or glutamine resulted in significant reduction in enzymatic activity. By examining the structure of *Mycobacterium tuberculosis* QPRTase with just quinolinic acid bound in the active site, it can be seen that the side chain of this arginine residue (Arg105') is not very close to quinolinic acid **10** and does not appear to bind to the C-2 carboxylate (Figure 5.12a). However, in the structure of *Mycobacterium tuberculosis* QPRTase with bound phthalic acid **25** and PRPCP **33**, stable substrate analogues of quinolinic acid **10** and PRPP **15** respectively, it can be seen that the side chain of this arginine residue appears to swing round and bind to both the C-2 carboxylate of phthalic acid **25** and one of the phosphate groups of PRPCP **33** (Figure 5.12b). This residue could therefore be involved in holding the two substrates in the correct orientation for reaction. This would explain the significant reduction in enzymatic activity observed when this arginine residue was replaced with alanine or glutamine; neither residue is capable of forming what are clearly important electrostatic interactions between the enzyme and the substrates.

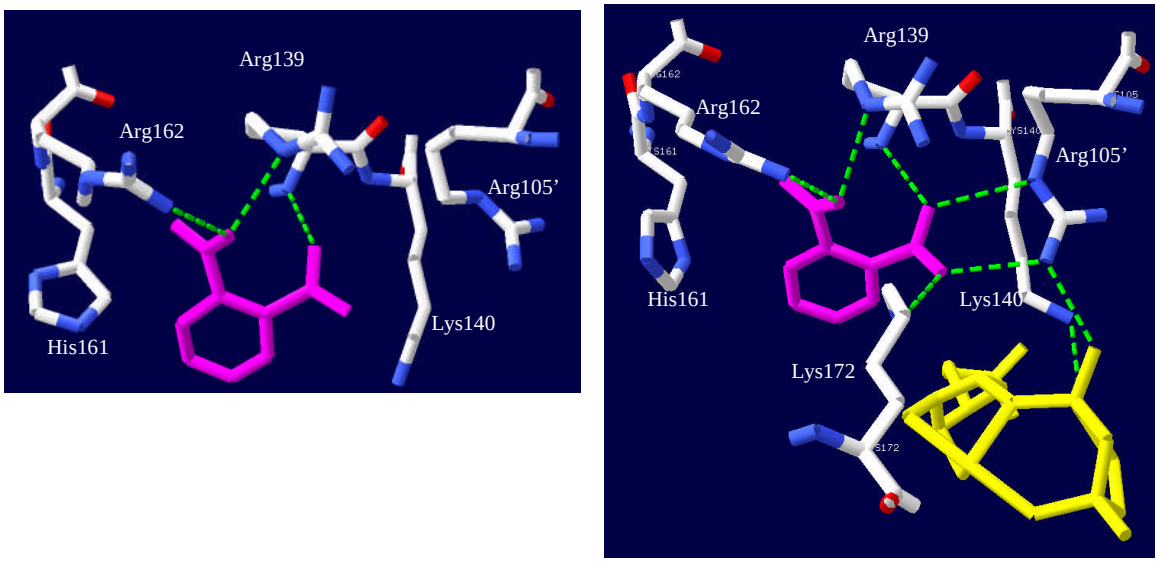

Figure 5.12: *Active site of Mycobacterium tuberculosis QPRTase with (a) quinolinic acid bound (pink) [Protein Data Bank 1QPQ] and (b) phthalic acid (pink) and PRPCP (yellow) bound [Protein Data Bank 1QPR].*

5.2.4.5 Mutation of Lys171

The site-directed mutagenesis studies showed that residue Lys171 is critical for the enzymatic activity of human brain QPRTase. Mutation of this residue to either alanine or serine resulted in complete loss of enzymatic activity. Structural studies on *Mycobacterium tuberculosis* QPRTase have also suggested this residue plays an important role in the QPRTase catalysed reaction.

In the structure of the *Mycobacterium tuberculosis* QPRTase apoenzyme, the side chain of this lysine residue (Lys172 in the *Mycobacterium tuberculosis* enzyme) interacts with the side chains of residues Asn174 and Glu104' (Figure of 5.13). Binding of quinolinic acid **10** is accompanied by reorientation of the side chain of the lysine residue towards the C-2 carboxylate of the substrate (Figure 5.13). This results in a 5 Å movement of the lysine side chain Nε atom and a 2 Å displacement of its Cα atom.[8]

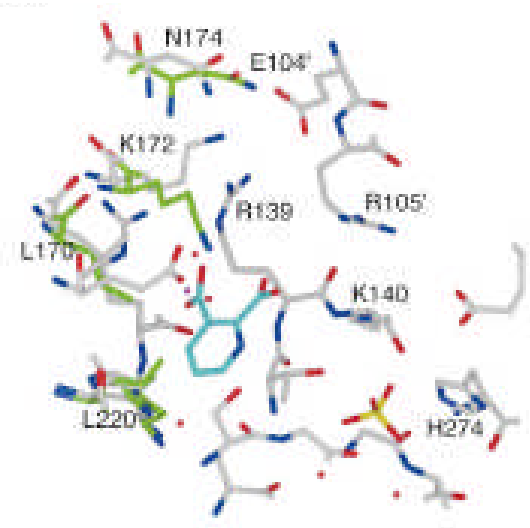

Figure 5.13: *Superimposition of the active sites in the Mycobacterium tuberculosis QPRTase apoenzyme and QPRTase-quinolinic acid complex structures.*[8] *Carbon atoms are depicted in grey (apoenzyme), green (quinolinic acid bound enzyme) or cyan (quinolinic acid); nitrogen atoms are shown in blue and oxygen atoms in red. For the QPRTase-quinolinc acid complex, only residues that undergo substrate induced conformational changes are shown.*

The site-directed mutagenesis studies on human brain QPRTase showed that replacing this lysine residue with either alanine or serine results in complete loss of enzymatic activity suggesting this is a key interaction between the enzyme and the substrate. This is consistent with the results from the inhibition studies on human brain QPRTase, which showed that the C-2 carboxylate group is essential for binding in the active site (Chapter 3). Nicotinic acid **27** lacks the C-2 carboxylate and is therefore not capable of forming this essential interaction with Lys171 in the QPRTase active site.

Furthermore, by examining the active site of the *Mycobacterium tuberculosis* QPRTase-NAMN complex, it can be seen that the overall conformation of the active site appears to be more similar to that of the apoenzyme and the conformational changes observed in the QPRTase-quinolinic acid complex are absent in the QPRTase-NAMN complex (Figure 5.14). Again, this is consistent with the role of the C-2 carboxylate group in inducing the conformational changes.

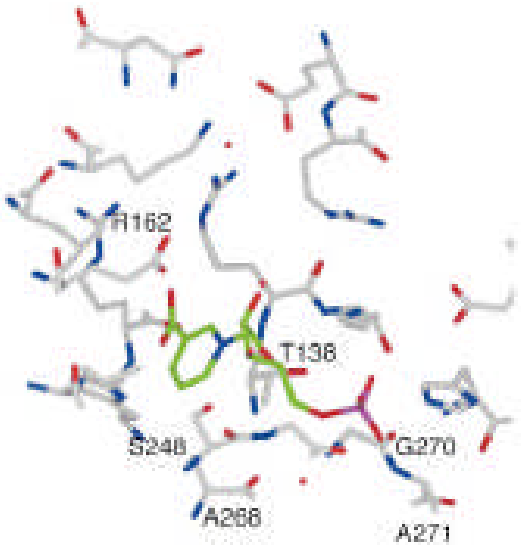

Figure 5.14: *Stereoview of the active site of Mycobacterium tuberculosis QPRTase with bound NAMN (green carbon atoms).*[8]

It would appear, therefore, that QPRTase has two conformers: a relaxed conformer, observed in the structures of the apoenzyme and its complex with the product NAMN, and an active conformer, seen in its complex with substrate quinolinic acid. The reorientation of the side chain of Lys171 has important implications for the mechanism of the QPRTase catalysed reaction.

5.2.4.6 Mechanistic information from the site-directed mutagenesis studies

QPRTase is an unusual phosphoribosyltransferase enzyme in that it appears to catalyse a second reaction, decarboxylation of the quinolinic acid mononucleotide **16** to form the corresponding nicotinic acid mononucleotide **11**. This decarboxylation reaction is considered to have an analogous mechanism to that observed for the decarboxylation of pyridine carboxylic acids in chemical studies. The mechanism proposed by Hammick *et al.* involves loss of carbon dioxide to form a nitrogen ylide, which is then protonated to give the product.[11] However, enzymatic involvement in the decarboxylation step has yet to be conclusively proven.

Based on the initial structural studies on human brain QPRTase, which identified the active site residues, and the site-directed mutagenesis studies, which showed how important these residues are for enzymatic activity, it is now possible to propose a mechanism involving QPRTase in the decarboxylation step (Scheme 5.2). Key to this mechanism is the active site residue Lys171, which the site-directed mutagenesis studies showed is essential for enzymatic activity.

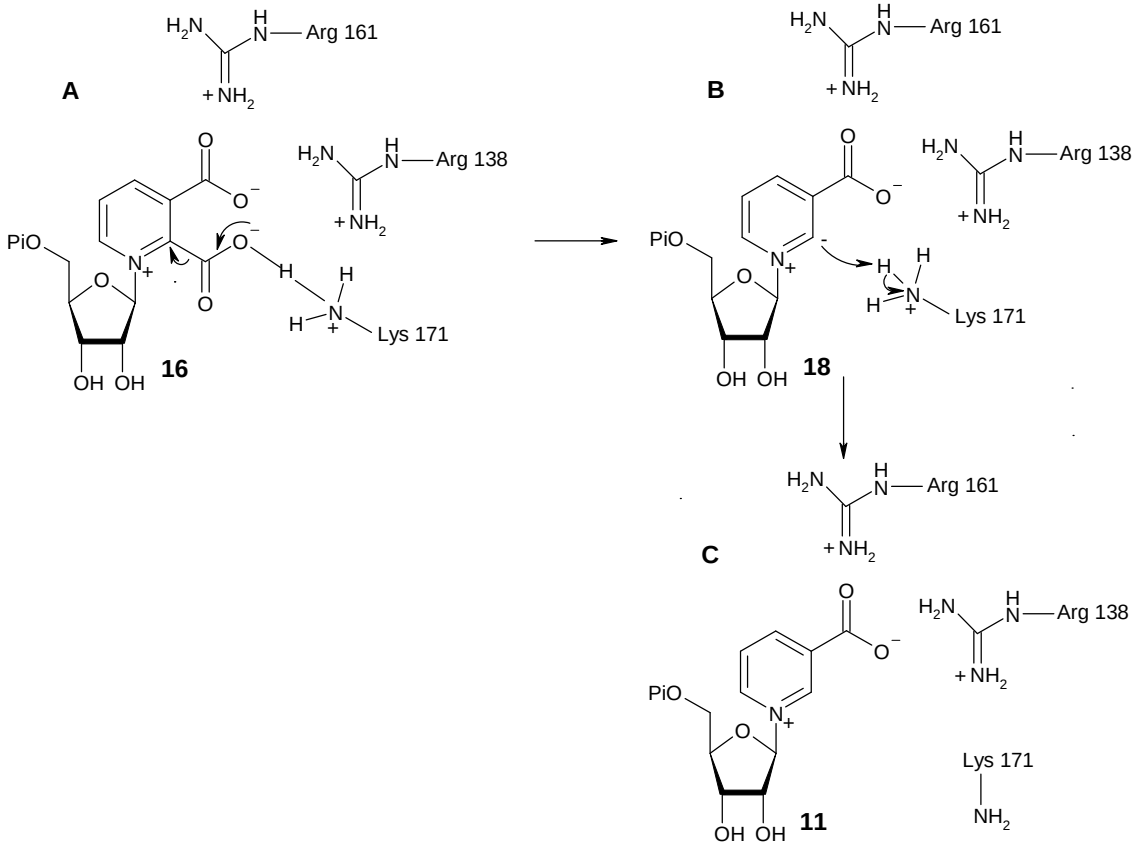

Scheme 5.2: *Proposed mechanism for QPRTase catalysed decarboxylation of QAMN.*

Firstly, interaction between Lys171 and the C-2 carboxylate may facilitate decarboxylation of QAMN **16** to form the nitrogen ylide intermediate **18** (Scheme 5.2A). Residue Lys171 is then perfectly positioned to reprotonate the ylide intermediate **18** to form the product, NAMN **11** (Scheme 5.2B). Finally, the lack of any interaction at the C-2 position would lead to reorientation of the side chain of Lys171 and a switch in conformation from active to relaxed thereby facilitating the release of the product, NAMN **11**, from the active site (Scheme 5.2C).

As discussed in section 1.5.3, orotidine 5'-monophosphate decarboxylase (OMP decarboxylase, EC 4.1.1.23) carries out a very similar decarboxylation reaction to QPRTase (Scheme 5.3). A mechanism involving a nitrogen ylide intermediate has also been proposed for OMP decarboxylase.[116] This ylide mechanism was supported by inhibition studies,[117] kinetic isotope effect studies[119,120] and structural studies.[121]

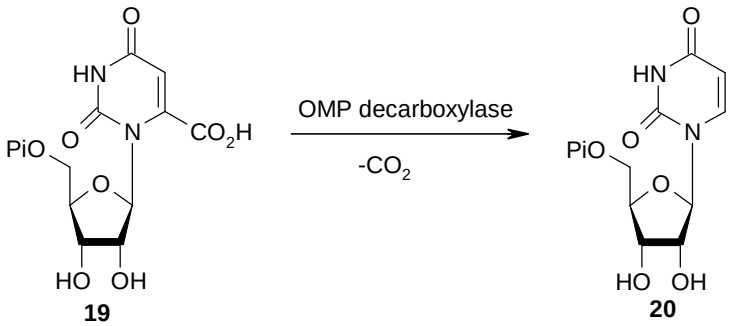

Scheme 5.3: *Decarboxylation of orotidine 5'-monophosphate.*

Furthermore, identification of the active site by structural studies enabled the elucidation of the residues involved in the decarboxylation mechanism for this enzyme.[121] The proposed mechanism is similar in many respects to the enzymatic mechanism proposed here for the decarboxylation of QAMN by QPRTase. In the mechanism reported for OMP decarboxylase, the key residue responsible for reprotonation of the ylide intermediate was also a lysine residue. The catalytic importance of this lysine residue was confirmed by site-directed mutagenesis studies carried out on yeast OMP decarboxylase.[122]

5.2.5 Summary

By employing the megaprimer method for PCR site-directed mutagenesis, nine QPRTase mutants were successfully generated. The desired mutations and the sequence integrity of the QPRTase gene were confirmed by automated DNA sequencing. No additional secondary mutations were observed in any of the sequences.

The mutant QPRTase proteins were successfully over-expressed from the pEHISTEV-QPRTase construct in *E. coli* strain BL21 (DE3). The proteins were purified by nickel affinity chromatography followed by gel filtration. Digestion of the proteins with trypsin followed by MALDI-MS analysis of the resulting peptides confirmed the presence of the desired amino acid substitution in each QPRTase mutant.

The kinetic studies showed the QPRTase mutants were either inactive or had very low activity. The loss of activity resulting from mutagenesis of the target residues does not appear to be a consequence of gross changes in enzyme structure, as indicated by comparison of the CD spectra of the mutant and wild-type enzymes. Therefore, it would appear that all the residues that were targeted in the mutagenesis studies are important for binding and/or catalysis.

Based on the initial structural studies on human brain QPRTase, which identified the active site residues, and the site-directed mutagenesis studies, which showed how important these residues are for enzymatic activity, a possible mechanism involving QPRTase in the decarboxylation of quinolinic acid mononucleotide was proposed. The proposed mechanism is similar in many respects to the mechanism reported for OMP decarboxylase.

5.2.6 Further work

Isothermal titration calorimetry (ITC) is a thermodynamic technique that allows the study of the interactions between two species. When two species interact, heat is either generated or absorbed and by measuring the heat of interaction it is possible to determine thermodynamic parameters of interactions such as binding affinity. This technique has therefore been applied to measuring protein-substrate interactions. The role of the QPRTase active site residues in substrate binding could be further investigated by performing ITC studies on both the wild-type and the mutant enzymes. For example, the complete loss of enzymatic activity observed for Arg138Gln QPRTase was explained by the loss of essential binding interactions between the enzyme and the C-2 and C-3 carboxylate groups of quinolinic acid. ITC studies may be used to confirm that quinolinic acid does not bind in the active site of this QPRTase mutant.

Having performed kinetic analysis of the mutant proteins, the next stage would be to undertake structural studies. Detailed structural studies on both wild-type human brain QPRTase and the mutant enzymes, with and without substrates and products, are required to elucidate the proposed decarboxylation mechanism more thoroughly.

5.3 References

1. H. Taguchi and K. Iwai, *Biochim. Biophys. Acta*, 1976, **422**, 29-37.
2. H. Taguchi and K. Iwai, *Agric. Biol. Chem.*, 1976, **40**, 385-389.
3. H. Taguchi and K. Iwai, *J. Nutr. Sci. Vitaminol.*, 1974, **20**, 283-291.
4. K. Shibata and K. Iwai, *Agric. Biol. Chem.*, 1980, **44**, 293-300.
5. R. Gaur, T. Roberts and K. Calvo, *Protein Pept. Lett.*, 2006, **13**, 163-167.
6. M.J. Zoller and M. Smith, *Nucleic Acids Res.*, 1982, **10**, 6487-6500.
7. M.J. Zoller and M. Smith, *Methods Enzymol.*, 1987, **154**, 329-350.
8. V. Sharma, C. Grubmeyer and J.C. Sacchettini, *Structure*, 1998, **6**, 1587-1599.
9. J. Brons-Poulsen, N.E. Petersen, M. Horder and K. Kristiansen, *Mol. Cell. Probes*, 1998, **12**, 345-348.
10. W. Tao, C. Grubmeyer and J.S. Blanchard, *Biochemistry*, 1996, **35**, 14-21.
11. M.R.F. Ashworth, R.P. Daffern and D.L. Hammick, *J. Chem. Soc.*, 1939, 809-812.
12. P. Beak and B. Siegel, *J. Am. Chem. Soc.*, 1976, **98**, 3601-3606.
13. H. L. Levine, R.S. Brody and F.H. Westheimer, *Biochemistry*, 1980, **19**, 4993-4999.
14. S.A. Acheson, J.B. Bell, M.E. Jones and R. Wolfenden, *Biochemistry*, 1990, **29**, 3198-3202.
15. J.A. Smiley, P. Paneth, M.H. O'Leary, J.B. Bell and M.E. Jones, *Biochemistry*, 1991, **30**, 6216-6223.
16. P. Harris, J.C. Navarro-Poulsen, K.F. Jensen and S. Larsen, *Biochemistry*, 2000, **39**, 4217-4224.
17. J.A. Smiley and M.E. Jones, *Biochemistry*, 1992, **31**, 12162-12168.

Chapter Six

Conclusions and Further Work

Conclusions and further work

Human brain QPRTase was successfully expressed in *E. coli* BL21 (DE3) from the pEHISTEV-QPRTase construct and the protein was efficiently purified by nickel affinity chromatography.

The structure of the fully active enzyme was solved using multiwavelength methods to a resolution of 1.9 Å. In the crystal structure, human brain QPRTase was found to adopt an energetically stable hexameric arrangement in which each subunit makes extensive contacts with four other monomers. The enzyme was also found to exist as a hexamer during gel filtration under physiological conditions.

Kinetic studies allowed the measurement of the kinetic parameters for quinolinic acid. The data gave a K_m of 13.4 ± 1.0 μM and a V_{max} of 0.92 ± 0.01 μM min^{-1}. There was no evidence for cooperative binding of quinolinic acid to the six subunits of the QPRTase hexamer. Previous kinetic studies on human brain QPRTase showed pronounced substrate inhibition by PRPP at high concentrations. The mixed inhibition observed suggested that PRPP not only binds to an active site (competitive) but also to a second site which perturbs and inhibits the active site (noncompetitive). The hexameric structure observed for human brain QPRTase offers a possible explanation for the complex kinetics this enzyme exhibits.

The structural studies enabled identification of the active site residues. The active site is a deep pocket with a highly positive electrostatic surface composed of three arginine residues (Arg161, Arg138 and Arg102'), two lysine residues (Lys139 and Lys171) and one histidine residue (His160). These residues are highly conserved among QPRTase enzymes.

A series of QPRTase mutants were successfully generated and characterised (Arg102Gln, Arg102Ala, Arg138Gln, Arg161Ala, Arg161Gln, Lys139Ala, Lys139Ser, Lys171Ala and Lys171Ser). The kinetic studies showed the QPRTase mutants were either inactive or had very low activity. The loss of activity resulting from mutagenesis of the target residues does not appear to be a consequence of gross

changes in enzyme structure, as indicated by comparison of the CD spectra of the mutant and wild-type enzymes. Therefore, it would appear that all the residues that were targeted in the mutagenesis studies are important for binding and/or catalysis.

Based on the initial structural studies on human brain QPRTase, which identified the active site residues, and the site-directed mutagenesis studies, which showed how important these residues are for enzymatic activity, a possible mechanism involving QPRTase in the decarboxylation of quinolinic acid mononucleotide was proposed. Key to this mechanism is the active site residue Lys171, which the site-directed mutagenesis studies showed is essential for enzymatic activity. The proposed decarboxylation mechanism is similar in many respects to the mechanism reported for OMP decarboxylase.

Detailed structural studies on both wild-type human brain QPRTase and the mutant enzymes, with and without substrates and products, are required to elucidate the proposed decarboxylation mechanism more thoroughly. The availability of the crystal structures of QPRTase with and without its substrates and products would provide a detailed perspective for the active site interactions in pre-catalytic, catalytic and post-catalytic stages of the enzyme. Hence useful information could be obtained concerning the mechanism of the QPRTase reaction.

The study of the inhibition of human brain QPRTase by quinolinic acid analogues provided further insight into the interactions in the active site and highlighted some structural features that are required for potent competitive inhibition and can thus be incorporated into future inhibitor design. The free carboxylic acid groups are required for binding. The 3-carboxylic acid group is somewhat important for substrate interaction with the enzyme because when this group was absent, the compounds became less effective as inhibitors. The carboxylic acid group at the 2-position appears to be essential for binding. The studies showed that aromaticity is important for tight binding. However, the aromatic ring does not have to be a pyridine ring as is present in the substrate quinolinic acid. Of the compounds tested, phthalic acid **25** proved to be the most effective competitive inhibitor and therefore it would appear that the ring nitrogen is not essential for binding.

The inhibition studies have thus far shown that there appears to be a certain degree of steric hindrance at the 4- and 5-positions of the pyridine ring. Furthermore, it was found that introducing small hydrophobic *N*-substituents leads to weaker binding in the active site. Increasing the similarity of the *N*-substituent to that in the putative reaction intermediate, quinolinic acid mononucleotide, might lead to tighter binding in the active site and thus increased inhibition. In addition, compounds of this type might be useful substrates for further enzymatic decarboxylation studies. Quinolinic acid mononucleotide itself remains a key synthetic target since access to this compound would enable the unambiguous determination of the enzymatic involvement in the decarboxylation reaction.

Chapter Seven

Experimental

7.1 Molecular Biology

7.1.1 Materials and instrumentation

The expression plasmid pEHISTEV and 6 x His-TEV protease were provided by Dr Huanting Liu (The Centre for Biomolecular Science, University of St Andrews). *E. coli* strains DH5α and BL21 (DE3) were supplied by Stratagene. All the primers used in the site-directed mutagenesis studies were synthesised by Eurogentic. All restriction endonucleases, deoxyribonucleotides, T4 DNA ligase and Vent DNA polymerase were purchased from Promega, Amersham or New England BioLabs. Bradford's stain was purchased from Sigma.

Sonication was carried out using a Sanyo Soniprep 150.

Centrifugation was carried out using a Beckman L-60, Beckman J2-21, Beckman J6-HC or a MSE Microcentaur.

7.1.2 General methods

7.1.2.1 DNA sequencing

To prepare the samples for DNA sequencing, 5 μL of the pure mutant plasmid DNA was mixed with 3.2 μM T7 promoter primer or 3.2 μM T7 terminator primer in 7 μL of sterile water. The sequences were determined by automated sequencing (The Sequencing Service, School of Life Sciences, University of Dundee).

7.1.2.2 Preparation of competent cells

To prepare competent cells, an *E. coli* (DH5α or BL21 (DE3)) overnight culture (1 mL) was inoculated into L-broth medium (100 mL). The culture was incubated at 37 °C with a shaking speed of 120 rpm for 2 hours to a log growth stage. The culture was then chilled on ice for 30 minutes before centrifugation at 2800 rpm for 5 minutes at 4 °C. The pellet was gently resuspended in 12.5 mL of 100 mM $CaCl_2$ and

12.5 mL of 40 mM $MgSO_4$ which had been cooled on ice. The competent cells were stored on ice for at least 2 hours prior to use.

7.1.2.3 Sodium dodecyl sulfate–polyacrylamide gel electrophoresis

Sodium dodecyl sulfate–polyacrylamide gel electrophoresis (SDS-PAGE) was carried out using a 12% resolving gel and a 5% stacking gel. Samples (10 μL) were mixed with 2 x SDS-PAGE loading buffer (10 μL) and boiled for 3 minutes at 100 °C prior to loading on to the gel. Electrophoresis was carried out at room temperature with a constant voltage of 180 V. Gels were stained with 0.25% Coomassie blue, destained and photographed.

7.1.2.4 Bradford's assay to measure protein concentration[1]

A series of standards of known protein concentration were prepared by adding Bradford's stain (1 mL) to 2 μL, 5 μL, 10μL and 20 μL of BSA (1 μg/μL). Similarly, solutions of pure QPRTase were prepared by adding Bradford's stain (1 mL) to 2 μL and 5 μL of the concentrated protein. After mixing well, the samples were left to stand for 30 minutes to allow the blue colour to develop. The absorbance of each sample at 595 nm was then measured against the Bradford's stain as a blank. A calibration curve was then compiled by plotting A_{595} as a function of the amount of protein in the assay mixture for the BSA standards. Using the A_{595} of the QPRTase solutions, the amount of protein in the assay mixture, and hence the concentration of the pure QPRTase, were determined.

7.1.3 Expression and purification of wild-type human brain QPRTase

7.1.3.1 Expression of HISTEV-QPRTase in E. coli

A glycerol stock (stored at -80 °C) of *E. coli* strain BL21 (DE3) competent cells containing the recombinant plasmid pEHISTEV-QPRTase was spread on to an L-agar plate containing kanamycin. The plate was incubated at 37 °C overnight. A single colony of *E. coli* containing pEHISTEV-QPRTase was picked and transferred into L-broth medium (10 mL) containing kanamycin (50 μg/mL medium). The culture was grown at 37 °C with a shaking speed of 200 rpm overnight.

To express HISTEV-QPRTase, the *E. coli* overnight culture (10 mL) was inoculated into L-broth medium (1 litre) containing kanamycin (50 μg/mL medium). The cells were grown at 37 °C with a shaking speed of 200 rpm to an optical density of 0.4. The cell culture was cooled moderately to 20 °C and was grown with a shaking speed of 200 rpm to an optical density of 0.6. Expression was then induced by the addition of 0.4 mM isopropyl-β-D-thiogalactoside (IPTG). The culture was incubated at 20 °C with a shaking speed of 200 rpm overnight.

The cells were harvested by centrifugation at 4000 rpm for 15 minutes at 4 °C. The supernatant was discarded and the pellet was resuspended and washed in PBS (20 ml) and centrifuged at 5000 rpm for 10 minutes at 4 °C. The supernatant was discarded and the pellet was stored at -70 °C, for later purification. The expression of HISTEV-QPRTase was analysed by SDS-PAGE.

7.1.3.2 Purification of HISTEV-QPRTase

The harvested cells from a 1 litre culture were resuspended in 10 mL of sample buffer (1 x PBS, 0.3 M NaCl, 10 mM imidazole) which contained protease inhibitor (PIT) (1 tablet/10 mL sample buffer) and 1 mM dithiothreitol (DTT). The cells were sonicated on ice three times each for 30 seconds with 1 minute intervals. The suspended cells were centrifuged at 5000 rpm for 10 minutes at 4 °C. The supernatant was collected and the pellet was resuspended in standard sample buffer

(no PIT or DTT). The cells were sonicated as before and then centrifuged at 5000 rpm for 10 minutes at 4 °C. The combined supernatants were then centrifuged at 18000 rpm for 1 hour at 4 °C. The supernatant was then collected and passed through a 0.2 μm syringe filter and loaded on to a nickel column with a flow rate of 2 mL/min. After washing the column with wash buffer (1 x PBS, 0.3 M NaCl, 20 mM imidazole, 1 mM PMSF, 100 mL), HISTEV-QPRTase was eluted from the column using elution buffer (1 x PBS, 0.3 M NaCl, 100 mM imidazole, 1 mM PMSF, 100 mL). Protein elution was monitored using Bradford's stain. The HISTEV-QPRTase containing fractions were analysed by SDS-PAGE and pooled.

7.1.3.3 TEV protease digestion

The pooled HISTEV-QPRTase containing fractions were dialysed in dialysis buffer (1 x sterile water, 0.3 M NaCl, 50 mM Tris pH 7.5, 1 mM DTT) overnight at 4 °C. The buffer was then changed to fresh dialysis buffer and dialysis was carried out for a further 2 hours. After dialysis, 1 mM DTT (1 μL/mL sample) was added to the HISTEV-QPRTase, followed by the addition of TEV protease (1 μg/mg protein). The digestion was carried out overnight at room temperature. The product was analysed by SDS-PAGE.

7.1.3.4 Removal of the His-tag and TEV protease

Dialysis was then carried out in a final dialysis buffer (1 x sterile water, 50 mM Tris pH 7.5, 200 mM NaCl) for 1 hour at room temperature. The buffer was then changed to an imidazole containing buffer (1 x sterile water, 50 mM Tris pH 7.5, 200 mM NaCl, 20 mM imidazole) and dialysis was carried out for a further 1 hour at room temperature.

The sample was then loaded on to the nickel column and QPRTase was eluted with wash buffer (1 x sterile water, 0.3 M NaCl, 20 mM imidazole, 1 mM PMSF, 100 mL). The fractions containing QPRTase were pooled and concentrated. The purified QPRTase was analysed by SDS-PAGE, and the concentration of the protein was determined by a Bradford's assay. The concentrated QPRTase was stored at -20 °C.

7.1.4 Site-directed mutagenesis studies

7.1.4.1 Generation of the mutant QPRTase DNA

Site-directed mutagenesis was performed on a pEHISTEV-QPRTase clone based on the megaprimer PCR method[2] by Dr Huanting Liu (The Centre for Biomolecular Science, University of St Andrews). The primers used for the generation of the QPRTase mutants are shown in Table 7.1.

Primer		Sequence	Notes
Flanking primer A[a]		5'CTAGTCATGAACGCTGAAGGCCTG3'	Forward
Internal mutagenic primers B[b]	Arg102Ala	5'CGTGTTGAGGGCCAC**CGC**TTCCCCCAGCAG3'	Reverse
	Arg102Gln	5'CGTGTTGAGGGCCAC**CTG**TTCCCCCAGCAG3'	Reverse
	Arg138Gln	5'GCCTGGCGTGGTCTT**CTG**CGTGCCTGCCAC3'	Reverse
	Lys139Ala	5'GAAGCCTGGCGTGGT**CGC**CCTCGTGCCTGC3'	Reverse
	Lys139Ser	5'GAAGCCTGGCGTGGT**CGA**CCTCGTGCCTGC3'	Reverse
	Arg161Ala	5'TCCCAGGTCGTA**CGC**GTGCGAGGCGGC3'	Reverse
	Arg161Gln	5'TCCCAGGTCGTA**CTG**GTGCGAGGCGGC3'	Reverse
	Lys171Ala	5'CACCACATGGTTATC**CGC**CACCATCACCAG3'	Reverse
	Lys171Ser	5'CACCACATGGTTATC**CGA**CACCATCACCAG3'	Reverse
Flanking primer C[c]		5'ATGCGGATCCCTAGTGGATTTTGGGC 3'	Reverse

Table 7.1: *Primers used for the generation of the QPRTase mutants. (a. BspHI site is underlined, b. The mutated genetic codes are highlighted in bold, c. BamHI site is underlined).*

In the first round of PCR, the outside flanking primer (primer A) and the internal mutagenic primer (primer B), containing the desired base substitution(s), were used to generate a double stranded megaprimer containing the mutations introduced by the mutagenic primer. The megaprimer was isolated by extraction from an agarose gel. In the second round of PCR, the purified megaprimer was used together with the second flanking primer (primer C) to generate the complete mutant QPRTase DNA sequence.

7.1.4.2 Restriction endonuclease digestion of the mutant QPRTase DNA and the plasmid pEHISTEV

The megaprimer PCR generated mutant QPRTase DNA (1 μg) was digested with the restriction enzymes BspHI (1 unit) and BamHI (1 unit) in 1x NEBuffer 4 (total volume 30 μL) as described by the manufacturer (New England Biolabs). The digestion mixture was incubated at 37 °C for two hours.

The plasmid pEHISTEV was digested with the restriction endonucleases NcoI and BamHI as described above.

*7.1.4.3 Construction of the expression vector pEHISTEV-QPRTase**

The BspHI / BamHI digested mutant QPRTase gene fragment (30 ng) was ligated into NcoI / BamHI digested pEHISTEV (10 ng) using T4 DNA ligase (1 μL) in 1x ligation buffer (total volume 20 μL). Ligation was carried out at 14 °C overnight.

7.1.4.4 Transformation in E. coli

DH5α competent cells (100 μL) were mixed with the ligation mixture and chilled on ice for 30 minutes. The competent cells were then heat shocked for 4 minutes at 42 °C, then immediately returned to ice for 15 minutes. L-Broth medium (1 mL) was added to the heat shocked competent cells which were then incubated at 37 °C for 1 hour. The competent cells were centrifuged at 10000 rpm for 3 minutes. The pellet was resuspended in L-broth medium (100 μL) and spread on to an L-agar plate containing kanamycin (50 μg/mL). The plates were incubated at 37 °C overnight.

The number of colonies on each agar plate was counted and a single colony was picked and transferred into L-broth medium (10 mL) containing kanamycin (50 μg/mL medium). The culture was grown at 37 °C with a shaking speed of 200 rpm overnight. The cells were then harvested by centrifugation at 4000 rpm for 10 minutes.

7.1.4.5 Isolation of the pure mutant plasmid DNA (pEHISTEV-QPRTase)*

The pure mutant plasmid DNA was isolated using a QIAprep Miniprep Kit. The pelleted bacterial cells were resuspended in buffer P1 (250 μL) containing LyseBlue reagent. The bacterial cells were lysed under alkaline conditions by adding buffer P2 and mixing gently until a homogeneously blue coloured suspension was obtained. The lysate was then neutralised and adjusted to high-salt binding conditions by adding buffer N3 (350 μL). The suspension was mixed gently until all traces of blue were removed and a homogeneously colourless suspension was obtained, indicating that SDS from the lysis buffer had been effectively precipitated. The suspension was centrifuged at 13000 rpm for 10 minutes. The supernatant was applied to a QIAprep spin column and centrifuged at 13000 rpm for 1 minute. The flow-through was discarded. The column was then washed sequentially with buffer PB (0.5 mL) to remove any endonucleases followed by buffer PE (0.75 mL) to remove salts. After centrifugation at 13000 rpm for 1 minute, the flow-through was discarded and the column was centrifuged for a further 1 minute to remove any residual wash buffer. The QIAprep column was then placed in a clean eppendorf. To elute the DNA, buffer EB (50 μL) was added to the centre of the QIAprep column. After 1 minute, the pure plasmid DNA was eluted by centrifugation at 13000 rpm for one minute. All the mutations and sequence integrity of the QPRTase gene were confirmed by automated DNA sequencing.

7.1.4.6 Expression and purification of the mutant QPRTases

The purified plasmids containing the human brain QPRTase gene with the designed mutations (pEHISTEV-QPRTase*) were transformed into *E. coli* strain BL21 (DE3) competent cells. Preparations and transformations were carried out as described previously. A single colony of *E. coli* containing pEHISTEV-QPRTase* was grown in L-broth (10 mL) containing kanamycin (50 μg/mL medium) at 37 °C with a shaking speed of 200 rpm overnight.

Expression and purification of the mutant QPRTase proteins were then carried out as described previously for wild-type QPRTase (sections 7.1.3.1 and 7.1.3.2).

7.2 Kinetic studies on human brain QPRTase

7.2.1 Standard activity assay[3]

The activity of QPRTase was determined using a continuous spectrophotometric assay based on the difference in extinction coefficients between quinolinic acid and nicotinic acid mononucleotide at 266 nm ($\Delta\varepsilon_{266}$ = 920 $M^{-1}cm^{-1}$). Typical assay mixtures contained 0.3 mM quinolinic acid, 0.1 mM PRPP and 6 mM $MgCl_2$ in 50 mM K_2HPO_4/KH_2PO_4 buffer (pH 7.2). Each assay was initiated by the addition of QPRTase (14 μg). The absorbance at 266 nm was then measured over a 30 minute period at 37 °C.

7.2.2 Determination of the kinetic parameters for wild-type QPRTase

The kinetic parameters K_m and V_{max} for quinolinic acid were determined by measuring the rate of the enzymatic reaction at a range of different quinolinic acid concentrations (10 – 300 μM) at a fixed and saturating concentration of PRPP (0.1 mM). The reaction was linear over the time course studied and the rates were measured in triplicate.

[Quinolinic acid] (μM)	ΔA_{266}	Δ[NAMN] (μM)	Rate of formation of NAMN (μM min^{-1})	Average rate of formation of NAMN (μM min^{-1})
10	0.0090 0.0097 0.0105	9.78 10.54 11.41	0.36 0.39 0.42	0.39
25	0.0137 0.0142 0.0156	14.89 15.43 16.95	0.55 0.57 0.63	0.58
50	0.0179 0.0185 0.0193	19.46 20.11 20.98	0.72 0.74 0.78	0.75
100	0.0197 0.0204 0.0209	21.41 22.17 22.72	0.79 0.82 0.84	0.82
200	0.0205 0.0209 0.0219	22.23 22.72 23.80	0.82 0.84 0.88	0.85
300	0.0211 0.0216 0.0223	22.93 23.48 24.24	0.85 0.87 0.90	0.87

Kinetic parameters were then evaluated by fitting the initial rate data to the Michaelis-Menten equation using non-linear regression with GraphPad Prism 3 software. K_m and V_{max} for quinolinic acid were determined as 13.4 ± 1.0 μM and 0.92 ± 0.01 μM min^{-1}, respectively.

7.2.3 Determination of the kinetic parameters for wild-type HISTEV-QPRTase

The kinetic parameters K_m and V_{max} for quinolinic acid were determined by measuring the rate of the enzymatic reaction at a range of different quinolinic acid concentrations (10 – 300 μM) at a fixed and saturating concentration of PRPP (0.1 mM). The reaction was linear over the time course studied and the rates were measured in triplicate.

[Quinolinic acid] (μM)	ΔA_{266}	Δ[NAMN] (μM)	Rate of formation of NAMN (μM min^{-1})	Average rate of formation of NAMN (μM min^{-1})
10	0.0097 0.0102 0.0112	10.52 11.09 12.17	0.39 0.41 0.45	0.42
25	0.0126 0.0132 0.0141	13.71 14.35 15.32	0.51 0.53 0.57	0.54
50	0.0194 0.0199 0.0202	21.09 21.63 21.96	0.78 0.80 0.81	0.80
100	0.0205 0.0206 0.0211	22.28 22.39 22.93	0.83 0.83 0.85	0.84
200	0.0213 0.0218 0.0219	23.15 23.70 23.83	0.86 0.88 0.88	0.87
300	0.0208 0.0209 0.0214	22.60 22.72 23.26	0.84 0.84 0.86	0.85

Kinetic parameters were then evaluated by fitting the initial rate data to the Michaelis-Menten equation using non-linear regression with GraphPad Prism 3 software. K_m and V_{max} for quinolinic acid were determined as 13.1 ± 1.9 μM and 0.93 ± 0.03 μM min^{-1}, respectively.

7.2.4 pH rate profile for QPRTase

The pH rate profile for human brain QPRTase was determined by utilising the standard UV activity assay to measure the rate of the enzymatic reaction in a series of 50 mM K_2HPO_4/KH_2PO_4 buffers of varying pH (pH 4.5 – 9) at fixed concentrations of quinolinic acid (0.3 mM) and PRPP (0.1 mM). Each reaction was initiated by the addition of QPRTase (14 μg). The reaction was linear over the time course studied and the rates were measured in triplicate. The table represents the overall data for the profile, which can be seen in graphical form in section 2.4.4.

pH	ΔA_{266}	Δ[NAMN] (μM)	Rate of formation of NAMN (μM min^{-1})	Average rate of formation of NAMN (μM min^{-1})
4.50	0.0328 0.0345 0.0360	35.67 37.48 39.09	1.32 1.39 1.45	1.39
5.03	0.0392 0.0393 0.0395	42.61 42.70 42.93	1.58 1.58 1.59	1.58
5.50	0.0468 0.0472 0.0475	50.81 51.33 51.64	1.88 1.90 1.91	1.90
6.00	0.0473 0.0479 0.0487	51.41 52.08 52.97	1.90 1.93 1.96	1.93
6.51	0.0358 0.0385 0.0393	38.92 41.80 42.70	1.44 1.55 1.58	1.52
7.02	0.0236 0.0272 0.0283	25.69 29.51 30.73	0.95 1.09 1.14	1.06
7.51	0.0178 0.0199 0.0252	19.36 21.64 27.35	0.72 0.80 1.01	0.84
8.00	0.0122 0.0132 0.0148	13.17 14.36 16.11	0.49 0.53 0.60	0.54
8.50	0.0115 0.0135 0.0137	12.49 14.60 14.85	0.46 0.54 0.55	0.52
8.98	0.0107 0.0123 0.0135	11.67 13.29 14.64	0.43 0.49 0.54	0.49

7.2.5 Solvent isotope effect studies on QPRTase

The solvent isotope effects were determined by measuring the rate of the enzymatic reaction in equivalent 50 mM potassium phosphate buffers in H_2O and D_2O at a fixed concentration of quinolinic acid (0.3 mM) and PRPP (0.1 mM). Each reaction was initiated by the addition of QPRTase (14 μg). The reaction was linear over the time course studied and the rates were measured in triplicate. The solvent isotope effects were determined at pL 7.2, pL 6.3 and pL 5.3 (L = H or D).

pL	ΔA_{266}	Δ[NAMN] (μM)	Rate of formation of NAMN (μM min^{-1})	Average rate of formation of NAMN (μM min^{-1})	Solvent isotope effect (k_H/k_D)
pH 7.2	0.0213 0.0216 0.0223	23.15 23.48 24.24	0.86 0.87 0.90	0.88	1.16
pD 7.2	0.0186 0.0190 0.0194	20.22 20.65 21.09	0.75 0.76 0.78	0.76	
pH 6.3	0.0425 0.0437 0.0447	46.20 47.50 48.59	1.71 1.76 1.80	1.75	0.85
pD 6.3	0.0482 0.0514 0.0529	52.39 55.87 57.50	1.94 2.07 2.13	2.05	
pH 5.3	0.0427 0.0430 0.0437	46.41 46.74 47.50	1.72 1.73 1.76	1.74	0.90
pD 5.3	0.0472 0.0485 0.0488	51.33 52.72 53.04	1.90 1.95 1.96	1.94	

7.2.6 Determination of the kinetic parameters for Arg161Ala HISTEV-QPRTase

The kinetic parameters K_m and V_{max} for quinolinic acid were determined by measuring the rate of the enzymatic reaction at a range of different quinolinic acid concentrations (50 – 1000 μM) at a fixed concentration of PRPP (0.1 mM). The reaction was linear over the time course studied and the rates were measured in triplicate.

[Quinolinic acid] (μM)	ΔA_{266}	Δ[NAMN] (μM)	Rate of formation of NAMN (μM min^{-1})	Average rate of formation of NAMN (μM min^{-1})
50	0.0023 0.0041 0.0045	2.50 4.34 4.81	0.09 0.16 0.18	0.14
100	0.0044 0.0051 0.0060	4.73 5.49 6.48	0.18 0.20 0.24	0.21
200	0.0050 0.0051 0.0074	5.47 5.55 7.99	0.20 0.21 0.30	0.24
300	0.0062 0.0075 0.0082	6.74 8.07 8.93	0.25 0.30 0.33	0.29
400	0.0084 0.0096 0.0099	9.12 10.43 10.78	0.34 0.39 0.40	0.39
500	0.0095 0.0104 0.0114	10.30 11.33 12.39	0.38 0.42 0.46	0.42
600	0.0107 0.0112 0.0119	11.63 12.17 12.91	0.43 0.45 0.48	0.45
800	0.0116 0.0125 0.0134	12.61 13.54 14.55	0.47 0.50 0.54	0.50
1000	0.0132 0.0135 0.0139	14.37 14.58 15.16	0.53 0.54 0.56	0.54

Kinetic parameters were then evaluated by fitting the initial rate data to the Michaelis-Menten equation using non-linear regression with GraphPad Prism 3 software. K_m and V_{max} for quinolinic acid were determined as 319 ± 60 μM and 0.71 ± 0.06 μM min^{-1}, respectively.

7.3 Inhibition studies on human brain QPRTase

7.3.1 Inhibition studies (with respect to quinolinic acid as the variable substrate)

Preliminary screening of potential inhibitors was carried out by assessing the % inhibition of QPRTase activity at a fixed concentration of quinolinic acid and PRPP (0.1 mM). The inhibition of QPRTase by a number of compounds was then examined in detail by assaying the activity at various concentrations of quinolinic acid (10-300 μM) and a fixed concentration of PRPP (0.1 mM). The reactions were linear over the time course studied and the rates were measured in triplicate. The kinetic parameters, K_m and V_{max}, were calculated by fitting initial rate data to the Michaelis-Menten equation using non-linear regression with Graph Pad Prism 3 software on a PC. Each inhibitor was compared to a standard assay at quinolinic acid concentrations 10-300 μM. K_i values were determined using linear regression plots of $K_{m(app)}$ versus inhibitor concentration (competitive inhibition) or $1/V_{max(app)}$ versus inhibitor concentration (noncompetitive inhibition).

7.3.2 Inhibition studies (with respect to PRPP as the variable substrate)

Preliminary screening of potential inhibitors was carried out by assessing the % inhibition of QPRTase activity at a fixed concentration of quinolinic acid and PRPP (0.1 mM). The inhibition of QPRTase by a number of compounds was then examined in detail by assaying the activity at various concentrations of PRPP (10-300 μM) and a fixed concentration of quinolinic acid (0.3 mM). The reactions were linear over the time course studied and the rates were measured in triplicate. The kinetic parameters, K_m and V_{max}, were calculated by fitting initial rate data to the Michaelis-Menten equation using non linear regression with Graph Pad Prism 3 software on a PC. Each inhibitor was compared to a standard assay at PRPP concentrations 10-300 μM. K_i values were determined using linear regression plots of $K_{m(app)}$ versus inhibitor concentration.

N-Methylquinolinic acid (41)

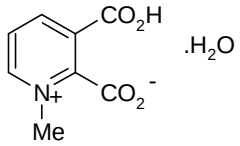

[Quinolinic acid] (mM)	Rate (μM min^{-1}) (No inhibitor)	Rate (μM min^{-1}) (0.1 mM inhibitor)	Rate (μM min^{-1}) (0.2 mM inhibitor)	Rate (μM min^{-1}) (0.3 mM inhibitor)
0.3	0.86, 0.88, 0.88	0.84, 0.84, 0.87	0.80, 0.80, 0.81	0.73, 0.73, 0.76
0.2	0.88, 0.89, 0.89	0.75, 0.75, 0.80	0.73, 0.73, 0.75	0.66, 0.70, 0.71
0.1	0.83, 0.86, 0.86	0.58, 0.60, 0.65	0.50, 0.53, 0.58	0.46, 0.48, 0.50
0.05	0.72, 0.74, 0.75	0.48, 0.49, 0.49	0.35, 0.39, 0.42	0.33, 0.33, 0.35
0.025	0.53, 0.58, 0.59	0.35, 0.37, 0.38	0.26, 0.28, 0.30	0.16, 0.17, 0.23
0.010	0.40, 0.42, 0.44	0.19, 0.20, 0.26	0.12, 0.13, 0.17	-

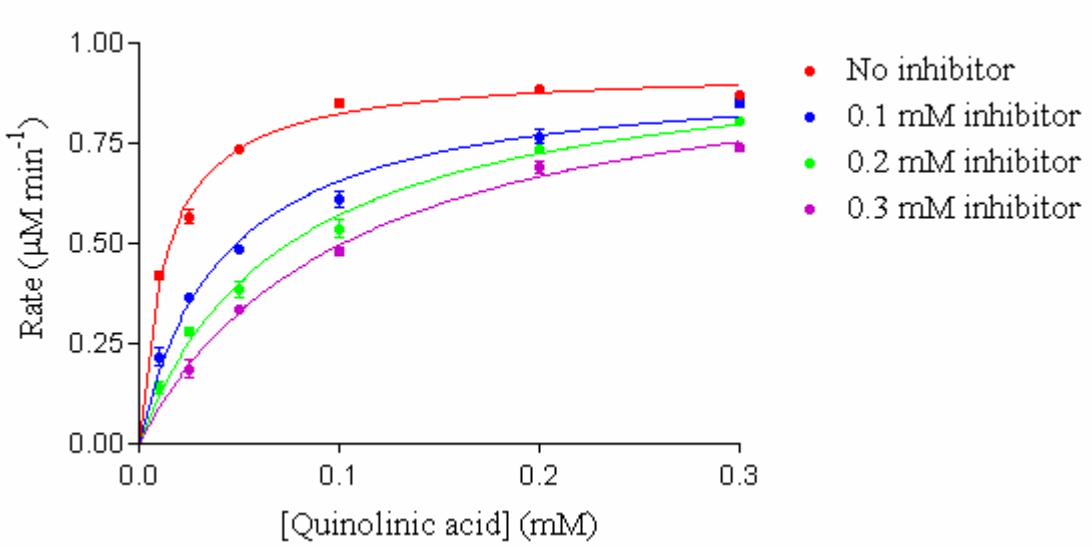

[Inhibitor] (μM)	$K_{m(app)}$ (μM)	$V_{max(app)}$ (μM min^{-1})
0	13.6 ± 1.2	0.94 ± 0.02
100	42.4 ± 4.1	0.93 ± 0.03
200	74.1 ± 6.7	0.99 ± 0.04
300	106.8 ± 8.6	1.02 ± 0.04

N-Ethylquinolinic acid (42)

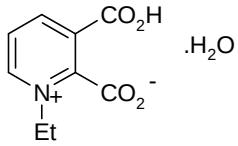

[Quinolinic acid] (mM)	Rate (μM min^{-1}) (No inhibitor)	Rate (μM min^{-1}) (0.1 mM inhibitor)	Rate (μM min^{-1}) (0.2 mM inhibitor)	Rate (μM min^{-1}) (0.3 mM inhibitor)
0.3	0.86, 0.87, 0.87	0.81, 0.82, 0.82	0.75, 0.76, 0.76	0.67, 0.67, 0.68
0.2	0.79, 0.80, 0.83	0.68, 0.68, 0.79	0.65, 0.66, 0.67	0.45, 0.54, 0.55
0.1	0.69, 0.69, 0.79	0.65, 0.66, 0.67	0.45, 0.47, 0.53	0.38, 0.39, 0.44
0.05	0.71, 0.84, 0.84	0.52, 0.52, 0.56	0.37, 0.42, 0.44	0.29, 0.32, 0.33
0.025	0.50, 0.51, 0.56	0.32, 0.34, 0.38	0.20, 0.22, 0.24	0.16, 0.18, 0.20
0.010	0.36, 0.37, 0.41	0.22, 0.26, 0.27	0.14, 0.17, 0.18	-

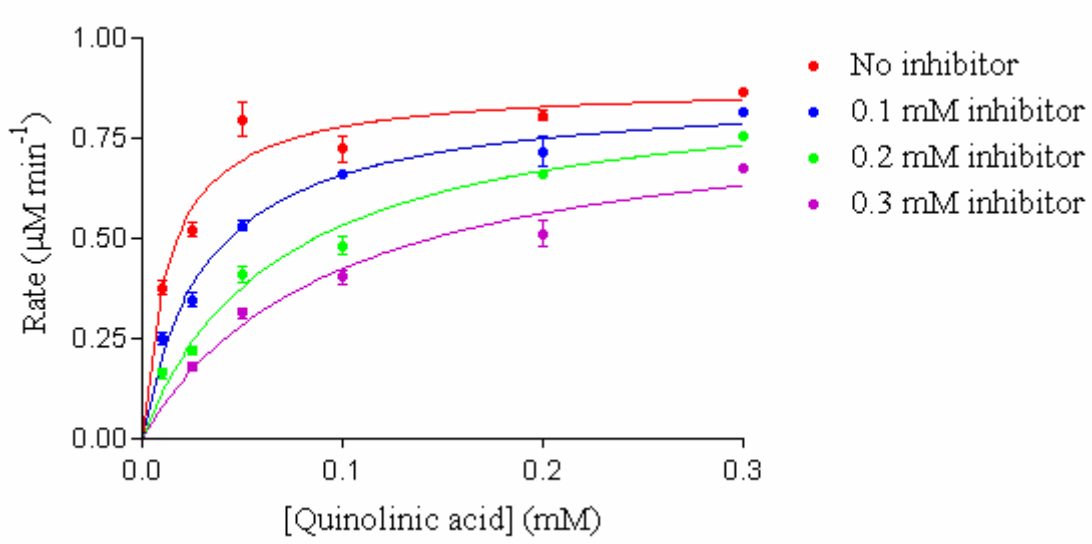

[Inhibitor] (μM)	$K_{m(app)}$ (μM)	$V_{max(app)}$ (μM min^{-1})
0	13.6 ± 2.3	0.89 ± 0.05
100	32.1 ± 3.2	0.87 ± 0.03
200	70.5 ± 6.9	0.91 ± 0.04
300	98.0 ± 9.8	0.83 ± 0.08

5-Ethylquinolinic acid (43)

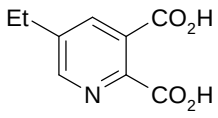

[Quinolinic acid] (mM)	Rate (μM min^{-1}) (No inhibitor)	Rate (μM min^{-1}) (0.6 mM inhibitor)	Rate (μM min^{-1}) (0.8 mM inhibitor)	Rate (μM min^{-1}) (1.0 mM inhibitor)
0.3	0.85, 0.87, 0.90	0.85, 0.87, 0.89	0.79, 0.82, 0.84	0.72, 0.73, 0.74
0.2	0.82, 0.84, 0.88	0.83, 0.87, 0.89	0.67, 0.70, 0.75	0.53, 0.55, 0.65
0.1	0.79, 0.82, 0.84	0.67, 0.70, 0.74	0.57, 0.60, 0.64	0.44, 0.47, 0.50
0.05	0.72, 0.74, 0.78	0.59, 0.61, 0.64	0.47, 0.47, 0.48	0.34, 0.39, 0.42
0.025	0.55, 0.57, 0.63	0.43, 0.45, 0.47	0.34, 0.41, 0.43	0.20, 0.23, 0.26
0.010	0.36, 0.39, 0.42	0.15, 0.18, 0.22	0.08, 0.12, 0.14	-

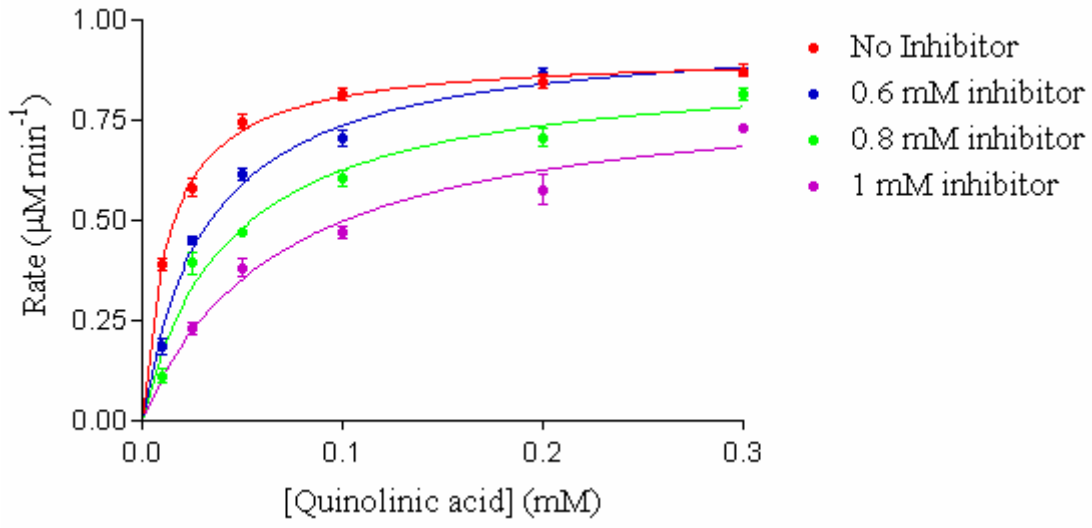

[Inhibitor] (μM)	$K_{m(app)}$ (μM)	$V_{max(app)}$ (μM min^{-1})
0	13.4 ± 1.0	0.92 ± 0.01
600	33.2 ± 2.9	0.98 ± 0.04
800	44.9 ± 5.9	0.90 ± 0.06
1000	74.1 ± 12.1	0.86 ± 0.07

5-Ethyl-N-methylquinolinic acid (46)

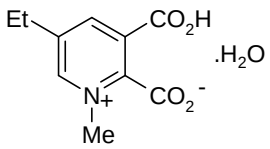

[Quinolinic acid] (mM)	Rate (μM min^{-1}) (No inhibitor)	Rate (μM min^{-1}) (0.6 mM inhibitor)	Rate (μM min^{-1}) (0.8 mM inhibitor)	Rate (μM min^{-1}) (1.0 mM inhibitor)
0.3	0.85, 0.87, 0.90	0.88, 0.88, 0.89	0.83, 0.84, 0.85	0.77, 0.79, 0.80
0.2	0.82, 0.84, 0.88	0.79, 0.85, 0.87	0.75, 0.77, 0.79	0.62, 0.63, 0.69
0.1	0.79, 0.82, 0.84	0.71, 0.81, 0.83	0.62, 0.63, 0.70	0.55, 0.57, 0.60
0.05	0.72, 0.74, 0.78	0.63, 0.68, 0.70	0.52, 0.55, 0.57	0.40, 0.43, 0.45
0.025	0.55, 0.57, 0.63	0.45, 0.46, 0.46	0.34, 0.38, 0.41	0.25, 0.29, 0.31
0.010	0.36, 0.39, 0.42	0.20, 0.22, 0.27	0.15, 0.19, 0.21	0.11, 0.15, 0.18

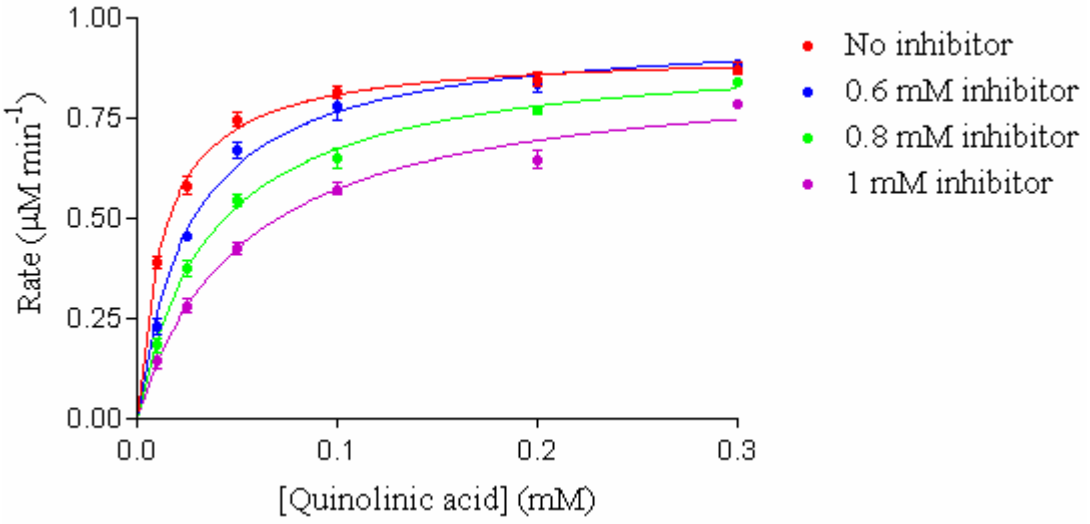

[Inhibitor] (μM)	$K_{m(app)}$ (μM)	$V_{max(app)}$ (μM min^{-1})
0	13.4 ± 1.0	0.92 ± 0.01
600	26.8 ± 2.5	0.97 ± 0.02
800	37.5 ± 3.3	0.93 ± 0.02
1000	54.6 ± 8.4	0.88 ± 0.04

Quinolinic acid N-oxide (62)

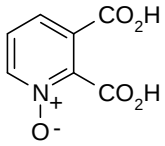

[Quinolinic acid] (mM)	Rate (μM min^{-1}) (No inhibitor)	Rate (μM min^{-1}) (0.05 mM inhibitor)	Rate (μM min^{-1}) (0.1 mM inhibitor)	Rate (μM min^{-1}) (0.2 mM inhibitor)
0.3	0.85, 0.88, 0.89	0.86, 0.86, 0.88	0.83, 0.84, 0.87	0.77, 0.79, 0.81
0.2	0.87, 0.89, 0.90	0.79, 0.80, 0.82	0.75, 0.77, 0.80	0.65, 0.68, 0.72
0.1	0.83, 0.85, 0.87	0.66, 0.69, 0.72	0.58, 0.61, 0.65	0.50, 0.53, 0.55
0.05	0.72, 0.74, 0.77	0.49, 0.50, 0.56	0.40, 0.44, 0.47	0.28, 0.33, 0.35
0.025	0.56, 0.57, 0.59	0.35, 0.39, 0.40	0.27, 0.31, 0.33	0.17, 0.20, 0.24
0.010	0.39, 0.42, 0.46	0.25, 0.27, 0.30	0.15, 0.17, 0.22	-

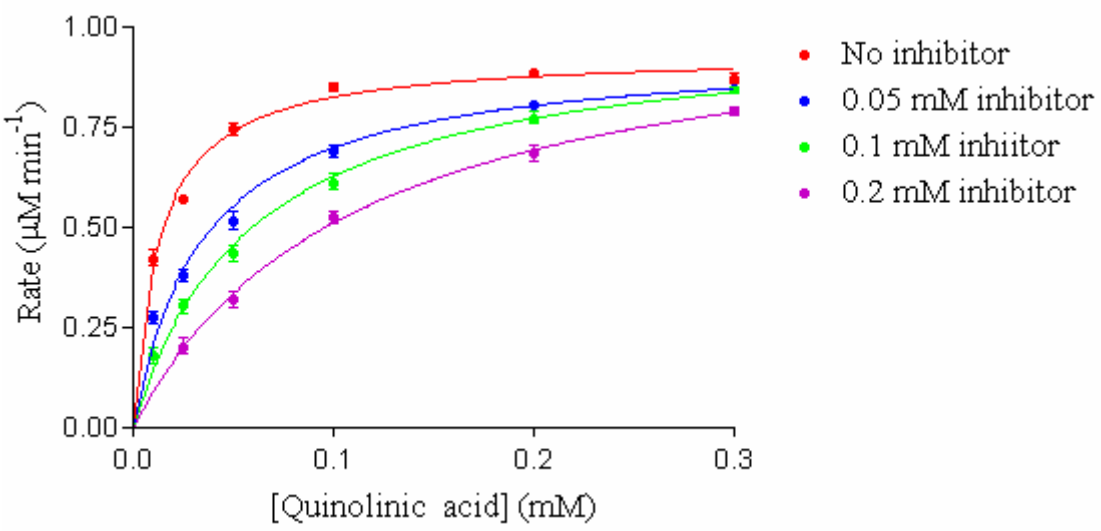

[Inhibitor] (μM)	$K_{m(app)}$ (μM)	$V_{max(app)}$ (μM min^{-1})
0	13.5 ± 1.6	0.94 ± 0.02
50	35.7 ± 3.5	0.94 ± 0.03
100	60.7 ± 5.1	1.00 ± 0.03
200	111.0 ± 10.0	1.07 ± 0.04

Phthalic acid (25)

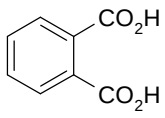

[Quinolinic acid] (mM)	Rate (μM min^{-1}) (No inhibitor)	Rate (μM min^{-1}) (0.05 mM inhibitor)	Rate (μM min^{-1}) (0.1 mM inhibitor)	Rate (μM min^{-1}) (0.2 mM inhibitor)
0.3	0.86, 0.87, 0.87	0.85, 0.85, 0.88	0.78, 0.81, 0.82	0.68, 0.69, 0.72
0.2	0.88, 0.91, 0.93	0.70, 0.71, 0.74	0.64, 0.65, 0.69	0.56, 0.56, 0.58
0.1	0.83, 0.84, 0.87	0.55, 0.55, 0.57	0.44, 0.45, 0.51	0.38, 0.42, 0.43
0.05	0.78, 0.79, 0.88	0.37, 0.43, 0.44	0.31, 0.34, 0.34	0.18, 0.19, 0.26
0.025	0.56, 0.57, 0.62	0.24, 0.29, 0.30	0.22, 0.22, 0.25	0.10, 0.11, 0.17
0.010	0.39, 0.39, 0.42	0.14, 0.15, 0.20	0.09, 0.10, 0.17	-

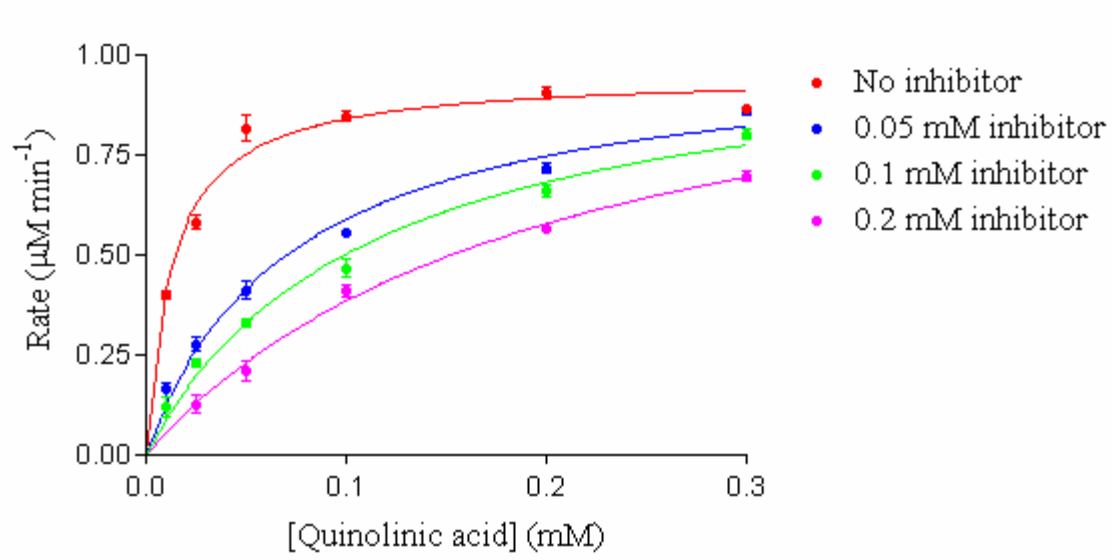

[Inhibitor] (μM)	$K_{m(app)}$ (μM)	$V_{max(app)}$ (μM min^{-1})
0	13.5 ± 1.4	0.96 ± 0.02
50	74.0 ± 7.4	1.03 ± 0.04
100	109.7 ± 11.2	1.06 ± 0.06
200	203.0 ± 28.9	1.17 ± 0.09

2,3-Naphthalene dicarboxylic acid (104)

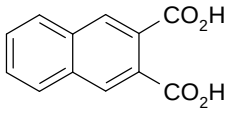

[Quinolinic acid] (mM)	Rate (μM min^{-1}) (No inhibitor)	Rate (μM min^{-1}) (0.1 mM inhibitor)	Rate (μM min^{-1}) (0.2 mM inhibitor)	Rate (μM min^{-1}) (0.3 mM inhibitor)
0.3	0.86, 0.87, 0.87	0.85, 0.87, 0.88	0.83, 0.84, 0.85	0.80, 0.82, 0.83
0.2	0.88, 0.91, 0.93	0.83, 0.84, 0.86	0.79, 0.80, 0.80	0.76, 0.79, 0.82
0.1	0.83, 0.84, 0.87	0.76, 0.78, 0.80	0.65, 0.67, 0.70	0.59, 0.62, 0.64
0.05	0.78, 0.79, 0.88	0.58, 0.62, 0.66	0.49, 0.53, 0.55	0.42, 0.46, 0.46
0.025	0.56, 0.57, 0.62	0.43, 0.45, 0.48	0.35, 0.37, 0.40	0.27, 0.30, 0.32
0.010	0.39, 0.39, 0.42	0.27, 0.29, 0.32	0.21, 0.24, 0.25	0.16, 0.20, 0.20

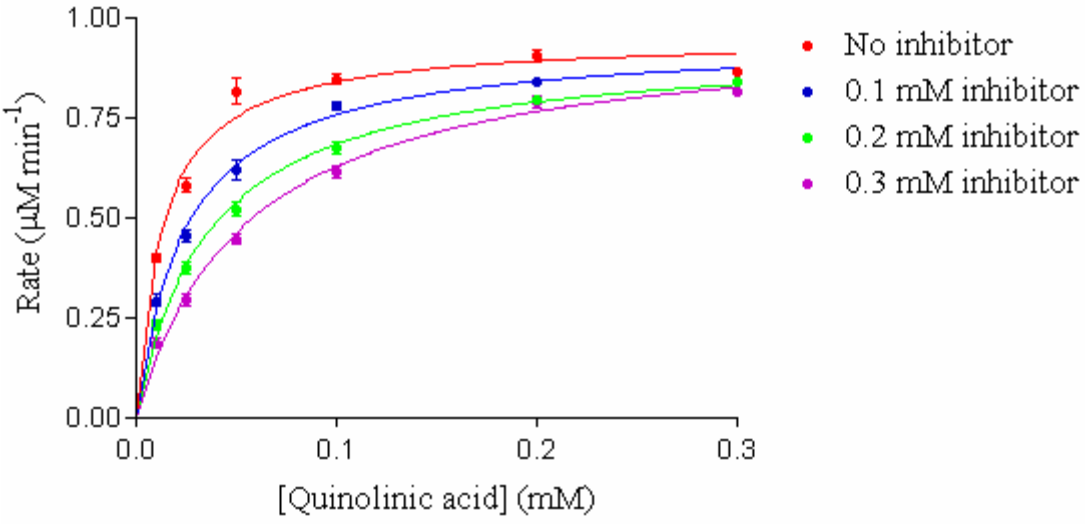

[Inhibitor] (μM)	$K_{m(app)}$ (μM)	$V_{max(app)}$ (μM min^{-1})
0	13.5 ± 1.4	0.96 ± 0.02
100	25.4 ± 2.0	0.95 ± 0.02
200	37.8 ± 3.2	0.94 ± 0.02
300	55.1 ± 4.3	0.98 ± 0.03

Picolinic acid (26)

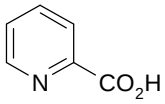

[Quinolinic acid] (mM)	Rate (μM min^{-1}) (No inhibitor)	Rate (μM min^{-1}) (0.1 mM inhibitor)	Rate (μM min^{-1}) (0.2 mM inhibitor)	Rate (μM min^{-1}) (0.3 mM inhibitor)
0.3	0.86, 0.86, 0.88	0.86, 0.86, 0.87	0.82, 0.83, 0.84	0.78, 0.78, 0.82
0.2	0.88, 0.89, 0.90	0.78, 0.79, 0.85	0.76, 0.78, 0.80	0.71, 0.73, 0.75
0.1	0.82, 0.84, 0.88	0.74, 0.74, 0.76	0.64, 0.65, 0.68	0.59, 0.59, 0.60
0.05	0.73, 0.74, 0.74	0.59, 0.65, 0.66	0.47, 0.57, 0.59	0.37, 0.52, 0.54
0.025	0.53, 0.55, 0.62	0.40, 0.42, 0.44	0.28, 0.30, 0.34	0.20, 0.24, 0.26
0.010	0.39, 0.41, 0.45	0.18, 0.19, 0.22	0.08, 0.09, 0.11	-

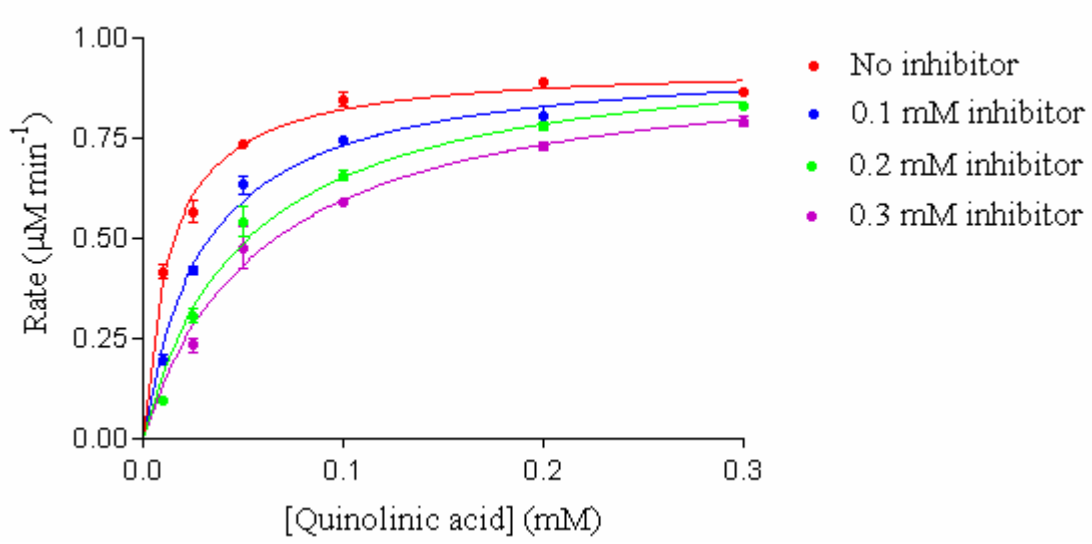

[Inhibitor] (μM)	$K_{m(app)}$ (μM)	$V_{max(app)}$ (μM min^{-1})
0	13.5 ± 1.1	0.94 ± 0.02
100	30.6 ± 2.5	0.96 ± 0.02
200	51.4 ± 6.1	0.99 ± 0.04
300	69.8 ± 8.9	0.99 ± 0.05

N-Methylpicolinic acid (50)

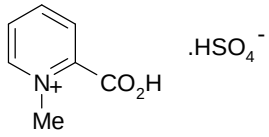

[Quinolinic acid] (mM)	Rate (μM min^{-1}) (No inhibitor)	Rate (μM min^{-1}) (0.1 mM inhibitor)	Rate (μM min^{-1}) (0.2 mM inhibitor)	Rate (μM min^{-1}) (0.3 mM inhibitor)
0.3	0.86, 0.86, 0.88	0.88, 0.89, 0.89	0.86, 0.86, 0.87	0.83, 0.84, 0.84
0.2	0.88, 0.89, 0.90	0.84, 0.86, 0.88	0.77, 0.80, 0.85	0.79, 0.80, 0.81
0.1	0.82, 0.84, 0.88	0.78, 0.79, 0.80	0.72, 0.79, 0.81	0.67, 0.75, 0.77
0.05	0.73, 0.74, 0.74	0.66, 0.66, 0.67	0.58, 0.59, 0.60	0.44, 0.47, 0.55
0.025	0.53, 0.55, 0.62	0.45, 0.47, 0.54	0.38, 0.40, 0.44	0.35, 0.37, 0.39
0.010	0.39, 0.41, 0.45	0.27, 0.32, 0.35	0.22, 0.24, 0.26	0.14, 0.16, 0.20

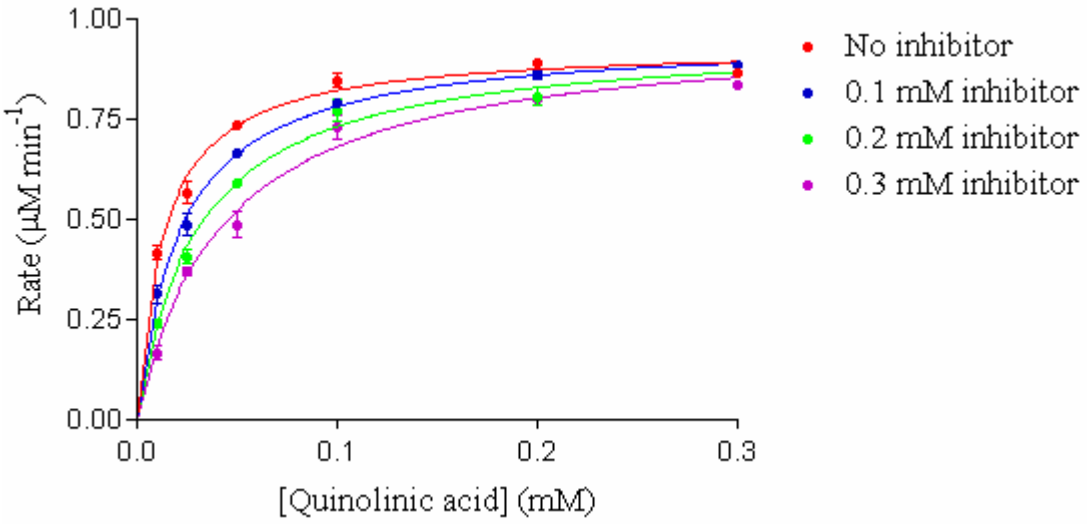

[Inhibitor] (μM)	$K_{m(app)}$ (μM)	$V_{max(app)}$ (μM min^{-1})
0	13.5 ± 1.1	0.94 ± 0.02
100	22.4 ± 1.3	0.96 ± 0.01
200	30.6 ± 2.5	0.95 ± 0.02
300	43.4 ± 4.4	0.98 ± 0.04

N-Ethylpicolinic acid (51)

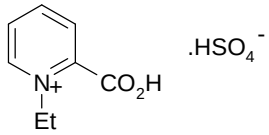

[Quinolinic acid] (mM)	Rate (μM min^{-1}) (No inhibitor)	Rate (μM min^{-1}) (0.1 mM inhibitor)	Rate (μM min^{-1}) (0.2 mM inhibitor)	Rate (μM min^{-1}) (0.3 mM inhibitor)
0.3	0.86, 0.86, 0.88	0.86, 0.87, 0.87	0.84, 0.86, 0.87	0.83, 0.84, 0.87
0.2	0.88, 0.89, 0.90	0.85, 0.86, 0.87	0.82, 0.85, 0.86	0.80, 0.85, 0.87
0.1	0.82, 0.84, 0.88	0.76, 0.77, 0.79	0.70, 0.75, 0.76	0.67, 0.69, 0.71
0.05	0.73, 0.74, 0.74	0.57, 0.60, 0.65	0.52, 0.55, 0.59	0.48, 0.49, 0.55
0.025	0.53, 0.55, 0.62	0.47, 0.51, 0.53	0.42, 0.44, 0.46	0.31, 0.33, 0.37
0.010	0.39, 0.41, 0.45	029, 0.31, 0.33	0.25, 0.27, 0.28	0.19, 0.22, 0.24

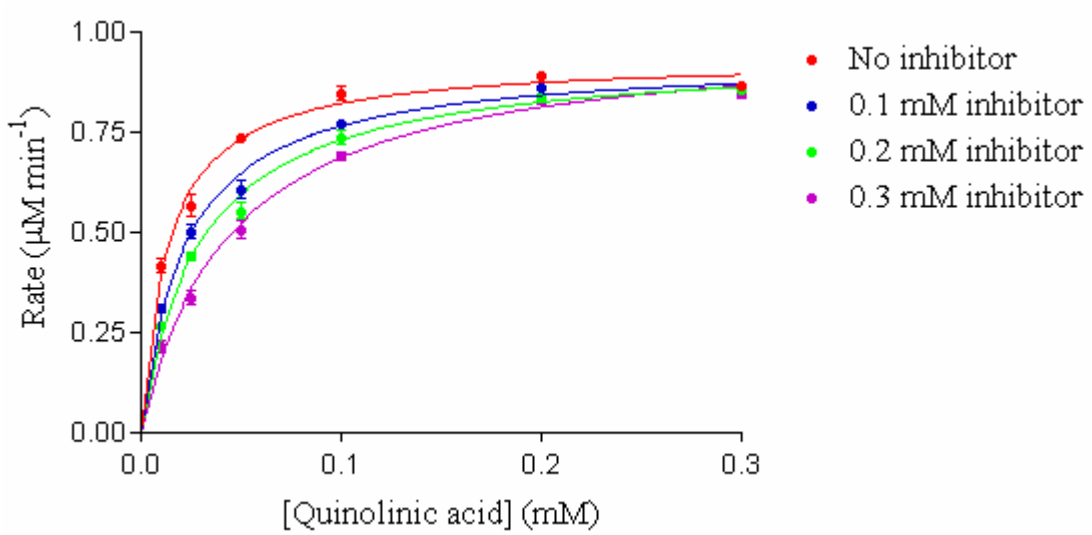

[Inhibitor] (μM)	$K_{m(app)}$ (μM)	$V_{max(app)}$ (μM min^{-1})
0	13.5 ± 1.1	0.94 ± 0.02
100	22.5 ± 1.5	0.94 ± 0.02
200	29.7 ± 2.2	0.95 ± 0.03
300	44.6 ± 3.8	0.99 ± 0.03

Picolinic acid N-oxide (105)

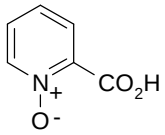

[Quinolinic acid] (mM)	Rate (μM min^{-1}) (No inhibitor)	Rate (μM min^{-1}) (0.1 mM inhibitor)	Rate (μM min^{-1}) (0.2 mM inhibitor)	Rate (μM min^{-1}) (0.3 mM inhibitor)
0.3	0.85, 0.88, 0.89	0.84, 0.84, 0.88	0.81, 0.83, 0.85	0.75, 0.76, 0.78
0.2	0.87, 0.89, 0.90	0.83, 0.85, 0.87	0.75, 0.77, 0.80	0.68, 0.71, 0.74
0.1	0.83, 0.85, 0.87	0.80, 0.85, 0.87	0.59, 0.69, 0.71	0.60, 0.65, 0.66
0.05	0.72, 0.74, 0.77	0.59, 0.63, 0.67	0.50, 0.52, 0.55	0.43, 0.46, 0.48
0.025	0.56, 0.57, 0.59	0.47, 0.50, 0.51	0.36, 0.38, 0.41	0.25, 0.29, 0.33
0.010	0.39, 0.42, 0.46	0.27, 0.28, 0.33	0.18, 0.22, 0.26	0.12, 0.15, 0.17

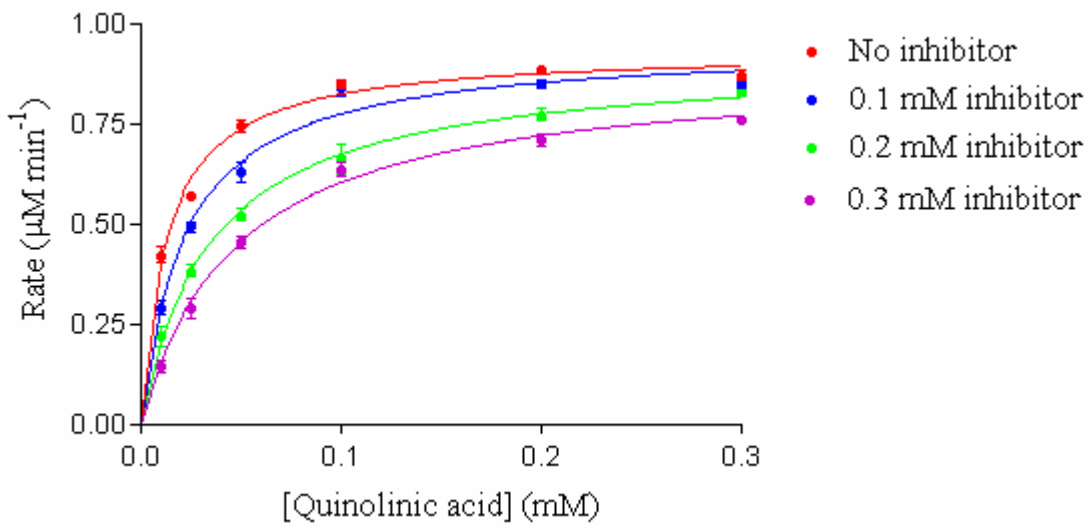

[Inhibitor] (μM)	$K_{m(app)}$ (μM)	$V_{max(app)}$ (μM min^{-1})
0	13.5 ± 1.6	0.94 ± 0.02
100	22.6 ± 2.1	0.95 ± 0.02
200	35.6 ± 2.4	0.91 ± 0.02
300	47.0 ± 4.6	0.89 ± 0.03

Quinoline-2-carboxylic acid (52)

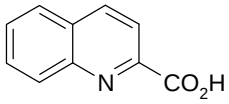

[Quinolinic acid] (mM)	Rate (μM min^{-1}) (No inhibitor)	Rate (μM min^{-1}) (0.3 mM inhibitor)	Rate (μM min^{-1}) (0.5 mM inhibitor)	Rate (μM min^{-1}) (0.7 mM inhibitor)
0.3	0.86, 0.87, 0.87	0.90, 0.91, 0.91	0.88, 0.90, 0.91	0.84, 0.85, 0.87
0.2	0.88, 0.91, 0.93	0.88, 0.92, 0.94	0.84, 0.88, 0.90	0.79, 0.84, 0.85
0.1	0.83, 0.84, 0.87	0.76, 0.78, 0.80	0.63, 0.65, 0.72	0.56, 0.60, 0.63
0.05	0.78, 0.79, 0.88	0.55, 0.57, 0.66	0.51, 0.55, 0.60	0.42, 0.45, 0.48
0.025	0.56, 0.57, 0.62	0.42, 0.46, 0.48	0.27, 0.28, 0.36	0.24, 0.26, 0.28
0.010	0.39, 0.39, 0.42	0.20, 0.23, 0.24	0.15, 0.17, 0.20	0.08, 0.11, 0.16

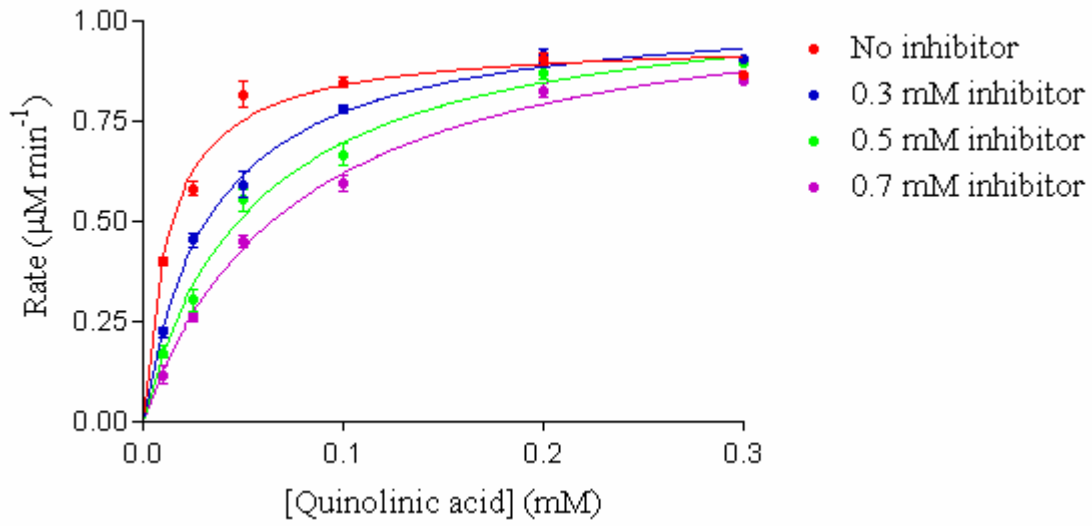

[Inhibitor] (μM)	$K_{m(app)}$ (μM)	$V_{max(app)}$ (μM min^{-1})
0	13.5 ± 1.4	0.96 ± 0.02
300	35.2 ± 2.6	1.04 ± 0.02
500	56.3 ± 5.6	1.09 ± 0.05
700	76.4 ± 6.8	1.10 ± 0.08

N-Methylquinoline-2-carboxylic acid (55)

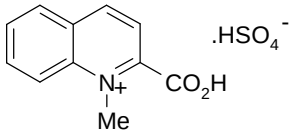

[Quinolinic acid] (mM)	Rate (μM min^{-1}) (No inhibitor)	Rate (μM min^{-1}) (0.3 mM inhibitor)	Rate (μM min^{-1}) (0.5 mM inhibitor)	Rate (μM min^{-1}) (0.7 mM inhibitor)
0.3	0.86, 0.87, 0.87	0.90, 0.90, 0.91	0.88, 0.89, 0.91	0.82, 0.86, 0.89
0.2	0.88, 0.91, 0.93	0.89, 0.89, 0.91	0.85, 0.88, 0.90	0.80, 0.84, 0.87
0.1	0.83, 0.84, 0.87	0.78, 0.80, 0.84	0.73, 0.75, 0.77	0.66, 0.69, 0.72
0.05	0.78, 0.79, 0.88	0.62, 0.64, 0.67	0.52, 0.55, 0.60	0.45, 0.48, 0.52
0.025	0.56, 0.57, 0.62	0.50, 0.50, 0.51	0.42, 0.44, 0.48	0.34, 0.37, 0.39
0.010	0.39, 0.39, 0.42	0.26, 0.28, 0.30	0.18, 0.20, 0.24	0.14, 0.16, 0.20

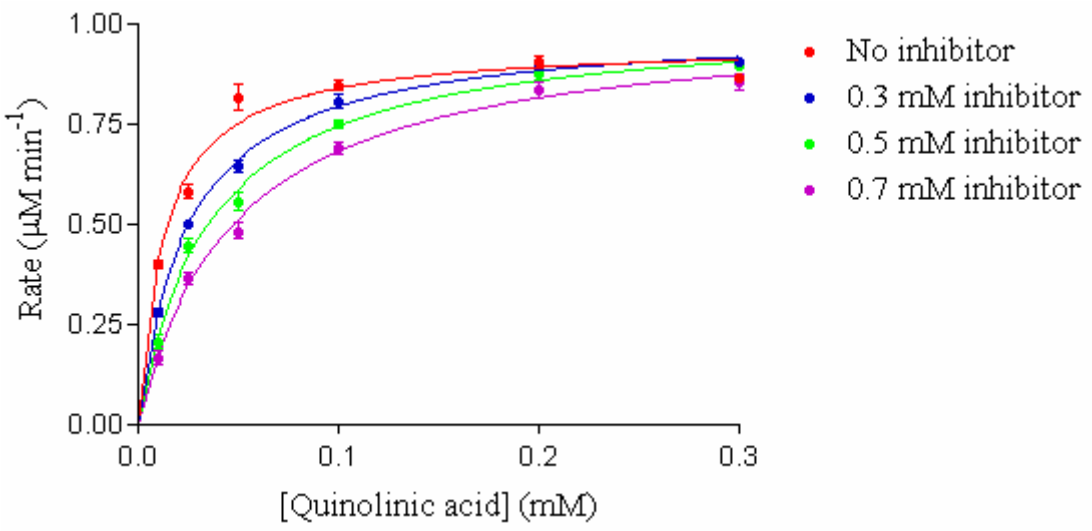

[Inhibitor] (μM)	$K_{m(app)}$ (μM)	$V_{max(app)}$ (μM min^{-1})
0	13.5 ± 1.4	0.96 ± 0.02
300	25.5 ± 1.7	1.00 ± 0.02
500	35.5 ± 2.7	1.01 ± 0.03
700	49.0 ± 4.0	1.02 ± 0.03

Adenosine 5'-monophosphate (107) - Inhibition with respect to quinolinic acid

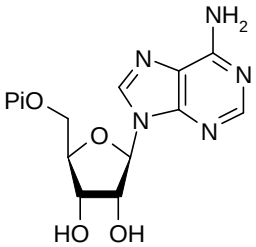

[Quinolinic acid] (mM)	Rate (μM min^{-1}) (No inhibitor)	Rate (μM min^{-1}) (0.1 mM inhibitor)	Rate (μM min^{-1}) (0.2 mM inhibitor)	Rate (μM min^{-1}) (0.3 mM inhibitor)
0.3	0.86, 0.87, 0.87	0.77, 0.79, 0.84	0.67, 0.69, 0.70	0.58, 0.65, 0.68
0.2	0.88, 0.91, 0.93	0.70, 0.72, 0.78	0.65, 0.67, 0.69	0.54, 0.57, 0.61
0.1	0.83, 0.84, 0.87	0.68, 0.68, 0.71	0.57, 0.59, 0.63	0.48, 0.50, 0.54
0.05	0.78, 0.79, 0.88	0.57, 0.60, 0.64	0.51, 0.53, 0.55	0.42, 0.44, 0.48
0.025	0.56, 0.57, 0.62	0.47, 0.51, 0.55	0.42, 0.48, 0.52	0.35, 0.36, 0.42
0.010	0.39, 0.39, 0.42	0.34, 0.36, 0.38	0.27, 0.30, 0.33	0.25, 0.28, 0.31

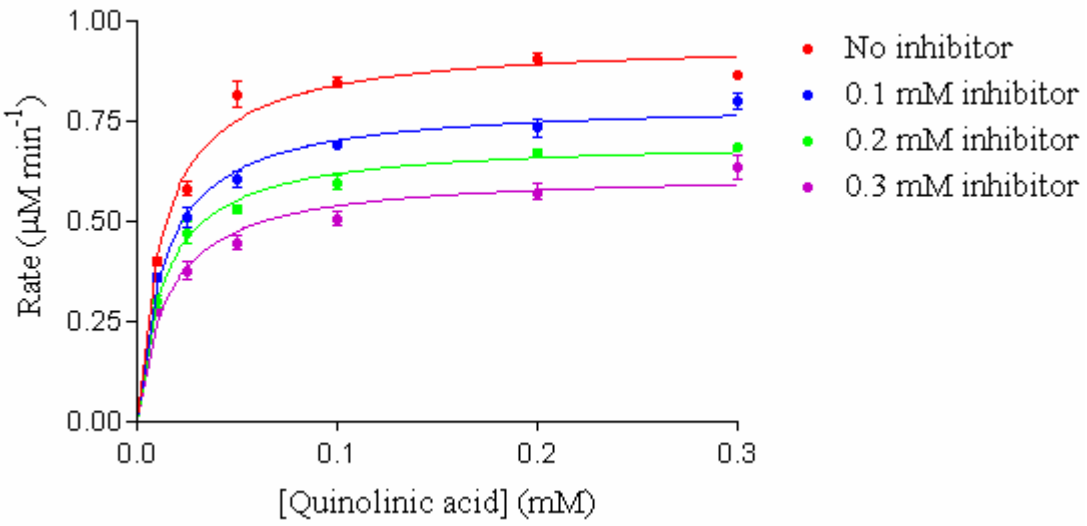

[Inhibitor] (μM)	$K_{m(app)}$ (μM)	$V_{max(app)}$ (μM min^{-1})
0	13.5 ± 1.4	0.96 ± 0.02
100	13.7 ± 1.8	0.80 ± 0.02
200	13.9 ± 1.4	0.71 ± 0.02
300	15.3 ± 3.3	0.62 ± 0.03

Adenosine 5'-monophosphate (107) - Inhibition with respect to PRPP

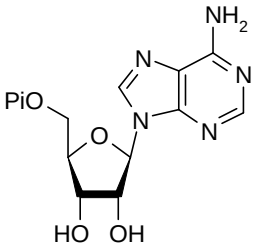

[PRPP] (mM)	Rate (μM min^{-1}) (No inhibitor)	Rate (μM min^{-1}) (0.3 mM inhibitor)	Rate (μM min^{-1}) (0.5 mM inhibitor)	Rate (μM min^{-1}) (0.7 mM inhibitor)
0.3	0.90, 0.92, 0.94	0.83, 0.85, 0.88	0.79, 0.80, 0.82	0.70, 0.72, 0.75
0.2	0.83, 0.85, 0.91	0.81, 0.81, 0.84	0.74, 0.78, 0.83	0.64, 0.68, 0.71
0.1	0.81, 0.89, 0.91	0.61, 0.62, 0.68	0.55, 0.57, 0.63	0.51, 0.53, 0.54
0.05	0.65, 0.67, 0.71	0.53, 0.55, 0.58	0.43, 0.46, 0.51	0.36, 0.39, 0.41
0.025	0.45, 0.48, 0.53	0.30, 0.32, 0.37	0.24, 0.26, 0.33	0.16, 0.20, 0.24
0.010	0.29, 0.34, 0.37	0.17, 0.19, 0.22	0.11, 0.15, 0.18	-

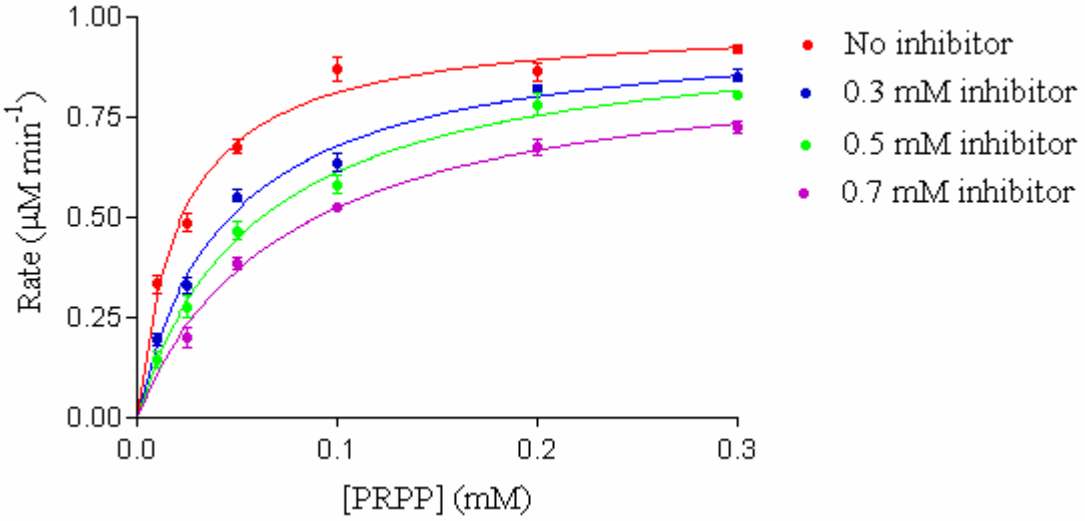

[Inhibitor] (μM)	$K_{m(app)}$ (μM)	$V_{max(app)}$ (μM min^{-1})
0	22.1 ± 2.3	0.99 ± 0.03
300	44.9 ± 4.0	0.98 ± 0.04
500	58.2 ± 5.9	0.97 ± 0.04
700	73.7 ± 7.6	0.92 ± 0.04

Guanosine 5'-monophosphate (108) - Inhibition with respect to quinolinic acid

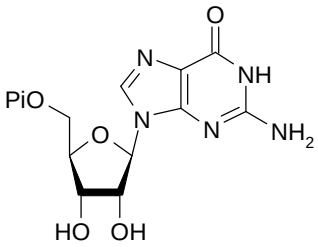

[Quinolinic acid] (mM)	Rate (μM min^{-1}) (No inhibitor)	Rate (μM min^{-1}) (0.1 mM inhibitor)	Rate (μM min^{-1}) (0.2 mM inhibitor)	Rate (μM min^{-1}) (0.3 mM inhibitor)
0.3	0.86, 0.87, 0.87	0.78, 0.82, 0.85	0.68, 0.71, 0.72	0.61, 0.64, 0.66
0.2	0.88, 0.91, 0.93	0.75, 0.77, 0.77	0.64, 0.68, 0.72	0.56, 0.58, 0.60
0.1	0.83, 0.84, 0.87	0.68, 0.70, 0.73	0.58, 0.60, 0.63	0.49, 0.52, 0.55
0.05	0.78, 0.79, 0.88	0.60, 0.62, 0.66	0.51, 0.55, 0.57	0.45, 0.48, 0.50
0.025	0.56, 0.57, 0.62	0.50, 0.53, 0.55	0.45, 0.47, 0.51	0.33, 0.36, 0.43
0.010	0.39, 0.39, 0.42	0.36, 0.38, 0.41	0.29, 0.32, 0.34	0.26, 0.29, 0.31

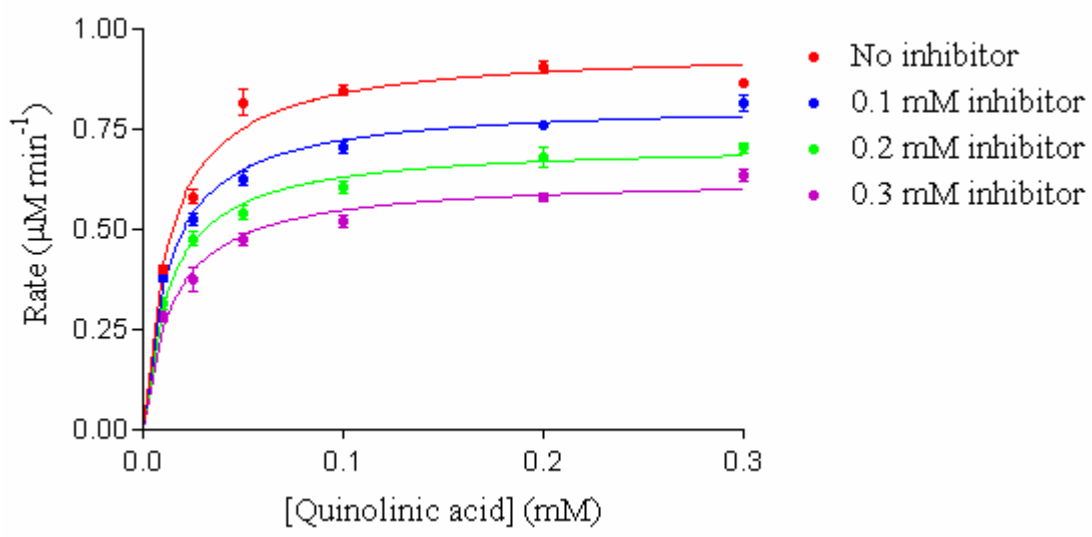

[Inhibitor] (μM)	$K_{m(app)}$ (μM)	$V_{max(app)}$ (μM min^{-1})
0	13.5 ± 1.4	0.96 ± 0.02
100	13.0 ± 1.6	0.82 ± 0.02
200	13.1 ± 1.3	0.72 ± 0.02
300	14.9 ± 2.0	0.63 ± 0.03

Guanosine 5'-monophosphate (108) - Inhibition with respect to PRPP

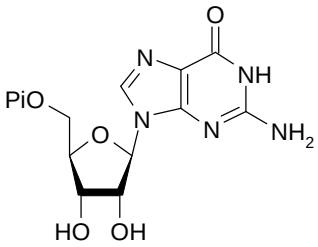

[PRPP] (mM)	Rate (μM min^{-1}) (No inhibitor)	Rate (μM min^{-1}) (0.3 mM inhibitor)	Rate (μM min^{-1}) (0.5 mM inhibitor)	Rate (μM min^{-1}) (0.7 mM inhibitor)
0.3	0.90, 0.92, 0.94	0.85, 0.86, 0.88	0.80, 0.83, 0.85	0.75, 0.78, 0.79
0.2	0.83, 0.85, 0.91	0.80, 0.83, 0.84	0.76, 0.78, 0.79	0.70, 0.72, 0.73
0.1	0.81, 0.89, 0.91	0.68, 0.71, 0.74	0.61, 0.64, 0.65	0.55, 0.61, 0.62
0.05	0.65, 0.67, 0.71	0.53, 0.55, 0.58	0.46, 0.49, 0.52	0.40, 0.43, 0.44
0.025	0.45, 0.48, 0.53	0.34, 0.38, 0.40	0.26, 0.30, 0.33	0.21, 0.22, 0.25
0.010	0.29, 0.34, 0.37	0.18, 0.20, 0.23	0.13, 0.16, 0.19	0.08, 0.10, 0.13

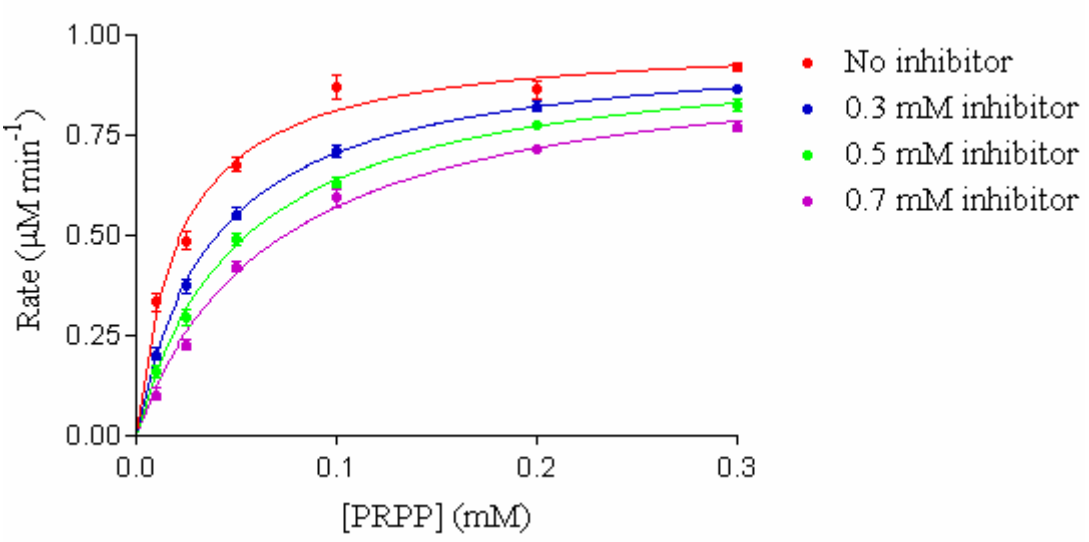

[Inhibitor] (μM)	$K_{m(app)}$ (μM)	$V_{max(app)}$ (μM min^{-1})
0	22.1 ± 2.3	0.99 ± 0.03
300	39.6 ± 2.1	0.98 ± 0.02
500	53.2 ± 3.4	0.98 ± 0.02
700	69.7 ± 5.7	0.97 ± 0.04

Cytidine 5'-monophosphate (109) - Inhibition with respect to quinolinic acid

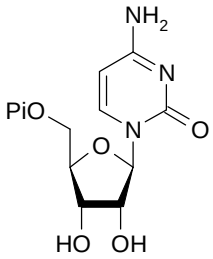

[Quinolinic acid] (mM)	Rate (μM min^{-1}) (No inhibitor)	Rate (μM min^{-1}) (0.1 mM inhibitor)	Rate (μM min^{-1}) (0.2 mM inhibitor)	Rate (μM min^{-1}) (0.3 mM inhibitor)
0.3	0.86, 0.87, 0.87	0.74, 0.78, 0.80	0.63, 0.63, 0.64	0.51, 0.57, 0.59
0.2	0.88, 0.91, 0.93	0.68, 0.68, 0.74	0.58, 0.60, 0.63	0.50, 0.53, 0.55
0.1	0.83, 0.84, 0.87	0.63, 0.65, 0.68	0.53, 0.56, 0.60	0.48, 0.49, 0.51
0.05	0.78, 0.79, 0.88	0.53, 0.56, 0.58	0.45, 0.47, 0.53	0.40, 0.44, 0.47
0.025	0.56, 0.57, 0.62	0.45, 0.47, 0.49	0.37, 0.40, 0.43	0.29, 0.32, 0.37
0.010	0.39, 0.39, 0.42	0.32, 0.36, 0.39	0.28, 0.32, 0.36	0.24, 0.27, 0.34

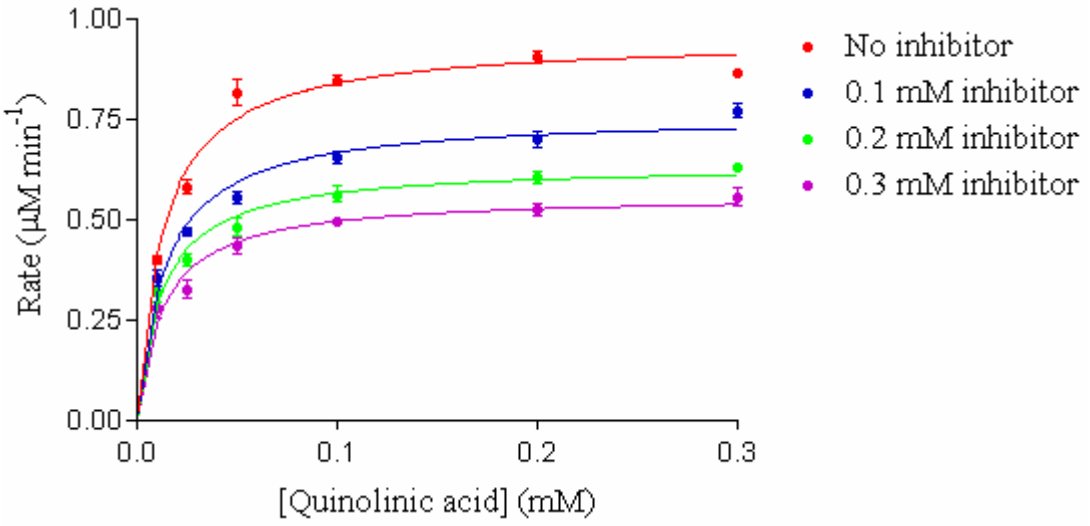

[Inhibitor] (μM)	$K_{m(app)}$ (μM)	$V_{max(app)}$ (μM min^{-1})
0	13.5 ± 1.4	0.96 ± 0.02
100	13.9 ± 2.6	0.76 ± 0.03
200	12.3 ± 2.1	0.63 ± 0.02
300	13.4 ± 2.6	0.56 ± 0.02

Cytidine 5'-monophosphate (109) - Inhibition with respect to PRPP

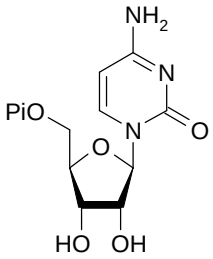

[PRPP] (mM)	Rate (μM min^{-1}) (No inhibitor)	Rate (μM min^{-1}) (0.3 mM inhibitor)	Rate (μM min^{-1}) (0.5 mM inhibitor)	Rate (μM min^{-1}) (0.7 mM inhibitor)
0.3	0.90, 0.92, 0.94	0.83, 0.86, 0.90	0.79, 0.82, 0.84	0.73, 0.75, 0.78
0.2	0.83, 0.85, 0.91	0.77, 0.80, 0.82	0.69, 0.72, 0.75	0.65, 0.68, 0.70
0.1	0.81, 0.89, 0.91	0.59, 0.60, 0.68	0.55, 0.58, 0.60	0.50, 0.55, 0.56
0.05	0.65, 0.67, 0.71	0.49, 0.53, 0.55	0.42, 0.44, 0.47	0.33, 0.39, 0.41
0.025	0.45, 0.48, 0.53	0.30, 0.33, 0.37	0.21, 0.26, 0.30	0.16, 0.19, 0.21
0.010	0.29, 0.34, 0.37	0.17, 0.19, 0.22	0.08, 0.10, 0.13	-

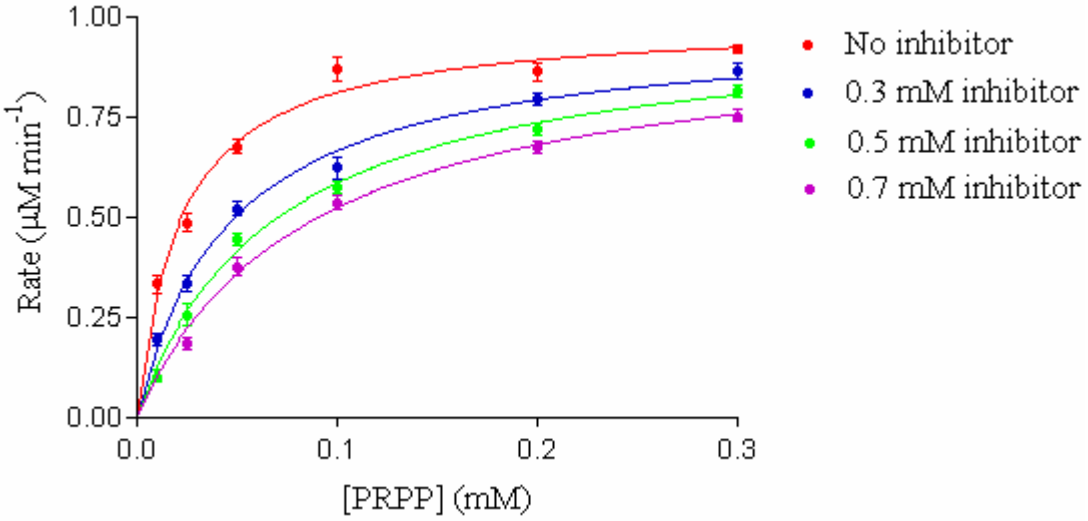

[Inhibitor] (μM)	$K_{m(app)}$ (μM)	$V_{max(app)}$ (μM min^{-1})
0	22.1 ± 2.3	0.99 ± 0.03
300	48.3 ± 4.4	0.98 ± 0.04
500	70.0 ± 6.0	1.00 ± 0.03
700	88.6 ± 9.0	0.98 ± 0.04

Thymidine 5'-monophosphate (110) - Inhibition with respect to quinolinic acid

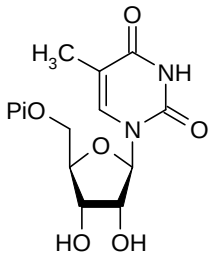

[Quinolinic acid] (mM)	Rate (μM min^{-1}) (No inhibitor)	Rate (μM min^{-1}) (0.1 mM inhibitor)	Rate (μM min^{-1}) (0.2 mM inhibitor)	Rate (μM min^{-1}) (0.3 mM inhibitor)
0.3	0.86, 0.87, 0.87	0.69, 0.74, 0.76	0.64, 0.68, 0.71	0.53, 0.62, 0.64
0.2	0.88, 0.91, 0.93	0.62, 0.65, 0.71	0.54, 0.56, 0.58	0.41, 0.43, 0.50
0.1	0.83, 0.84, 0.87	0.61, 0.63, 0.65	0.48, 0.52, 0.54	0.43, 0.46, 0.48
0.05	0.78, 0.79, 0.88	0.50, 0.52, 0.55	0.44, 0.46, 0.49	0.39, 0.42, 0.44
0.025	0.56, 0.57, 0.62	0.40, 0.42, 0.48	0.33, 0.37, 0.41	0.29, 0.32, 0.35
0.010	0.39, 0.39, 0.42	0.30, 0.31, 0.36	0.26, 0.30, 0.32	0.21, 0.24, 0.28

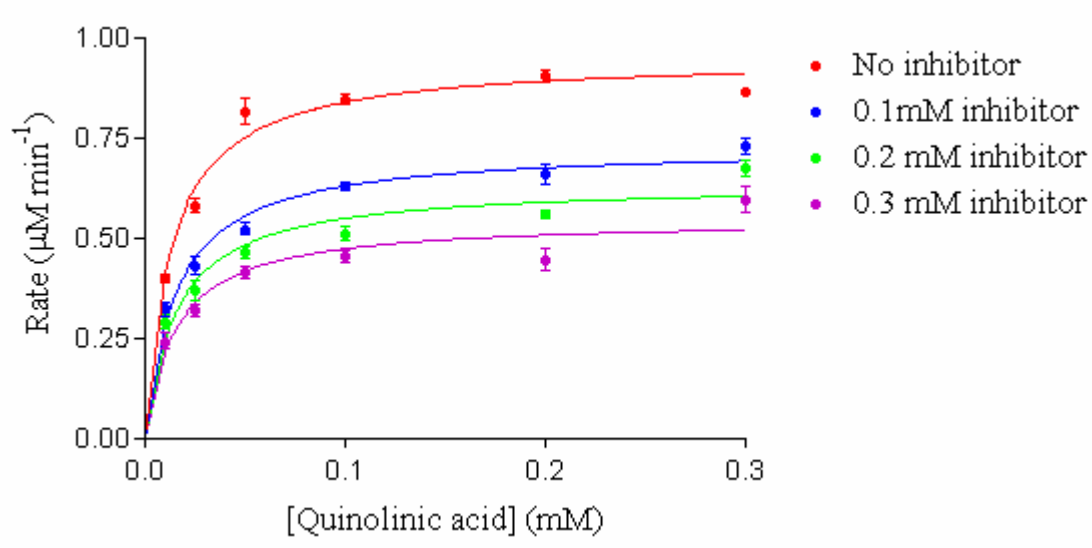

[Inhibitor] (μM)	$K_{m(app)}$ (μM)	$V_{max(app)}$ (μM min^{-1})
0	13.5 ± 1.4	0.96 ± 0.02
100	15.6 ± 2.7	0.73 ± 0.02
200	15.9 ± 2.8	0.64 ± 0.02
300	15.6 ± 3.5	0.55 ± 0.03

Thymidine 5'-monophosphate (110) - Inhibition with respect to PRPP

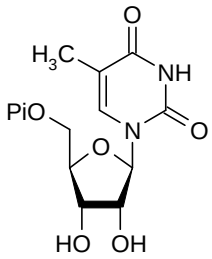

[PRPP] (mM)	Rate (μM min^{-1}) (No inhibitor)	Rate (μM min^{-1}) (0.3 mM inhibitor)	Rate (μM min^{-1}) (0.5 mM inhibitor)	Rate (μM min^{-1}) (0.7 mM inhibitor)
0.3	0.90, 0.92, 0.94	0.86, 0.88, 0.91	0.81, 0.82, 0.85	0.76, 0.78, 0.80
0.2	0.83, 0.85, 0.91	0.77, 0.79, 0.82	0.73, 0.75, 0.77	0.64, 0.67, 0.69
0.1	0.81, 0.89, 0.91	0.55, 0.58, 0.68	0.58, 0.60, 0.63	0.51, 0.53, 0.54
0.05	0.65, 0.67, 0.71	0.51, 0.51, 0.53	0.41, 0.44, 0.47	0.33, 0.37, 0.41
0.025	0.45, 0.48, 0.53	0.32, 0.33, 0.38	0.24, 0.27, 0.32	0.18, 0.20, 0.24
0.010	0.29, 0.34, 0.37	0.15, 0.17, 0.20	0.08, 0.10, 0.13	-

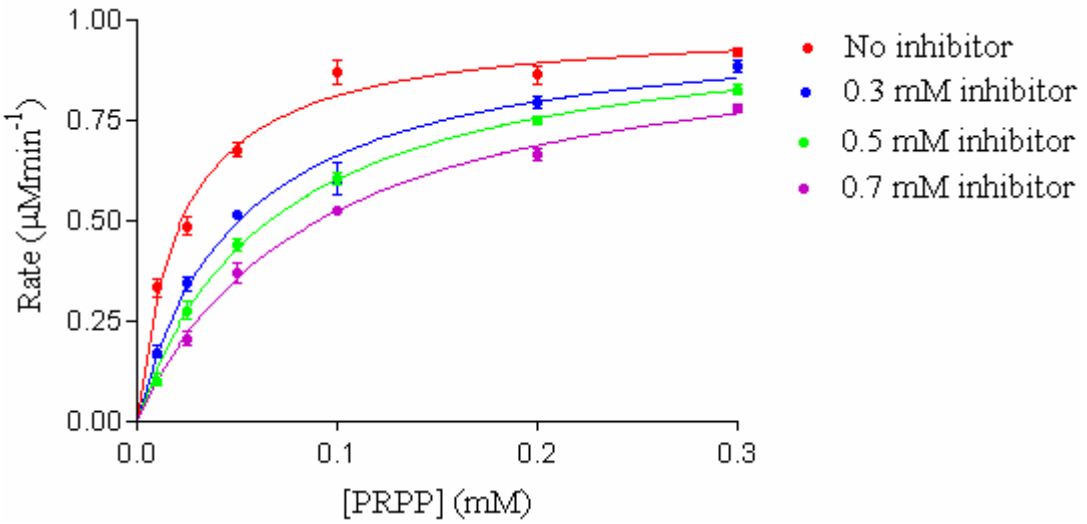

[Inhibitor] (μM)	$K_{m(app)}$ (μM)	$V_{max(app)}$ (μM min^{-1})
0	22.1 ± 2.3	0.99 ± 0.04
300	51.2 ± 5.5	1.00 ± 0.03
500	68.6 ± 4.9	1.02 ± 0.03
700	88.8 ± 7.6	1.00 ± 0.03

7.4 Synthesis of potential inhibitors of human brain QPRTase

7.4.1 General methods

NMR data were collected using a Bruker AV-300 operating at 300 MHz for ^{1}H and 75.46 MHz for ^{13}C. Chemical shifts for proton and carbon resonances are reported in ppm relative to chloroform (δ 7.25, 77.0 respectively), methanol (δ 3.35, 49.0 respectively), dimethylsulfoxide (δ 2.5, 39.7 respectively) or water (δ 4.70). The coupling constants are given in Hz. The multiplicity is given as follows, singlet: s, doublet: d, triplet: t, quartet: q, multiplet: m, doublet of doublets: dd, doublet of doublets of doublets: ddd, triplet of doublets: td, broad signal: br.

Electrospray mass spectra were recorded on a Micromass LCT spectrometer. Dominant fractions are reported as percentages of the base peak intensity.

Infrared spectra were recorded on a Perkin-Elmer 1420 spectrophotometer. The samples were prepared as nujol mulls (solids) or as thin films (liquids) between sodium chloride plates. Absorption maxima are reported in wavenumbers (cm^{-1}).

Elemental analyses were carried out by the University of St Andrews microanalytical laboratory.

Melting points were determined using Gallenkamp melting point apparatus and are uncorrected.

Thin layer chromatography was performed on 0.20 mm silica gel plates (60F 245) (Allied signal).

Flash chromatography was performed according to the procedure of Still *et al*. using sorbisil C60 (40-60 mm mesh) silica gel.[4]

Solvents were dried and purified according to the methods of Perrin and Armarego.[5]

7.4.2 Synthesis of N-substituted compounds

Synthesis of dimethyl quinolinate (38)

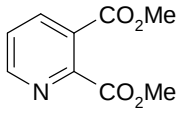

38

To a suspension of quinolinic acid (12.06 g, 72 mmol) in methanol (100 mL) was added concentrated sulfuric acid (12 mL), dropwise with stirring. Upon heating, quinolinic acid dissolved and the resulting solution was heated under reflux overnight. The reaction was quenched by pouring on to crushed ice. Concentrated ammonia solution was added until the solution was strongly alkaline (pH 10). The product was then extracted with diethyl ether (3 × 150 mL). The combined diethyl ether extracts were dried ($MgSO_4$) and the solvent was removed under reduced pressure to give a white solid (7.90 g). The crude product was recrystallised from methanol to give the pure product as a white crystalline solid (7.58 g, 54%); mp 55-56 °C (lit.[6] 52-53 °C); ν_{max} (nujol / cm^{-1}) 1760 (C=O stretch); δ_H (300 MHz; $CDCl_3$) 3.94 (3 H, s, CO_2CH_3), 4.01 (3 H, s, CO_2CH_3), 7.50 (1 H, dd, $J_{5,6}$ 5 and $J_{4,5}$ 8, H-5), 8.17 (1 H, dd, $J_{4,6}$ 2 and $J_{4,5}$ 8, H-4) and 8.77 (1 H, dd, $J_{4,6}$ 2 and $J_{5,6}$ 5, H-6); δ_C (75.46 MHz; $CDCl_3$) 53.4 ($CO_2\underline{C}H_3$), 53.5 ($CO_2\underline{C}H_3$), 125.5 (C-5), 126.9 (C-3), 138.0 (C-4), 151.1 (C-6), 152.2 (C-2), 166.2 ($\underline{C}O_2CH_3$) and 167.0 ($\underline{C}O_2CH_3$); *m/z* (ES^+) 218 ($(M+Na)^+$, 100%) and 196 ($(M+H)^+$, 8%).

Synthesis of N-methylquinolinic acid (41)

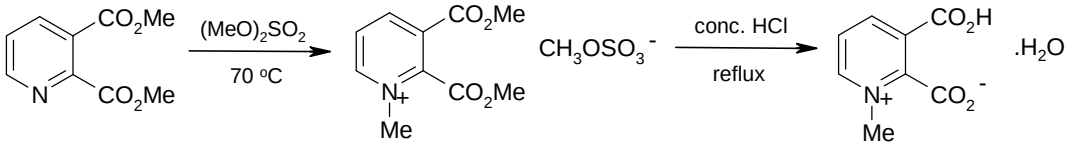

38 **39** **41**

Dimethyl sulfate (1.1 mL, 12 mmol) was added slowly, with stirring, to dimethyl quinolinate **38** (2.33 g, 12 mmol) and the reaction was heated at 70 °C for 2 hours under a nitrogen atmosphere. Upon cooling, the reaction mixture crystallised, forming a white solid. ^{1}H and ^{13}C NMR spectroscopy showed the reaction had reached completion and the desired product **39** had been formed exclusively. δ_H (300 MHz; $CDCl_3$) 3.60 (3 H, s, $CH_3OSO_3^-$), 3.97 (3 H, s, CO_2CH_3), 4.09 (3 H, s, CO_2CH_3), 4.50 (3 H, s, NCH_3), 8.42 (1 H, dd, $J_{5,6}$ 6 and $J_{4,5}$ 8, H-5), 9.00 (1 H, dd, $J_{4,6}$ 1 and $J_{4,5}$ 8, H-4) and 9.77 (1 H, dd, $J_{4,6}$ 1 and $J_{5,6}$ 6, H-6); δ_C (75.46 MHz; $CDCl_3$) 50.2 ($CH_3OSO_3^-$), 53.1 ($CO_2\underline{C}H_3$), 53.4 ($CO_2\underline{C}H_3$), 58.0 (NCH_3), 131.8 (C-5), 132.2 (C-3), 149.3 (C-4), 150.6 (C-6), 153.1 (C-2), 163.6 ($\underline{C}O_2CH_3$) and 165.1 ($\underline{C}O_2CH_3$).

The intermediate dimethyl *N*-methylquinolinate **39** (3.75 g) was then dissolved in concentrated hydrochloric acid (30 mL) and the resulting solution was heated under reflux (100 °C) for 3 hours. Excess hydrochloric acid was removed under reduced pressure to give a white solid. Recrystallisation from water gave the product **41** as white crystals (1.94 g, 81%, over 2 steps); mp 156-158 °C; (Found: C 48.55; H 4.60; N 7.02. Calc. For $C_8H_9NO_5$: C 48.25; H 4.55; N 7.02%); ν_{max} (nujol / cm^{-1}) 3000 (O─H stretch) and 1750 (C=O stretch); δ_H (300 MHz; D_2O) 4.36 (3 H, s, NCH_3), 8.15 (1 H, dd, $J_{5,6}$ 6 and $J_{4,5}$ 8, H-5), 9.03 (1 H, dd, $J_{4,6}$ 1 and $J_{4,5}$ 8, H-4) and 9.06 (1 H, dd, $J_{4,6}$ 1 and $J_{5,6}$ 6, H-6); δ_C (75.46 MHz; d_6-DMSO) 49.6 (NCH_3), 128.9 (C-5), 131.6 (C-3), 150.1 (C-4), 150.3 (C-6), 150.6 (C-2), 161.1 (CO_2H) and 161.9 (CO_2H); *m/z* (ES^+) 182 (M^+, 100%).

Synthesis of N-ethylquinolinic acid (42)

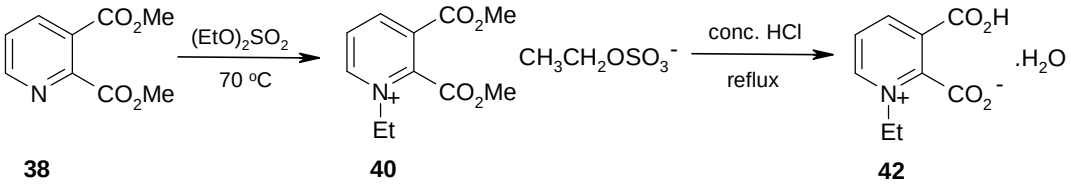

38 **40** **42**

Diethyl sulfate (1.5 mL, 12 mmol) was added slowly, with stirring, to dimethyl quinolinate **38** (2.33 g, 12 mmol) and the reaction was heated at 70 °C overnight under a nitrogen atmosphere. The reaction was then allowed to cool to room temperature. ^{1}H and ^{13}C NMR spectroscopy showed the reaction had reached completion and the desired product **40** had been formed exclusively. δ_H (300 MHz; $CDCl_3$) 1.26 (3 H, t, *J* 7, $C\underline{H}_3CH_2OSO_3^-$), 1.71 (3 H, t, *J* 8, $C\underline{H}_3CH_2N$), 3.98 (3 H, s, CO_2CH_3), 4.05 (3 H, s, CO_2CH_3), 4.10 (2 H, q, *J* 7, $CH_3C\underline{H}_2OSO_3^-$), 4.78 (2 H, q, *J* 8, $CH_3C\underline{H}_2N$), 8.55 (1 H, dd, $J_{5,6}$ 6 and $J_{4,5}$ 8, H-5), 9.10 (1 H, dd, $J_{4,6}$ 1 and $J_{4,5}$ 8, H-4) and 9.63 (1 H, dd, $J_{4,6}$ 1 and $J_{5,6}$ 6, H-6); δ_C (75.46 MHz; $CDCl_3$) 15.6 ($\underline{C}H_3CH_2OSO_3^-$), 17.6 ($\underline{C}H_3CH_2N$), 53.0 ($CO_2\underline{C}H_3$), 53.2 ($CO_2\underline{C}H_3$), 53.4 ($CH_3\underline{C}H_2OSO_3^-$), 65.6 ($CH_3\underline{C}H_2N$), 129.0 (C-5), 131.1 (C-3), 146.9 (C-4), 147.7 (C-6), 151.0 (C-2), 160.1 ($\underline{C}O_2CH_3$) and 161.1 ($\underline{C}O_2CH_3$).

The intermediate dimethyl *N*-ethylquinolinate **40** (4.10 g) was then dissolved in concentrated hydrochloric acid (30 mL) and the resulting solution was heated under reflux (100 °C) for 3 hours. Excess hydrochloric acid was removed under reduced pressure to produce a white solid. Recrystallisation from water gave the product **42** as white crystals (2.02 g, 79%, over 2 steps); mp 145-147 °C; (Found: C 50.89; H 5.03; N 6.47. Calc. For $C_9H_{11}NO_5$: C 50.71; H 5.20; N 6.57%); ν_{max} (nujol / cm^{-1}) 3020 (O─H stretch) and 1720 (C=O stretch); δ_H (300 MHz; D_2O) 1.50 (3 H, t, *J* 7, $NCH_2C\underline{H}_3$), 4.53 (2 H, q, *J* 7, $NC\underline{H}_2CH_3$), 7.96 (1 H, dd, $J_{5,6}$ 6 and $J_{4,5}$ 8, H-5), 8.85 (1 H, dd, $J_{4,6}$ 1 and $J_{4,5}$ 8, H-4) and 8.89 (1 H, dd, $J_{4,6}$ 1 and $J_{5,6}$ 6, H-6); δ_C (75.46 MHz; d_6-DMSO) 18.8 ($NCH_2\underline{C}H_3$), 58.6 ($N\underline{C}H_2CH_3$), 129.2 (C-5), 129.4 (C-3), 148.5 (C-4), 150.2 (C-6), 150.5 (C-2), 166.0 (CO_2H) and 166.7 (CO_2H); *m/z* (ES^+) 196 (M^+, 100%).

Synthesis of dimethyl 5-ethylquinolinate (44)[7]

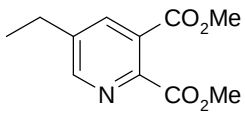

44

To a suspension of 5-ethylquinolinic acid (2.50 g, 13 mmol) in methanol (30 mL) was added concentrated sulfuric acid (3 mL), dropwise with stirring. The resulting solution was heated under reflux overnight. The solution was then cooled and poured on to crushed ice. Concentrated ammonia solution was added until the solution was strongly alkaline (pH 10). The product was then extracted with diethyl ether (3 × 60 mL). The combined diethyl ether extracts were dried ($MgSO_4$) and the solvent was removed under reduced pressure to give a yellow oil (1.60 g). The crude product was purified by column chromatography on silica with dichloromethane / ethyl acetate (4:1) as the eluting solvent. This gave the desired product as a colourless oil (1.38 g, 48%); ν_{max} (nujol / cm^{-1}) 1750 (C=O stretch); δ_H (300 MHz; $CDCl_3$) 1.28 (3H, t, *J* 8, $C\underline{H}_3CH_2$), 2.74 (2 H, q, *J* 8, $CH_3C\underline{H}_2$), 3.91 (3 H, s, CO_2CH_3), 3.97 (3 H, s, CO_2CH_3), 7.92 (1 H, d, $J_{4,6}$ 2, H-4) and 8.56 (1 H, d, $J_{4,6}$ 2, H-6); δ_C (75.46 MHz; $CDCl_3$) 15.2 ($\underline{C}H_3CH_2$), 26.1 ($CH_3\underline{C}H_2$), 53.3 ($CO_2\underline{C}H_3$), 53.4 ($CO_2\underline{C}H_3$), 127.4 (C-5), 136.8 (C-3), 141.9 (C-4), 147.8 (C-6), 151.7 (C-2), 166.8 ($\underline{C}O_2CH_3$) and 166.9 ($\underline{C}O_2CH_3$); *m/z* (ES^+) 246 ($(M+Na)^+$, 100%) and 224 ($(M+H)^+$, 8%).

Synthesis of 5-ethyl-N-methylquinolinic acid (46)

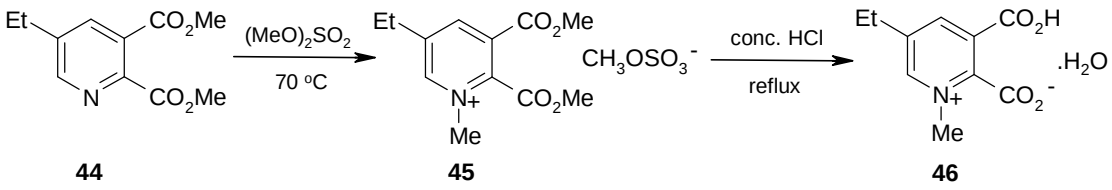

44 **45** **46**

Dimethyl sulfate (0.4 mL, 4.5 mmol) was added slowly, with stirring, to dimethyl 5-ethylquinolinate **44** (1.00 g, 4.5 mmol) and the reaction was heated at 70 °C overnight under a nitrogen atmosphere. The reaction was then allowed to cool to room temperature. ^{1}H and ^{13}C NMR spectroscopy showed the reaction had reached completion and the desired product **45** had been formed exclusively. δ_H (300 MHz; $CDCl_3$) 1.19 (3H, t, *J* 8, $C\underline{H}_3CH_2$), 2.83 (2 H, q, *J* 8, $CH_3C\underline{H}_2$), 3.59 (3H, s, $CH_3OSO_3^-$), 3.89 (3 H, s, CO_2CH_3), 4.01 (3 H, s, CO_2CH_3), 4.23 (3 H, s, NCH_3), 8.85 (1 H, d, $J_{4,6}$ 2, H-4) and 8.89 (1 H, d, $J_{4,6}$ 2, H-6); δ_C (75.46 MHz; $CDCl_3$) 13.6 ($\underline{C}H_3CH_2$), 25.8 ($CH_3\underline{C}H_2$), 47.0 ($CH_3OSO_3^-$), 54.6 ($CO_2\underline{C}H_3$), 55.6 ($CO_2\underline{C}H_3$), 56.7 (NCH_3), 128.8 (C-5), 136.2 (C-3), 146.7 (C-4), 147.1 (C-6), 149.3 (C-2), 161.9 ($\underline{C}O_2CH_3$) and 163.3 ($\underline{C}O_2CH_3$).

The intermediate dimethyl 5-ethyl-*N*-methylquinolinate **45** (1.50 g) was then dissolved in concentrated hydrochloric acid (20 mL) and the resulting solution was heated under reflux (100 °C) for 3 hours. Excess hydrochloric acid was removed under reduced pressure to give a white solid. Recrystallisation from water gave the product **46** as white crystals (0.91 g, 89%, over 2 steps); mp 177-179 °C; (Found: C 52.98; H 5.70; N 6.07. Calc. For $C_{10}H_{13}NO_5$: C 52.86; H 5.73; N 6.17%); ν_{max} (nujol / cm^{-1}) 3000 (O─H stretch) and 1710 (C=O stretch); δ_H (300 MHz; D_2O) 1.15 (3H, t, *J* 8, $C\underline{H}_3CH_2$), 2.74 (2 H, q, *J* 8, $CH_3C\underline{H}_2$), 4.14 (3 H, s, NCH_3), 8.59 (1 H, d, $J_{4,6}$ 2, H-4) and 8.72 (1 H, d, $J_{4,6}$ 2, H-6); δ_C (75.46 MHz; d_6-DMSO) 13.7 ($\underline{C}H_3CH_2$), 25.4 ($CH_3\underline{C}H_2$), 46.3 (NCH_3), 127.5 (C-5), 137.0 (C-3), 143.8 (C-4), 147.1 (C-6), 151.3 (C-2), 165.3 ($\underline{C}O_2CH_3$) and 165.8 ($\underline{C}O_2CH_3$); *m/z* (ES^+) 210 (M^+, 100%).

Synthesis of methyl picolinate (47)[8]

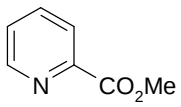

47

To a suspension of picolinic acid (8.85 g, 72 mmol) in methanol (100 mL) was added concentrated sulfuric acid (12 mL), dropwise with stirring. Upon heating, picolinic acid dissolved and the resulting solution was heated under reflux overnight. The reaction was quenched by pouring on to crushed ice. Concentrated ammonia solution was added until the solution was strongly alkaline (pH 10). The product was then extracted with diethyl ether (3 × 150 mL). The combined diethyl ether extracts were dried ($MgSO_4$) and the solvent was removed under reduced pressure to give a yellow oil (7.03 g). The crude product was purified by column chromatography on silica with dichloromethane / ethyl acetate (4:1) as the eluting solvent. This gave the desired product as a colourless oil (6.80g, 69%); ν_{max} (nujol / cm^{-1}) 1710 (C=O stretch); δ_H (300 MHz; CD_3OD) 3.58 (3 H, s, CO_2CH_3), 7.20 (1 H, ddd, $J_{3,5}$ 1.5, $J_{5,6}$ 5 and $J_{4,5}$ 8, H-5), 7.48 (1 H, td, $J_{4,6}$ 2 and $J_{3,4} = J_{4,5}$ 8, H-4), 7.53 (1 H, ddd, $J_{3,6}$ 1, $J_{3,5}$ 1.5 and $J_{3,4}$ 8, H-3) and 7.97 (1 H, ddd, $J_{3,6}$ 1, $J_{4,6}$ 2 and $J_{5,6}$ 5, H-6); δ_C (75.46 MHz; $CDCl_3$) 52.9 ($CO_2\underline{C}H_3$), 128.9 (C-5), 129.7 (C-3), 138.0 (C-4), 151.1 (C-6), 152.2 (C-2) and 167.0 ($\underline{C}O_2CH_3$); *m/z* (ES^+) 160 ($(M+Na)^+$, 100%) and 138 ($(M+H)^+$, 10%).

Synthesis of N-methylpicolinic acid (50)

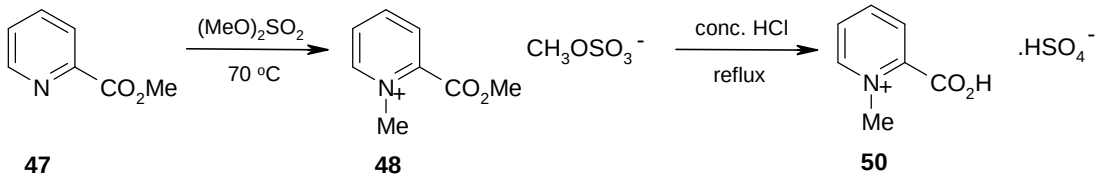

47 **48** **50**

Dimethyl sulfate (1.1 mL, 12 mmol) was added slowly, with stirring, to methyl picolinate **47** (1.64 g, 12 mmol) and the reaction was heated at 70 °C for 6 hours under a nitrogen atmosphere. Upon cooling, the reaction mixture crystallised, forming a white solid. ^{1}H and ^{13}C NMR spectroscopy showed the reaction had reached completion and the desired product **48** had been formed exclusively. δ_H (300 MHz; $CDCl_3$) 3.49 (3 H, s, $CH_3OSO_3^-$), 4.11 (3 H, s, CO_2CH_3), 4.60 (3 H, s, NCH_3), 7.38-7.40 (1 H, m, H-5), 7.73 (1 H, dd, $J_{3,5}$ 1 and $J_{3,4}$ 8, H-3), 8.04 (1 H, td, $J_{4,6}$ 1 and $J_{3,4} = J_{4,5}$ 8, H-4) and 8.65 (1 H, dd, $J_{4,6}$ 1 and $J_{5,6}$ 6, H-6); δ_C (75.46 MHz; $CDCl_3$) 49.1 ($CH_3OSO_3^-$), 53.1 ($CO_2\underline{C}H_3$), 54.0 (NCH_3), 130.3 (C-5), 130.8 (C-3), 142.5 (C-4), 147.2 (C-6), 150.0 (C-2) and 159.6 ($\underline{C}O_2CH_3$).

The intermediate methyl *N*-methylpicolinate **48** (3.10 g) was then dissolved in concentrated hydrochloric acid (25 mL) and the resulting solution was heated under reflux (100 °C) for 2 hours. Excess hydrochloric acid was removed under reduced pressure to give a white solid. Recrystallisation from methanol gave the product **50** as white crystals (2.59 g, 92%, over 2 steps); mp 169-172 °C (lit.[9] 170-173 °C); (Found: C 35.64; H 3.74; N 5.91. Calc. For $C_7H_9NSO_6$: C 35.74; H 3.85; N 5.95%); ν_{max} (nujol / cm^{-1}) 3050 (O─H stretch) and 1760 (C=O stretch); δ_H (300 MHz; D_2O) 4.24 (3 H, s, NCH_3), 7.83-7.86 (1 H, m, H-5), 7.99 (1 H, dd, $J_{3,5}$ 1 and $J_{3,4}$ 8, H-3), 8.39 (1 H, td, $J_{4,6}$ 1 and $J_{3,4} = J_{4,5}$ 8, H-4) and 8.59 (1 H, dd, $J_{4,6}$ 1 and $J_{5,6}$ 6, H-6); δ_C (75.46 MHz; d_6-DMSO) 50.7 (NCH_3), 131.6 (C-5), 132.0 (C-3), 147.5 (C-4), 149.1 (C-6), 150.5 (C-2) and 164.9 (CO_2H); *m/z* (ES^+) 138 (M^+, 100%).

Synthesis of N-ethylpicolinic acid (51)

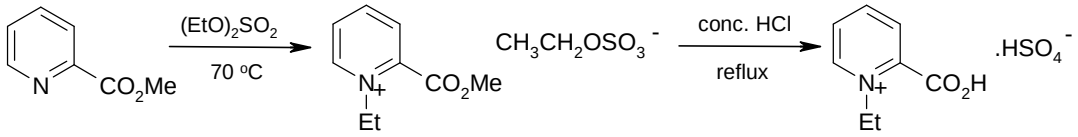

47 **49** **51**

Diethyl sulfate (1.5 mL, 12 mmol) was added slowly, with stirring, to methyl picolinate **47** (1.64 g, 12 mmol) and the reaction was heated at 70 °C overnight under a nitrogen atmosphere. The reaction was then allowed to cool to room temperature. ^{1}H and ^{13}C NMR spectroscopy showed the reaction had reached completion and the desired product **49** had been formed exclusively. δ_H (300 MHz; $CDCl_3$) 1.47 (3 H, t, *J* 8, $C\underline{H}_3CH_2OSO_3^-$), 1.68 (3 H, t, *J* 8, $C\underline{H}_3CH_2N$), 3.97 (3 H, s, CO_2CH_3), 4.54 (2 H, q, *J* 8, $CH_3C\underline{H}_2OSO_3^-$), 5.06 (2 H, q, *J* 8, $CH_3C\underline{H}_2N$), 8.38-8.41 (1 H, m, H-5), 8.47 (1 H, dd, $J_{3,5}$ 1 and $J_{3,4}$ 8, H-3), 8.76 (1 H, td, $J_{4,6}$ 1 and $J_{3,4} = J_{4,5}$ 8, H-4) and 9.50 (1 H, dd, $J_{4,6}$ 1 and $J_{5,6}$ 6, H-6); δ_C (75.46 MHz; $CDCl_3$) 15.4 ($\underline{C}H_3CH_2OSO_3^-$), 17.4 ($\underline{C}H_3CH_2N$), 53.1 ($CO_2\underline{C}H_3$), 58.5 ($CH_3\underline{C}H_2OSO_3^-$), 65.1 ($CH_3\underline{C}H_2N$), 131.1 (C-5), 132.0 (C-3), 142.5 (C-4), 147.8 (C-6), 149.3 (C-2) and 159.9 ($\underline{C}O_2CH_3$).

The intermediate methyl *N*-ethylpicolinate **49** (3.40 g) was then dissolved in concentrated hydrochloric acid (25 mL) and the resulting solution was heated under reflux (100 °C) for 2 hours. Excess hydrochloric acid was removed under reduced pressure to give a white solid. Recrystallisation from methanol gave the product **51** as white crystals (2.00 g, 67%, over 2 steps); 230-232 °C; (Found: C 38.45; H 4.52; N 5.66. Calc. For $C_8H_{11}NSO_6$: C 38.55; H 4.42; N 5.62%); ν_{max} (nujol / cm^{-1}) 3000 (O─H stretch) and 1720 (C=O stretch); δ_H (300 MHz; D_2O) 1.42 (3 H, t, *J* 7, $NCH_2C\underline{H}_3$), 4.58 (2 H, q, *J* 7, $NC\underline{H}_2CH_3$) 7.84-7.87 (1 H, m, H-5), 7.92 (1 H, dd, $J_{3,5}$ 1 and $J_{3,4}$ 8, H-3), 8.37 (1 H, td, $J_{4,6}$ 1 and $J_{3,4} = J_{4,5}$ 8, H-4) and 8.64 (1 H, dd, $J_{4,6}$ 1 and $J_{5,6}$ 6, H-6); δ_C (75.46 MHz; d_6-DMSO) 18.6 ($\underline{C}H_3CH_2N$), 58.6 ($CH_3\underline{C}H_2N$), 130.8 (C-5), 131.5 (C-3), 148.3 (C-4), 149.0 (C-6), 150.9 (C-2) and 166.6 (CO_2H); *m/z* (ES^+) 152 (M^+, 100%).

Synthesis of methyl quinoline-2-carboxylate (53)

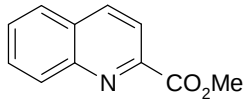

53

To a suspension of quinoline-2-carboxylic acid (5.00 g, 29 mmol) in methanol (40 mL) was added concentrated sulfuric acid (4 mL), dropwise with stirring. The resulting solution was heated under reflux overnight. The solution was then cooled and poured on to crushed ice. Upon addition of concentrated ammonia solution, a white solid precipitated from solution and was collected by filtration. The crude product was recrystallised from methanol to give the pure product as a white crystalline solid (4.50 g, 83%); mp 81-83 °C (lit.[10] 78 °C); ν_{max} (nujol / cm^{-1}) 1740 (C=O stretch); δ_H (300 MHz; $CDCl_3$) 4.03 (3 H, s, CO_2CH_3), 7.56-7.63 (1 H, m, H-6), 7.70-7.77 (1 H, m, H-7), 8.14 (1 H, d, $J_{3,4}$ 8, H-3), 8.20 (1 H, dd, $J_{5,7}$ 1.5 and $J_{5,6}$ 8, H-5), 8.26 (1 H, dd, $J_{6,8}$ 1.5 and $J_{7,8}$ 8, H-8) and 8.42 (1 H, d, $J_{3,4}$ 8, H-4); δ_C (75.46 MHz; $CDCl_3$) 53.3 ($CO_2\underline{C}H_3$), 121.0 (C-3), 127.6 (C-6), 128.7 (C-5), 129.4 (C-4a), 130.4 (C-8), 130.7 (C-7), 137.4 (C-4), 147.5 (C-8a), 147.9 (C-2) and 165.9 ($\underline{C}O_2CH_3$); *m/z* (ES^+) 210 ($(M+Na)^+$, 100%) and 188 ($(M+H)^+$, 10%).

Synthesis of N-methylquinoline-2-carboxylic acid (55)[11]

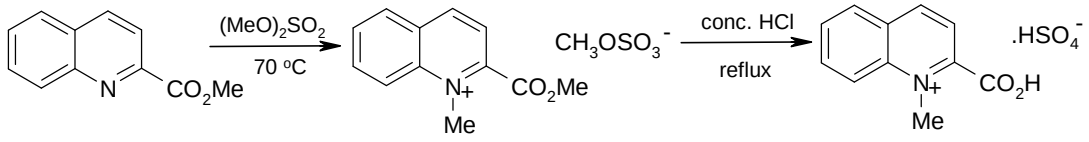

53 **54** **55**

Dimethyl sulfate (1.0 mL, 10.7 mmol) was added slowly, with stirring, to methyl quinoline-2-carboxylate **53** (2.00 g, 10.7 mmol) and the reaction was heated at 70 °C overnight under a nitrogen atmosphere. The reaction was then allowed to cool to room temperature. ^{1}H and ^{13}C NMR spectroscopy showed the reaction had reached completion and the desired product **54** had been formed exclusively. δ_H (300 MHz; $CDCl_3$) 3.27 (3 H, s, $CH_3OSO_3^-$), 3.55 (3 H, s, CO_2CH_3), 4.40 (3 H, s, NCH_3), 7.80-7.85 (1 H, m, H-6), 8.00-8.06 (1 H, m, H-7), 8.18 (1 H, d, $J_{3,4}$ 8, H-3), 8.20-8.28 (2 H, m, H-5 and H-8) and 8.50 (1 H, d, $J_{3,4}$ 8, H-4); δ_C (75.46 MHz; $CDCl_3$) 48.8 ($CH_3OSO_3^-$), 54.6 ($CO_2\underline{C}H_3$), 55.3 (NCH_3), 121.3 (C-3), 129.0 (C-6), 130.6 (C-5), 130.9 (C-4a), 136.2 (C-8), 138.6 (C-7), 141.1 (C-4), 148.3 (C-8a), 149.2 (C-2) and 165.4 ($\underline{C}O_2CH_3$).

The intermediate methyl *N*-methylquinoline-2-carboxylate **54** (3.20 g) was then dissolved in concentrated hydrochloric acid (25 mL) and the resulting solution was heated under reflux (100 °C) for 3 hours. Excess hydrochloric acid was removed under reduced pressure to give a yellow solid. Recrystallisation from methanol gave the product **55** as white crystals (1.89 g, 62%, over 2 steps); mp 105-107 °C; (Found: C 46.47; H 3.91; N 4.83. Calc. For $C_{11}H_{11}NSO_6$: C 46.32; H 3.86; N 4.91%); ν_{max} (nujol / cm^{-1}) 3050 (O─H stetch) and 1720 (C=O stretch); δ_H (300 MHz; D_2O) 4.35 (3 H, s, NCH_3), 7.75-7.87 (1 H, m, H-6), 7.98-8.07 (1 H, m, H-7), 8.17 (1 H, d, $J_{3,4}$ 8, H-3), 8.20-8.29 (2 H, m, H-5 and H-8) and 8.54 (1 H, d, $J_{3,4}$ 8, H-4); δ_C (75.46 MHz; d_6-DMSO) 47.9 (NCH_3), 120.7 (C-3), 129.0 (C-6), 130.8 (C-5), 131.2 (C-4a), 136.0 (C-8), 138.8 (C-7), 141.2 (C-4), 147.8 (C-8a), 148.4 (C-2) and 166.0 ($\underline{C}O_2H$); *m/z* (ES^+) 188 (M^+, 100%).

Synthesis of methyl nicotinate (56)

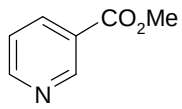

56

To a suspension of nicotinic acid (8.85 g, 72 mmol) in methanol (100 mL) was added concentrated sulfuric acid (12 mL), dropwise with stirring. Upon heating, nicotinic acid dissolved and the resulting solution was heated under reflux overnight. The reaction was quenched by pouring on to crushed ice. Concentrated ammonia solution was added until the solution was strongly alkaline (pH 10). The product was then extracted with diethyl ether (3 × 150 mL). The combined diethyl ether extracts were dried ($MgSO_4$) and the solvent was removed under reduced pressure to give an off-white solid (7.93 g). The crude product was recrystallised from methanol to give the pure product as a white crystalline solid (7.49 g, 76%); mp 40-43 °C (lit.[12] 37-39 °C); ν_{max} (nujol / cm^{-1}) 1720 (C=O stretch); δ_H (300 MHz; $CDCl_3$) 3.84 (3 H, s, CO_2CH_3), 7.43 (1 H, ddd, $J_{2,5}$ 1, $J_{5,6}$ 6 and $J_{4,5}$ 8, H-5), 8.19 (1 H, ddd, $J_{4,6}$ 1.5, $J_{2,4}$ 2 and $J_{4,5}$ 8, H-4), 8.47 (1 H, dd, $J_{4,6}$ 1.5 and $J_{5,6}$ 6, H-6) and 8.85 (1 H, dd, $J_{2,5}$ 1 and $J_{2,4}$ 2, H-2); δ_C (75.46 MHz; $CDCl_3$) 52.4 ($CO_2\underline{C}H_3$), 128.3 (C-5), 130.7 (C-3), 139.1 (C-4), 149.0 (C-6), 151.5 (C-2) and 164.1 ($\underline{C}O_2CH_3$); *m/z* (ES^+) 160 ($(M+Na)^+$, 100%) and 138 ($(M+H)^+$, 8%).

Synthesis of N-methylnicotinic acid (59)

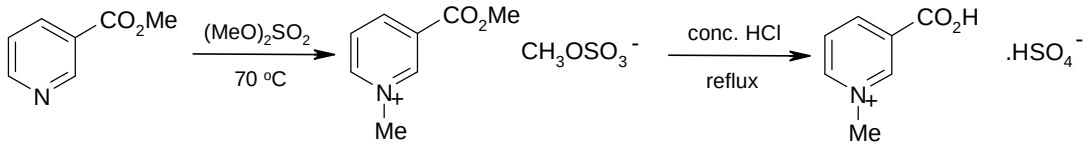

56 **57** **59**

Dimethyl sulfate (1.1 mL, 12 mmol) was added slowly, with stirring, to methyl nicotinate **56** (1.64 g, 12 mmol) and the reaction was heated at 70 °C for 6 hours under a nitrogen atmosphere. Upon cooling, the reaction mixture crystallised, forming a white solid. ^{1}H and ^{13}C NMR spectroscopy showed the reaction had reached completion and the desired product **57** had been formed exclusively. δ_H (300 MHz; $CDCl_3$) 3.29 (3 H, s, $CH_3OSO_3^-$), 4.24 (3 H, s, CO_2CH_3), 4.38 (3 H, s, NCH_3), 8.08 (1 H, ddd, $J_{2,5}$ 1, $J_{5,6}$ 6 and $J_{4,5}$ 8, H-5), 8.73 (1 H, ddd, $J_{4,6}$ 1.5, $J_{2,4}$ 2 and $J_{4,5}$ 8, H-4), 8.97 (1 H, dd, $J_{4,6}$ 1.5 and $J_{5,6}$ 6, H-6) and 9.19 (1 H, dd, $J_{2,5}$ 1 and $J_{2,4}$ 2, H-2); δ_C (75.46 MHz; $CDCl_3$) 49.5 ($CH_3OSO_3^-$), 53.4 ($CO_2\underline{C}H_3$), 54.6 (NCH_3), 128.9 (C-5), 130.7 (C-3), 145.1 (C-4), 147.0 (C-6), 149.5 (C-2) and 162.1 ($\underline{C}O_2CH_3$).

The intermediate methyl *N*-methylnicotinate **57** (3.10 g) was then dissolved in concentrated hydrochloric acid (25 mL) and the resulting solution was heated under reflux (100 °C) for 2 hours. Excess hydrochloric acid was removed under reduced pressure to give a white solid. Recrystallisation from methanol gave the product **59** as white crystals (2.54 g, 90%, over 2 steps); mp 166-168 °C; (Found: C 36.14; H 3.90; N 6.00. Calc. For $C_7H_9NSO_6$: C 35.74; H 3.85; N 5.95%); ν_{max} (nujol / cm^{-1}) 3050 (O─H stretch) and 1760 (C=O stretch); δ_H (300 MHz; D_2O) 4.32 (3 H, s, NCH_3), 8.02 (1 H, dd, $J_{5,6}$ 6 and $J_{4,5}$ 8, H-5), 8.81-8.86 (2 H, m, H-4 and H-6) and 9.22 (1 H, br s, H-2); δ_C (75.46 MHz; d_6-DMSO) 51.3 (NCH_3), 130.9 (C-5), 147.7 (C-3), 148.3 (C-4), 149.5 (C-6), 150.8 (C-2) and 164.2 (CO_2H); *m/z* (ES^+) 138 (M^+, 100%).

Synthesis of N-ethylnicotinic acid (60)

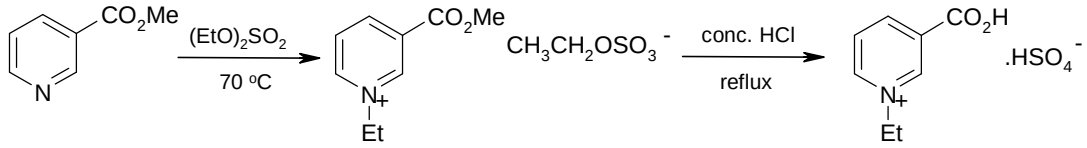

56 **58** **60**

Diethyl sulfate (1.5 mL, 12 mmol) was added slowly, with stirring, to methyl nicotinate **56** (1.64 g, 12 mmol) and the reaction was heated at 70 °C overnight under a nitrogen atmosphere. The reaction was then allowed to cool to room temperature. ^{1}H and ^{13}C NMR spectroscopy showed the reaction had reached completion and the desired product **58** had been formed exclusively. δ_H (300 MHz; $CDCl_3$) 1.21 (3 H, t, *J* 8, $C\underline{H}_3CH_2OSO_3^-$), 1.68 (3 H, t, *J* 8, $C\underline{H}_3CH_2N$), 3.97 (3 H, s, CO_2CH_3), 4.03 (2 H, q, *J* 8, $CH_3C\underline{H}_2OSO_3^-$), 4.88 (2 H, q, *J* 8, $CH_3C\underline{H}_2N$), 8.27 (1 H, ddd, $J_{2,5}$ 1, $J_{5,6}$ 6 and $J_{4,5}$ 8, H-5), 8.90 (1 H, ddd, $J_{4,6}$ 1.5, $J_{2,4}$ 2 and $J_{4,5}$ 8, H-4), 9.33 (1 H, dd, $J_{4,6}$ 1.5 and $J_{5,6}$ 6, H-6) and 9.36 (1 H, dd, $J_{2,5}$ 1 and $J_{2,4}$ 2, H-2); δ_C (75.46 MHz; $CDCl_3$) 15.7 ($\underline{C}H_3CH_2OSO_3^-$), 17.4 ($NCH_2\underline{C}H_3$), 53.5 ($CO_2\underline{C}H_3$), 58.8 ($CH_3\underline{C}H_2OSO_3^-$), 63.8 ($N\underline{C}H_2CH_3$), 129.6 (C-5), 131.5 (C-3), 145.4 (C-4), 145.9 (C-6), 149.2 (C-2) and 161.7 ($\underline{C}O_2CH_3$).

The intermediate methyl *N*-ethylnicotinate **58** (3.40 g) was then dissolved in concentrated hydrochloric acid (25 mL) and the resulting solution was heated under reflux (100 °C) for 2 hours. Excess hydrochloric acid was removed under reduced pressure to give a white solid. Recrystallisation from methanol gave the product **60** as white crystals (2.15 g**,** 72%, over 2 steps); mp 234-236 °C; (Found: C 38.46; H 4.51; N 5.67. Calc. For $C_8H_{11}NSO_6$: C 38.55; H 4.42; N 5.62%); ν_{max} (nujol / cm^{-1}) 3000 (O─H stretch) and 1730 (C=O stretch); δ_H (300 MHz; D_2O) 1.49 (3 H, t, *J* 7, $NCH_2C\underline{H}_3$), 4.54 (2 H, q, *J* 7, $NC\underline{H}_2CH_3$), 8.05 (1 H, dd, $J_{5,6}$ 6 and $J_{4,5}$ 8, H-5), 8.85-8.89 (2 H, m, H-4 and H-6) and 9.19 (1 H, br s, H-2); δ_C (75.46 MHz; d_6-DMSO) 18.3 ($NCH_2\underline{C}H_3$), 60.6 ($N\underline{C}H_2CH_3$), 131.2 (C-5), 134.0 (C-3), 148.0 (C-4), 148.4 (C-6), 149.8 (C-2) and 167.1 (CO_2H); *m/z* (ES^+) 152 (M^+, 100%).

Attempted synthesis of quinolinic acid N-oxide (62)

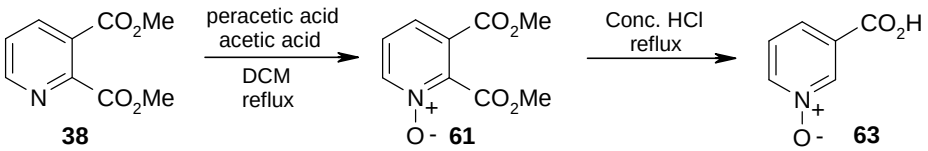

Peroxyacetic acid (15 mL of a 32 wt% solution in dilute acetic acid, 63 mmol) was added to dichloromethane (40 mL) and the solution was stirred at 0 °C. To this solution was added a solution of dimethyl quinolinate **38** (1.00g, 5 mmol) in dichloromethane (10 mL) dropwise, with stirring. The resulting solution was allowed to slowly warm to room temperature and was then heated under reflux for 6 hours. The reaction was then cooled to room temperature and the solvent was removed under reduced pressure to give a colourless oil. To the residue was added dichloromethane (50 mL) followed by water (50 mL). The organic layer was washed with water (50 mL), dried ($MgSO_4$) and the solvent was removed under reduced pressure to give a white solid. Recrystallisation from methanol gave the desired product **61** as a white solid (0.25 g, 24%); mp 141-143 °C (lit.[13] (140-141 °C); ν_{max} (nujol/cm^{-1}) 1760 (C=O stretch) and 1300 (N^+—O^- stretch); δ_H (300 MHz; $CDCl_3$) 3.88 (3 H, s, CO_2CH_3), 3.99 (3 H, s, CO_2CH_3), 7.35 (1 H, dd, $J_{5,6}$ 6 and $J_{4,5}$ 8, H-5), 7.82 (1 H, dd, $J_{4,6}$ 1 and $J_{4,5}$ 8, H-4) and 8.30 (1 H, dd, $J_{4,6}$ 1 and $J_{5,6}$ 6, H-6); δ_C (75.46 MHz; d_6-DMSO) 54.6 ($CO_2\underline{C}H_3$), 55.6 ($CO_2\underline{C}H_3$), 127.4 (C-5), 129.7 (C-3), 132.7 (C-4), 141.6 (C-6), 143.0 (C-2), 161.8 ($\underline{C}O_2CH_3$) and 163.9 ($\underline{C}O_2CH_3$); *m/z* (ES^+) 212 ($(M+H)^+$, 100%).

A solution of dimethyl quinolinate *N*-oxide **61** (0.14 g, 0.7 mmol) in concentrated hydrochloric acid (10 mL) was heated under reflux for 6 hours. The excess hydrochloric acid was removed under reduced pressure. The product was recrystallised from water to give a white solid (85 mg, 88%). The product was identified as nicotinic acid *N*-oxide **63**; mp 249-252 °C (dec.) (lit.[14] 249 °C (dec.)); ν_{max} (nujol / cm^{-1}) 3000 (O—H stretch), 1720 (C=O stretch) and 1295 (N^+—O^- stretch); δ_H (300 MHz; D_2O) 7.62 (1 H, ddd, $J_{2,5}$ 1, $J_{5,6}$ 6 and $J_{4,5}$ 8, H-5), 8.18 (1 H, ddd, $J_{4,6}$ 1.5, $J_{2,4}$ 2 and $J_{4,5}$ 8, H-4), 8.42 (1 H, dd, $J_{4,6}$ 1.5 and $J_{5,6}$ 6, H-6) and 8.75 (1 H, dd, $J_{2,5}$ 1 and $J_{2,4}$ 2, H-2); δ_C (75.46 MHz; d_6-DMSO) 127.5 (C-5), 131.2 (C-3), 139.5 (C-4), 142.1 (C-6), 142.5 (C-2) and 164.2 (CO_2H); *m/z* (ES^+) 140 ($(M+H)^+$, 100%).

Synthesis of quinolinic acid N-oxide (62)

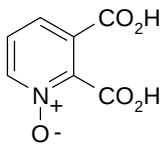

62

A mixture of quinolinic acid (0.50 g, 3 mmol) and peroxyacetic acid (10 mL of a 32 wt% solution in dilute acetic acid, 42 mmol) was gently heated. Upon heating, quinolinic acid dissolved and the resulting solution was heated at 60 °C. After 4 hours, a white precipitate began to separate. The reaction was heated at 60 °C for a further 2 hours and was then allowed to cool to room temperature. The white precipitate was collected by suction filtration. Recrystallisation from water gave the desired product **62** as a white solid (0.16 g, 30%); mp 263-265 °C (dec.) (lit.[15] mp 260-262 °C (dec.)); (Found: C 45.95; H 2.75; N 7.70. Calc. For $C_7H_5NO_5$: C 45.90; H 2.73; N 7.65%); ν_{max} (nujol / cm^{-1}) 3000 (O─H stretch), 1730 (C=O stretch) and 1250 (N^+─O^- stretch); δ_H (300 MHz; D_2O) 7.58 (1 H, dd, $J_{5,6}$ 6 and $J_{4,5}$ 8, H-5), 8.16 (1 H, dd, $J_{4,6}$ 1 and $J_{4,5}$ 8, H-4) and 8.38 (1 H, dd, $J_{4,6}$ 1 and $J_{5,6}$ 6, H-6); δ_C (75.46 MHz; d_6-DMSO) 126.4 (C-5), 126.7 (C-3), 127.8 (C-4), 142.0 (C-6), 143.3 (C-2), 162.0 (CO_2H) and 163.9 (CO_2H); *m/z* (ES^+) 184 ($(M+H)^+$, 100%).

Attempted synthesis of N-(2-hydroxyethyl)quinolinic acid (64)

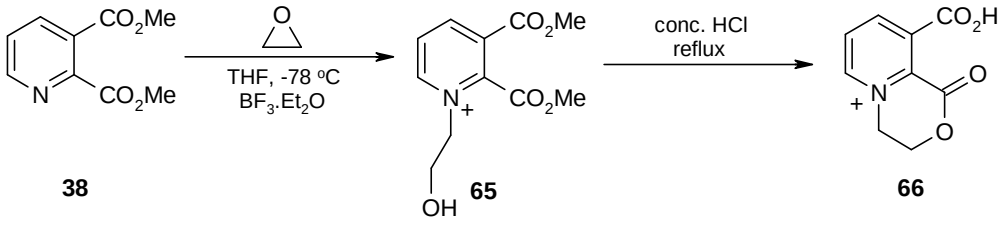

38 **65** **66**

To a solution of dimethyl quinolinate **38** (1.28 g, 6.6 mmol) in dry tetrahydrofuran (20 mL) was added boron trifluoride diethyl etherate (2.5 mL, 20 mmol). The resulting solution was cooled to -78 °C and ethylene oxide (0.5 g, 11.4 mmol) was swiftly decanted to the flask. After stirring at -78 °C under a nitrogen bubbler for 2 hours, the reaction was allowed to slowly warm to room temperature overnight. The solvent was removed under reduced pressure. Water (50 mL) was added to the residue and the insoluble white solid was removed by filtration. The water was removed under reduced pressure to give a pale yellow solid (1.32 g, 82%); δ_H (300 MHz; D_2O) 3.38 (2 H, t, *J* 7, CH_2), 3.82 (3 H, s, CO_2CH_3), 3.87 (3 H, s, CO_2CH_3), 4.05 (2 H, t, *J* 7, CH_2O), 7.62 (1 H, dd, $J_{5,6}$ 5 and $J_{4,5}$ 8, H-5), 8.20 (1 H, dd, $J_{4,6}$ 1.5 and $J_{4,5}$ 8, H-4) and 8.60 (1 H, dd, $J_{4,6}$ 1.5 and $J_{5,6}$ 5, H-6); δ_C (75.46 MHz; d_6-DMSO) 51.2 ($CO_2\underline{C}H_3$), 52.7 ($CO_2\underline{C}H_3$), 60.8 (CH_2), 62.4 (CH_2), 126.8 (C-5), 129.2 (C-3), 145.9 (C-4), 149.0 (C-6), 151.7 (C-2), 158.6 ($\underline{C}O_2CH_3$) and 161.1 ($\underline{C}O_2CH_3$); *m/z* (ES^+) 240 (M^+, 100%).

A solution of dimethyl *N*-(2-hydroxyethyl)quinolinate **65** (1.20 g) in concentrated hydrochloric acid (20 mL) was heated under reflux for 6 hours. The reaction was then cooled to room temperature and the excess hydrochloric acid was removed under reduced pressure to give a pale brown solid (0.95 g). All attempts to purify the product failed. The product was identified as the bicyclic compound **66**; δ_H (300 MHz; D_2O) 3.45 (2 H, t, *J* 7, CH_2), 4.10 (2 H, t, *J* 7, CH_2), 7.97 (1 H, dd, $J_{5,6}$ 5 and $J_{4,5}$ 8, H-5), 8.70 (1 H, dd, $J_{4,6}$ 1.5 and $J_{4,5}$ 8, H-4) and 8.74 (1 H, dd, $J_{4,6}$ 1.5 and $J_{5,6}$ 5, H-6); δ_C (75.46 MHz; d_6-DMSO) 57.7 (CH_2), 58.9 (CH_2), 127.0 (C-5), 130.3 (C-3), 148.2 (C-4), 149.5 (C-6), 152.4 (C-2), 157.8 (C=O) and 163.0 (CO_2H); *m/z* (ES^+) 194 (M^+, 100%).

7.4.3 Routes to 4-substituted quinolinic acid derivatives

7.4.3.1 Route 1 – Directed ortho-metalation

Synthesis of diisopropyl quinolinate (69)[16]

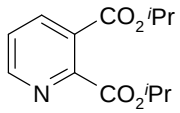

69

To a suspension of quinolinic acid (4.98 g, 29.8 mmol) in isopropanol (40 mL) was added concentrated sulfuric acid (6 mL), dropwise with stirring. Upon heating, quinolinic acid dissolved and the resulting solution was heated under reflux overnight. The solution was then cooled and poured on to crushed ice. Concentrated ammonia solution was added until the solution was strongly alkaline (pH 10). The product was then extracted with diethyl ether (3 × 100 mL). The combined diethyl ether extracts were dried ($MgSO_4$) and the solvent was removed under reduced pressure to give a yellow oil (3.46 g). The crude product was purified by column chromatography on silica with dichloromethane / ethyl acetate (4:1) as the eluting solvent. This gave the desired product as a colourless oil (3.02 g, 40%); ν_{max} (nujol / cm^{-1}) 1740 (C=O stretch); δ_H (300 MHz; CD_3OD) 1.36 (6 H, d, *J* 5, 2 × CH_3), 1.39 (6 H, d, *J* 5, 2 × CH_3), 5.17-5.31 (2 H, m, 2 × C<u>H</u>$(CH_3)_2$), 7.63 (1 H, dd, $J_{5,6}$ 5 and $J_{4,5}$ 8, H-5), 8.28 (1 H, dd, $J_{4,6}$ 1.5 and $J_{4,5}$ 8, H-4) and 8.72 (1 H, dd, $J_{4,6}$ 1.5 and $J_{5,6}$ 5, H-6); δ_C (75.46 MHz; $CDCl_3$) 23.6 (2 × CH_3), 23.7 (2 × CH_3), 71.4 (CH (^{i}Pr)), 71.9 (CH (^{i}Pr)), 124.9 (C-5), 126.8 (C-3), 138.0 (C-4), 152.0 (C-6), 152.1 (C-2), 165.0 (<u>C</u>$O_2{}^i$Pr) and 166.3 (<u>C</u>$O_2{}^i$Pr); *m/z* (ES^+) 290 ($(M+K)^+$, 5%), 274 ($(M+Na)^+$, 100%) and 252 ($(M+H)^+$, 10%).

Attempted synthesis*[17] *of diisopropyl 4-trimethylsilylquinolinate (70)

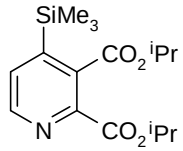

70

To a solution of 2,2,6,6-tetramethylpiperidine (1.0 mL, 6.0 mmol) in dry tetrahydrofuran (10 mL) was added n-butyllithium (4.2 mL of a 1.6 M solution in hexane, 6.6 mmol) with stirring at -78 °C, under a nitrogen atmosphere. After 25 minutes, a solution of trimethylsilyl chloride (3.8 mL, 30.0 mmol) in dry tetrahydrofuran (5 mL) was added, followed by the dropwise addition of a solution of diisopropyl quinolinate (0.77 g, 3.0 mmol) in dry tetrahydrofuran (10 mL) over 15 minutes. After stirring at -78 °C for 2 hours, the solution was allowed to gradually warm up to room temperature. The reaction was quenched by pouring the reaction mixture over 5% aqueous sodium hydrogen carbonate solution (10 mL). The organic material was extracted with diethyl ether (3 × 50 mL), washed with water (15 mL) and brine (2 × 20 mL) and dried (K_2CO_3). Removal of the solvent under reduced pressure gave a brown oil (0.84 g). An attempt was made to separate the components of the crude product by column chromatography on silica, employing gradient elution 5:1 hexane / ethyl acetate to 1:1 hexane / ethyl acetate. The major product isolated was identified as diisopropyl 4,6-di(trimethylsilyl)quinolinate **71** (0.18 g, 15%); δ_H (300 MHz; $CDCl_3$) 0.25 (9 H, s, $Si(CH_3)_3$), 0.27 (9 H, s, $Si(CH_3)_3$), 1.29 (6 H, d, *J* 6, 2 × CH_3), 1.34 (6 H, d, *J* 6, 2 × CH_3), 5.13-5.24 (2 H, m, 2 × $C\underline{H}(CH_3)_2$) and 7.66 (1 H, s, H-5); δ_C (75.46 MHz; $CDCl_3$) 0.0 (2 × $Si(CH_3)_3$), 22.1 (4 × CH_3 (^{i}Pr)), 70.3 (CH (^{i}Pr)), 70.4 (CH (^{i}Pr)), 124.9 (C-5), 126.9 (C-3), 134.2 (C-4), 149.1 (C-6), 152.0 (C-2), 165.0 ($\underline{C}O_2{}^i$Pr) and 166.5 ($\underline{C}O_2{}^i$Pr); *m/z* (ES^+) 418 ($(M+Na)^+$, 100%) and 396 ($(M+H)^+$, 25%).

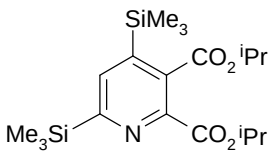

71

7.4.3.2 Route 2 - Addition to N-acylpyridinium salts[18]

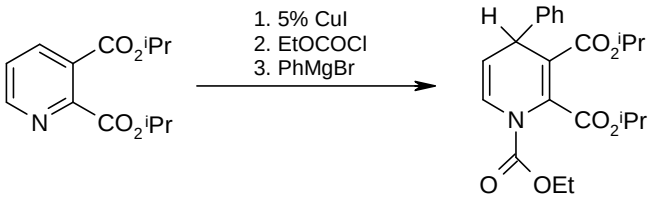

69 **78**

To a solution of diisopropyl quinolinate **69** (1.00 g, 4.0 mmol) in dry tetrahydrofuran (20 mL) under nitrogen was added CuI (57 mg, 0.3 mmol) and the mixture was stirred at room temperature until it became homogeneous. The reaction was cooled to approximately -30 ^{o}C (dry ice / xylene) then ethyl chloroformate (0.6 mL, 6.0 mmol) was added, with stirring. After 10 minutes, phenyl magnesium bromide (2 mL of a 3 M solution in diethyl ether, 6.0 mmol) in dry tetrahydrofuran (10 mL) was added slowly via cannula. The resulting orange solution was stirred for 2 hours at approximately -30 ^{o}C (dry ice / xylene) and then at room temperature for 2 hours. The reaction was quenched by addition of 20% aqueous ammonium chloride solution (20 mL) followed by diethyl ether (25 mL). The organic layer was separated and washed sequentially with 20% aqueous ammonium chloride / ammonium hydroxide solution (50:50, 20 mL), water (20 mL), 10% HCl (20 mL), water (20 mL) and brine (20 mL). After drying ($MgSO_4$), the solution was filtered and evaporated to yield a yellow oil (2.69 g). TLC and ^{1}H NMR analysis of the crude product showed no reaction had occurred.

7.4.3.3 Route 3 – Oxidation of 4-substituted quinolines

7.4.3.3.1 Synthesis of 4-substituted quinolines

Attempted synthesis*[19] *of 4-isobutylquinoline (87) (I)

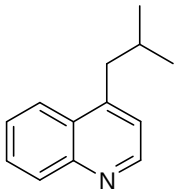

87

To a solution of n-butyllithium (2.8 mL of a 2.5 M solution in hexane, 7.0 mmol) in dry diethyl ether (20 mL) was added a solution of 4-methylquinoline **84** (1.00 g, 7.0 mmol) in diethyl ether (5 mL), under nitrogen. The reaction mixture turned bright red/orange. After 10 minutes, a solution of isopropyl bromide (0.33 mL, 3.5 mmol) in dry diethyl ether (3 mL) was added slowly over 20 minutes. The resulting solution was heated under reflux, under nitrogen, for 1 hour. The reaction mixture was allowed to cool to room temperature and was then poured over crushed ice. The two phases were separated and the aqueous layer was extracted with diethyl ether (3 x 75 mL). The combined diethyl ether extracts were dried (Na_2SO_4) and the solvent was removed under reduced pressure to give a yellow oil (0.98 g). No attempt was made to purify the crude product. The major product was identified as 2-butyl-4-methyl-1,2-dihydroquinoline **88**; δ_H (300 MHz; $CDCl_3$) 0.83 (3 H, t, *J* 7, CH_3), 1.18-1.33 (4 H, m, 2 x CH_2), 1.43-1.52 (2 H, m, CH_2), 1.90 (3 H, s, 4-CH_3), 3.68 (1 H, br s, NH), 4.03-4.09 (1 H, m, H-2), 5.30-5.33 (1 H, m, H-3), 6.32 (1 H, dd, $J_{5,7}$ 1 and $J_{5,6}$ 8, H-5), 6.49-6.55 (1 H, m, H-6), 6.85-6.90 (1 H, m, H-7) and 6.93 (1 H, dd, $J_{6,8}$ 1 and $J_{7,8}$ 8, H-8); *m/z* (ES^+) 202 ($(M+H)^+$, 10%). The minor product was identified as 2-butyl-4-methylquinoline **89**; δ_H (300 MHz; $CDCl_3$) 0.88 (3 H, t, *J* 7, CH_3), 1.10-1.18 (2 H, m, CH_2), 1.31-1.40 (2 H, m, CH_2), 1.66-1.76 (2 H, m, CH_2), 2.59 (3 H, s, 4-CH_3), 7.06 (1 H, s, H-3), 7.38-7.44 (1 H, m, H-6), 7.56-7.61 (1 H, m, H-7), 7.85-7.88 (1 H, m, H-5) and 7.95-7.99 (1 H, m, H-8); *m/z* (ES^+) 200 ($(M+H)^+$, 100%).

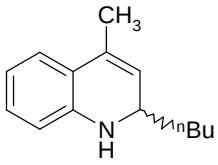

88

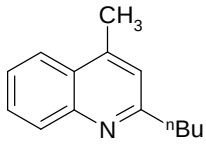

89

Attempted synthesis*[19] *of 4-isobutylquinoline (87) (II)

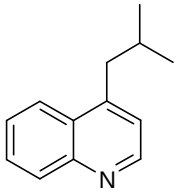

87

To a solution of methyllithium (4.4 mL of a 1.6 M solution in diethyl ether, 7.0 mmol) in dry diethyl ether (20 mL) was added a solution of 4-methylquinoline **84** (1.00 g, 7.0 mmol) in diethyl ether (5 mL), under nitrogen. The resulting solution was heated under reflux for 30 minutes. A solution of isopropyl bromide (0.33 mL, 3.5 mmol) in dry diethyl ether (3 mL) was then added slowly and the resulting solution was heated under reflux, under nitrogen, for 2.5 hours. The reaction mixture was allowed to cool to room temperature and was then poured over crushed ice. The two phases were separated and the aqueous layer was extracted with diethyl ether (3 x 75 mL). The combined ether extracts were dried (Na_2SO_4) and the solvent was removed under reduced pressure to give a yellow oil (0.72 g). No attempt was made to purify the crude product. The product was identified as 2,4-dimethyl-1,2-dihydroquinoline **90**; δ_H (300 MHz; $CDCl_3$) 1.17 (3 H, d, *J* 6, 2-CH_3), 1.89 (3 H, s, 4-CH_3), 3.68 (1H, br s, NH), 4.20-4.28 (1 H, m, H-2), 5.26-5.29 (1 H, m, H-3), 6.33 (1 H, dd, $J_{5,7}$ 1 and $J_{5,6}$ 8, H-5), 6.51-6.57 (1 H, m, H-6), 6.85-6.91 (1 H, m, H-7) and 6.93 (1 H, dd, $J_{6,8}$ 1 and $J_{7,8}$ 8, H-8); *m/z* (ES^+) 160 ($(M+H)^+$, 100%).

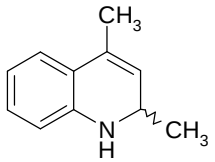

90

Attempted synthesis of 4-isobutylquinoline (87) (III)

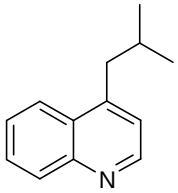

87

Dry diisopropylamine (1.00 mL, 7.0 mmol) was stirred under nitrogen in dry tetrahydrofuran (25 mL) at -78 °C for 10 minutes. n-Butyllithium (2.8 mL of a 2.5 M solution in hexane, 7.0 mmol) was added and the mixture was allowed to slowly reach room temperature. The resulting lithium diisopropylamide solution was then cooled to -78 °C and transferred slowly via cannula to a solution of 4-methylquinoline **84** (1.00 g, 7.0 mmol) in dry tetrahydrofuran (25 mL) that was also previously cooled to -78 °C. The mixture was left to stir at -30 °C for 1 hour then the resulting red solution was again cooled to -78 °C. A solution of isopropyl bromide (0.65 mL, 6.7 mmol) in dry tetrahydrofuran (8 mL) that was previously cooled to -78 °C was then added slowly via cannula. The resulting solution was stirred under nitrogen overnight, slowly allowing the reaction to warm to room temperature. The reaction mixture was then added to water (100 mL) and stirred for 10 minutes before extracting with diethyl ether (3 × 100 mL). The diethyl ether extracts were washed with water (100 mL), dried (Na_2SO_4) and evaporated under reduced pressure. This gave the crude product as a brown oil (1.54 g). TLC and ^1H NMR analysis of the crude product showed no reaction had occurred.

Synthesis*[20,21] *of 4-isobutylquinoline (87)

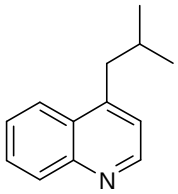

87

To liquid ammonia (120 mL) was added iron (III) nitrate (0.05 g) with vigorous stirring. To the resulting orange solution was added clean sodium (1.21 g, 52.5 mmol) in small pieces over a period of 30 minutes. Stirring was continued until the initial dark blue colour was replaced by a grey suspension of sodium amide. 4-Methylquinoline **84** (5.02 g, 35.1 mmol) was then added dropwise. After stirring the resulting solution for 30 minutes, isopropyl bromide (6.46 g, 52.5 mmol) was added at such a rate that the reaction did not become unduly vigorous. The reaction was stirred for 1 hour and then ammonium chloride was added to quench the reaction. The ammonia was allowed to evaporate overnight. To the resulting orange residue was added diethyl ether (100 mL) followed by water (100 mL). The two phases were separated and the aqueous phase was extracted further with diethyl ether (100 mL). The combined diethyl ether extracts were extracted with 6*N* hydrochloric acid solution (4 x 25 mL). The acid extracts were then made strongly alkaline by the addition of solid sodium hydroxide. A brown oil formed on the surface and was separated. The aqueous layer was extracted with diethyl ether (3 x 100 mL). The combined upper layer (brown oil) and diethyl ether extracts were dried (sodium sulfate) and the solvent was removed under reduced pressure to give a dark brown oil (5.04 g). The crude product was purified by column chromatography on silica employing gradient elution 3:1 petroleum ether / ethyl acetate to 1:1 petroleum ether / ethyl acetate. This gave the desired product **87** as a pale yellow oil (2.79 g, 43%); ν_{max}/cm^{-1} 3025, 1600 and 1510; δ_H (300 MHz; $CDCl_3$) 0.90 (6 H, d, *J* 7, 2 x CH_3), 1.94-2.07 (1 H, m, CH), 2.84 (2 H, d, *J* 7, CH_2), 7.11 (1 H, d, $J_{2,3}$ 5, H-3), 7.43-7.49 (1 H, m, H-6), 7.58-7.64 (1 H, m, H-7), 7.94 (1 H, ddd, $J_{5,6}$ 8, $J_{5,7}$ 1.5 and $J_{5,8}$ 0.5, H-5), 8.03 (1 H, ddd, $J_{7,8}$ 8, $J_{6,8}$ 1.5 and $J_{5,8}$ 0.5, H-8) and 8.71 (1 H, d, $J_{2,3}$ 5, H-2); δ_C (75.46 MHz; $CDCl_3$) 23.0 (2 x CH_3), 29.6 (CH), 41.8 (CH_2), 122.1 (C-3), 124.2 (C-6), 126.4 (C-5), 128.2 (C-4a), 129.2 (C-8), 130.4 (C-7), 147.9 (C-4), 148.7 (C-8a) and 150.2 (C-2); *m/z* (ES^+) 208 ($(M+Na)^+$, 15%) and 186 ($(M+H)^+$, 100%).

Synthesis*[20,21] *of 4-benzylquinoline (91)

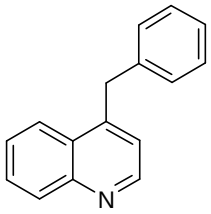

91

To liquid ammonia (120 mL) was added iron (III) nitrate (0.04 g) with vigorous stirring. To the resulting orange solution was added clean sodium (1.21 g, 52.5 mmol) in small pieces over a period of 30 minutes. Stirring was continued until the initial dark blue colour was replaced by a grey suspension of sodium amide. 4-Methylquinoline **84** (5.02 g, 35.1 mmol) was then added dropwise. After stirring the resulting solution for 30 minutes, bromobenzene (8.24 g, 52.5 mmol) was added at such a rate that the reaction did not become unduly vigorous. After stirring for 1 hour, the reaction was quenched by addition of ammonium chloride and the ammonia was allowed to evaporate overnight. To the resulting orange residue was added diethyl ether (100 mL) followed by water (100 mL). The two phases were separated and the aqueous phase was extracted further with diethyl ether (100 mL). The combined diethyl ether extracts were extracted with 6*N* hydrochloric acid solution (4 x 25 mL). The acid extracts were then made strongly alkaline by the addition of solid sodium hydroxide. A brown oil formed on the surface and was separated. The aqueous layer was extracted with diethyl ether (3 x 100 mL). The combined upper layer (brown oil) and diethyl ether extracts were dried (Na_2SO_4) and the solvent was removed under reduced pressure to give a dark brown oil (4.24 g). The crude product was purified by column chromatography on silica employing gradient elution 3:1 petroleum ether / ethyl acetate to 1:1 petroleum ether / ethyl acetate. This gave the desired product **91** as a pale yellow oil (1.66 g, 22%); ν_{max}/cm^{-1} 3029, 1591 and 1508; δ_H (300 MHz; $CDCl_3$) 4.44 (2 H, s, CH_2), 7.13 (1 H, d, $J_{2,3}$ 5, H-3), 7.19-7.34 (5 H, m, 5 × Ar-H), 7.50-7.56 (1 H, m, H-6), 7.67-7.73 (1 H, m, H-7), 8.03 (1 H, ddd, $J_{5,6}$ 8, $J_{5,7}$ 1.5 and $J_{5,8}$ 0.5, H-5), 8.15 (1 H, ddd, $J_{7,8}$ 8, $J_{6,8}$ 1.5 and $J_{5,8}$ 0.5, H-8) and 8.83 (1 H, d, $J_{2,3}$ 5, H-2); δ_C (75.46 MHz; $CDCl_3$) 38.6 (CH_2), 122.3 (C-3), 124.3 (C-6), 127.0 (C-5), 127.1 (C-4'), 128.0 (C-4a), 129.1, 129.3 (C-2', C-3', C-5' and C-6'), 129.6 (C-8), 130.6 (C-7), 139.0 (C-1'), 147.0 (C-4), 148.8 (C-8a) and 150.7 (C-2); *m/z* (ES^+) 220 ($(M+H)^+$, 100%).

Synthesis*[20,21] *of 4-phenethylquinoline (94)

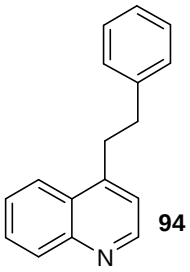

94

To liquid ammonia (50 mL) was added iron (III) nitrate (0.02 g) with vigorous stirring. To the resulting orange solution was added clean sodium (0.24 g, 10.5 mmol) in small pieces over a period of 30 minutes. Stirring was continued until the initial dark blue colour was replaced by a grey suspension of sodium amide. 4-Methylquinoline **84** (1.00 g, 7.0 mmol) was then added dropwise. After stirring the resulting solution for 30 minutes, benzyl bromide (1.80 g, 10.5 mmol) was added at such a rate that the reaction did not become unduly vigorous. The reaction mixture was stirred for a further 1 hour and then ammonium chloride was added to quench the reaction and the ammonia was allowed to evaporate overnight. To the orange residue was added diethyl ether (50 mL) followed by water (50 mL). The two phases were separated and the diethyl ether phase was extracted with 6*N* hydrochloric acid solution (4 x 20 mL). The acid extracts were then made strongly alkaline by the addition of solid sodium hydroxide. A brown oil formed on the surface and was separated. The aqueous layer was extracted with diethyl ether (3 x 50 mL). The combined upper layer (brown oil) and diethyl ether extracts were dried (Na_2SO_4) and the solvent was removed under reduced pressure to give a dark brown oil (0.73 g). The crude product was purified by column chromatography on silica employing gradient elution 3:1 petroleum ether / ethyl acetate to 1:1 petroleum ether / ethyl acetate. This gave the desired product **94** as a pale yellow solid (0.40 g, 24%); mp 98-100 °C (lit.[22] mp 101-103 °C); ν_{max}/cm^{-1} 3030, 1595 and 1510; δ_H (300 MHz; $CDCl_3$) 3.01 (2 H, t, *J* 8, CH_2), 3.32 (2 H, t, *J* 8, CH_2), 7.10-7.27 (6 H, m, 6 x Ar-H), 7.48-7.54 (1 H, m, H-6), 7.62-7.68 (1 H, m, H-7), 8.01 (1 H, ddd, $J_{5,6}$ 8, $J_{5,7}$ 1.5 and $J_{5,8}$ 0.5, H-5), 8.07 (1 H, ddd, $J_{7,8}$ 8, $J_{6,8}$ 1.5 and $J_{5,8}$ 0.5, H-8) and 8.72 (1 H, d, $J_{2,3}$ 5, H-2); δ_C (75.46 MHz; $CDCl_3$) 34.5 (CH_2), 36.6 (CH_2), 121.3 (C-3), 123.8 (C-6), 126.7 (C-5), 126.8 (C-4'), 128.0 (C-4a), 128.8, 129.0 (C-2', C-3', C-5' and C-6'), 129.5 (C-8), 130.7 (C-7), 141.4 (C-1'), 147.8 (C-4), 148.8 (C-8a) and 150.6 (C-2); *m/z* (ES^+) 256 ($(M+Na)^+$, 5%) and 234 ($(M+H)^+$, 100%).

7.4.3.3.2 Oxidation of 4-substituted quinolines

Synthesis*[23] *of 4-methylquinolinic acid (95)

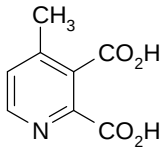

95

To a biphasic mixture of dichloromethane (75 mL) and sodium hypochlorite solution (50 mL diluted with 155 mL of water, 1.0 mol) was added ruthenium (IV) oxide (24 mg, 175 μmol) under vigorous stirring at room temperature. When the reaction mixture was yellow, 4-methylquinoline **84** (1.00 g, 7.0 mmol) was added dropwise. After stirring at room temperature for 7.5 hours, the mixture became black. TLC analysis (dichloromethane:methanol, 95:5) showed that the conversion was not complete and an additional amount of sodium hypochlorite solution (20 mL, 0.4 mol) was added. After stirring overnight at room temperature, the aqueous phase was separated, washed with diethyl ether (2 x 100 mL) and acidified to pH 1 with 37% hydrochloric acid. Evaporation to dryness gave the crude product as a yellow solid (23.20 g). Desalinisation of the crude product was attempted by adding *N*,*N*-dimethylformamide (100 mL), then removing the insoluble salt by filtration. The filtrate was evaporated and the resulting orange solid was washed with toluene (4 x 50 mL) followed by chloroform (3 x 50 mL). Recrystallisation from ethanol gave the product **95** as an orange solid (0.88 g, 69%, impure); mp 180 °C (dec.) (lit.[24] mp 188–190 °C); $\lambda_{max}(H_2O)$/nm 276 (log ε 1.96) (lit.[24] 276 (log ε 3.69)); ν_{max}/cm^{-1} 3000 (O─H stretch) and 1725 (C=O stretch); δ_H (300 MHz; D_2O) 2.52 (3 H, s, 4-CH_3), 7.91 (1 H, d, $J_{5,6}$ 6, H-5) and 8.49 (1 H, d, $J_{5,6}$ 6, H-6); δ_C (75.46 MHz; CD_3OD) 19.6 (CH_3), 130.0 (C-5), 135.0 (C-3), 146.5 (C-4), 149.2 (C-6), 152.0 (C-2), 167.5 (CO_2H) and 171.4 (CO_2H); *m/z* (ES^+) 182 ($(M+H)^+$, 100%).

7.5 References

1. M.M. Bradford, *Anal. Biochem.*, 1976, **72**, 248-254.
2. J. Brons-Poulsen, N.E. Petersen, M. Horder and K. Kristiansen, *Mol. Cell. Probes*, 1998, **12**, 345-348.
3. H. Cao, B.L. Pietrak and C. Grubmeyer, *Biochemistry*, 2002, **41**, 3520-3528.
4. W.C. Still, M. Khan and J. Mitra, *J. Org. Chem.*, 1978, **43**, 2923-2925.
5. D.D. Perrin, W.L.F. Armarego and D.R. Perrin, *Purification of Laboratory Chemicals*, Pergammon Press, Oxford, 1980.
6. R.C. Elderfield and M. Green, *J. Org. Chem.*, 1952, **17**, 431-441.
7. L.M. Spiessens and M.O. Anteunis, *Bull. Soc. Chim. Belg.*, 1980, **89**, 205-231.
8. R. Levine and J.K. Sneed, *J. Am. Chem. Soc.*, 1951, **73**, 5614-5616.
9. H. Neunberg, *Ber.*, 1935, **68**, 1474-1475.
10. B. Vaitilingam, A. Nayyar, P.B. Palde, V. Monga, R. Jain, S. Kaur and P.P. Singh, *Bioorg. Med. Chem.*, 2004, **12**, 4179-4188.
11. W.H. Mills and F.M. Hamer, *J. Chem. Soc. Trans.*, 1922, **121**, 2008-2014.
12. J.S. Foot, H. Kanno, G.M.P. Gerard and R.J.K. Taylor, *Synthesis*, 2003, **7**, 1055-1064.
13. D.B. Paul, *Aust. J. Chem.*, 1984, **37**, 87-93.
14. G.R. Clemo and H. Koenig, *J. Chem. Soc.*, 1949, 231-239.
15. B.M. Bain and J.E. Saxton, *J. Chem. Soc.*, 1961, 5216-5223.
16. P. Monje, P. Grana, M.R. Paleo and F.J. Sardina, *Org. Lett.*, 2006, **8**, 951-954.
17. T.D. Krizan and J.C. Martin, *J. Am. Chem. Soc.*, 1983, **105**, 6155-6157.
18. D.L. Comins and A.H Abdullah, *J. Org. Chem.*, 1982, **47**, 4315-4319.
19. C. Osuch and R. Levine, *J. Am. Chem. Soc.*, 1956, **78**, 1723-1725.
20. B.S. Furniss, A.J. Hannaford, P.W.G Smith and A.R. Tatchell, *Vogel's Textbook of Practical Organic Chemistry*, 5th Edition, Longman Scientific and Technical, 1989, 1171-1172.
21. M.J. Weiss and C.H. Hauser, *J. Am. Chem. Soc.*, 1949, **71**, 2023-2026.
22. H. Gilman, J.L. Towle and R.K. Ingham, *J. Am. Chem. Soc.*, 1954, **76**, 2920-2923.
23. M.D. La Bas, C. Guéret, C. Perrio, M.C. Lasne and L. Barré, *Synthesis*, 2001, **16**, 2495-2499.
24. C. O'Murchu, *Synthesis*, 1989, **10**, 880-882.

Appendices

Appendix 1

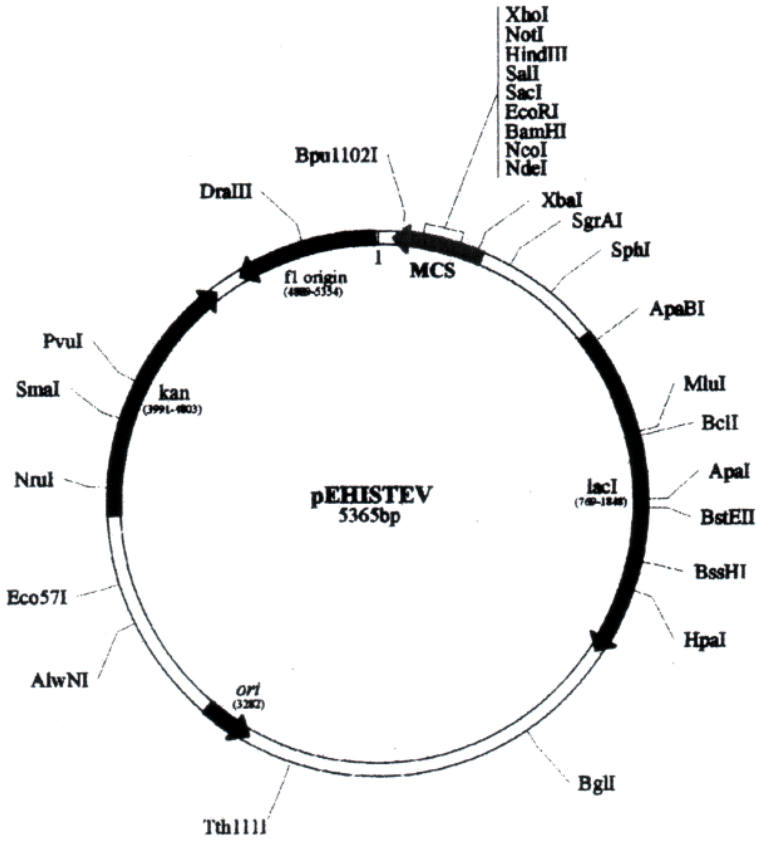

T7 Pro seq primer

T7 promoter lac operator *Xba* I

ATCGATCTCGATCCCGCGAAATTAATACGACTCACTATAGGGGAATTGTGAGCGGATAACAATTCCCCTCTAGAAATAATTTTG

rbs *Nde* I 6xHis

TTTAACTTTAAGAAGGAGATATACAT ATG TCG TAC TAC CAT CAC CAT CAC CAT CAC GAT TAC GAT ATC CCA

M S Y Y H H H H H H D Y D I P

TEV protease site *Nco* I *BamH* I *EcoR* I *Sac* I

ACG ACC GAA AAC CTG TAT TTT CAG GGC GCC ATG GCT GAT ATC GGA TCC GAA TTC GAG CTC CGT

T T E N L Y F Q* G A M D D I G S E F E L R

Sal I *Hind* III *Not* I *Xho* I

CGA CAA GCT TGC GGC CGC ACT CGA GCA CCA CCA CCA CCA CCA CTG AGA TCC GGC TGC TAA CAA

R Q A C G R T R A P P P P P L R S G C end

Bpu1102I T7 terminator

AGCCCGAAAGGAAGCTGAGTTGGCTGCTGCCACCGCTGAGCAATAACTAGCATAACCCCTTGGGGCCTCTAAACGGGTCTTGAGG

T7 Ter seq primer

GGTTTTTTGCTGAA